Modelling and Optimization of an Intelligent Home Energy Management System (HEMS) in Microgrid

Xin Lin

A thesis submitted to Auckland University of Technology in fulfilment of the requirements for the degree of Doctor of Philosophy (PhD)

2022

School of Engineering, Computer and Mathematical Sciences

Auckland University of Technology

New Zealand

Preface

This thesis has been prepared at School of Engineering, Computer and Mathematical Sciences, Auckland University of Technology, New Zealand in fulfillment of the requirements for the award of a degree of Doctor of Philosophy (PhD). The work has been carried out in the period from April 2018 to November 2022 under the supervision of Dr. Ramon Zamora and Dr. Craig A. Baguley. The purpose of this thesis is to develop an energy management system for smart houses with photovoltaics (PV) and hybrid energy storage system (HESS) aimed at reducing electricity costs while satisfying user comfort demands. The research work carried out in this thesis was mainly divided in two parts. The first part of the thesis is mainly to study microgrid technology and develop a local level energy management system for HESS in a DC microgrid. The second part of the thesis is to develop a system level energy management system including load forecasting and power optimization for a residential DC microgrid. The work carried out in both parts of the thesis was presented in the form of manuscripts. An introductory preface to each chapter explains the work in each manuscript and its relevance to the main idea of the thesis. Furthermore, each chapter describes the work presented in the manuscripts.

Abstract

Recently, carbon emissions and depletion of fossil fuels are exacerbated by the high demand for electrical energy in the residential sector. Renewable energy sources (RES) as an environmentally friendly energy source have been widely installed in residential buildings. However, the intermittent of RES makes it challenging to providing stable power to residential customers. To solve this problem, an energy storage system (ESS) is integrated into homes to improve the quality of electrical energy. This kind of power system integrating RES and ESS in the house can be defined as a home microgrid. The home energy management system (HEMS) plays an important role in the home microgrid, which can collect data information through the home local area network and the Internet to predict the user's energy usage. Then, the HEMS will use the predicted data to formulate an optimal power scheduling plan, so as to reduce the operating cost of the system and improve the utilization efficiency of RES. Furthermore, the HEMS is beneficial to both utility and home customers. For the utility, the HEMS can moderate the household's power demand from the utility during peak periods, thereby reducing the supply pressure on the main grid. The HEMS can increase the penetration of RES installations in the residential sector, thereby reducing carbon emissions. For home users, the HEMS can enable users to change from traditional consumers to prosumers that actively participate in the energy trading market. In addition, the HEMS can change the user's energy usage patterns, thereby reducing household energy consumption. Therefore, it is necessary to study the application of the HEMS in modern smart grids.

The purpose of this study is to develop an energy management system for a smart home with photovoltaics (PV) and hybrid energy storage system (HESS), with the aim of reducing electricity costs while meeting occupant comfort needs. The research work carried out by this study is mainly divided into two parts. The first part is the local level energy management system, which can be further divided into two sub-parts presented in separate independent chapters. The two subparts are the decentralized control method for single type energy storage and the multifunctional control method for HESS, respectively. The second part is the system level energy management control, which is also divided into two parts and presented in separate independent chapters. These two subparts are load prediction and power optimization respectively.

Chapter 1 provides the background and motivation of this thesis. It also points out the research gaps, research questions and specific contributions of the thesis. Chapter 2 provides a comprehensive review of smart energy management systems in home microgrids. This part first introduces the concept and structure of household microgrid in detail, including HESS composed of high energy density storage (HES) and high power density storage (HPS). Further, this part describes the role and function of HEMS in the home microgrid. These functions can be grouped into load forecasting, optimization and control. Each function is categorized and analyzed in

detail. Then, a case study is provided to verify the feasibility of HEMS containing HESS. Finally, this chapter reveals the flaws and gaps in intelligent HEMS research, which constitute a part of the research questions of this thesis.

The proposed method starts with a fully decentralized control approach for battery storage systems in the local level energy management system which is presented in Chapter 3. This part of the study develops a state of charge (SoC) balance control method to address the SoC imbalance among batteries regardless of whether the batteries have the same capacity. In this way, a battery with a higher SoC and capacity can deliver more power in discharging mode than ones with a lower SoC and capacity. During charging mode, the battery with higher SoC and lower capacity is controlled to draw less power than the ones with higher capacity and lower SoC. Therefore, SoC balance can be achieved among distributed BSUs. Then, a high-pass filter (HPF) based power droop method is designed to realize voltage regulation and power sharing. In this method, the secondary voltage restoration control is equivalent to an HPF, thereby eliminating the communication connection between the primary control and the secondary control. This part also establishes a processor-in-the-loop (PIL) simulation platform to verify the performance of the method.

Chapter 4 proposes a comprehensive multifunctional control method for multiple HESSs composed of batteries and supercapacitors (SCs) in a DC microgrid. The study in this part develops a novel droop-based coordinated control to realize power sharing between battery and SC. At the same time, the method can also realize voltage regulation without an additional voltage recovery control method, thereby reducing the complexity of control. Among them, v-dP is proposed to regulate the battery to provide the average power provided, while the traditional droop control is used to adjust the SC to deliver the instantaneous power. Different line resistances in the system reduce the accuracy of power distribution among the batteries. Therefore, a voltage compensator based on a consensus algorithm is developed to simultaneously achieve accurate power sharing and SoC balancing among batteries. Then, an SoC recovery control of the SCs is adopted to ensure the continuous operation of the SCs. Finally, a power management system is presented to prevent the batteries overuse in different operating mode.

After completing the design of the energy management system at the local level, the research work moved into the development of the system level energy management system. Chapter 5 proposes a hybrid approach for improving the accuracy of short-term household load forecasting. The hybrid approach consists of two models. The first model is an ensemble model used to predict home heat and air conditioning (HAC) load usage. The ensemble model includes support vector machine (SVM), back propagation neural network (BPNN), and generalized regression neural network (GRNN). Among them, genetic algorithm is adopted to optimize SVM and BPNN to enhance their performance. Then, a thermal dynamic model is developed to track the indoor

temperature which is used as one of the inputs to the ensemble model. Another model is a deep ensemble model used to track the consumption of lighting and other loads. The deep ensemble model consists of three bidirectional long short-term memory (Bi-LSTM) networks. Among them, the Bayesian algorithm is used to optimize the hyperparameters of LSTM. Finally, a trimmed algorithm is used to integrate the results of the ensemble and deep ensemble models to remove undesired outliers.

The prediction data obtained according to the method in Chapter 5 will be sent to the optimization layer in the system level energy management system to generate the optimal power scheduling plan. Therefore, the purpose of Chapter 6 is to develop an optimization technique to formulate an optimal power scheduling plan with the objectives of minimizing the operating cost and maximizing the user comforts. Furthermore, this chapter also presents the interaction between system level and local level energy management systems. Therefore, Chapter 6 proposes a multi-level HEMS for a DC home microgrid, which consists of two parts. The first part is the long- and short-time optimization methods based on model predictive control (MPC). This long-term optimization is proposed to minimize the operating cost of the system and maximize the user comfort. In addition, the degradation models of batteries and SCs are designed to evaluate their degradation costs. Hence, the total operating cost covers electricity cost, PV power generation cost, battery and SC wear costs. Then, a predicted mean vote - percentage people dissatisfied (PMV-PPD) model is adopted to evaluate thermal environment comfort. An illuminance model is employed to assess the indoor visual comfort. The purpose of this short-time optimization is to alleviate the power fluctuations caused by the randomness of end-user behaviors and PV generation, as well as to ensure the capacity of the SC within a safe range. The second part of this chapter is the local level energy management system, which method is further improved based on the method in Chapter 4. Furthermore, the local level energy management system is more simplified and has better performance compared to the method presented in Chapter 4.

Table of Contents

Attestation of Authorship

I hereby declare that this submission is my own work and that the work presented in this thesis is solely based on my own research. The content of this PhD work is original, except where the work is referenced. I also declare that this work has not been submitted in whole or in part for the purpose of degree or qualification at any degree-awarding institute. I declare that this thesis is my own work and contains nothing as an outcome of work done in internal and/or external collaboration.

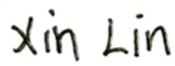

……

Xin Lin

November 2022

Co-Authored Works

Chapter Title	Author	Contribution (%)
Chapter 2: An overview of intelligent energy management system in a home microgrid	X. Lin R. Zamora C. Baguley	85 10 5
Chapter 3: A fully filter-based decentralized control with state of charge balancing strategy for battery energy storage systems in autonomous dc microgrid applications	X. Lin R. Zamora C. Baguley	85 10 5
Chapter 4: A comprehensive multi-functional controller for hybrid energy storage systems in DC microgrids	X. Lin R. Zamora C. Baguley	85 10 5
Chapter 5: A hybrid short-term load forecasting approach for individual residential customer	X. Lin R. Zamora C. Baguley A. K. Srivastava	80 10 5 5
Chapter 6: A multi-level energy management system (HEMS) suited to DC-based home microgrid	X. Lin R. Zamora C. Baguley Y. Jiang A. K. Srivastava	80 8 4 4 4

We, the undersigned, hereby agree to the participation percentages and contribution to the chapters identified in the table above.

……..…….

Dr Ramon Zamora
(Primary Supervisor)

……..…….

Dr Craig Baguley
(Secondary Supervisor)

……..…….

Dr Yazhou Jiang
(Collaborator)

……..…….

Prof Anurag K. Srivastava
(Collaborator)

Published Works during the PhD Programme

Published works included in this thesis

1. X. Lin, R. Zamora, and C. Baguley, "An overview of intelligent energy management system in a home microgrid," *Renewable and Sustainable Energy Reviews*, 2022 (**To be submitted**)
2. X. Lin, R. Zamora, C. Baguley, Yazhou Jiang and Anurag K. Srivastava, "A multi-level energy management system (HEMS) suited to DC-based home microgrid," *IEEE Trans. Sustain. Energy*, 2022 (**To be submitted**)
3. X. Lin, R. Zamora, C. Baguley, and Anurag K. Srivastava, "A hybrid short-term load forecasting approach for individual residential customer," *IEEE Trans. Power Del.* 2022. **(Published)**
4. X. Lin, R. Zamora, and C. Baguley, "A comprehensive multi-functional controller for hybrid energy storage systems in DC microgrids," *IEEE Trans. Ind. Appl*. **(Under first review)**
5. X. Lin, R. Zamora, and C. Baguley, "A fully filter-based decentralized control with state of charge balancing strategy for battery energy storage systems in autonomous dc microgrid applications," *IEEE Access*, vol. 9, pp. 15028–15040, Jan. 2021. **(Published)**

Published works excluded from this thesis

1. X. Lin and R. Zamora, "Controls of hybrid energy storage systems in microgrids: Critical review, case study and future trends," *Journal Energy Storage*, vol. 47, pp. 103884, March 2022. **(Published)**
2. X. Lin, R. Zamora, and C. Baguley, "A coordinated droop controls and power management scheme for hybrid energy storage systems in DC microgrids," *in Proc. AUPEC*, Perth, Australia, 2021, pp.1-6. **(Published)**
3. X. Lin, R. Zamora, and C. Baguley, "Droop control based on improved virtual impedance in a stand-alone microgrid," *IEEE PES GTD Asia 2019 Conference,* Bangkok, Thailand. **(Published)**

Acknowledgement

This doctoral thesis represents the compilation of the research outputs during my time as a research student at Auckland University of Technology (AUT), Auckland, New Zealand. Many people have contributed to the success of the PhD research in one way or another to help and support the realization of this thesis.

I would like to express my heartfelt gratitude to my primary supervisor, Dr Ramon Zamora, who provides tremendous support during my Master to PhD journey. I am grateful for his guidance and patience during my research study. I appreciate his invaluable time in reviewing all manuscripts and providing precious comments and suggestions. Without his motivation and encouragement, this thesis would not have been possible. My sincere thanks also go to my secondary supervisor, Dr Craig Baguley, for providing me with invaluable suggestions, insights, inspiration, and support.

I would also like to express my sincere appreciation to Prof Anurag K. Srivastava and Dr Leo Yazhou Jiang for the fruitful collaborations in writing and publishing journal articles. I would also like to thank the members of Renewable Energy and Power Systems Group under Dr Ramon Zamora for constructive discussions, questions and suggestions. Special appreciations to Dr Nicholas Mukisa, Dr Peter Makolo, Dr Jun Su, Ifedayo Oladeji, Asaad Mohammad, Uvini Perera, Avy Sheina and all master students who happened to participate in our research group.

I am very grateful to AUT for the Vice-Chancellor's Scholarship which enabled me to pursue my PhD. I would also like to thank the AUT staffs for their help and support during my PhD study.

I would also like to thank my beloved family and friends for their support in my PhD study and help in my life. May God bless you all.

Introduction

Chapter 1: Introduction

1.1. Background and motivation

The growth in energy demand caused by human activities leads to an increase in the carbon dioxide emissions and depletion of fossil fuel. According statistics of the International Energy Agency (IEA) statistic, the global electricity consumption has reached 29 trillion kWh in 2020, approximately one-third of it was contributed to the residential sector [1]. Similar energy statistics and research reports have also been carried out in some countries, such as the United States and New Zealand [2], [3]. These reports recommend the development of novel electricity technologies to reduce energy usage in the residential sector without causing environmental problems. Therefore, renewable energy sources (RES) as non-polluting and environmentally friendly energy sources have been integrated into residential buildings by several research projects to reduce electricity demand from utility [4]–[6]. However, the intermittent and random nature of RES makes it challenging to provide users with stable electric power, thereby failing to meet the energy demands of customers. Therefore, an energy storage system (ESS) can be installed in a residence as an energy buffer to suppress power fluctuations caused by a mismatch between power generation and demand and to ensure stable operation of the system. In a residence, the RES such as photovoltaic (PV), ESS and household appliances form a small-scale power system, which can be defined as a home microgrid [7].

Typically, ESSs in the home microgrids are a single type of energy storage. For instance, the methods in [8]–[10] employ batteries with a low dynamic response and high energy capacity density characteristics to supply household loads. However, the random behavior of end users can cause frequent load fluctuations in the house. Due to the characteristics of the battery, it may not be able to suppress high frequency power oscillations, and the degradation of the battery is accelerated, thereby reducing its lifespan [11]. Therefore, supercapacitor (SC), with a fast dynamic response but a low energy density, may be employed to serve loads with high and rapid power fluctuations [12]. So far, no existing energy storage type has characteristics that suit all load and user demands. Therefore, hybrid energy storage systems (HESS) comprising multiple energy storage types can be presented as an effective solution in the home microgrid.

In the home microgrid, the output power of PV and ESS acts on the system in the form of DC, and a large number of DC electrical loads are adopted in the houses, such as air conditioners and LED lights. Therefore, DC-based microgrids is more suitable for residential scenarios, which simplifies energy conversion and increases the energy efficiency of the system by up to 5% compared to traditional AC-based microgrids [13], [14]. In DC home microgrid, the home energy management system (HEMS) is a key challenge, which can achieve the stable and economical operation of the system through the coordination and management of distributed energy sources

and energy transactions with the main grid [15]. The HEMS also encourages end customers to actively participate in the energy interaction mechanism, adjust customers' electricity consumption behavior, and then turn them into prosumers [16].

The HEMS can be composed of three parts: day-ahead load forecasting, optimization and control. Day-ahead load forecasting stage predicts the household load consumption on the next day by collecting meteorological and historical load datasets. Generally, time series models are the typical method applied to load forecasting, including autoregressive integrated moving average models [17], grey model [18], and regression analysis model [19]. However, these models are insufficient to deal with nonlinear problems and will lead to lower prediction accuracy. Therefore, nonlinear forecasting models, including support vector regression [20] and artificial neural networks [21], have been employed to solve nonlinear problems in load forecasting. However, these methods use a single predictive model. Due to the performance limitations of a single predictor, the predicted output may have outliers, and hence, the deviation will increase [22], [23]. For this reason, the ensemble forecasting model that including multiple predictors such as in [24]–[26] is proposed to eliminate the outliers of the predicted output to improve the forecasting accuracy. However, the above methods mainly focus on the users' total power prediction and do not include the power consumption prediction of high-power equipment, such as heating and air conditioning (HAC). Since HAC occupies a large proportion of electricity, regulating the HAC loads is a potential for energy-saving [27]. Furthermore, the power consumption forecast for HAC can enable users to understand the specific situation of the power usage, so as to make necessary adjustments to achieve the goal of power-saving [28]. There are three prediction methods for HAC systems: physics-based, data-driven, and hybrid models [29]. The physics-based model predicts the load by establishing a complex physical model. However, the parameters of the physical model are often difficult to measure [30]. Data-driven uses machine learning and time-series statistical analysis methods to predict load, but it requires a lot of historical data [31]. In order to solve these issues, a hybrid model including physical-based and data-driven models is presented because it only requires a simple physical model and less historical data, such as methods in [32], [33]. Afterwards, the obtained prediction data including house load and weather conditions is transferred to the system optimization stage.

The optimization layer of HEMS will minimize the operating cost of the home microgrid and ensure its stable operation according to the predicted data and real-time electricity price. The optimization methods is a fundamental challenge in the HMES, which can be divided into offline and online optimization [34], [35]. Offline optimization is based on the premise that RES and house load is determined to reduce system energy consumption and cost operation [36]. However, uncertainties in RES and house load reduce the accuracy of offline optimization. For this reason, online optimization such as in [37]–[39] is proposed to solve these problems. The optimization layer consists of three main factors: time frame, constraints and objective function. The time

frame consists of time horizon and time resolution. Depending on the scenario, the time horizon can change from a few hours to several days, such as the operating cost management [40], [41]. Time resolution can range from a few minutes to an hour [42], [43]. According to the house microgrid requirements and user demands, the constraints can be classified into technical and environmental constraints. The technical constraints mainly include power balance, power limits, load demand limits, load on/off time, state of charge (SoC) and depth of discharge (DoD) limits [16], [44], [45]. The environmental constraints mainly consist of temperature limits, heating (cooling) coefficient limits, and predicted mean vote (PMV) thermal comfort limits [46], [47]. Then, the objective function refers to the goal of the optimization of the system, which can be divided into single or multiple objectives, such as operating cost, power usage and energy storage degradation cost [48], [49]. The objective function is to be solved by suitable optimization algorithm such as model predictive control (MPC), heuristic algorithm and mixed integer programing within constraint conditions and time horizons [50], [51]. Then, the optimized results are sent to the control layer to regulate power converter system (PCS) based HESS via the communication system.

The control system will generate a pulse width modulation (PWM) signal according to the decision made by the optimization layer to regulate the PCS based HESS to supply power to the system load and ensure the bus voltage within a safe range. The control system should simultaneously satisfy the versatility, stability and independent operation ability. Therefore, the development of control technology in the HEMS is a new challenge facing in the home microgrid. The control technology can be broadly summarized into three types: (a) decentralized, (b) centralized, and (c) distributed. In decentralized method, each converter is controlled by its local controllers (LCs) that only receive local data and are not aware of the overall status of the system as well as the working conditions of other controllers. In addition, there is no communication network among the controllers [52]. For instance, a droop-based control method is the classic decentralized control, which is used to achieve power sharing in the HESS [53]. In the centralized control, a central controller (CC) is required to adjust an LC, such as voltage recovery control, through the communication system [54]. The CC collects system data and makes decisions for the LCs. In distributed multi-agent control, each controller is considered as individual agent, which will receive local information and will also collect data from neighboring agents through a sparse communication network to achieve coordinated control, such as voltage recovery and SoC balancing controls [55].

1.2. Research gaps

The review of the existing approaches related to the HEMS in home microgrid indicates that:

- There is a need for a novel and enhanced complete HEMS that should take into account the interaction among control, forecasting and optimization layers.

Although many research works have studied HEMS algorithm, HEMS considering operating costs, comfort management and HESS is not covered in the published works. Besides, most of the existing methods in HEMS focus on developing the optimization algorithm but neglect the integrity and independence of the HEMS.

- There is a need to develop a novel HESS control system which should have versatility and simplicity. The new control method should consider accurate power distribution, voltage restoration, SoC balance and recovery for the batteries and SCs.

The control approach in HEMS refers to the HESS control system. The existing HESS control methods achieve multiple functions, such as power sharing, voltage regulation and SoC recovery of SC. More functions mean that the control system becomes more complex, and the order of the system becomes higher. Then, the control system parameters need to be carefully designed to avoid the potential influence between control loops with different functions, thereby avoiding the instability of the system. The new HESS control technology should be more effective, less complex, and considering more functions.

- There is a need to develop a novel load forecasting technology which should have high accuracy and require large amounts of historical data.

Load forecasting plays an important role in HEMS, which enables users to understand electricity consumption and control the operation of electrical appliances to reduce electricity tariffs. So far, the existing methods mainly focus on the study of load forecasting for large-scale systems (e.g., more than thousands of residential users) rather than an individual residential customer. Since the individual load has the characteristics of fast changing and randomness, its prediction is still a challenge. In addition, most methods use a single predictor and require a large amount of historical data to achieve load forecasting. Furthermore, the results of a single predictor may have unexpected outliers, which reduces the accuracy of the forecast.

- There is a need to develop a novel optimization technology which should consider operating cost, HESS degradation cost, thermal and visual comforts.

Load optimization in HEMS can improve energy efficiency and reduce electricity bills. Currently, the published works mainly focus on reducing the operating cost of the system within a set comfort range. However, these works ignore the maximization of user comfort and the degradation of energy storage devices. Besides, these research works do not consider power fluctuations generated by RES and user behavior randomness and uncertainty.

1.3. Research questions and objectives

Based on the research gaps mentioned in the previous section, the research questions can be summarized as follows:

1. How can the control method be optimally designed to achieve power-sharing, power-split, SoC balance and restoration for HESS with multiple batteries and SCs?
2. How can HEMS algorithm be designed to optimize power consumption and customer comfort?

Based on research questions, the objectives of this PhD thesis are to develop a novel HESS control system and minimize the operating cost of the home microgrid as well as maximize the residential user comfort. Specifically, the mentioned objectives can be further separated into four sub-objectives as shown below:

1. To develop a control method to address SoC imbalance and DC bus deviations in a DC microgrid including distributed battery energy storages.
2. To develop and simplify a control approach to address inaccurate power sharing between batteries, dc bus deviations, SoC imbalance of batteries and insufficient energy use of SCs.
3. To develop a novel load forecasting method to improve the prediction accuracy.
4. To develop an advanced HEMS to minimize operation cost and to maximize the residential user comfort level.

1.4. Research contributions

The work presented in this PhD thesis is divided in the form of manuscripts, and each manuscript corresponds to a significant contribution. The contributions of the thesis are as follows.

1. A novel filter-based droop control with SoC balancing scheme for DC microgrids is proposed, which does not require any local communication systems among PCS.
2. A comprehensive multi-functional controller is proposed for HESS including batteries and SCs in DC microgrid.
3. A hybrid load forecasting method is proposed to improve the prediction accuracy for the individual residential user.
4. A multi-level HEMS is proposed to minimize operating cost and maximize user comfort in the DC home microgrid.

1.5. Thesis outline

This PhD thesis follows the Auckland University of Technology (AUT) institution's doctoral thesis Format Two, also referred to as the "Manuscript Format". Chapter 1 describes the thesis introduction. Chapter 2 presents a literature review of the current application of HEMS technology in the home microgrids. Chapter 3 states a fully decentralized control technique for battery energy storage in an autonomous DC microgrid. Next, a comprehensive multifunctional controller for HESS in a DC microgrid is presented in Chapter 4. Chapter 5 describes a hybrid forecasting model for predicting short-term consumption of household loads. Chapter 6 covers a novel multi-level HEMS for optimizing home power usage while meeting user comfort needs. Finally, Chapter 7 gives this thesis's conclusion and describes the future trend related to the application of the HEMS in home microgrid. The thesis structure, chapter titles and the titles of the manuscripts for Chapters 2 - 6 are shown in Fig. 1.

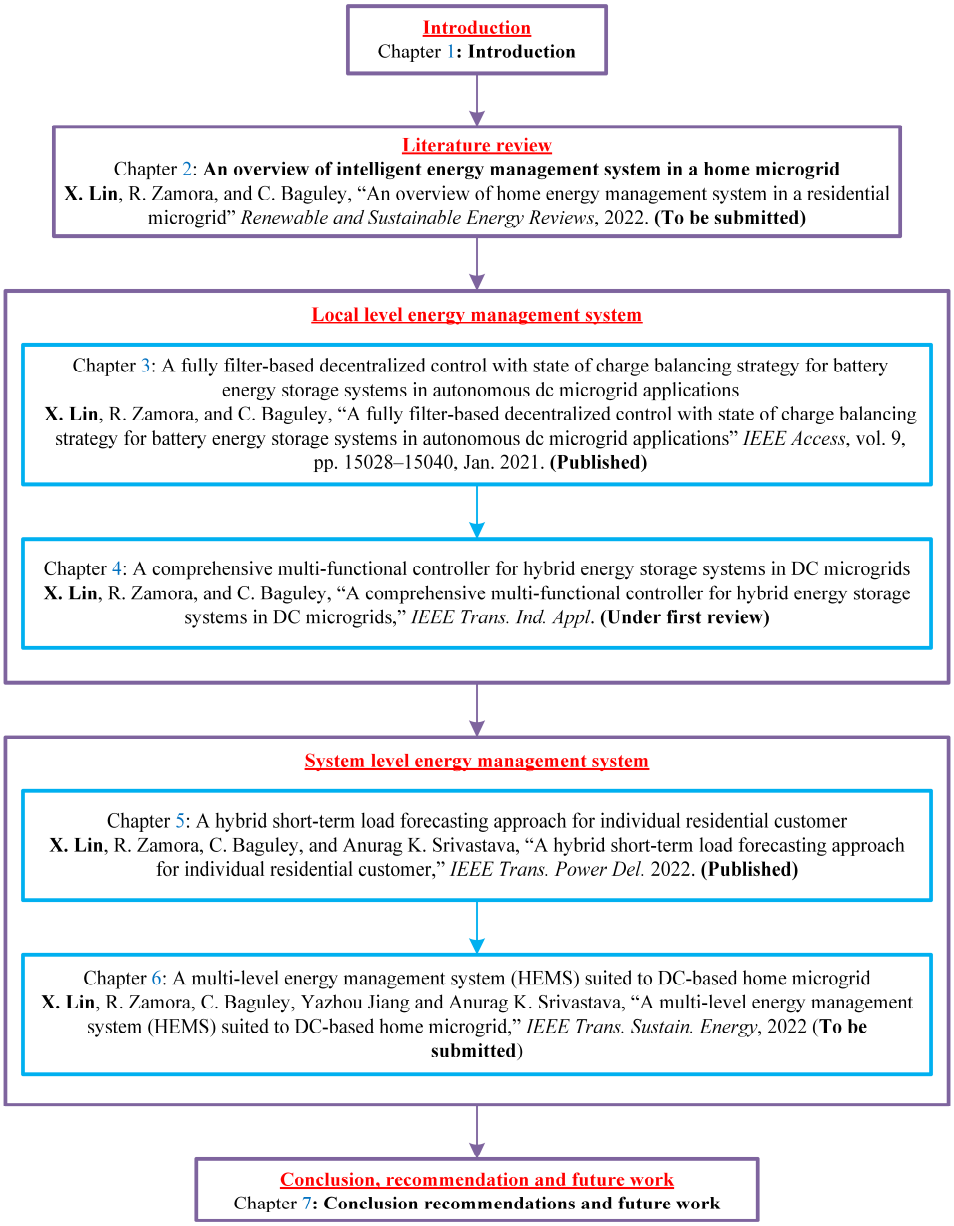

Fig.1. Thesis structure.

References

[1] IEA, "Electricity demand by sector and scenario 2018-2040," *IEA*, 2022. https://www.iea.org/data-and-statistics/charts/electricity-demand-by-sector-and-scenario-2018-2040

[2] EIA, "Electricity consumption in the United States was about 3.9 trillion kilowatthours (kWh) in 2021," *EIA*, 2022. https://www.eia.gov/energyexplained/electricity/use-of-electricity.php

[3] C. Dortans, M. W. Jack, B. Anderson, and J. Stephenson, "Lightening the load: quantifying the potential for energy-efficient lighting to reduce peaks in electricity demand," *Energy Effic.*, vol. 13, no. 6, pp. 1105–1118, 2020, doi: 10.1007/s12053-020-09870-8.

[4] H. T. Nguyen, D. T. Nguyen, and L. B. Le, "Energy management for households with solar assisted thermal load considering renewable energy and price uncertainty," *IEEE Trans. Smart Grid*, vol. 6, no. 1, pp. 301–314, 2015, doi: 10.1109/TSG.2014.2350831.

[5] L. Martirano *et al.*, "Aggregation of users in a residential/commercial building managed by a Building Energy Management System (BEMS)," *IEEE Trans. Ind. Appl.*, vol. 55, no. 1, pp. 26–34, 2019, doi: 10.1109/TIA.2018.2866155.

[6] V. Pilloni, A. Floris, A. Meloni, and L. Atzori, "Smart Home Energy Management Including Renewable Sources: A QoE-Driven Approach," *IEEE Trans. Smart Grid*, vol. 9, no. 3, pp. 2006–2018, 2018, doi: 10.1109/TSG.2016.2605182.

[7] F. Luo, G. Ranzi, S. Wang, and S. Member, "Hierarchical Energy Management System for Home Microgrids," *IEEE Trans. Smart Grid*, vol. 10, no. 5, pp. 5536–5546, 2019.

[8] A. Chub, D. Vinnikov, R. Kosenko, E. Liivik, and I. Galkin, "Bidirectional DC-DC Converter for Modular Residential Battery Energy Storage Systems," *IEEE Trans. Ind. Electron.*, vol. 67, no. 3, pp. 1944–1955, 2020, doi: 10.1109/TIE.2019.2902828.

[9] T. Li and M. Dong, "Residential Energy Storage Management With Bidirectional Energy Control," *IEEE Trans. Smart Grid*, vol. 10, no. 4, pp. 3596–3611, Jul. 2019, doi: 10.1109/TSG.2018.2832621.

[10] E. Rodriguez-Diaz, E. J. Palacios-Garcia, A. Anvari-Moghaddam, J. C. Vasquez, and J. M. Guerrero, "Real-time Energy Management System for a hybrid AC/DC residential microgrid," *2017 IEEE 2nd Int. Conf. Direct Curr. Microgrids, ICDCM 2017*, pp. 256–261, 2017, doi: 10.1109/ICDCM.2017.8001053.

[11] X. Qiu, T. A. Nguyen, and M. L. Crow, "Heterogeneous Energy Storage Optimization for Microgrids," *IEEE Trans. Smart Grid*, vol. 7, no. 3, pp. 1453–1461, 2016, doi: 10.1109/TSG.2015.2461134.

[12] D. B. W. Abeywardana, B. Hredzak, V. G. Agelidis, and G. D. Demetriades, "Supercapacitor sizing method for energy-controlled filter-based hybrid energy storage

systems," *IEEE Trans. Power Electron.*, vol. 32, no. 2, pp. 1626–1637, 2017, doi: 10.1109/TPEL.2016.2552198.

[13] A. Chub, D. Vinnikov, E. Liivik, and T. Jalakas, "Multiphase Quasi-Z-Source DC-DC Converters for Residential Distributed Generation Systems," *IEEE Trans. Ind. Electron.*, vol. 65, no. 10, pp. 8361–8371, 2018, doi: 10.1109/TIE.2018.2801860.

[14] U. Boeke, R. Weiß, A. Mauder, L. Hamimilton, and L. Ott, "Efficienncy advantages of ±380 V DC grids in comparison with 230 V/400 V AC grids," *NIAC Jt. Undertaking, White Pap.*, 2014.

[15] A. Nawaz, M. Zhou, J. Wu, and C. Long, "A comprehensive review on energy management, demand response, and coordination schemes utilization in multi-microgrids network," *Appl. Energy*, vol. 323, no. July, p. 119596, 2022, doi: 10.1016/j.apenergy.2022.119596.

[16] M. Shafie-Khah and P. Siano, "A stochastic home energy management system considering satisfaction cost and response fatigue," *IEEE Trans. Ind. Informatics*, vol. 14, no. 2, pp. 629–638, 2018, doi: 10.1109/TII.2017.2728803.

[17] J. C. Lopez, M. J. Rider, and Q. Wu, "Parsimonious Short-Term Load Forecasting for Optimal Operation Planning of Electrical Distribution Systems," *IEEE Trans. Power Syst.*, vol. 34, no. 2, pp. 1427–1437, 2019, doi: 10.1109/TPWRS.2018.2872388.

[18] A. Dejamkhooy, A. Dastfan, and A. Ahmadyfard, "Modeling and Forecasting Nonstationary Voltage Fluctuation Based on Grey System Theory," *IEEE Trans. Power Deliv.*, vol. 32, no. 3, pp. 1212–1219, 2017, doi: 10.1109/TPWRD.2014.2386696.

[19] J. Zhao and X. Liu, "A hybrid method of dynamic cooling and heating load forecasting for office buildings based on artificial intelligence and regression analysis," *Energy Build.*, vol. 174, pp. 293–308, 2018, doi: 10.1016/j.enbuild.2018.06.050.

[20] Y. Wang, Q. Chen, T. Hong, and C. Kang, "Review of Smart Meter Data Analytics: Applications, Methodologies, and Challenges," *IEEE Trans. Smart Grid*, vol. 10, no. 3, pp. 3125–3148, May 2019, doi: 10.1109/TSG.2018.2818167.

[21] C. Cecati, J. Kolbusz, P. Rózycki, P. Siano, and B. M. Wilamowski, "A Novel RBF Training Algorithm for Short-Term Electric Load Forecasting and Comparative Studies," *IEEE Trans. Ind. Electron.*, vol. 62, no. 10, pp. 6519–6529, 2015, doi: 10.1109/TIE.2015.2424399.

[22] A. O. Hoori, A. Al Kazzaz, R. Khimani, Y. Motai, and A. J. Aved, "Electric Load Forecasting Model Using a Multicolumn Deep Neural Networks," *IEEE Trans. Ind. Electron.*, vol. 67, no. 8, pp. 6473–6482, 2020, doi: 10.1109/TIE.2019.2939988.

[23] H. Y. Su, T. Y. Liu, and H. H. Hong, "Adaptive residual compensation ensemble models for improving solar energy generation forecasting," *IEEE Trans. Sustain. Energy*, vol. 11, no. 2, pp. 1103–1105, 2020, doi: 10.1109/TSTE.2019.2931154.

[24] M. Q. Raza, N. Mithulananthan, J. Li, and K. Y. Lee, "Multivariate Ensemble Forecast

Framework for Demand Prediction of Anomalous Days," *IEEE Trans. Sustain. Energy*, vol. 11, no. 1, pp. 27–36, Jan. 2020, doi: 10.1109/TSTE.2018.2883393.

[25] M. Zhou and M. Jin, "Holographic Ensemble Forecasting Method for Short-Term Power Load," *IEEE Trans. Smart Grid*, vol. 10, no. 1, pp. 425–434, 2019, doi: 10.1109/TSG.2017.2743015.

[26] D. H. Tran, D. L. Luong, and J. S. Chou, "Nature-inspired metaheuristic ensemble model for forecasting energy consumption in residential buildings," *Energy*, vol. 191, p. 116552, 2020, doi: 10.1016/j.energy.2019.116552.

[27] Y. Yu, S. You, H. Zhang, T. Ye, Y. Wang, and S. Wei, "A review on available energy saving strategies for heating, ventilation and air conditioning in underground metro stations," *Renew. Sustain. Energy Rev.*, vol. 141, no. October 2020, p. 110788, 2021, doi: 10.1016/j.rser.2021.110788.

[28] Y. Chen, G. Fu, and X. Liu, "Air-Conditioning Load Forecasting for Prosumer Based on Meta Ensemble Learning," *IEEE Access*, vol. 8, pp. 123673–123682, 2020, doi: 10.1109/ACCESS.2020.2994119.

[29] Y. Ding, H. Su, X. Kong, and Z. Zhang, "Ultra-short-term building cooling load prediction model based on feature set construction and ensemble machine learning," *IEEE Access*, vol. 8, pp. 178733–178745, 2020, doi: 10.1109/ACCESS.2020.3027061.

[30] A. Foucquier, S. Robert, F. Suard, L. Stéphan, and A. Jay, "State of the art in building modelling and energy performances prediction: A review," *Renew. Sustain. Energy Rev.*, vol. 23, pp. 272–288, 2013, doi: 10.1016/j.rser.2013.03.004.

[31] J. S. Chou, S. C. Hsu, N. T. Ngo, C. W. Lin, and C. C. Tsui, "Hybrid Machine Learning System to Forecast Electricity Consumption of Smart Grid-Based Air Conditioners," *IEEE Syst. J.*, vol. 13, no. 3, pp. 3120–3128, 2019, doi: 10.1109/JSYST.2018.2890524.

[32] F. Massa Gray and M. Schmidt, "A hybrid approach to thermal building modelling using a combination of Gaussian processes and grey-box models," *Energy Build.*, vol. 165, pp. 56–63, 2018, doi: 10.1016/j.enbuild.2018.01.039.

[33] B. Dong, Z. Li, S. M. M. Rahman, and R. Vega, "A hybrid model approach for forecasting future residential electricity consumption," *Energy Build.*, vol. 117, pp. 341–351, 2016, doi: 10.1016/j.enbuild.2015.09.033.

[34] K. Rahbar, J. Xu, and R. Zhang, "Real-time energy storage management for renewable integration in microgrid: An off-line optimization approach," *IEEE Trans. Smart Grid*, vol. 6, no. 1, pp. 124–134, 2015, doi: 10.1109/TSG.2014.2359004.

[35] M. S. Taha, H. H. Abdeltawab, and Y. A. R. I. Mohamed, "An online energy management system for a grid-connected hybrid energy source," *IEEE J. Emerg. Sel. Top. Power Electron.*, vol. 6, no. 4, pp. 2015–2030, 2018, doi: 10.1109/JESTPE.2018.2828803.

[36] J. M. Raya-Armenta, N. Bazmohammadi, J. G. Avina-Cervantes, D. Sáez, J. C. Vasquez, and J. M. Guerrero, "Energy management system optimization in islanded microgrids: An

overview and future trends," *Renew. Sustain. Energy Rev.*, vol. 149, no. June, p. 111327, 2021, doi: 10.1016/j.rser.2021.111327.

[37] J. Wu and X. Guan, "Coordinated multi-microgrids optimal control algorithm for smart distribution management system," *IEEE Trans. Smart Grid*, vol. 4, no. 4, pp. 2174–2181, 2013, doi: 10.1109/TSG.2013.2269481.

[38] Z. Wang, B. Chen, J. Wang, and J. Kim, "Decentralized Energy Management System for Networked Microgrids in Grid-Connected and Islanded Modes," *IEEE Trans. Smart Grid*, vol. 7, no. 2, pp. 1097–1105, 2016, doi: 10.1109/TSG.2015.2427371.

[39] K. Rahbar, C. C. Chai, and R. Zhang, "Energy cooperation optimization in microgrids with renewable energy integration," *IEEE Trans. Smart Grid*, vol. 9, no. 2, pp. 1482–1493, 2018, doi: 10.1109/TSG.2016.2600863.

[40] A. J. Litchy and M. H. Nehrir, "Real-time energy management of an islanded microgrid using multi-objective Particle Swarm Optimization," *IEEE Power Energy Soc. Gen. Meet.*, vol. 2014-Octob, no. October, pp. 1–5, 2014, doi: 10.1109/PESGM.2014.6938997.

[41] J. Yan, M. Menghwar, E. Asghar, M. Kumar Panjwani, and Y. Liu, "Real-time energy management for a smart-community microgrid with battery swapping and renewables," *Appl. Energy*, vol. 238, no. August 2018, pp. 180–194, 2019, doi: 10.1016/j.apenergy.2018.12.078.

[42] A. Sobu and G. Wu, "Dynamic optimal schedule management method for microgrid system considering forecast errors of renewable power generations," *2012 IEEE Int. Conf. Power Syst. Technol. POWERCON 2012*, 2012, doi: 10.1109/PowerCon.2012.6401287.

[43] J. D. Lara, D. E. Olivares, and C. A. Cañizares, "Robust energy management of isolated microgrids," *IEEE Syst. J.*, vol. 13, no. 1, pp. 680–691, 2019, doi: 10.1109/JSYST.2018.2828838.

[44] X. Wei *et al.*, "Two-Stage Cooperative Intelligent Home Energy Management System for Optimal Scheduling," *IEEE Trans. Ind. Appl.*, vol. 9994, no. c, pp. 1–1, 2022, doi: 10.1109/tia.2022.3172669.

[45] B. Jeddi, Y. Mishra, and G. Ledwich, "Differential Dynamic Programming Based Home Energy Management Scheduler," *IEEE Trans. Sustain. Energy*, vol. 11, no. 3, pp. 1427–1437, 2020, doi: 10.1109/TSTE.2019.2927237.

[46] A. Anvari-Moghaddam, H. Monsef, and A. Rahimi-Kian, "Optimal smart home energy management considering energy saving and a comfortable lifestyle," *IEEE Trans. Smart Grid*, vol. 6, no. 1, pp. 324–332, 2015, doi: 10.1109/TSG.2014.2349352.

[47] F. Luo, G. Ranzi, C. Wan, Z. Xu, and Z. Y. Dong, "A Multistage Home Energy Management System with Residential Photovoltaic Penetration," *IEEE Trans. Ind. Informatics*, vol. 15, no. 1, pp. 116–126, 2019, doi: 10.1109/TII.2018.2871159.

[48] A. Ahmad and J. Y. Khan, "Real-Time Load Scheduling, Energy Storage Control and Comfort Management for Grid-Connected Solar Integrated Smart Buildings," *Appl.*

Energy, vol. 259, no. August 2019, p. 114208, 2020, doi: 10.1016/j.apenergy.2019.114208.

[49] H. Ekhteraei Toosi, A. Merabet, and A. Swingler, "Impact of battery degradation on energy cost and carbon footprint of smart homes," *Electr. Power Syst. Res.*, vol. 209, no. December 2021, p. 107955, 2022, doi: 10.1016/j.epsr.2022.107955.

[50] Y. Zhang, R. Wang, T. Zhang, Y. Liu, and B. Guo, "Model predictive control-based operation management for a residential microgrid with considering forecast uncertainties and demand response strategies," *IET Gener. Transm. Distrib.*, vol. 10, no. 10, pp. 2367–2378, 2016, doi: 10.1049/iet-gtd.2015.1127.

[51] S. Pal and R. Kumar, "Electric Vehicle Scheduling Strategy in Residential Demand Response Programs With Neighbor Connection," *IEEE Trans. Ind. Informatics*, vol. 14, no. 3, pp. 980–988, 2018.

[52] D. Y. Yamashita, I. Vechiu, and J. P. Gaubert, "A review of hierarchical control for building microgrids," *Renew. Sustain. Energy Rev.*, vol. 118, no. October 2019, p. 109523, 2020, doi: 10.1016/j.rser.2019.109523.

[53] Q. Xu *et al.*, "A Decentralized Dynamic Power Sharing Strategy for Hybrid Energy Storage System in Autonomous DC Microgrid," *IEEE Trans. Ind. Electron.*, vol. 64, no. 7, pp. 5930–5941, 2017, doi: 10.1109/TIE.2016.2608880.

[54] O. Salari, K. Hashtrudi-Zaad, A. Bakhshai, M. Z. Youssef, and P. Jain, "A Systematic Approach for the Design of the Digital Low-Pass Filters for Energy Storage Systems in EV Applications," *IEEE J. Emerg. Sel. Top. Ind. Electron.*, vol. 1, no. 1, pp. 67–79, 2020, doi: 10.1109/jestie.2020.2999508.

[55] R. Zhang, B. Hredzak, and T. Morstyn, "Distributed Control with Virtual Capacitance for the Voltage Restorations, State of Charge Balancing and Load Allocations of Heterogeneous Energy Storages in a DC Datacenter Microgrid," *IEEE Trans. Energy Convers.*, vol. 34, no. 3, pp. 1296–1308, 2018, doi: 10.1109/TEC.2018.2889065.

Literature review

Chapter 2: An overview of intelligent energy management system in a home microgrid

Citation:

X. Lin, R. Zamora, and C. Baguley, "An overview of intelligent energy management system in a home microgrid," *Renewable and Sustainable Energy Reviews*, 2022. **(To be submitted)**

Preamble:

Chapter 2 presents the motivation and background of this study. It provides a comprehensive literature review of home energy management system (HEMS) for home microgrids. This chapter specifically discusses the concept and structure of the home microgrid, and at the same time points out the defects of the traditional home microgrid and introduces the concept and structure of the hybrid energy storage system (HESS). This chapter also divides HEMS into three main parts according to its functions, which consist of load forecasting, optimization and control. This chapter specifically categorizes load forecasting methods into physics-based, data-driven and hybrid methods, each of which is described and discussed in detail including advantages and disadvantages. Next, this chapter also reviews past and current optimization techniques for HEMS, which are divided into model predictive control (MPC), metaheuristic algorithms, mixed integer linear program (MILP), mixed integer non-linear program (MINLP) and other methods according to the optimization methods. Then, this chapter also provides a review of the control methods of HESS, which are classified into centralized, decentralized and distributed methods. After that, the chapter also specially provides a case study to verify the possibility and performance of considering HESS in HEMS.

Abstract:

A home microgrid is a small-scale power system with environmental affinity, and integration of production and consumption. The home energy management system (HEMS) plays an important role in the home microgrid, which can coordinate the output of various distributed energy resources (DERs) and the on/off of household appliances through the collected real-time information. As a result, the cost of electricity for households can be reduced and the demand for electricity from the main grid during peak periods can be moderated. For this reason, the HEMS has received extensive attentions from academia and industry. The purpose of this article is to provide an overview of HEMS. The concept and structure of the home microgrid are analyzed in detail. At the same time, the article also introduces the concept and structure of a hybrid energy storage system (HESS) composed of high energy density storage (HES) and high power density storage (HPS), which is used to replace the traditional single energy storage system to suppress the high frequency power fluctuation of the system. Then, the HEMS is mainly divided into load

forecasting, optimization and control according to its functions. Each subfunction is categorized in detail, while the relevant literature is also provided for discussion and analysis. Then, a case study is provided to verify the feasibility of considering HESS in HEMS. Based on the literature review and case analysis, an insight into the future trend of HEMS is presented, which covers household load forecasting, optimization techniques and control methods.

1. Introduction

Human activities such as industrialization and urbanization have led to a substantial increase in global energy demand, thereby increasing the consumption of fossil fuels and carbon emissions. According to the survey and statistics of the International Energy Agency (IEA), the global electricity energy demand grows at an annual rate of 2.1% [1]. By 2020, the global electricity consumption has reached 29 trillion kWh, of which approximately 24.2 % is contributed to the residential sector [2]. In this regard, many countries have also carried out investigations on domestic household electricity consumption. For instance, a report by the U.S. Energy Information Administration (EIA) shows that the United States has consumed 3.9 trillion kWh of electricity in 2021, of which the residential sector consumes about one-third of the total electricity [3]. Other countries such as China [4] and the Netherlands [5] have conducted similar surveys. These studies have shown that household electricity consumption has a high proportion in the total electricity use and continues to increase [6]. Therefore, there is a need to develop an advanced and intelligent power technology to reduce household electricity consumption, thereby reducing the power supply pressure on the main grid [7].

Renewable energy source (RES) such as solar and wind have received a lot of attention due to their non-polluting nature and environmental friendliness [8]. Many research projects have integrated RESs into the residential buildings to study changes in domestic energy consumption and costs [9–11]. However, the randomness and intermittent nature of the RES makes it challenging to continuously supply stable power to the households, thus reducing the stability of the system and failing to meet the electricity demand of the users [12]. An energy storage system (ESS) is proposed to solve this issue. When the power produced by RESs is higher than the demand side consumption, ESS will be operated in charging mode to absorb the surplus power. On the other hand, when the power generated by RESs is lower than load demand, the ESS will supply power to the load demand [13]. Therefore, the ESS can be regarded as an energy buffer to suppress the system power fluctuation and to ensure the stable operation of the system [14]. The integration of a small-scale power system including RES and ESS in residential buildings can be defined as home microgrid or residential microgrid [15,16].

The home microgrid provides an opportunity for end customers to actively participate in energy exchange mechanisms and change consumption patterns. Therefore, the home microgrid transforms the end customer from a traditional consumer role to a prosumer [17]. The operation

mode of the home microgrid is similar to the traditional microgrid, which can be divided into two types: grid-connected and islanded modes [18]. In the grid-connected mode, the home microgrid decides to purchase/sell electric power from/to the main grid and other home microgrids according to the power generation of the RESs, flexible load demand and real-time electricity prices. Furthermore, the home microgrid regulates the change of the bidirectional power flow with the goal of the lowest cost in this mode [19]. When the power quality of the main grid fails, the operation mode of the home microgrid switches to the islanded mode. The home microgrid formulates a load scheduling plan according to the power generation of the RESs, and conduct power transactions with other home microgrids to meet the electricity demand of users [20]. Home microgrid can realize the above automatic operation relying on an advanced intelligent system which can be called home energy management system (HEMS) [21].

Since the HEMS plays a significant role in home microgrids, it has received considerable attention from industry [22]. According to the market investigating report, the market share of the HEMS has reached 2.1 billion US dollars in 2021 and is expected to reach 6 billion US dollars in 2027 [23]. HEMS can make household load scheduling by collecting information such as electricity rates and weather conditions to minimize electricity tariff and simultaneously ensure end user comfort [24]. The operating procedure of the HEMS can be divided into data monitoring, forecasting, optimization and control, which can be described as below [25,26]:

- Data monitoring: benefiting from advanced information and communication technology, HEMS can monitor and collect household load usage data, energy cost, dynamic real-time electricity price and weather data through home area network and internet. These collected datasets will be passed to the prediction layer. In addition, end customers can access these datasets at any time through mobile phones and computers to understand the electricity cost of households.
- Forecasting: the HEMS will analyze the characteristics of the collected datasets, and then predict the necessary data of the system such as weather conditions, hourly electricity prices and load consumption at the next timescale. The timescale can be in minutes, hours and days.
- Optimization: the HEMS generates a power dispatch scheduling based on the predicted dataset with optimization objectives such as electricity cost and user comfort under technical constraints such as power limits and state of charge (SoC) limit.
- Control: the power dispatch plan includes control reference signals and switching signals for household appliances. Typically, a control reference signals are sent to the power converter system (PCS) to regulate the power variation of the distributed energy resource (DER). The switch signals directly manage the on/off of the household appliances.

Table 1
An overview of previous and recent review articles on HEMS research.

Ref.	Year	Contributions
[38]	2011	The article focusses on overview the HEMS based on nonintrusive load monitoring technology.
[27]	2013	The article discusses HEMS in smart houses including policy, user behavior, utility-side and customer-side enabling technologies.
[31]	2015	The article focuses on reviewing the infrastructure, communication protocols, system software, and end-user roles in HEMS.
[32]	2015	The article provides a comparative analysis of the literature on HEMS model including demand response, consumer well-being, uncertainty and multiple objectives.
[26]	2016	The article outlines the concept and structure of HEMS. The article also investigates the utilization of RES and different power scheduling strategies.
[39]	2017	The article reviews individual household load models considering demand response and demand-side management, as well as neighborhood coordination mechanisms and techniques.
[34]	2018	The article reviews HEMS model including demand response strategies, smart technologies, and load dispatch. The article also discusses the application of artificial intelligence in load scheduling.
[28]	2019	The article provides overview of the optimization techniques in HEMS.
[30]	2020	The article discusses different demand response strategies and load optimization algorithms in HEMS.
[40]	2020	The article reviews the application of reinforcement learning in HEMS.
[41]	2021	The article reviews demand-side flexible resource technologies including RES and ESS. In addition, the article provides an overview of coordination and negotiation techniques, which consist of multi-agent systems, optimization, and game theory.
[42]	2021	The article provides overview of the application of artificial intelligence in smart buildings, which mainly includes monitoring, making decision and optimization algorithm.
[43]	2021	The article presents a comprehensive review of demand side management including deployment, communication system and optimization technologies.
[33]	2022	The article outlines the framework structure of HEMS including RES, communication network system and monitoring equipment. The demand response and optimized power scheduling schemes are also studied.
[44]	2022	The article focuses on the detection and positioning methods of HEMS includes information and communication technologies. The article collected and discussed related research between 2010-2021, and also provided solutions for potential challenges.

A number of review works such as refs. [27–30] have investigated and summarized HEMS studies. Ref. [31] focuses on reviewing the infrastructure, communication protocols, system software, and end-user roles in HEMS. In addition, the article summarizes and discusses HEMS models published between 1970 and 2014. Ref. [32] presents a comparative analysis of the literature on HEMS, which is mainly about the method of the model and the impact of the model on HEMS. This optimization model incorporates demand response, consumer well-being, uncertainty and multiple objectives. Additionally, the article discusses computational constraints and timescales. In [26], the concept and structure of HEMS is outlined. The article also investigates the utilization of RES in residential buildings. In addition, different power scheduling strategies are also discussed. Ref. [33] outlines the framework structure of HEMS including RES, communication network system and monitoring equipment. The article studies and classifies different types of demand response strategies. Furthermore, optimized power scheduling schemes are investigated in this article. Ref. [34] reviews previous and current HEMS model including demand response strategies, smart technologies, and load dispatch. Then, the application of artificial intelligence such as neural networks and fuzzy logic systems in load scheduling is also discussed. Table 1 provides an overview of review articles on HEMS research.

Although the articles mentioned in Table 1 have reviewed different models and approaches for HEMS, their shortcomings can be summarized as follows:

- The home microgrid is the cornerstone of the operation of HEMS, and the above literature does not discuss the microgrid technology in depth. In addition, the intermittent nature of RES and uncertainty in end-customer behavior can cause high-frequency changes in household loads [35,36]. In this regard, the current ESSs of home microgrids are high energy density storage (HES), which cannot handle high-frequency load changes [37]. Therefore, it is proposed to integrate high power density storage (HPS) into home microgrids.
- The mentioned works in Table 1 focus on reviewing and investigating optimization algorithms, demand response strategies, infrastructure, monitoring, and communication technologies in HEMS. However, forecasting and control in HEMS are not specifically analyzed and discussed.

The shortcomings mentioned above are completely addressed in this review article. The main contributions of this article are summarized as follows:

- This article studies home microgrid technology. In this regard, this paper also discusses and analyzes the application of hybrid energy storage system (HESS) including HES and HPS in home microgrids. Finally, the article also provides a case study to verify the feasibility of HESS application in home microgrid.
- This article delves into load forecasting in HEMS, which is classified as data-based, physics-based, and hybrid methods.
- The article also studies different optimization algorithms in depth.
- The article discusses control methods in HEMS, which are divided into centralized, decentralized and distributed methods.

The rest of this article is organized as follows. Section 2 presents the concept and structure of the home microgrid. Section 3 reviews the different load forecasting methods in HEMS. Section 5 describes and classifies the optimization algorithm in HMES. The control approaches in HEMS are discussed in Section 6. Section 7 gives the future trends. The conclusion is described in Section 8.

2. Home microgrid studies

Home microgrids are the cornerstone of HEMS operations, which can benefit both the main grid and end customers, as summarized below:

- Benefits for the main grid: the home microgrid can serve as a dispatchable load or generation unit to provide power and auxiliary services to satisfy the demands of the upstream network [45]. In addition, the home microgrid can reduce the dependence on the main grid during power peak periods, thereby alleviating the supply pressure on the main grid. Compared with traditional power generation equipment, the home microgrid adopts DERs including RES and ESS as power sources, thereby reducing greenhouse gas emissions and increasing environmental affinity [46].
- Benefits for end customers: home microgrids can transform end users from traditional consumers to prosumers who can benefit from participating in energy market trading mechanisms [47]. Home microgrids can enable end users to understand the composition of energy consumption, thereby changing users' consumption behavior and achieving the purpose of saving energy. Then, the home microgrid can provide users with voltage and frequency support to ensure the quality of home electricity consumption. When the power quality of the utility fails, the home microgrid can still provide electricity to users continuously [48].

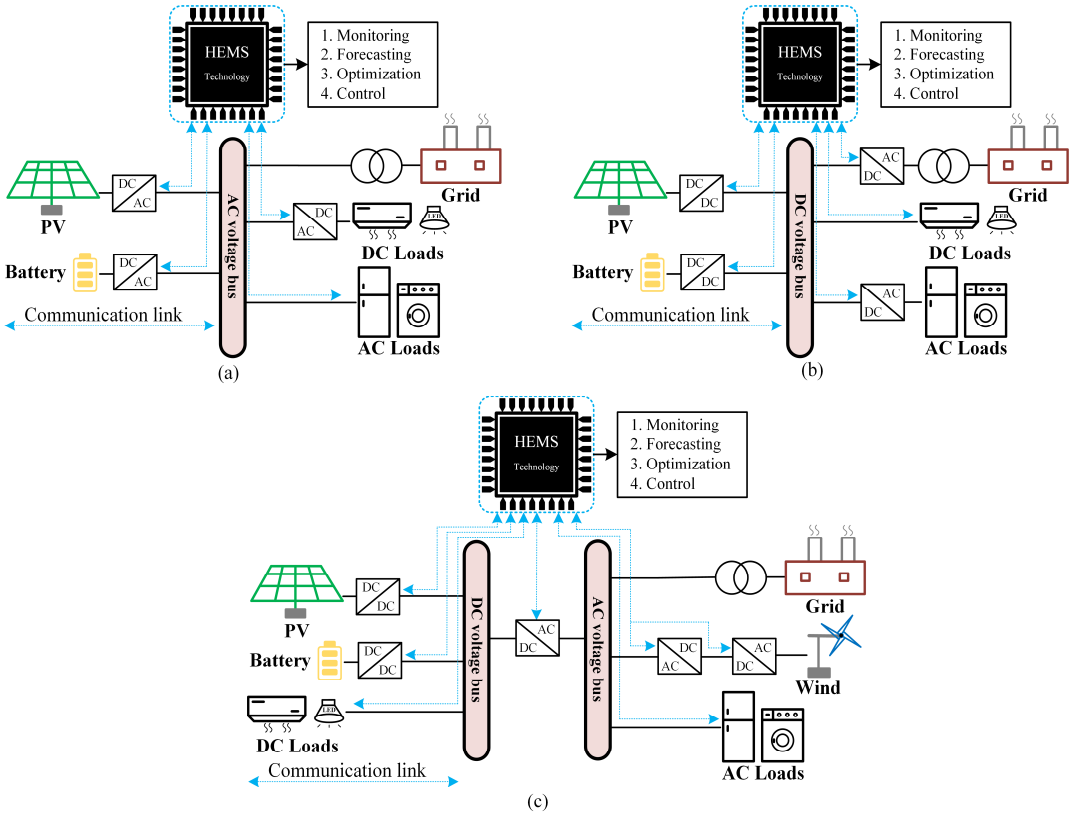

Fig. 1. The schematic diagram of different types home microgrids: (a) AC home microgrid, (b) DC home microgrid, (c) hybrid AC/DC home microgrid

Similar to traditional microgrids, house microgrids can be divided into three types: AC microgrids, DC microgrids, and hybrid AC/DC microgrids. The schematic diagram of the home microgrid is displayed in Fig. 1.

The structure of the AC home microgrid is shown in Fig. 1(a). DERs including PV and battery systems need to convert DC power to AC power through DC/AC inverters, which are then connected to the AC common bus. AC/DC power converters convert AC power to DC power to supply DC loads. The AC common bus can directly supply the power demand for AC loads without any power electronic converters. AC home microgrids can be directly integrated into the main grid as long as the phases are synchronized. Some research works such as [49–51] propose different HEMS models based on AC home microgrid. However, both PV and battery systems are DC power sources that require DC/AC inverters for power conversion to operate in AC microgrids. For this reason, there may be a power loss during the conversion process [52].

Due to the DC characteristics of RES and ESS and the popularity of DC loads in homes, DC microgrids have received extensive attention. Besides, some published works such as [53,54] demonstrated that the energy efficiency of DC-based microgrids is about 5% higher than that of conventional AC systems. Many research topics such as [55–58] apply DC-based microgrids in homes. The equivalent structure of this DC microgrid is depicted in Fig. 1(b). The PV and battery systems only need to be connected to the DC bus through a DC-DC converter without AC-DC conversion. The DC bus can directly provide the power demand for the DC load and is connected to the AC load through the inverter. The DC microgrid needs to be connected to the main grid through a DC-AC inverter as an energy interface.

The hybrid AC/DC microgrid contains two individual AC and DC microgrids. Several research works such as [59–62] have applied hybrid AC/DC microgrids to residential buildings. The equivalent structure of the hybrid AC/DC microgrid is shown in Fig. 1 (c). DC microgrid contain PV, ESS and DC loads, while AC microgrid consists of wind generation and AC loads. The main grid is connected to the hybrid microgrid through the AC bus. A bidirectional DC/AC power converter acts as an energy interface to connect DC and AC microgrids. The bidirectional DC/AC power converter can regulate the power flow between AC and DC microgrid, and stabilize the DC bus voltage, AC bus voltage and frequency [63,64].

Table 2
The characteristics of different ESSs.

ESS type	Power density (W/kg)	Energy density (Wh/kg)	Cost ($/kWh)	Response	Lifespan (year)
Lithium-ion	150-300	200-350	600-2500	3-5 ms	5-15
SC	200-23000	0.1-5	300-2400	<5 ms	10-30
Compressed air	0.5-2	3-6	2-50	3-10 min	20-40
Superconducting magnetic	500-2000	0.5-10	350	1-10 ms	15-20
Flywheel	1000	80-200	1000-10000	>10 ms	15-20
Lead-acid	75-300	30-50	200-400	3-5 ms	5-15

In home microgrid, RESs such as PV and wind are the main electrical energy sources. However, RES has the characteristics of uncertainty and interruption, and it cannot provide constant power

for the system, thereby reducing the stability of the system operation [65]. To solve this issue, the ESS is used to suppress power fluctuations and improve power quality, so that the high penetration of the RES can be realized [66]. Table 2 summarizes some ESS characteristics [66–68]. For instance, compared with other types of energy storage, a lithium-ion battery has a higher energy density. Hence, it can be considered as HES. Also, it has higher installation cost and lower lifespan. In contrast, a supercapacitor (SC) is a type of HPS that have a long service life.

The randomness of end-customer behavior can lead to high-frequency household load fluctuations. Meanwhile, most HEMS models in home microgrid only consider the HES as the ESS for the home microgrid [51,69,70]. For this reason, the HES is always frequently subjected to irregular deep charge and discharge, which reduces the service life of the HES and increases the maintenance and replacement cost of the HES [71]. Therefore, HESS consisting of HES and HPS is a promising solution to solve the mentioned problems [72]. Currently, very few research topics consider HESS in HEMS. For example, ref. [73] proposed a fuzzy logic control-based HEMS for residential DC microgrid including batteries and fuel cells. The proposed method can effectively improve the operating cost of the system. However, this method does not consider HPS. The battery may not be able to meet the high frequency power demands. Although ref. [74] and [75] consider HES and HPS in residential microgrid, these methods focus on power distribution between HES and HPS without considering economic benefits. Therefore, it is still a challenge to integrate HESS technology in HEMS in home microgrid.

Compared with a single ESS, HESS has a more complex topology, which can be divided into passive topology, semi-active topology and active topology [76]. The diagram of equivalent topology is plotted in Fig. 2. The passive topology is a low cost and simple structure. The HESS is directly connected to the DC bus without installing any DC-DC power converter, as shown in Fig. 2(a). In this configuration, the HESS needs to pre-set the desired voltage level to ensure the stability of the DC bus voltage. The power distribution between HES and HPS is mainly determined by the internal resistance and the characteristics of voltage and current [77]. Typically, HPS compensates for high frequency power fluctuations. The disadvantages of this structure are summarized as follows [78]:

- The controllability of HESS is poor.
- The voltage of the HESS must be consistent with the bus voltage.

In the semi-active topology, an energy storage device in the HESS is connected to the DC bus through a bidirectional DC-DC power converter. Then, a control method is developed to regulate the power converter to provide power to the system. Another energy storage device is directly connected to the bus [79]. Therefore, there are two types of semi-active topologies. One is that the HES is connected to the DC bus through a power converter, while the HPS is directly

connected to the DC bus, as shown in Fig. 2(b). The other is that the HPS is connected to the DC bus through a power converter, while the HES is directly connected to the DC bus, as shown in Fig. 2(c). The disadvantages of this structure are summarized as follows [80]:

- This configuration provides only partial energy storage controllability.
- One type of storage voltage in the HESS is still consistent with the bus voltage.

In the active topology, both the HES and the HPS in the HESS are merged into the DC bus through a DC-DC power converter, as shown in Fig. 2(d). A coordinated control method needs to be devised to regulate the HES and HPS for power sharing and bus voltage stability [81]. This active topology improves the controllability of the HESS. However, this structure still has the following drawbacks [82]:

- Investment and installation costs are high.
- The addition of power converters increases power losses.

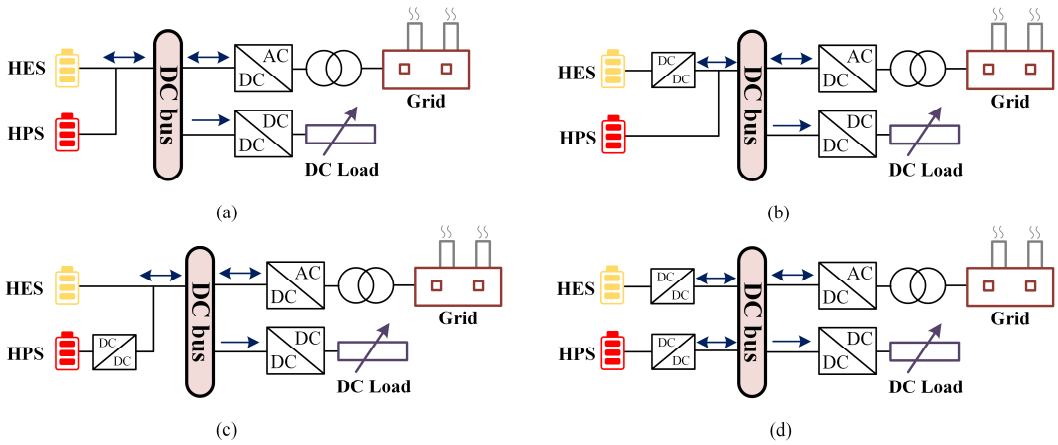

Fig. 2. The structure of the HESS: (a) Passive topology, (b) Semi-active topology (HES with converter), (c) Semi-active topology (HPS with converter), (d) Active topology.

3. Forecasting technology in HEMS

Home load forecasting plays an important role in HEMS. Through load prediction, HEMS can make power scheduling in real time, thereby improving economic efficiency. End customers can track and assess future energy consumption and manage household appliances to reduce electricity costs. Load forecasting can be divided into short-term, medium-term and long-term forecasts according to the time horizon [83,84]. The time range of the short-term forecast is usually between a few minutes and a week, which is used to formulate a short-term energy scheduling strategy. The time horizon for the medium-term forecast is between one week to one year. The time horizon of long-term forecasting is more than one year. Typically, mid- and long-term forecasts are used for mid- to long-term operating cost planning. There are three main types of forecasting methods: physical-based method, data-driven method, and hybrid method [85].

3.1. Physical-based method

A physics-based approach, which may also be referred to as a white-box approach or an engineering approach, is to model building components and to analyze energy consumption through thermodynamic theory [86]. This method needs to collect building and environmental information including climate, sky conditions, building physical information, etc. to evaluate the energy consumption of the building by a thermal dynamic model. In this regard, such models usually include heating models, air conditioning system models, ventilation models, etc. Besides, some building energy assessment software such as EnergyPlus, TRNSYS, SPARK, etc. integrate these models to improve the accuracy of energy assessment [87].

Many existing works such as [88–92] have studied the physics-based methods. The method in [88] evaluates the distribution of indoor temperature and airflow by creating building blocks in SPARK software. In [90], an energy management system for residential and commercial buildings is developed to improve the switching performance of heating, ventilation, and air-conditioning (HVAC) systems. The proposed method is implemented in EnergyPlus software. The results show that the proposed method can improve the energy use efficiency of the HVAC system by 19%. In [93], a thermal comfort control method based on a parallel temporal convolutional neural network (PTCN) and an improved chimpanzee optimization algorithm (ICHOA) was developed to track future indoor comfort and energy consumption. In the proposed method, PTCN is used to predict thermal comfort and energy consumption, while ICHOA is used to optimize the set objective function. Finally, TRNSYS platform is used to verify the feasibility of the proposed method. In [94], a systematic building model is developed to assess the building's interior and HVAC energy use. In addition, the method also takes into account the user's behavioral patterns and natural heat. The proposed method is validated on Dymola software.

The physics-based method does not require extensive historical load data for load tracking. However, the disadvantage of this method is that it needs more data to ensure the accuracy of load evaluation [95]. This information content includes building and user characteristic information. Building information is mainly composed of area, height, material, geographic location information, weather and meteorological conditions. User characteristic information covers behavior patterns and comfort sensitivity. The above mentioned information is difficult to obtain from public databases except weather data [96]. Therefore, the use of this method has certain limitations.

3.2. Data-driven method

Data-driven models can also be defined as black-box models that build associations between inputs and predicted targets through statistical models and machine learning [97]. In contrast to physics-based methods, data-driven models do not require the development of building physical

models and the collection of building data information. To this end, the data-driven model does not require any knowledge and experience of building physics. Usually, this method only needs to collect historical data and weather information of load consumption to track future load usage [98]. Data-driven models can be mainly divided into support vector machines (SVM), artificial neural networks (ANN) and ensemble models.

3.2.1. SVM models

SVM is a very popular and promising artificial intelligence algorithm, which was introduced by Vapnik in 1995 [99]. SVM is an efficient model for solving nonlinear problems; hence, it is widely used to solve classification and regression problems. It is worth noting that SVM used for regression problems can also be called support vector regression (SVR). The goal of SVM is to maximize the margins between different classes of data. The equivalent diagram of SVM is plotted in Fig. 3. The SVM introduces a kernel function such as Radial basis function (RBF), which can map the input space to the high dimensions space (Hilbert space) to realize the dataset division [100]. Ref. [101] proposes an online SVR method to predict short-term usage of occupancy loads. The cuckoo optimization algorithm is used to optimize hyperparameters for SVR. The dataset from the Irish Commission for Energy Regulation is used to validate the predictive performance of the proposed method.

In [102], a sequential grid approach based support vector regression (SGA-SVR) method is proposed to improve the accuracy and speed of short-term load forecasting. Then, a grid algorithm is employed to fit the parametric regression surface. The simulation results show that the prediction accuracy and computing speed of the proposed method are obviously better than the traditional SVR method. In [103], the performances of four intelligent algorithms for short-term prediction of household loads are compared and analyzed. The four methods consist of back propagation neural network (BPNN), RBF, general regression neural network (GRNN), and SVR. The results show that the prediction accuracy and stability of SVR are better than other methods. In [104], a novel SVR model is proposed to track short-term load consumption. The method uses the ambient temperature data of two hours before the occurrence of the demand response strategy as the input variable of the SVR. In addition, the method proposes selection criteria for ambient drying temperature, which is used to verify the optimal ambient temperature of two hours before demand response event. In [105], a sensor-based SVR model is proposed for predicting energy consumption in multi-building dwellings in New York City. The method also examines the impact of monitoring time (minutes, hours and days) and spatial (unit, floor and total building) scales on prediction accuracy. The results show that selecting time and spatial as hours and floors can effectively improve the prediction accuracy.

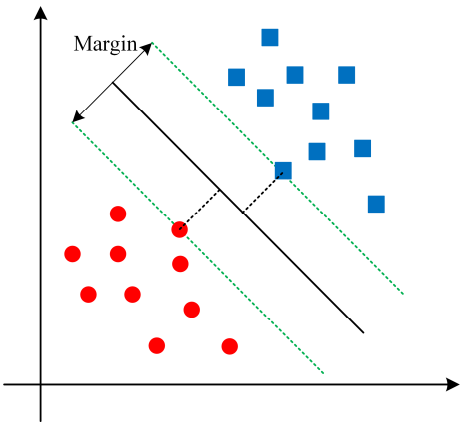

Fig. 3. The equivalent schematic of SVM model.

3.2.2. ANN models

ANN is an intelligent algorithm inspired by biological neural networks, which was introduced by McCulloch and Pitts in 1943 [106]. Typically, ANN is composed of input layer, hidden layer and output layer, as shown in Fig. 4. The input layer is mainly used to receive data information such as load data and weather data. In the hidden layer, ANN will repeatedly train the weights and biases in the activation function according to the characteristics of the data, so as to maximize the fit of the ANN model to the input data, thereby improving the accuracy of prediction. The output layer displays the results from the hidden layers. It should be noted that the number of hidden layers and neurons needs to be reasonably selected, which will affect the prediction accuracy and computational burden [107].

In [108], a deep recurrent neural network (RNN) is proposed for mid- to long-term residential and commercial load forecasting at an hour time resolution. Then, a sequential model-based optimization (SMBO) algorithm is used to optimize the hyperparameters of the RNN. In addition, the method is capable of repairing missing parts of load history data. Load data for a public safety building in Salt Lake City, Utah, and a residential building in Austin, Texas are used to validate the predictive performance of the proposed method. In [109], a radial basis function neural network (RBFNN) based forecasting model is proposed for predicting electrical load consumption in buildings. The method employs real historical building load data and different weather conditions as inputs to the prediction model to validate the performance of the proposed model. Ref. [110] proposes an improved Elman neural network (ENN) to track changes in household load power. The method also takes the user comfort index as an input to the prediction model. Furthermore, the softmax function is employed as the activation function for the hidden layers in the ENN. Different types of loads such as weekend and seasonal loads are used to verify the prediction accuracy of the method. Ref. [111] proposes a deep neural network with household appliance consumption sequence based on long short-term memory (LSTM) to solve the problem of low prediction accuracy caused by the random behavior of end users. This method is compared

with other prediction methods such as feedforward neural network (FNN) and k nearest neighbor (KNN) to verify its superiority. In [112], an advanced pool-based RNN is proposed to improve the prediction performance of household loads. The method also addresses the overfitting problem of the model by increasing the diversity and quantity of the data. The proposed method compares autoregressive integrated moving average (ARIMA), SVR, and typical RNN to verify its efficiency.

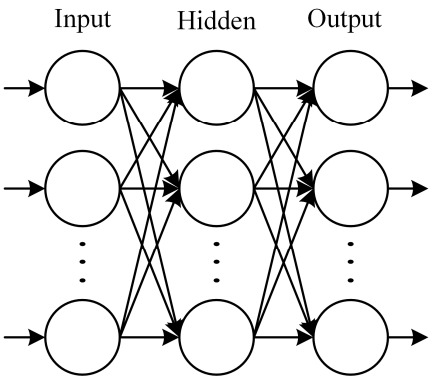

Fig. 4. The equivalent schematic of ANN model.

3.2.3. Ensemble models

Predictive models that contain only a single learning algorithm such as the models presented in [104,105,109] may lead to unexpected outliers in the forecasting results. Therefore, the ensemble model (EM) is proposed to address this problem [113]. The EM method can also be thought of as a predictive framework that incorporates multiple identical or different learning algorithms. Each learning algorithm then gets its own different forecasting outcomes [107]. These results will eventually be combined through the aggregation algorithms, such as trimmed algorithm and Bayesian algorithm [114]. The main purpose of EM is to remove outliers, thereby improving the accuracy of prediction methods. In [115], an EM method is proposed for tracking the energy consumption of building heating equipment. The EM contains three predictors: FNN, RBFNN and adaptive neuro-fuzzy interference system (ANFIS). The results of each predictor are finally combined by ordinary averaging and weighting methods. The results show that the accuracy of the EM method is significantly higher than that of a single predictor. Ref. [116] proposes an advanced EM method for predicting occupancy energy usage. In this method, an unscented Kalman filter (UKF) is used to denoise the time series of input variables. Next, an improved coupled generative adversarial stacking autoencoder (ICo-GASA) was developed to track changes in occupancy loads. The ICo-GASA is composed of three generative adversarial networks (GANs). Each GAN contains two deep belief networks (DBNs). Finally, the prediction results of ICo-GASA are merged by self-organizing map (SOM).

In [117], an evolutionary neural machine inference model (ENMIM) is propose to track future energy consumption of residential buildings. The model consists of two single supervised learning

machines - least squares support vector regression (LSSVR) and RBFNN. A symbiotic organisms search (SOS) is used to search for the optimal hyperparameters of the predictors. Load data of residential buildings in Ho Chi Minh City, Vietnam are used to verify the performance of the proposed method. In [118], an advanced EM method is proposed for predicting the energy consumption of photovoltaic-integrated smart buildings. The method is composed of five different prediction algorithms: ENN, ARIMA, FNN, RBF, backpropagation neural network (BPNN) and its wavelet transform (WT) model. Among them, WT is used to eliminate outliers in the load input data. Then, a particle swarm optimization (PSO) is used to optimize the FNN and RBF. Finally, the outputs of each predictor are integrated by the Bayesian model. Ref. [119] compares the performance of different prediction algorithms in evaluating the consumption of cooling and heating loads. These algorithms include SVR, ANN, classification and regression trees (CART), chi-square automatic interaction detector (CHAID), and general linear regression (GLR). Then, the algorithms with higher prediction performance are screened out to form the EM framework. The method aims to improve the prediction accuracy of cooling and heating loads.

3.3. Hybrid method

The previous two sub-sections have studied physics-based methods and data-driven methods. However, both methods have some limitations in residential building energy consumption prediction. The physics-based approach requires specialized construction-related knowledge and experience. In addition, this method also requires a large amount of accurate data information such as building area, height, material, etc., which is difficult to obtain from public websites [120]. The data-driven approach requires a large amount of historical load data of residential buildings under different conditions (e.g., different climatic and weather conditions). Predictive models then analyze and learn characteristics of this data to assess the future energy use of residential buildings. If there is insufficient data, prediction accuracy may decrease [95]. To address these issues, a hybrid method (also called grey box) consisting of physics-based and data-driven approach is proposed for predicting building energy usage. In this method, the physics-based method usually adopts the lumped capacitance model method, which is composed of resistance (R) and capacitance (C). The method aims to represent the thermal dynamic model inside the building in the form of an electrical circuit diagram. In this circuit, a resistance represents the thermal impedance which represents the strength of the object blocking the flow of heat, while a capacitance represents the heat capacity which represents the ability of the object to store thermal energy [121,122]. The values of R and C can be estimated based on the relationship between the input and output by employing algorithms such as Kalman filtering [123]. Typically, RC models can be used to evaluate indoor temperature changes and the use of cooling and heating loads. The data-driven approach in the hybrid model also uses artificial intelligence algorithms such as ANN and SVM. Unlike the method in sub-section 3.2, the data-driven method here will receive the

feature data generated by the RC model as input, thereby improving the prediction accuracy without requiring a large amount of historical data information [100].

Several works such as [124–127] have studied the hybrid methods. In [125], a reduced-order RC grey model is proposed for tracking changes in building thermal loads. The model also takes into account the uncertainty of the input variables. In [127], a hybrid model is proposed for predicting the energy consumption of buildings. In this model, an RC thermal dynamic model is developed taking into account the uncertainty of the building conditions. ARIMA is then used to search for unknown parameters of the thermal dynamic model. In [128], a hybrid model is proposed for short-term prediction of household load. This method develops an RC-based thermal dynamic model to evaluate indoor temperature changes and energy consumption of air conditioning (AC). Then, an LSSVM is used to track non-AC energy usage. Finally, the method is compared with other algorithms (ANN, SVR, LSSVM, Gaussian process regression (GPR) and Gaussian mixture model (GMM)) to verify its superiority. In [129], a hybrid model incorporates RC thermal dynamics and Gaussian process for tracking building energy consumption and indoor temperature. Compared with a single predictor, the accuracy of the proposed method is significantly improved. In [130], a hybrid forecasting method is proposed to improve the accuracy of short-term single-family load forecasting. This method separates household loads into heat and air conditioning (HAC), lights, and other loads. Then, an EM framework and 7R4C thermal dynamic model are developed to evaluate the HAC energy consumption. The EM framework consists of BPNN, SVM, and GRNN. A genetic algorithm (GA) is used to optimize the weights of BPNN and SVM to improve their performance. Next, a deep EM (DEM) framework is designed to predict changes in lights and other loads. The DEM contains three bidirectional long short-term memory networks (Bi-LSTM). Bayesian algorithm is used to search the hyperparameters of Bi-LSTM. Finally, a trimmed algorithm is used to integrate the results of EM and DEM. The method is compared with BPNN, RBF and ELM to show its superiority.

4. Optimization methods in HEMS

The future home load usage can be obtained through advanced load forecasting techniques, which have been described in previous sections. These forecasting data are then sent to the optimization layer in HEMS [25]. It is the responsibility of the optimization layer to use these prediction datasets to generate an optimal power scheduling plan by considering different objectives and the operating constraints [40]. The optimization objective covers electricity cost, operating cost, load scheduling, battery degradation, etc. [28,39]. The operational constraints include demand response, indoor temperature, power balance, physical constraints of batteries, power constraints of batteries and grid, etc. [43]. Currently, model predictive control (MPC), metaheuristic algorithms, mixed integer linear program (MILP), mixed integer non-linear program (MINLP) and other methods have been widely used in optimization layer.

4.1. MPC

The MPC is also commonly referred to as receding horizon control, which reduces prediction errors by updating control decisions online. The MPC needs to develop a mathematical model of the system and define a predictive horizon. Next, an objective function is defined to evaluate the performance of the model. Finally, the first control signal in the predictive horizon is used in the model, and the predictive horizon is moved by one time interval at the next time [131]. In [132], an MPC-based multi-time scales control structure is proposed for home energy management. The method takes into account the real-time electricity price and the electricity available in the energy market. Ref. [133] proposes a hierarchical HEMS that incorporates forecasting, day-ahead scheduling, and real-time operations. In the forecasting phase, an ANN is used to achieve day-ahead forecasting of household loads. Next, a home energy model based on peak-to-average ratio constraints is used in the day-ahead scheduling phase. Finally, MPC is employed to perform short-term energy optimization. In this process, a natural aggregation algorithm (NAA) is used to solve the objective function. The results show that the proposed method can reduce the cost of electricity and keep the users' comfort within an acceptable range.

In [134], a two-level energy management system is proposed to reduce the operating cost of a home microgrid. The method also takes into account the markdown cost of the battery and the self-depletion of the PV. In the upper layer, an MPC is used to calculate the home energy usage plan for the next 24 hours including energy storage configuration and appliance running time. The lower layer is a real-time controller, which is used to compensate the prediction error and the optimization error of the upper layer, thereby reducing the waste of household energy. Experimental results show that household energy costs can be reduced by 27.8% using the proposed method. Ref. [135] proposes a two-layer MPC enhanced by two data-driven modules for energy management of home microgrids. The home microgrid includes batteries and fuel cells. This data-driven module is used to improve the accuracy of battery and hydrogen storage models. The proposed method can determine the daily energy storage operation plan according to the annual operating cost of the microgrid, thereby reducing the degradation cost of energy storage and the operating cost of the microgrid. Simulation results show that this approach can reduce annual costs by 5%. Ref. [136] proposes a shrinking horizon MPC for managing household appliance usage, thereby reducing daily electricity costs. In addition, the method also takes into account user comfort and different electricity price scenarios.

4.2. Metaheuristic algorithms

A metaheuristic algorithm is a search algorithm that can solve complex optimization problems according to set constraints. The GA and PSO are currently the most popular meta-heuristic algorithms, and they have been widely used in HEMS optimization problems. In [70], a robust

index model is designed to improve the robustness level of home energy local network (HELN) to reduce the negative impact of user uncertainty on home energy usage. A robust optimization is used in load switching management, while a PSO is employed to optimize the load scheduling plan. Ref. [137] proposes a multi-timescale HEMS based on cooperative particle swarm optimization (CPSO), which considers electric vehicles, thermoelectric appliances and uncontrollable equipment. This approach is designed to reduce electricity costs and end-user discomfort with temperature. Ref. [138] proposes an intelligent residential energy management system (IREMS) for smart homes. The proposed IREMS aims to reduce residential electricity bills and constrain the electricity demand within the maximum demand based on the operation of household appliances and RESs. A GA is hired to choose the size of RES and energy storage so as to maximize the utilization of renewable energy.

Ref. [139] proposes an energy management system framework based on smart home area network (HAN) to reduce electricity cost and peak-to-average ratio (PAR). The home gateway (HG) receives real-time electricity price information from the demand response program and sends it to the energy management controller (EMC). Then, the EMC will generate the optimal load dispatch plan according to the demand response strategy and send it to the home smart appliances in the form of instructions. Additionally, the method incorporates real-time electricity prices and an inclined block rate (IBR) model. Finally, a GA is used to solve the objective function. In [140], a second-life battery energy storage system (SL-BESS) from electric vehicles is applied to the HEMS. Then, the article also establishes a variety of indicators of occupant satisfaction, which includes equipment use satisfaction, thermal comfort and acoustic comfort. The proposed HEMS will formulate an optimal load scheduling plan according to the electric energy cost, SL-BESS life cycle, user satisfaction and PAR. Finally, a reference point-based non-dominated sorting genetic algorithm (NSGA-III) is designed to solve the target problem.

4.3. MILP and MINLP

MILP/MINLP refers to the linear/nonlinear relationship between the optimization objective and variables. Besides, this objective function needs to obey linear/nonlinear constraints with integer variables. Ref. [141] designs an MILP-based HEMS. The proposed method can obtain the optimal load scheduling plan under different constraints and keep the indoor temperature within an acceptable range. Public data from the national renewable energy laboratory (NREL) is used to validate the performance of the method. In [142], an MILP-based two-horizon algorithm is developed for home energy management. The algorithm aims to formulate an optimal power scheduling strategy with high time resolution, thereby reducing electricity costs. At the same time, this method can also limit the calculation time to improve the calculation efficiency. Compared with the moving window algorithm, this method has obvious advantages. A two-stage scheduling optimization model based on flexible quantification in [143] is developed to achieve collaboration

between distribution system operators (DSOs) and households. Among them, the intelligent home energy management system (IHEMS) is designed to minimize electricity costs and ensure user satisfaction according to user electricity consumption patterns. Then, an MINLP-based DSO optimization model is developed to reduce network operating costs while considering the uncertainty of the distribution system caused by wind power. In [144], a double-layers building energy management system (BEMS) is designed for domestic dwellings aimed at optimizing energy scheduling and bidding. Energy scheduling and bidding strategies are formulated as MILP problems. The upper-level system determines the bid for the energy quantity by taking into account the operating costs. The underlying systems are used to ensure an optimal operating mix of building loads and distributed energy resources. Finally, the article uses real data of Sydney, Australia housing to verify the feasibility of the proposed method.

A multi-objective MINLP model in [145] is designed to optimize household energy consumption. The proposed method integrates objective functions under different constraints and user needs aimed at reducing household energy consumption, and electricity costs, while ensuring thermal comfort for end users. The real data is adopted to verify the performance of the proposed method in different scenarios. Ref. [146] proposes an MINLP-based home energy management framework aimed at reducing home energy usage costs and carbon emissions. Within this framework, a technology-independent model of battery degradation was developed to address wear and tear caused by irregular cycling of batteries in residential buildings. Simulation results show that the proposed method can reduce the cost, capacity loss and carbon emission of the system to 78%, 81% and 30%, respectively. Ref. [147] proposes an economical and efficient HEMS for household power dispatching strategy. The delay tasks of household appliances are divided into interruptible, non-interruptible, power non-adjustable and power adjustable tasks, and mathematical models of constraints are established. Then, an optimization model for end-user comfort is considered in the HEMS model, which represents the MINLP problem. Finally, the proposed HEMS is tested under different conditions.

4.4. Other methods

Other methods such as stochastic programming, dynamic programming and artificial intelligence algorithms are also used to solve optimization problems in HEMS. Ref. [36] proposes a framework for home energy management based on stochastic programming, and this framework also considers the electric vehicle availability and RESs' uncertainty. The model minimizes the cost of electricity used by end customers in different demand responses, while developing a response fatigue to assess customer satisfaction. Household load data from Italy are used to verify the feasibility of the proposed method. Ref. [148] proposes a framework for smart home energy management based on a hybrid robust stochastic optimization model aimed at ensuring the profitability of energy management for decision makers and the comfort of end users. The

optimization framework considers real-time energy markets and uses stochastic programming to model the uncertain characteristics of photovoltaic generation and energy prices. In [149], a stochastic dynamic programming framework is proposed for energy management in smart homes with plug-in electric vehicles (PEVs). This optimization framework aims to reduce electricity costs while meeting electricity demand and PEV charging requirements. The system operation mode is divided into vehicle-to-grid, vehicle-to-home and grid-to-vehicle. The performance of the proposed method is verified in different operating modes using real-time electricity prices.

Ref. [150] proposes a smart charging method for a home energy hub (HEH), which aims to improve the smart charging and discharging performance of electric vehicles. The optimal state of charge of batteries and electric vehicles in HEHs systems is determined by the Bellman-Ford-Moor algorithm (BFMA). The BFMA uses solar radiation, electricity price, and load history data to improve system yield based on user preferences. Ref. [151] develops an energy management system based on Lyapunov optimization technology for smart buildings integrating PV. The purpose of this method is to reduce the electricity price for the users by considering the real-time electricity price, battery degradation cost, thermal comfort and visual comfort of the users. Ref. [152] proposes a HEMS called forecast™, which aims to improve the operation mode of home appliances and satisfy the power demands of users under demand response program, thereby achieving cost reduction and energy efficiency improvement. The HEMS is established based on MPC with multiple objectives including energy cost, thermal comfort, user convenience and carbon emissions. Then, machine learning algorithms are employed to derive mathematical models and operating patterns of appliances, the purpose is to accurately predict energy usage and comfort needs. Ref. [153] proposes a data-driven approach to HEMS based on ANN and Q-learning algorithms, which is aimed to reduce the operating cost of the system. An ELM is used to predict future electricity prices and PV generation. The real datasets are used to verify the performance of the proposed HEMS.

In summary, the above subsections have studied different optimization methods in HEMS. However, these methods still have some drawbacks that are summarized as follows:

- The above optimization method only considers the battery energy storage system. Random behavior of users may cause high-frequency fluctuations in household load. The battery is a HES which may not be able to handle the high frequency power fluctuations, thereby reducing the life of the battery.
- Although some of the above optimization methods consider the thermal comfort of the user, most of them only ensure the thermal comfort range of the user rather than the optimal thermal comfort. In addition, thermal comfort cannot only consider the indoor temperature level, but also factors such as humidity, clothing insulation, etc.

5. Control methods in HEMS

Due to the intermittent and random nature of RES, it cannot provide continuous and stable power demand for end users. Therefore, the HESS is adopted to suppress the high and low power fluctuations of the system. In HEMS, the control layer will receive the control signal generated by the optimization layer. The control signal will directly regulate the charging and discharging operation mode of HESS, aiming at improving the power quality and ensuring the stable operation of the system. Compared with the traditional single ESS, the structure of HESS is more complicated. This also means that the controller design of HESS is more difficult. Therefore, this chapter provides an overview of current HESS control methods. The control methods of the HESS can be classified into three types: centralized, decentralized and distributed types.

5.1. Centralized methods

In the centralized type, a centralized controller will collect the status information of HES and HPS through the communication system. The controller then generates pulse width modulated (PWM) signals, which are sent to the power converters of the HES and HPS to regulate their charging and discharging, respectively. The structural principle of the centralized control method is shown in Fig. 5. There are many control methods used in centralized control types, such as filtration-based control (FBC), fuzzy logic control (FLC), MPC, ANN, and optimization-based control.

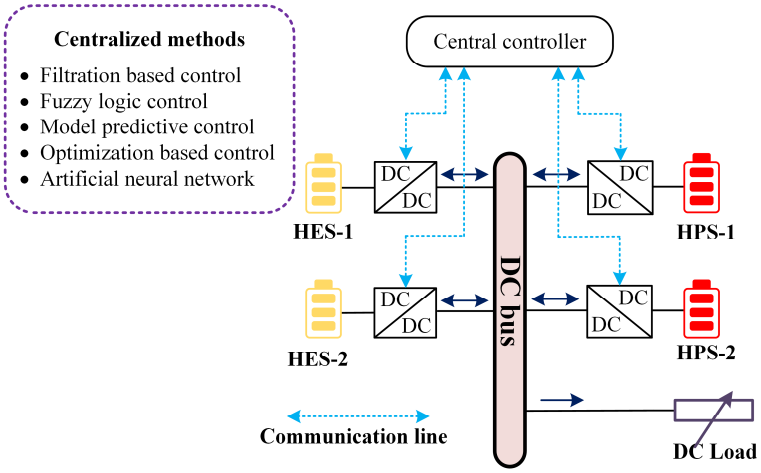

Fig. 5. The equivalent circuit diagram of the centralized control.

The FBC uses a low-pass filter (LPF) to decouple the total current of the system into low-frequency and high-frequency currents. These currents with different frequencies will be defined as current reference values, which will be respectively sent to the current controllers of the HES and HPS to adjust the corresponding power converters [154–157]. For instance, ref. [154] proposes a FBC strategy for HESS consisting of battery and SC, which aims to suppress sudden power changes of the system. In the proposed method, the battery is used to provide low-frequency power, while the SC suppresses high-frequency power fluctuations. The advantage of

this method is that the transient power of the system is transferred to the SC, thereby reducing the maximum peak value of the transient power of the battery and improving the service period of the battery. This paper verifies the feasibility of the method through experiments. In [156], an FBC-based supervisory control algorithm is proposed for battery-SC energy storage system in a small wind power generation. The purpose of this method is to solve the irregularity of battery charge and discharge caused by the uncertainty of wind power generation, thereby reducing the life of the battery and increasing the operating cost. The proposed method is able to transfer short-term charging/discharging cycles to SC to prolong the battery life cycle.

The FLC method is typically used to generate the reference current/power for HES and HPS controls [158–161]. In [158], an FLC-based energy storage management system is designed for battery-SC energy storage system in a medium-voltage DC shipboard power system. This method is designed to meet the peak current requirements while allowing the access of pulsed loads. The battery and SC in the system are connected to the DC bus through a bidirectional DC-DC converters with a dual active bridge configuration. It is proposed that the energy storage management system will generate reference power for the battery and SC according to the demand of the system load. The proposed method is modeled and verified in SimPowerSystems, and also compared with the proportional-integral based energy storage management system to show the superiority of the proposed method. Ref. [161] designs a multiple FLC approach for a HESS consisting of battery, SC, and fuel cell in a hybrid green power system. The purpose of this control method is to suppress the irregular power fluctuation caused by the uncertainty of RESs. This paper uses real data to simulate a hybrid green power system composed of wind power, PV generation and HESS. The results confirmed the importance of SC in this system, which can reduce the peak power of the system. In addition, the current fluctuation of the battery is also reduced.

The MPC is also a popular method widely used in HESS control [162–165]. Ref. [162] proposes an advanced MPC method for a battery-SC energy storage system. The MPC predicts PWM signals based on the SoC status, current and voltage constraints of the battery and SC, which are used to control the DC-DC converters. In addition, the method also adds the voltage of the SC to the objective function, the purpose of which is to minimize the voltage variation of the SC. Therefore, this method can ensure that the SC has enough power for future use. The proposed method distributes the fast current to the SC, while the battery only needs to supply the average current. Therefore, the life cycle of the battery can be extended. In [165], a novel MPC approach is proposed for voltage control and power sharing of battery-SC energy storage system in a DC microgrid. The MPC method will perform a one-step prediction based on the state information of the HESS and the preset constraints to obtain the PWM signals, which will be used to adjust the DC bus voltage and improve the anti-interference ability of the DC microgrid. In addition, the method is able to perform power allocation between the battery and SC according to the remaining

capacity of the HESS, thus ensuring that they are not overused. The proposed method is verified in MATLAB/Simulink for its feasibility.

The ANN is trained through the collected data to optimize the control parameters of the HESS [166–169]. Ref. [166] proposes an online-trained ANN-based control system for a hybrid AC/DC microgrid consisting of PV generation, wind power generation, fuel cell and battery energy storage. In this method, an adaptive ANN is used to track the maximum power of renewable energy sources while controlling the energy exchange between microgrids and utilities. Then, the FLC-based energy management system is designed to reduce the cost of electricity usage. The feasibility of this method was verified under different conditions. In [168], a novel power management strategy (PMS) based on hybrid bat search and artificial neural network (HBSANN) is proposed for controlling battery-SC energy storage system in a DC microgrid. The proposed PMS is capable of power distribution and DC bus voltage regulation within the constraints of the SoC. In this method, the high-frequency power fluctuations are compensated by the SC, and thus, the life cycle of the battery can be extended. In addition, the method also analyzes the harmonic distortion of the AC voltage. A hardware-in-the-loop (HIL) platform is built to verify the performance of the proposed method.

The optimization-based controls are also widely used in HESS to achieve power distribution, bus voltage regulation and reduce investment costs [170–173]. In [170], a multi-objective optimization based power sharing control strategy is proposed for HESS in a photovoltaic power generation system. The optimization objectives of this method cover the energy loss, the SoC of the SC and the charging/discharging frequency of the battery. Then, the paper also develops a linear weighted summation algorithm based on variable weights to address the multi-objective problem to generate the current reference values of battery and SC. The experimental simulation platform is established to verify the feasibility of the proposed method. In [172], the paper proposes a simulated annealing PSO algorithm for user battery-SC energy storage system in PV-wind power generation system. The purpose of the algorithm is to minimize the operating and investment costs of the system taking into account the system energy loss constraints, battery and SC current constraints. The proposed method can increase the diversity of particle swarms and avoid prematureness, thereby improving the global optimization ability of PSO.

The above literature has studied the application of different centralized control methods in HESS. These approaches mainly focus on achieving power distribution between batteries and SCs, bus voltage regulation, and reduction in operating costs. However, these methods all require a communication network to be successfully implemented. This means that communication delays and sudden failures can degrade the performance of these controllers.

5.2. Decentralized methods

In decentralized control, each power converter is only regulated by local control (LC), which only receives local data without requiring neighbor information and without considering the state of the overall system. Therefore, the decentralized control method does not require any communication system and enables plug-and-play functionality. The equivalent structure of the decentralized method is given in Fig. 6. Currently, the droop-based control strategy is the most popular decentralized control method [174–179]. The droop control method includes two current-voltage and power-voltage droop methods, which can generate a reference voltage for a dual-loop control system. For instance, ref. [174] develops an integral droop (ID) control based on the charge and discharge characteristics of capacitors, which will form a coordinated control system with traditional power-voltage droop control. Among them, ID is used to adjust the SC converter to provide instantaneous power, while the traditional droop control is used to regulate the battery converter to provide average power for the system. Then, a minimum relative impedance criterion is developed to assess the stability of the system. Finally, the experimental results verify the feasibility of coordinated control. In [176], a decentralized energy management framework is proposed for battery-SC energy storage system in a DC microgrid. In this framework, a virtual capacitance droop control with SoC recovery is used to regulate SC converters to suppress high-frequency power fluctuations. A conventional current-voltage droop control is adopted to control the battery converter to compensate low-frequency power fluctuations. During the operation of the system, the SoC of the SC can automatically restore to the pre-set value, so as to ensure that the SC can continue to work. The article also gives guidelines for the design of control methods to ensure that there are no potential conflicts between controllers.

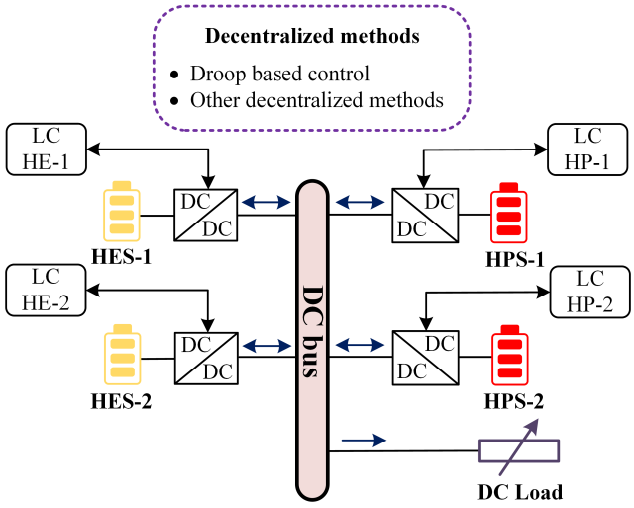

Fig. 6. The equivalent structure of the decentralized control.

In [177], a novel virtual resistor and capacitor droop (VRCD) control is designed to be applied in the HESS of shipboard medium voltage DC system. The HESS is composed of battery, SC and flywheel. The proposed control method is able to make the HESS respond to low-frequency, medium-frequency and high-frequency load fluctuations. In addition, the proposed method is also

able to restore the SoC level of SC to the set value. The design process of the controller is presented in detail. The proposed method verifies its performance in PSCAD/EMTDC. In [179], a coordinated control method and power management system is proposed for multiple battery-SC systems in a DC microgrid. The coordinated control is composed of v-dP and conventional droop control, which are used to manage the SC and battery converter, respectively. The advantage of the coordinated control is that power distribution and DC bus voltage regulation can be realized simultaneously without an additional voltage restoration system, thus simplifying the overall control system. In addition, the method also considers the SoC balance between batteries and the SoC recovery of SCs. The proposed power management system can effectively prevent the battery from overcharging and over discharging. A processor-in-the-loop (PIL) simulation platform is built to verify the performance of the proposed method.

There are still other decentralized methods applied to the HESS, such as [180–182]. In [180], a distributed control method based on frequency-coordinated virtual impedance is developed for a battery-SC energy storage system in a DC microgrid. In this control method, the virtual impedance is equivalent to an LPF and a high-pass filter (HPF), respectively, which can regulate the battery and SC to suppress low-frequency and high-frequency power fluctuations. In addition, the method also designs an SoC recovery system for the SC to ensure that the SC always has sufficient power. In [182], a droop control based on HPF and LPF is proposed for HESS in shipboard microgrid. Among them, the HPF-based droop controller is used to regulate the SC converter to suppress the high-frequency power fluctuation caused by the frequent start/stop of the shipboard. LPF based droop control is used to manage the power output of the battery converter. This method also ensures that the SoC of the SC is within a safe range.

Decentralized control methods have been reviewed in the literature above. Most of these approaches focus on power distribution, SoC restoration for SCs, and bus voltage regulation. A small number of articles consider the SoC balance between batteries. Since the decentralized approach has no communication system, it cannot obtain the data information of neighbors, therefore, the accuracy of power allocation and SoC balancing will be reduced.

5.3. Distributed methods

A distributed approach can be defined as a multi-agent system. The control system of each power converter can be defined as an agent, which will receive local information and collect data information from neighbor agents through a sparse communication network, so as to realize the coordinated control of the microgrid system. The equivalent structure of the distributed control is shown in Fig. 7. Many published works have studied the application of distributed control systems on HESS [183–188]. For instance, a coordinated droop control system with advanced voltage recovery control in [183] is developed for multiple HESSs in a DC microgrid. The virtual

resistance droop and virtual capacitance droop control methods are used to realize the power distribution between the battery and the SC. Since the droop control will lead to deviations in the bus voltage, a voltage recovery control system based on a consensus algorithm is developed to ensure that the DC bus voltage is within a safe range. Then, the SCs can always guarantee enough power for future use. The article also derives a small-signal model and analyze the stability of the system to ensure that the proposed voltage recovery control does not negatively affect the droop control. In [184], a distributed coordinated control strategy is proposed for multiple battery-SC energy storage systems. The method employs virtual impedance droop control, which can distribute the high-frequency and low-frequency components of the loads to the SCs and the batteries, respectively. Then, a consensus algorithm-based voltage restoration and SoC balance control method is developed to address bus voltage deviation and SoC imbalance between batteries. In addition, the SoC of the SC can automatically restore to the safety level. The performance of the proposed method is verified in RTDS Technologies real-time digital power system simulator under different conditions.

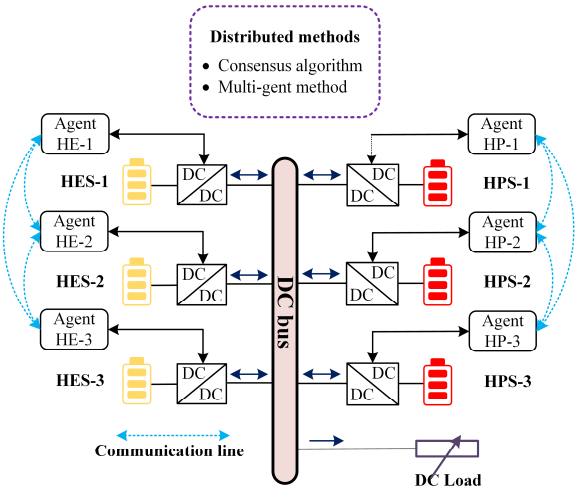

Fig. 7. The equivalent structure of the distributed control.

In [186], a consensus algorithm-based multifunctional control system is designed for multiple HESSs in a DC microgrid. The traditional droop control method and the ID control method are adopted to regulate the batteries and SCs to compensate the high and low frequency power fluctuations of the system. In addition, the proposed control method can automatically realize the regulation of DC bus voltage, SoC recovery of SCs and SoC balancing among batteries. The stability of the control system is also analyzed in the frequency domain. Finally, the performance of the proposed method is verified by the hardware platform. In [188], a distributed control system based on a leaderless consensus algorithm is proposed for battery-SC energy storage systems in an islanded DC microgrid. The control method implements power distribution between batteries and SCs, DC bus voltage regulation, SoC restoration of the SCs and SoC balancing between batteries through data information exchange between neighbors. The article studies the effect of

the design of the control parameters on the system. The feasibility and performance of the proposed method are validated through an experimental setup platform.

In summary, the above-mentioned distributed control method can realize multiple functions, which cover power distribution, voltage regulation, SoC recovery and balancing. However, this multifunctional control method will lead to the complexity of the overall control system. In addition, potential conflicts may arise between control methods. Finally, communication delays and failures can hinder data exchange between agents, reducing the performance of the control system.

6. Case study and discussion

The randomness of user behaviors and the uncertainties of RESs will cause high-frequency power fluctuations and power mismatch between hourly power scheduling and intra-hourly power consumption. To this end, the battery is forced to compensate the high-frequency power oscillations of the system, thereby reducing its service lifespan. Therefore, this article suggests that HPS such as SC should be incorporated into HEMS to suppress high-frequency power fluctuations. In this case, a HEMS based on multi-time MPC is presented in a home microgrid. This case is used to study the charging/discharging conditions of the battery and SC as well as the operating cost of the system under high-frequency power fluctuations.

In order to reduce the wear rate of the battery, a linear degradation model can be written as (1) and (2) [189].

$$\mathrm{LTT}_B^* = Q_B \times \mathrm{DoD}_B \times L_B \tag{1}$$

$$C_{B,\mathrm{per}}^* = \frac{B_{\mathrm{price}}}{\mathrm{LTT}_B \times \sqrt{\mu}} \tag{2}$$

where LTT_B^* is the lifetime throughput of battery (kWh). Q_B, DoD_B, and L_B are the battery capacity (kWh), battery DoD, and lifetime. B_{price} and μ are the replacement cost ($) and charging and discharging efficiency. Since the model in [189] cannot directly represent the relationship between battery degradation and power variation, the model needs to be modified appropriately.

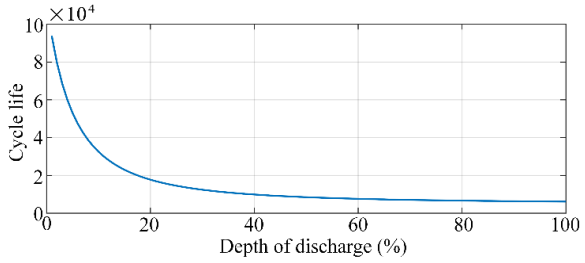

Fig. 8. Relationship between cycle life and DoD.

The relationship between life cycle and depth of discharge (DOD) is presented in Fig. 8. In this regard, the fitting function of the curve from Fig. 8 is written as (3) and (4) [190,191].

$$L_B(\mathrm{DoD}_B(\Delta t)) = a_B \times \mathrm{DoD}_B(\Delta t)^{-b_B} \times e^{c_B \times \mathrm{DoD}_B(\Delta t)} \tag{3}$$

$$\mathrm{DoD}_B(\Delta t) = \frac{P_B(t) \times \Delta t}{Q_B} \tag{4}$$

where a_B, b_B,- and c_B are the curve-fitting coefficients for equation (2). Δt is the time interval. $P_B(t)$ is the battery power at time t (kW). Then, combining (1)-(4), total battery degradation cost model can be expressed as (5).

$$C_B(t) = \frac{B_{\mathrm{price}} \times P_B(t) \times \Delta t}{Q_B \times \mathrm{DoD}_B(\Delta t) \times L_B(\mathrm{DoD}_B(\Delta t)) \times \sqrt{\mu}} \tag{5}$$

where C_B is the total battery degradation cost. Then, an SC degradation cost model can be written as (6).

$$C_{\mathrm{sc}}(t) = \frac{\mathrm{SC}_{\mathrm{price}}}{L_{\mathrm{sc}} \times 2 \times Q_{\mathrm{sc}}} \times P_{\mathrm{sc}}(t) \times \Delta t \tag{6}$$

where $\mathrm{SC}_{\mathrm{price}}$, Q_{sc} and L_{sc} are the SC price, SC capacity and total lifetime. $P_{\mathrm{sc}}(t)$ is SC power (kW). $\mathrm{SC}_{\mathrm{price}}/(L_{\mathrm{sc}} \times 2 \times Q_{\mathrm{sc}})$ refers to the degradation costper kWh. $P_{\mathrm{sc}}(t) \times \Delta t$ indicates the energy variation of SC during time interval Δt. The hourly cost of PV generation can be expressed as (7).

$$C_{\mathrm{pv}} = \frac{\mathrm{PV}_{\mathrm{price}}}{N_{\mathrm{year}} \times 365 \times 24} \tag{7}$$

where $\mathrm{PV}_{\mathrm{price}}$ and N_{year} are the PV price and number of guaranteed years of the PV. The utility electricity cost is written as (8).

$$C_g(t) = P_g(t) \times \eta_{\mathrm{pr}}(t) \times \Delta t \tag{8}$$

where $\eta_{\mathrm{pr}}(t)$ is the hourly electricity price at time t (\$), and $P_g(t)$ is the grid power at time t (kW).

The multi-time MPC framework used in this case study includes long-term optimization (LTO) and short-term optimization (STO). The LTO is used to reduce the operating cost and the STO is used to reduce the power mismatch. The specific content of the optimization process of multi-time MPC can be found in [135,192].

The power balance constraint can be written as (9).

$$P_L(t) = P_g(t) + P_{\text{pv}}(t) + P_B(t) + P_{\text{sc}}(t) \tag{9}$$

where $P_L(t)$ is the house load at time t (kW). $P_{\text{pv}}(t)$ is the PV power at time t (kW). The SoC models of the battery and SC can be expressed as (10) - (13).

$$\text{SoC}_B(t+1) = \text{SoC}_B(t) - \frac{\eta_B^c \times P_B(t) \times \Delta t}{Q_B}, P_B(t) \le 0 \tag{10}$$

$$\text{SoC}_B(t+1) = \text{SoC}_B(t) - \frac{P_B(t) \times \Delta t}{Q_B \times \eta_B^d}, P_B(t) > 0 \tag{11}$$

$$\text{SoC}_{\text{sc}}(t+1) = \text{SoC}_{\text{sc}}(t) - \frac{\eta_{\text{sc}}^c \times P_{\text{sc}}(t) \times \Delta t}{Q_{\text{sc}}}, P_{\text{sc}}(t) \le 0 \tag{12}$$

$$\text{SoC}_{\text{sc}}(t+1) = \text{SoC}_{\text{sc}}(t) - \frac{P_{\text{sc}}(t) \times \Delta t}{Q_{\text{sc}} \times \eta_{\text{sc}}^d}, P_{\text{sc}}(t) > 0 \tag{13}$$

where $\text{SoC}_B(t)$ and $\text{SoC}_{\text{sc}}(t)$ are the SoC of battery and SC. η_B^c, η_{sc}^c, η_B^d and η_{sc}^d are the charging and discharging coefficients for battery and SC. The SoC and power constraints of the battery and SC can be written as (14) - (18).

$$\text{SoC}_B^{\min} \le \text{SoC}_B(t) \le \text{SoC}_B^{\max} \tag{14}$$

$$\text{SoC}_{\text{sc}}^{\min} \le \text{SoC}_{\text{sc}}(t) \le \text{SoC}_{\text{sc}}^{\max} \tag{15}$$

$$P_B^{\min} \le P_B(t) \le P_B^{\max} \tag{16}$$

$$P_{\text{sc}}^{\min} \le P_{\text{sc}}(t) \le P_{\text{sc}}^{\max} \tag{17}$$

$$P_g^{\min} \le P_g(t) \le P_g^{\max} \tag{18}$$

where $\text{SoC}_B^{\min}$, $\text{SoC}_{\text{sc}}^{\min}$, $\text{SoC}_B^{\max}$ and $\text{SoC}_{\text{sc}}^{\max}$ are the minimum and maximum SoC of the battery and SC. $P_B^{\min}$, $P_{\text{sc}}^{\min}$, $P_g^{\min}$, $P_B^{\max}$, $P_{\text{sc}}^{\max}$ and $P_g^{\max}$ are the minimum and maximum power of the battery, SC and utility. The objective function of LTO is written as (19).

$$\min F_{\text{LTO}} = \sum_{t_{\text{LT}} \in \{1,\ldots,T_{\text{LT}}\}} (C_g(t_{\text{LT}}) + C_B(t_{\text{LT}}) + C_{\text{sc}}(t_{\text{LT}}) + C_{\text{pv}} \tag{19}$$

s.t. (5) – (18)

variables: $\{P_g(t_{\text{LT}}), P_B(t_{\text{LT}}), P_{\text{sc}}(t_{\text{LT}}), P_{\text{hac}}(t_{\text{LT}})\}_{t_{\text{LT}}=1}^{T_{\text{LT}}}$

where T_{LT} is the time horizon for LTO. t_{LT} is time in LTO. Then, the objective function of STO can be written as (20).

$$\min F_{\mathrm{STO}} = \sum_{t_{\mathrm{ST}} \in \{1,\ldots,T_{\mathrm{ST}}\}} C_{\mathrm{sc}}(t_{\mathrm{ST}}) + \left|P_B^{\mathrm{LT}}(t_{\mathrm{LT}}) - P_B^{\mathrm{ST}}(t_{\mathrm{ST}})\right| + \left|P_g^{\mathrm{LT}}(t_{\mathrm{LT}}) - P_g^{\mathrm{ST}}(t_{\mathrm{ST}})\right| \quad (20)$$

s.t. (5) – (18)

variables: $\{P_g(t_{\mathrm{ST}}), P_{\mathrm{sc}}(t_{\mathrm{ST}}), P_B(t_{\mathrm{ST}})\}_{t_{\mathrm{ST}}=1}^{T_{\mathrm{ST}}}$

The public datasets consisting of load and weather data for individual house are obtained from NREL database is used to validate the feasibility of the method [193]. The hourly electricity price data is collected from energy market company of Singapore [194]. The long-time and short-time scales are 1 h and 5 min, respectively. The errors (5%, 10%, and 20%) in the household load and PV data is randomly generated, which represent power mismatches. The results are given in Fig. 9 and Table 3.

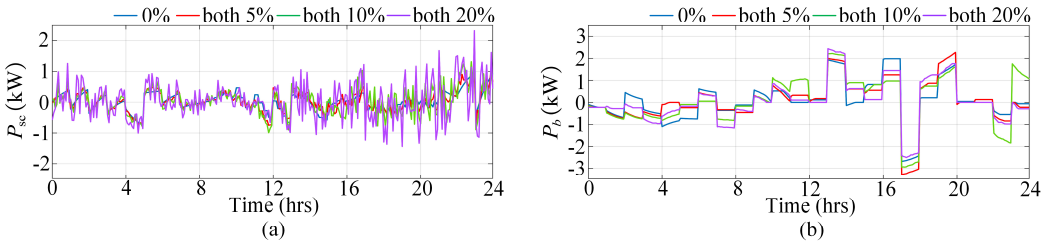

Fig. 9. Simulation results: (a) The output power of the SC, (b) the output power of the battery.

Table 3
The operating costs under different stochastic errors.

Errors	0 %	5 %	10 %	20 %
Operating cost ($)	12.1407	12.2046	12.0842	12.3540
Cost efficiency (%)	22.7790	22.3727	23.1380	21.4223

It can be seen from Fig. 9(a) that the HEMS automatically distributes the high-frequency component of the load to the SC energy storage. As the error increases, the SC will release/absorb power frequently to suppress system power fluctuations. In Fig. 9(b), the battery energy storage is responsible for providing low-frequency power demands, and its power output does not change frequently as the error increases. Therefore, the life cycle of the battery can be extended. It also can be observed from Table 3 that the operating cost and cost efficiency of the system are 12.1407 $ and 22.7790 % in the case of zero error. When the error of load and PV generation increase from 0% to 20%, the operating cost and cost efficiency of the system do not change considerably. Therefore, the integration of HEMS with HESS can ensure that the change of operating cost is within an acceptable range under the condition of error change.

7. The future trends of the HEMS

Currently, most HEMS approaches only consider a single type of HES such as a battery as an energy storage device for a home microgrid. Very few articles such as [74,75] consider HPS in home microgrids. However, these methods also only focus on power distribution and do not consider operating costs. The intermittent nature of RESs and the randomness of end-user behaviors results in the power mismatch between different time resolutions such as hourly and intra-hourly loads. Therefore, this article provides a suggestion on the integration of HPS systems such as SC in the home microgrids. To this end, this article presents a case for studying the charging/discharging of HESS and operating cost change of the system under power mismatch. It can be seen from the results that SC can effectively suppress high-frequency power fluctuations and prolong the service life of the battery. Besides, the operating costs of the system will not vary considerably. Therefore, HEMS integrating HES and HPS can be suggested as one of the research trends. Furthermore, the joint optimization of HES and HPS in HEMS considering different optimization objectives and constraints has not been deeply studied, which is still a challenge.

From the literature review, it can be concluded that most HEMSs are focused on reducing electricity and operating costs while maintaining user comfort. However, these HEMS are all aimed at reducing household electricity consumption, which may result in higher power generation at the utility than demand side electricity demand. Therefore, a mechanism for energy exchange between end users and distribution system operators should be developed to suppress this power mismatch problem. In addition, user comfort mentioned in most articles refers to thermal comfort, which is expressed by room temperature. According to ISO 7730:2005 standard, the thermal comfort model considers indoor temperature, humidity and clothing insulation [195]. Therefore, this article suggests that the thermal comfort model in ISO 7730:2005 should be integrated into HEMS to maximize the user's thermal comfort rather than setting a thermal comfort constraint. Then, the user comfort should not be limited to thermal comfort, visual comfort and air comfort should also be considered in HEMS.

Most published load forecasting methods are applied to large buildings and residential communities. A small amount of research work has focused on developing load forecasting methods for single households. However, the predictive accuracy of household load will be affected by load characteristics and user behavior randomness. To this end, this article suggests that household load characteristics, user behavior patterns and satisfaction should be considered in the design of household load prediction methods. The current control method of HESS can realize power sharing, voltage regulation, SoC balancing of battery and SoC recovery of SC simultaneously. However, the structure of this multifunctional controller is relatively complex, and the parameters of the controller need to be carefully designed to avoid conflicts between

control loops. Therefore, the simplification and versatility of the control method of HESS is still very challenge.

8. Conclusion

This article provides an overview of the literature on HEMS for home microgrids. The concept and structure of the home microgrid are discussed in detail. In this way, this article introduces HESS in the home microgrid to replace the traditional single energy storage system. The objective of the HESS is to suppress low- and high-frequency power fluctuations in home microgrid. Then, the structural characteristics of HESS are discussed in depth. This paper also provides an in-depth analysis of the functions of HEMS including load forecasting, optimization and control. Among them, the article classifies each function in detail, then analyzes and discusses the proposed method in depth. Then, the article provides a case to verify the feasibility of considering HESS in HEMS. Finally, this article gives insights into the future trends of HEMS including load forecasting, optimization methods and control techniques.

References

[1] IEA, "World energy outlook 2022," *IEA*, 2022. https://www.iea.org/reports/world-energy-outlook-2022/outlook-for-electricity

[2] IEA, "Electricity demand by sector and scenario 2018-2040," *IEA*, 2022. https://www.iea.org/data-and-statistics/charts/electricity-demand-by-sector-and-scenario-2018-2040

[3] EIA, "Electricity consumption in the United States was about 3.9 trillion kilowatthours (kWh) in 2021," *EIA*, 2022. https://www.eia.gov/energyexplained/electricity/use-of-electricity.php

[4] L. Li, Y. Yao, R. Yang, and K. Zhou, "Is it more effective to bring time-of-use pricing into increasing block tariffs ? Evidence from evaluation of residential electricity price policy in Anhui province," *J. Clean. Prod.*, vol. 181, pp. 703–716, 2018, doi: 10.1016/j.jclepro.2018.01.209.

[5] B. Mahapatra and A. Nayyar, "Home energy management system (HEMS): concept, architecture, infrastructure, challenges and energy management schemes," *Energy Syst.*, no. 0123456789, 2019, doi: 10.1007/s12667-019-00364-w.

[6] Z. Zhang, W. Cai, and X. Feng, "How do urban households in China respond to increasing block pricing in electricity? Evidence from a fuzzy regression discontinuity approach," *Energy Policy*, vol. 105, no. May 2016, pp. 161–172, 2017, doi: 10.1016/j.enpol.2017.02.025.

[7] H. Kim, H. Choi, H. Kang, J. An, S. Yeom, and T. Hong, "A systematic review of the smart energy conservation system: From smart homes to sustainable smart cities," *Renew.*

Sustain. Energy Rev., vol. 140, no. January, p. 110755, 2021, doi: 10.1016/j.rser.2021.110755.

[8] H. Hu, N. Xie, D. Fang, and X. Zhang, "The role of renewable energy consumption and commercial services trade in carbon dioxide reduction: Evidence from 25 developing countries," *Appl. Energy*, vol. 211, no. December 2017, pp. 1229–1244, 2018, doi: 10.1016/j.apenergy.2017.12.019.

[9] H. T. Nguyen, D. T. Nguyen, and L. B. Le, "Energy management for households with solar assisted thermal load considering renewable energy and price uncertainty," *IEEE Trans. Smart Grid*, vol. 6, no. 1, pp. 301–314, 2015, doi: 10.1109/TSG.2014.2350831.

[10] L. Martirano *et al.*, "Aggregation of users in a residential/commercial building managed by a Building Energy Management System (BEMS)," *IEEE Trans. Ind. Appl.*, vol. 55, no. 1, pp. 26–34, 2019, doi: 10.1109/TIA.2018.2866155.

[11] V. Pilloni, A. Floris, A. Meloni, and L. Atzori, "Smart Home Energy Management Including Renewable Sources: A QoE-Driven Approach," *IEEE Trans. Smart Grid*, vol. 9, no. 3, pp. 2006–2018, 2018, doi: 10.1109/TSG.2016.2605182.

[12] H. Masrur, H. O. R. Howlader, M. E. Lotfy, K. R. Khan, J. M. Guerrero, and T. Senjyu, "Analysis of techno-economic-environmental suitability of an isolated microgrid system located in a remote island of Bangladesh," *Sustain.*, vol. 12, no. 7, 2020, doi: 10.3390/su12072880.

[13] K. D. Hoang and H. H. Lee, "Accurate power sharing with balanced battery state of charge in distributed DC microgrid," *IEEE Trans. Ind. Electron.*, vol. 66, no. 3, pp. 1883–1893, 2019, doi: 10.1109/TIE.2018.2838107.

[14] K. A. Khan and M. Khalid, "Improving the Transient Response of Hybrid Energy Storage System for Voltage Stability in DC Microgrids Using an Autonomous Control Strategy," *IEEE Access*, vol. 9, pp. 10460–10472, 2021, doi: 10.1109/ACCESS.2021.3051144.

[15] F. Luo, G. Ranzi, S. Wang, and S. Member, "Hierarchical Energy Management System for Home Microgrids," *IEEE Trans. Smart Grid*, vol. 10, no. 5, pp. 5536–5546, 2019.

[16] A. Anvari-Moghaddam, J. M. Guerrero, J. C. Vasquez, H. Monsef, and A. Rahimi-Kian, "Efficient energy management for a grid-tied residential microgrid," *IET Gener. Transm. Distrib.*, vol. 11, no. 11, pp. 2752–2761, 2017, doi: 10.1049/iet-gtd.2016.1129.

[17] K. Vatanparvar and M. A. Al Faruque, "Design Space Exploration for the Profitability of a Rule-Based Aggregator Business Model Within a Residential Microgrid," *IEEE Trans. Smart Grid*, vol. 6, no. 3, pp. 1167–1175, 2015, doi: 10.1109/TSG.2014.2380318.

[18] A. Dagar, P. Gupta, and V. Niranjan, "Microgrid protection: A comprehensive review," *Renew. Sustain. Energy Rev.*, vol. 149, no. July, p. 111401, 2021, doi: 10.1016/j.rser.2021.111401.

[19] M. M. Gamil, T. Senjyu, H. Masrur, H. Takahashi, and M. E. Lotfy, "Controlled V2Gs and battery integration into residential microgrids: Economic and environmental impacts,"

Energy Convers. Manag., vol. 253, p. 115171, 2022, doi: 10.1016/j.enconman.2021.115171.

[20] M. Marzband, M. Javadi, S. A. Pourmousavi, and G. Lightbody, "An advanced retail electricity market for active distribution systems and home microgrid interoperability based on game theory," *Electr. Power Syst. Res.*, vol. 157, pp. 187–199, 2018, doi: 10.1016/j.epsr.2017.12.024.

[21] Y. Zhang, R. Wang, T. Zhang, Y. Liu, and B. Guo, "Model predictive control-based operation management for a residential microgrid with considering forecast uncertainties and demand response strategies," *IET Gener. Transm. Distrib.*, vol. 10, no. 10, pp. 2367–2378, 2016, doi: 10.1049/iet-gtd.2015.1127.

[22] M. S. Aliero, K. N. Qureshi, M. F. Pasha, and G. Jeon, "Smart Home Energy Management Systems in Internet of Things networks for green cities demands and services," *Environ. Technol. Innov.*, vol. 22, p. 101443, 2021, doi: 10.1016/j.eti.2021.101443.

[23] Imarc, "Home energy management systems market: global industry trends, share, size, growth, opportunity and forecast 2022-2027," *Imarc*, 2022. https://www.imarcgroup.com/home-energy-management-systems-market (accessed Nov. 02, 2022).

[24] J. Guerrero, D. Gebbran, S. Mhanna, A. C. Chapman, and G. Verbič, "Towards a transactive energy system for integration of distributed energy resources: Home energy management, distributed optimal power flow, and peer-to-peer energy trading," *Renew. Sustain. Energy Rev.*, vol. 132, no. June, 2020, doi: 10.1016/j.rser.2020.110000.

[25] M. F. Zia, E. Elbouchikhi, and M. Benbouzid, "Microgrids energy management systems: A critical review on methods, solutions, and prospects," *Appl. Energy*, vol. 222, no. April, pp. 1033–1055, 2018, doi: 10.1016/j.apenergy.2018.04.103.

[26] B. Zhou *et al.*, "Smart home energy management systems: Concept, configurations, and scheduling strategies," *Renew. Sustain. Energy Rev.*, vol. 61, pp. 30–40, 2016, doi: 10.1016/j.rser.2016.03.047.

[27] A. Zipperer *et al.*, "Electric energy management in the smart home: Perspectives on enabling technologies and consumer behavior," *Proc. IEEE*, vol. 101, no. 11, pp. 2397–2408, 2013, doi: 10.1109/JPROC.2013.2270172.

[28] N. Qayyum, A. Amin, U. Jamil, and A. Mahmood, "Optimization Techniques for Home Energy Management: A Review," *2019 2nd Int. Conf. Comput. Math. Eng. Technol.*, pp. 1–7, 2019.

[29] F. Etedadi Aliabadi, K. Agbossou, S. Kelouwani, N. Henao, and S. S. Hosseini, "Coordination of smart home energy management systems in neighborhood areas: A systematic review," *IEEE Access*, vol. 9, pp. 36417–36443, 2021, doi: 10.1109/ACCESS.2021.3061995.

[30] M. Shakeri *et al.*, "An Overview of the Building Energy Management System Considering

the Demand Response Programs, Smart Strategies and Smart Grid," *Energies*, vol. 13, no. 13, 2020, doi: 10.3390/en13133299.

[31] A. M. Vega, F. Santamaria, and E. Rivas, "Modeling for home electric energy management: A review," *Renew. Sustain. Energy Rev.*, vol. 52, pp. 948–959, 2015, doi: 10.1016/j.rser.2015.07.023.

[32] M. Beaudin and H. Zareipour, "Home energy management systems: A review of modelling and complexity," *Renew. Sustain. Energy Rev.*, vol. 45, pp. 318–335, 2015, doi: 10.1016/j.rser.2015.01.046.

[33] A. O. Ali, M. R. Elmarghany, M. M. Abdelsalam, M. N. Sabry, and A. M. Hamed, "Closed-loop home energy management system with renewable energy sources in a smart grid: A comprehensive review," *J. Energy Storage*, vol. 50, no. November 2021, p. 104609, 2022, doi: 10.1016/j.est.2022.104609.

[34] H. Shareef, M. S. Ahmed, A. Mohamed, and E. Al Hassan, "Review on Home Energy Management System Considering Demand Responses, Smart Technologies, and Intelligent Controllers," *IEEE Access*, vol. 6, pp. 24498–24509, 2018, doi: 10.1109/ACCESS.2018.2831917.

[35] W. Kong, Z. Y. Dong, Y. Jia, D. J. Hill, Y. Xu, and Y. Zhang, "Short-Term Residential Load Forecasting Based on LSTM Recurrent Neural Network," *IEEE Trans. Smart Grid*, vol. 10, no. 1, pp. 841–851, 2019, doi: 10.1109/TSG.2017.2753802.

[36] M. Shafie-Khah and P. Siano, "A stochastic home energy management system considering satisfaction cost and response fatigue," *IEEE Trans. Ind. Informatics*, vol. 14, no. 2, pp. 629–638, 2018, doi: 10.1109/TII.2017.2728803.

[37] X. Qiu, T. A. Nguyen, and M. L. Crow, "Heterogeneous Energy Storage Optimization for Microgrids," *IEEE Trans. Smart Grid*, vol. 7, no. 3, pp. 1453–1461, 2016, doi: 10.1109/TSG.2015.2461134.

[38] M. Zeifman and K. Roth, "Nonintrusive appliance load monitoring: Review and outlook," *IEEE Trans. Consum. Electron.*, vol. 57, no. 1, pp. 76–84, 2011, doi: 10.1109/TCE.2011.5735484.

[39] B. Celik, R. Roche, S. Suryanarayanan, D. Bouquain, and A. Miraoui, "Electric energy management in residential areas through coordination of multiple smart homes," *Renew. Sustain. Energy Rev.*, vol. 80, no. April 2016, pp. 260–275, 2017, doi: 10.1016/j.rser.2017.05.118.

[40] H. Zhang, D. Wu, and B. Boulet, "A review of recent advances on reinforcement learning for smart home energy management," *2020 IEEE Electr. Power Energy Conf. EPEC 2020*, vol. 3, 2020, doi: 10.1109/EPEC48502.2020.9320042.

[41] M. Hu, F. Xiao, and S. Wang, "Neighborhood-level coordination and negotiation techniques for managing demand-side flexibility in residential microgrids," *Renew. Sustain. Energy Rev.*, vol. 135, no. July 2020, p. 110248, 2021, doi:

10.1016/j.rser.2020.110248.

[42] J. Aguilar, A. Garces-Jimenez, M. D. R-Moreno, and R. García, “A systematic literature review on the use of artificial intelligence in energy self-management in smart buildings,” *Renew. Sustain. Energy Rev.*, vol. 151, no. May, p. 111530, 2021, doi: 10.1016/j.rser.2021.111530.

[43] S. Iqbal *et al.*, “A comprehensive review on residential demand side management strategies in smart grid environment,” *Sustain.*, vol. 13, no. 13, pp. 1–23, 2021, doi: 10.3390/su13137170.

[44] A. Natarajan, V. Krishnasamy, and M. Singh, “Occupancy detection and localization strategies for demand modulated appliance control in Internet ofThings enabled home energy management system,” *Renew. Sustain. Energy Rev.*, vol. 167, no. July, p. 112731, 2022, doi: 10.1016/j.rser.2022.112731.

[45] J. J. Justo, F. Mwasilu, J. Lee, and J. W. Jung, “AC-microgrids versus DC-microgrids with distributed energy resources: A review,” *Renew. Sustain. Energy Rev.*, vol. 24, pp. 387–405, 2013, doi: 10.1016/j.rser.2013.03.067.

[46] R. Zamora and A. K. Srivastava, “Controls for microgrids with storage: Review, challenges, and research needs,” *Renew. Sustain. Energy Rev.*, vol. 14, no. 7, pp. 2009–2018, 2010, doi: 10.1016/j.rser.2010.03.019.

[47] L. Bhamidi and S. Sivasubramani, “Optimal Sizing of Smart Home Renewable Energy Resources and Battery under Prosumer-Based Energy Management,” *IEEE Syst. J.*, vol. 15, no. 1, pp. 105–113, 2021, doi: 10.1109/JSYST.2020.2967351.

[48] Y. Han, K. Zhang, H. Li, and J. M. Guerrero, “MAS-Based Distributed Coordinated Control and Optimization in Microgrid and Microgrid Clusters: A Comprehensive Overview,” *IEEE Trans. Power Electron.*, vol. 33, no. 8, pp. 6488–6508, 2018, doi: 10.1109/TPEL.2017.2761438.

[49] F. Tooryan, H. HassanzadehFard, E. R. Collins, S. Jin, and B. Ramezani, “Optimization and energy management of distributed energy resources for a hybrid residential microgrid,” *J. Energy Storage*, vol. 30, no. April, p. 101556, 2020, doi: 10.1016/j.est.2020.101556.

[50] R. Singh, S. M. Amrr, and M. S. Jamil Asghar, “Supervisory control strategy for the effective solar energy utilization in a residential microgrid system using a cost-effective controller,” *Int. J. Electr. Power Energy Syst.*, vol. 132, no. April, p. 107170, 2021, doi: 10.1016/j.ijepes.2021.107170.

[51] J. Pascual, D. Arcos-Aviles, A. Ursúa, P. Sanchis, and L. Marroyo, “Energy management for an electro-thermal renewable–based residential microgrid with energy balance forecasting and demand side management,” *Appl. Energy*, vol. 295, p. 117062, 2021, doi: 10.1016/j.apenergy.2021.117062.

[52] A. Chakraborty, “Advancements in power electronics and drives in interface with growing

renewable energy resources," *Renew. Sustain. Energy Rev.*, vol. 15, no. 4, pp. 1816–1827, 2011, doi: 10.1016/j.rser.2010.12.005.

[53] U. Boeke, R. Weiß, A. Mauder, L. Hamimilton, and L. Ott, "Efficienncy advantages of ±380 V DC grids in comparison with 230 V/400 V AC grids," *NIAC Jt. Undertaking, White Pap.*, 2014.

[54] L. Ott, U. Böke, and R. Weiss, "Energy efficient dc-grids for commercial buildings," *ETG-Fachbericht*, vol. 2013-Novem, no. 139, 2013.

[55] M. Nasir, M. Anees, H. A. Khan, I. Khan, Y. Xu, and J. M. Guerrero, "Integration and Decentralized Control of Standalone Solar Home Systems for Off-Grid Community Applications," *IEEE Trans. Ind. Appl.*, vol. 55, no. 6, pp. 7240–7250, 2019, doi: 10.1109/TIA.2019.2911605.

[56] R. K. Chauhan, K. Chauhan, B. R. Subrahmanyam, A. G. Singh, and M. M. Garg, "Distributed and centralized autonomous DC microgrid for residential buildings: A case study," *J. Build. Eng.*, vol. 27, no. August 2019, p. 100978, 2020, doi: 10.1016/j.jobe.2019.100978.

[57] K. Palaniappan, S. Veerapeneni, R. Cuzner, and Y. Zhao, "Assessment of the feasibility of interconnected smart DC homes in a DC microgrid to reduce utility costs of low income households," *2017 IEEE 2nd Int. Conf. Direct Curr. Microgrids, ICDCM 2017*, pp. 467–473, 2017, doi: 10.1109/ICDCM.2017.8001087.

[58] A. Chub, D. Vinnikov, R. Kosenko, E. Liivik, and I. Galkin, "Bidirectional DC-DC Converter for Modular Residential Battery Energy Storage Systems," *IEEE Trans. Ind. Electron.*, vol. 67, no. 3, pp. 1944–1955, 2020, doi: 10.1109/TIE.2019.2902828.

[59] H. Çimen, N. Bazmohammadi, A. Lashab, Y. Terriche, J. C. Vasquez, and J. M. Guerrero, "An online energy management system for AC/DC residential microgrids supported by non-intrusive load monitoring," *Appl. Energy*, vol. 307, no. October 2021, p. 118136, 2022, doi: 10.1016/j.apenergy.2021.118136.

[60] E. Rodriguez-Diaz, E. J. Palacios-Garcia, A. Anvari-Moghaddam, J. C. Vasquez, and J. M. Guerrero, "Real-time Energy Management System for a hybrid AC/DC residential microgrid," *2017 IEEE 2nd Int. Conf. Direct Curr. Microgrids, ICDCM 2017*, pp. 256–261, 2017, doi: 10.1109/ICDCM.2017.8001053.

[61] A. Hamza, H. Bin Tahir, K. Siraj, and M. Nasir, "Hybrid AC/DC Microgrid for Residential Applications," in *2019 IEEE Third International Conference on DC Microgrids (ICDCM)*, May 2019, pp. 1–5. doi: 10.1109/ICDCM45535.2019.9232773.

[62] S. Paul and N. P. Padhy, "Resilient Scheduling Portfolio of Residential Devices and Plug-In Electric Vehicle by Minimizing Conditional Value at Risk," *IEEE Trans. Ind. Informatics*, vol. 15, no. 3, pp. 1566–1578, 2019, doi: 10.1109/TII.2018.2847742.

[63] M. Zolfaghari, G. B. Gharehpetian, M. Shafie-khah, and J. P. S. Catalão, "Comprehensive review on the strategies for controlling the interconnection of AC and DC microgrids,"

Int. J. Electr. Power Energy Syst., vol. 136, no. March 2021, p. 107742, 2022, doi: 10.1016/j.ijepes.2021.107742.

[64] E. Unamuno and J. A. Barrena, "Hybrid ac/dc microgrids—Part I: Review and classification of topologies," *Renew. Sustain. Energy Rev.*, vol. 52, pp. 1251–1259, Dec. 2015, doi: 10.1016/j.rser.2015.07.194.

[65] P. Bajpai and V. Dash, "Hybrid renewable energy systems for power generation in stand-alone applications: A review," *Renew. Sustain. Energy Rev.*, vol. 16, no. 5, pp. 2926–2939, 2012, doi: 10.1016/j.rser.2012.02.009.

[66] M. Aneke and M. Wang, "Energy storage technologies and real life applications – A state of the art review," *Appl. Energy*, vol. 179, pp. 350–377, 2016, doi: 10.1016/j.apenergy.2016.06.097.

[67] L. A. Wong, V. K. Ramachandaramurthy, P. Taylor, J. B. Ekanayake, S. L. Walker, and S. Padmanaban, "Review on the optimal placement, sizing and control of an energy storage system in the distribution network," *J. Energy Storage*, vol. 21, no. June 2018, pp. 489–504, 2019, doi: 10.1016/j.est.2018.12.015.

[68] X. Lin and R. Zamora, "Controls of hybrid energy storage systems in microgrids: Critical review, case study and future trends," *J. Energy Storage*, vol. 47, no. January, p. 103884, 2022, doi: 10.1016/j.est.2021.103884.

[69] M. Salgado, M. Negrete-Pincetic, Á. Lorca, and D. Olivares, "A low-complexity decision model for home energy management systems," *Appl. Energy*, vol. 294, no. April, p. 116985, 2021, doi: 10.1016/j.apenergy.2021.116985.

[70] X. Ran and S. Leng, "Enhanced Robust Index Model for Load Scheduling of a Home Energy Local Network with a Load Shifting Strategy," *IEEE Access*, vol. 7, pp. 19943–19953, 2019, doi: 10.1109/ACCESS.2018.2889762.

[71] S. Y. Kan, M. Verwaal, and H. Broekhuizen, "The use of battery-capacitor combinations in photovoltaic powered products," *J. Power Sources*, vol. 162, no. 2 SPEC. ISS., pp. 971–974, 2006, doi: 10.1016/j.jpowsour.2005.07.001.

[72] U. Manandhar *et al.*, "Energy management and control for grid connected hybrid energy storage system under different operating modes," *IEEE Trans. Smart Grid*, vol. 10, no. 2, pp. 1626–1636, 2019, doi: 10.1109/TSG.2017.2773643.

[73] F. J. Vivas, F. Segura, and J. M. Andújar, "Fuzzy logic-based energy management system for grid-connected residential DC microgrids with multi-stack fuel cell systems: A multi-objective approach," *Sustain. Energy, Grids Networks*, vol. 32, p. 100909, 2022, doi: 10.1016/j.segan.2022.100909.

[74] A. Latorre, C. A. Cortes, and W. Martinez, "EMS for bidirectional boost converters of a of a hybrid energy storage system for residential microgrid applications," *2018 20th Eur. Conf. Power Electron. Appl. EPE 2018 ECCE Eur.*, pp. 1–11, 2018.

[75] A. Traore, A. Taylor, M. A. Zohdy, and F. Z. Peng, "Modeling and simulation of a hybrid

energy storage system for residential grid-tied solar microgrid systems," *J. Power Energy Eng.*, vol. 05, no. 05, pp. 28–39, 2017, doi: 10.4236/jpee.2017.55003.

[76] L. Zhang *et al.*, "Hybrid electrochemical energy storage systems: An overview for smart grid and electrified vehicle applications," *Renew. Sustain. Energy Rev.*, vol. 139, no. November 2020, p. 110581, 2021, doi: 10.1016/j.rser.2020.110581.

[77] R. A. Dougal, S. Liu, and R. E. White, "Power and life extension of battery-ultracapacitor hybrids," *IEEE Trans. Components Packag. Technol.*, vol. 25, no. 1, pp. 120–131, 2002, doi: 10.1109/6144.991184.

[78] T. Ma, H. Yang, and L. Lu, "Development of hybrid battery-supercapacitor energy storage for remote area renewable energy systems," *Appl. Energy*, vol. 153, pp. 56–62, 2015, doi: 10.1016/j.apenergy.2014.12.008.

[79] Z. Song, H. Hofmann, J. Li, X. Han, X. Zhang, and M. Ouyang, "A comparison study of different semi-active hybrid energy storage system topologies for electric vehicles," *J. Power Sources*, vol. 274, pp. 400–411, 2015, doi: 10.1016/j.jpowsour.2014.10.061.

[80] W. Zhuang, J. Ye, Z. Song, G. Yin, and G. Li, "Comparison of semi-active hybrid battery system configurations for electric taxis application," *Appl. Energy*, vol. 259, no. November 2019, p. 114171, 2020, doi: 10.1016/j.apenergy.2019.114171.

[81] M. Momayyezan, D. B. W. Abeywardana, B. Hredzak, and V. G. Agelidis, "Integrated reconfigurable configuration for battery/ultracapacitor hybrid energy storage systems," *IEEE Trans. Energy Convers.*, vol. 31, no. 4, pp. 1583–1590, 2016, doi: 10.1109/TEC.2016.2589933.

[82] T. S. Babu, K. R. Vasudevan, V. K. Ramachandaramurthy, S. B. Sani, S. Chemud, and R. M. Lajim, "A Comprehensive Review of Hybrid Energy Storage Systems: Converter Topologies, Control Strategies and Future Prospects," *IEEE Access*, vol. 8, pp. 148702–148721, 2020, doi: 10.1109/ACCESS.2020.3015919.

[83] A. S. Ahmad *et al.*, "A review on applications of ANN and SVM for building electrical energy consumption forecasting," *Renew. Sustain. Energy Rev.*, vol. 33, pp. 102–109, 2014, doi: 10.1016/j.rser.2014.01.069.

[84] B. Yildiz, J. I. Bilbao, and A. B. Sproul, "A review and analysis of regression and machine learning models on commercial building electricity load forecasting," *Renew. Sustain. Energy Rev.*, vol. 73, no. February, pp. 1104–1122, 2017, doi: 10.1016/j.rser.2017.02.023.

[85] Y. Ding, H. Su, X. Kong, and Z. Zhang, "Ultra-short-term building cooling load prediction model based on feature set construction and ensemble machine learning," *IEEE Access*, vol. 8, pp. 178733–178745, 2020, doi: 10.1109/ACCESS.2020.3027061.

[86] G. Tardioli, R. Kerrigan, M. Oates, J. O. Donnell, and D. Finn, "Data driven approaches for prediction of building energy consumption at urban level," *Energy Procedia*, vol. 78, pp. 3378–3383, 2015, doi: 10.1016/j.egypro.2015.11.754.

[87] H. X. Zhao and F. Magoulès, "A review on the prediction of building energy

consumption," *Renew. Sustain. Energy Rev.*, vol. 16, no. 6, pp. 3586–3592, 2012, doi: 10.1016/j.rser.2012.02.049.

[88] M. Musy, F. Winkelmann, E. Wurtz, and A. Sergent, "Automatically generated zonal models for building air flow simulation: Principles and applications," *Build. Environ.*, vol. 37, no. 8–9, pp. 873–881, 2002, doi: 10.1016/S0360-1323(02)00050-1.

[89] Z. Zhai, M. H. Johnson, and M. Krarti, "Assessment of natural and hybrid ventilation models in whole-building energy simulations," *Energy Build.*, vol. 43, no. 9, pp. 2251–2261, 2011, doi: 10.1016/j.enbuild.2011.06.026.

[90] K. S. Cetin, M. H. Fathollahzadeh, N. Kunwar, H. Do, and P. C. Tabares-Velasco, "Development and validation of an HVAC on/off controller in EnergyPlus for energy simulation of residential and small commercial buildings," *Energy Build.*, vol. 183, pp. 467–483, 2019, doi: 10.1016/j.enbuild.2018.11.005.

[91] Z. Ma, J. Song, and J. Zhang, "Energy consumption prediction of air-conditioning systems in buildings by selecting similar days based on combined weights," *Energy Build.*, vol. 151, pp. 157–166, 2017, doi: 10.1016/j.enbuild.2017.06.053.

[92] Z. Liu, X. Zhou, W. Tian, X. Liu, and D. Yan, "Impacts of uncertainty in building envelope thermal transmittance on heating/cooling demand in the urban context," *Energy Build.*, vol. 273, p. 112363, 2022, doi: 10.1016/j.enbuild.2022.112363.

[93] H. Sun *et al.*, "Energy consumption optimization of building air conditioning system via combining the parallel temporal convolutional neural network and adaptive opposition-learning chimp algorithm," *Energy*, vol. 259, no. May, p. 125029, 2022, doi: 10.1016/j.energy.2022.125029.

[94] Y. Chen *et al.*, "Quantification of electricity flexibility in demand response: Office building case study," *Energy*, vol. 188, 2019, doi: 10.1016/j.energy.2019.116054.

[95] A. Foucquier, S. Robert, F. Suard, L. Stéphan, and A. Jay, "State of the art in building modelling and energy performances prediction: A review," *Renew. Sustain. Energy Rev.*, vol. 23, pp. 272–288, 2013, doi: 10.1016/j.rser.2013.03.004.

[96] X. Yang *et al.*, "Energy-saving potential prediction models for large-scale building: A state-of-the-art review," *Renew. Sustain. Energy Rev.*, vol. 156, no. June 2021, p. 111992, 2022, doi: 10.1016/j.rser.2021.111992.

[97] T. Ahmad, H. Chen, Y. Guo, and J. Wang, "A comprehensive overview on the data driven and large scale based approaches for forecasting of building energy demand: A review," *Energy Build.*, vol. 165, pp. 301–320, 2018, doi: 10.1016/j.enbuild.2018.01.017.

[98] Z. Wang and R. S. Srinivasan, "A review of artificial intelligence based building energy use prediction: Contrasting the capabilities of single and ensemble prediction models," *Renew. Sustain. Energy Rev.*, vol. 75, no. November 2016, pp. 796–808, 2017, doi: 10.1016/j.rser.2016.10.079.

[99] M. Bourdeau, X. qiang Zhai, E. Nefzaoui, X. Guo, and P. Chatellier, "Modeling and

forecasting building energy consumption: A review of data-driven techniques," *Sustain. Cities Soc.*, vol. 48, no. November 2018, p. 101533, 2019, doi: 10.1016/j.scs.2019.101533.

[100] A. A. A. Gassar and S. H. Cha, "Energy prediction techniques for large-scale buildings towards a sustainable built environment: A review," *Energy Build.*, vol. 224, p. 110238, 2020, doi: 10.1016/j.enbuild.2020.110238.

[101] P. Vrablecová, A. Bou Ezzeddine, V. Rozinajová, S. Šárik, and A. K. Sangaiah, "Smart grid load forecasting using online support vector regression," *Comput. Electr. Eng.*, vol. 65, no. 2018, pp. 102–117, 2018, doi: 10.1016/j.compeleceng.2017.07.006.

[102] Y. Yang, J. Che, C. Deng, and L. Li, "Sequential grid approach based support vector regression for short-term electric load forecasting," *Appl. Energy*, vol. 238, no. October 2018, pp. 1010–1021, 2019, doi: 10.1016/j.apenergy.2019.01.127.

[103] Z. Wang, R. S. Srinivasan, and J. Shi, "Artificial Intelligent Models for Improved Prediction of Residential Space Heating," *J. Energy Eng.*, vol. 142, no. 4, 2016, doi: 10.1061/(asce)ey.1943-7897.0000342.

[104] Y. Chen *et al.*, "Short-term electrical load forecasting using the Support Vector Regression (SVR) model to calculate the demand response baseline for office buildings," *Appl. Energy*, vol. 195, pp. 659–670, 2017, doi: 10.1016/j.apenergy.2017.03.034.

[105] R. K. Jain, K. M. Smith, P. J. Culligan, and J. E. Taylor, "Forecasting energy consumption of multi-family residential buildings using support vector regression: Investigating the impact of temporal and spatial monitoring granularity on performance accuracy," *Appl. Energy*, vol. 123, pp. 168–178, 2014, doi: 10.1016/j.apenergy.2014.02.057.

[106] W. S. McCulloch and W. Pitts, "A logical calculus of the ideas immanent in nervous activity," *Bull. Math. Biophys.*, vol. 5, no. 4, pp. 115–133, Dec. 1943, doi: 10.1007/BF02478259.

[107] Zeyu Wang and R. S. Srinivasan, "A review of artificial intelligence based building energy prediction with a focus on ensemble prediction models," in *2015 Winter Simulation Conference (WSC)*, Dec. 2015, vol. 75, pp. 3438–3448. doi: 10.1109/WSC.2015.7408504.

[108] A. Rahman, V. Srikumar, and A. D. Smith, "Predicting electricity consumption for commercial and residential buildings using deep recurrent neural networks," *Appl. Energy*, vol. 212, no. December 2017, pp. 372–385, 2018, doi: 10.1016/j.apenergy.2017.12.051.

[109] W. Mai, C. Y. Chung, T. Wu, and H. Huang, "Electric load forecasting for large office building based on radial basis function neural network," *IEEE Power Energy Soc. Gen. Meet.*, vol. 2014-Octob, no. October, pp. 1–5, 2014, doi: 10.1109/PESGM.2014.6939378.

[110] Y. Yu, X. Wang, and R. Bründlinger, "Improved Elman Neural Network Short-Term Residents Load Forecasting Considering Human Comfort Index," *J. Electr. Eng. Technol.*, vol. 14, no. 6, pp. 2315–2322, 2019, doi: 10.1007/s42835-019-00289-5.

[111] W. Kong, Z. Y. Dong, D. J. Hill, F. Luo, and Y. Xu, "Short-term residential load

forecasting based on resident behaviour learning," *IEEE Trans. Power Syst.*, vol. 33, no. 1, pp. 2017–2018, 2018, doi: 10.1109/TPWRS.2017.2688178.

[112] H. Shi, M. Xu, and R. Li, "Deep Learning for Household Load Forecasting-A Novel Pooling Deep RNN," *IEEE Trans. Smart Grid*, vol. 9, no. 5, pp. 5271–5280, 2018, doi: 10.1109/TSG.2017.2686012.

[113] H. Y. Su, T. Y. Liu, and H. H. Hong, "Adaptive residual compensation ensemble models for improving solar energy generation forecasting," *IEEE Trans. Sustain. Energy*, vol. 11, no. 2, pp. 1103–1105, 2020, doi: 10.1109/TSTE.2019.2931154.

[114] S. Hassan, A. Khosravi, and J. Jaafar, "Examining performance of aggregation algorithms for neural network-based electricity demand forecasting," *Int. J. Electr. Power Energy Syst.*, vol. 64, pp. 1098–1105, 2015, doi: 10.1016/j.ijepes.2014.08.025.

[115] R. Jovanović, A. A. Sretenović, and B. D. Živković, "Ensemble of various neural networks for prediction of heating energy consumption," *Energy Build.*, vol. 94, pp. 189–199, 2015, doi: 10.1016/j.enbuild.2015.02.052.

[116] G. Zhang and J. Guo, "A novel ensemble method for residential electricity demand forecasting based on a novel sample simulation strategy," *Energy*, vol. 207, p. 118265, 2020, doi: 10.1016/j.energy.2020.118265.

[117] D. H. Tran, D. L. Luong, and J. S. Chou, "Nature-inspired metaheuristic ensemble model for forecasting energy consumption in residential buildings," *Energy*, vol. 191, p. 116552, 2020, doi: 10.1016/j.energy.2019.116552.

[118] M. Q. Raza, M. Nadarajah, and C. Ekanayake, "Demand forecast of PV integrated bioclimatic buildings using ensemble framework," *Appl. Energy*, vol. 208, no. May 2017, pp. 1626–1638, 2017, doi: 10.1016/j.apenergy.2017.08.192.

[119] J. S. Chou and D. K. Bui, "Modeling heating and cooling loads by artificial intelligence for energy-efficient building design," *Energy Build.*, vol. 82, no. 2014, pp. 437–446, 2014, doi: 10.1016/j.enbuild.2014.07.036.

[120] Y. Chen, M. Guo, Z. Chen, Z. Chen, and Y. Ji, "Physical energy and data-driven models in building energy prediction: A review," *Energy Reports*, vol. 8, pp. 2656–2671, 2022, doi: 10.1016/j.egyr.2022.01.162.

[121] F. Belić, Ž. Hocenski, and D. Slišković, "Thermal modeling of buildings with RC method and parameter estimation," *Proc. 2016 Int. Conf. Smart Syst. Technol. SST 2016*, pp. 19–25, 2016, doi: 10.1109/SST.2016.7765626.

[122] D. Kim, J. Cai, K. B. Ariyur, and J. E. Braun, "System identification for building thermal systems under the presence of unmeasured disturbances in closed loop operation: Lumped disturbance modeling approach," *Build. Environ.*, vol. 107, pp. 169–180, 2016, doi: 10.1016/j.buildenv.2016.07.007.

[123] P. Bacher and H. Madsen, "Identifying suitable models for the heat dynamics of buildings," *Energy Build.*, vol. 43, no. 7, pp. 1511–1522, 2011, doi:

10.1016/j.enbuild.2011.02.005.

[124] R. Z. Homod, K. S. M. Sahari, H. A. F. Almurib, and F. H. Nagi, “Double cooling coil model for non-linear HVAC system using RLF method,” *Energy Build.*, vol. 43, no. 9, pp. 2043–2054, 2011, doi: 10.1016/j.enbuild.2011.03.023.

[125] M. H. Shamsi, U. Ali, E. Mangina, and J. O’Donnell, “A framework for uncertainty quantification in building heat demand simulations using reduced-order grey-box energy models,” *Appl. Energy*, vol. 275, no. June, p. 115141, 2020, doi: 10.1016/j.apenergy.2020.115141.

[126] A. Nutkiewicz, Z. Yang, and R. K. Jain, “Data-driven Urban Energy Simulation (DUE-S): A framework for integrating engineering simulation and machine learning methods in a multi-scale urban energy modeling workflow,” *Appl. Energy*, vol. 225, no. May, pp. 1176–1189, 2018, doi: 10.1016/j.apenergy.2018.05.023.

[127] X. Lü, T. Lu, C. J. Kibert, and M. Viljanen, “Modeling and forecasting energy consumption for heterogeneous buildings using a physical-statistical approach,” *Appl. Energy*, vol. 144, pp. 261–275, 2015, doi: 10.1016/j.apenergy.2014.12.019.

[128] B. Dong, Z. Li, S. M. M. Rahman, and R. Vega, “A hybrid model approach for forecasting future residential electricity consumption,” *Energy Build.*, vol. 117, pp. 341–351, 2016, doi: 10.1016/j.enbuild.2015.09.033.

[129] F. Massa Gray and M. Schmidt, “A hybrid approach to thermal building modelling using a combination of Gaussian processes and grey-box models,” *Energy Build.*, vol. 165, pp. 56–63, 2018, doi: 10.1016/j.enbuild.2018.01.039.

[130] X. Lin, R. Zamora, C. Baguley, and A. Srivastava, “A Hybrid Short-Term Load Forecasting Approach for Individual Residential Customer,” *IEEE Trans. Power Deliv.*, vol. 8977, no. c, 2022, doi: 10.1109/TPWRD.2022.3178822.

[131] B. Kouvaritakis and M. Cannon, *Model Predictive Control： Classical, Robust and Stochastic*. Cham: Springer Cham, 2016. doi: 10.1007/978-3-319-24853-0.

[132] A. Lefort, R. Bourdais, G. Ansanay-Alex, and H. Guéguen, “Hierarchical control method applied to energy management of a residential house,” *Energy Build.*, vol. 64, pp. 53–61, 2013, doi: 10.1016/j.enbuild.2013.04.010.

[133] F. Luo, G. Ranzi, C. Wan, Z. Xu, and Z. Y. Dong, “A Multistage Home Energy Management System with Residential Photovoltaic Penetration,” *IEEE Trans. Ind. Informatics*, vol. 15, no. 1, pp. 116–126, 2019, doi: 10.1109/TII.2018.2871159.

[134] M. Elkazaz, M. Sumner, E. Naghiyev, S. Pholboon, R. Davies, and D. Thomas, “A hierarchical two-stage energy management for a home microgrid using model predictive and real-time controllers,” *Appl. Energy*, vol. 269, no. February, p. 115118, 2020, doi: 10.1016/j.apenergy.2020.115118.

[135] D. Yassuda Yamashita, I. Vechiu, and J. P. Gaubert, “Two-level hierarchical model predictive control with an optimised cost function for energy management in building

microgrids," *Appl. Energy*, vol. 285, no. November 2020, p. 116420, 2021, doi: 10.1016/j.apenergy.2020.116420.

[136] A. Esmaeel Nezhad, A. Rahimnejad, P. H. J. Nardelli, S. A. Gadsden, S. Sahoo, and F. Ghanavati, "A Shrinking Horizon Model Predictive Controller for Daily Scheduling of Home Energy Management Systems," *IEEE Access*, vol. 10, pp. 29716–29730, 2022, doi: 10.1109/ACCESS.2022.3158346.

[137] Y. Liu, Y. Zhang, K. Chen, S. Z. Chen, and B. Tang, "Equivalence of Multi-Time Scale Optimization for Home Energy Management Considering User Discomfort Preference," *IEEE Trans. Smart Grid*, vol. 8, no. 4, pp. 1876–1887, 2017, doi: 10.1109/TSG.2015.2510222.

[138] S. L. Arun and M. P. Selvan, "Intelligent Residential Energy Management System for Dynamic Demand Response in Smart Buildings," *IEEE Syst. J.*, vol. 12, no. 2, pp. 1329–1340, Jun. 2018, doi: 10.1109/JSYST.2017.2647759.

[139] Z. Zhao, W. C. Lee, Y. Shin, and K. Bin Song, "An optimal power scheduling method for demand response in home energy management system," *IEEE Trans. Smart Grid*, vol. 4, no. 3, pp. 1391–1400, 2013, doi: 10.1109/TSG.2013.2251018.

[140] Y. Deng, Y. Zhang, F. Luo, and G. Ranzi, "Many-Objective HEMS Based on Multi-Scale Occupant Satisfaction Modelling and Second-Life BESS Utilization," *IEEE Trans. Sustain. Energy*, vol. 13, no. 2, pp. 934–947, 2022, doi: 10.1109/TSTE.2022.3140765.

[141] F. De Angelis, M. Boaro, D. Fuselli, S. Squartini, F. Piazza, and Q. Wei, "Optimal Home Energy Management Under Dynamic Electrical and Thermal Constraints," *IEEE Trans. Ind. Informatics*, vol. 9, no. 3, pp. 1518–1527, Aug. 2013, doi: 10.1109/TII.2012.2230637.

[142] M. Beaudin, H. Zareipour, A. Kiani Bejestani, and A. Schellenberg, "Residential Energy Management Using a Two-Horizon Algorithm," *IEEE Trans. Smart Grid*, vol. 5, no. 4, pp. 1712–1723, Jul. 2014, doi: 10.1109/TSG.2014.2310395.

[143] X. Wei *et al.*, "Two-Stage Cooperative Intelligent Home Energy Management System for Optimal Scheduling," *IEEE Trans. Ind. Appl.*, vol. 9994, no. c, pp. 1–1, 2022, doi: 10.1109/tia.2022.3172669.

[144] M. S. H. Nizami, M. J. Hossain, B. M. R. Amin, and E. Fernandez, "A residential energy management system with bi-level optimization-based bidding strategy for day-ahead bi-directional electricity trading," *Appl. Energy*, vol. 261, no. November 2019, p. 114322, 2020, doi: 10.1016/j.apenergy.2019.114322.

[145] A. Anvari-Moghaddam, H. Monsef, and A. Rahimi-Kian, "Optimal smart home energy management considering energy saving and a comfortable lifestyle," *IEEE Trans. Smart Grid*, vol. 6, no. 1, pp. 324–332, 2015, doi: 10.1109/TSG.2014.2349352.

[146] H. Ekhteraei Toosi, A. Merabet, and A. Swingler, "Impact of battery degradation on energy cost and carbon footprint of smart homes," *Electr. Power Syst. Res.*, vol. 209, no. December 2021, p. 107955, 2022, doi: 10.1016/j.epsr.2022.107955.

[147] G. Huang, J. Yang, and C. Wei, “Cost-effective and comfort-aware electricity scheduling for home energy management system,” *Proc. - 2016 IEEE Int. Conf. Big Data Cloud Comput. BDCloud 2016, Soc. Comput. Networking, Soc. 2016 Sustain. Comput. Commun. Sustain. 2016*, pp. 453–460, 2016, doi: 10.1109/BDCloud-SocialCom-SustainCom.2016.73.

[148] A. Akbari-Dibavar, S. Nojavan, B. Mohammadi-Ivatloo, and K. Zare, “Smart home energy management using hybrid robust-stochastic optimization,” *Comput. Ind. Eng.*, vol. 143, no. March, p. 106425, 2020, doi: 10.1016/j.cie.2020.106425.

[149] X. Wu, X. Hu, X. Yin, and S. J. Moura, “Stochastic Optimal Energy Management of Smart Home With PEV Energy Storage,” *IEEE Trans. Smart Grid*, vol. 9, no. 3, pp. 2065–2075, 2018, doi: 10.1109/TSG.2016.2606442.

[150] H. reza Gholinejad, J. Adabi, and M. Marzband, “Hierarchical Energy Management System for Home-Energy-Hubs Considering Plug-in Electric Vehicles,” *IEEE Trans. Ind. Appl.*, vol. 9994, no. c, pp. 1–10, 2022, doi: 10.1109/TIA.2022.3158352.

[151] A. Ahmad and J. Y. Khan, “Real-Time Load Scheduling, Energy Storage Control and Comfort Management for Grid-Connected Solar Integrated Smart Buildings,” *Appl. Energy*, vol. 259, no. August 2019, p. 114208, 2020, doi: 10.1016/j.apenergy.2019.114208.

[152] X. Jin, K. Baker, D. Christensen, and S. Isley, “Foresee: A user-centric home energy management system for energy efficiency and demand response,” *Appl. Energy*, vol. 205, no. August, pp. 1583–1595, 2017, doi: 10.1016/j.apenergy.2017.08.166.

[153] X. Xu, Y. Jia, Y. Xu, Z. Xu, S. Chai, and C. S. Lai, “A Multi-Agent Reinforcement Learning-Based Data-Driven Method for Home Energy Management,” *IEEE Trans. Smart Grid*, vol. 11, no. 4, pp. 3201–3211, 2020, doi: 10.1109/TSG.2020.2971427.

[154] S. K. Kollimalla, M. K. Mishra, and N. L. Narasamma, “Design and analysis of novel control strategy for battery and supercapacitor storage system,” *IEEE Trans. Sustain. Energy*, vol. 5, no. 4, pp. 1137–1144, 2014, doi: 10.1109/TSTE.2014.2336896.

[155] S. K. Kollimalla, M. K. Mishra, A. Ukil, and H. B. Gooi, “DC Grid Voltage Regulation Using New HESS Control Strategy,” *IEEE Trans. Sustain. Energy*, vol. 8, no. 2, pp. 772–781, 2017, doi: 10.1109/TSTE.2016.2619759.

[156] A. M. Gee, F. V. P. Robinson, and R. W. Dunn, “Analysis of battery lifetime extension in a small-scale wind-energy system using supercapacitors,” *IEEE Trans. Energy Convers.*, vol. 28, no. 1, pp. 24–33, 2013, doi: 10.1109/TEC.2012.2228195.

[157] N. R. Tummuru, M. K. Mishra, and S. Srinivas, “Dynamic Energy Management of Renewable Grid Integrated Hybrid Energy Storage System,” *IEEE Trans. Ind. Electron.*, vol. 62, no. 12, pp. 7728–7737, 2015, doi: 10.1109/TIE.2015.2455063.

[158] M. M. S. Khan, O. Faruque, and A. Newaz, “Fuzzy Logic Based Energy Storage Management System for MVDC Power System of All Electric Ship,” *IEEE Trans. Energy*

Convers., vol. 32, no. 2, pp. 798–809, 2017.

[159] A. Mohamed, V. Salehi, and O. Mohammed, "Real-time energy management algorithm for mitigation of pulse loads in hybrid microgrids," *IEEE Trans. Smart Grid*, vol. 3, no. 4, pp. 1911–1922, 2012, doi: 10.1109/TSG.2012.2200702.

[160] H. Shayeghi, F. Monfaredi, A. Dejamkhooy, M. Shafie-khah, and J. P. S. Catalão, "Assessing hybrid supercapacitor-battery energy storage for active power management in a wind-diesel system," *Int. J. Electr. Power Energy Syst.*, vol. 125, no. July 2020, 2021, doi: 10.1016/j.ijepes.2020.106391.

[161] R. Zahedi and M. M. Ardehali, "Power management for storage mechanisms including battery, supercapacitor, and hydrogen of autonomous hybrid green power system utilizing multiple optimally-designed fuzzy logic controllers," *Energy*, vol. 204, p. 117935, 2020, doi: 10.1016/j.energy.2020.117935.

[162] B. Hredzak, V. G. Agelidis, and M. Jang, "A model predictive control system for a hybrid battery-ultracapacitor power source," *IEEE Trans. Power Electron.*, vol. 29, no. 3, pp. 1469–1479, 2014, doi: 10.1109/TPEL.2013.2262003.

[163] J. Hou, Z. Song, H. Park, H. Hofmann, and J. Sun, "Implementation and evaluation of real-time model predictive control for load fluctuations mitigation in all-electric ship propulsion systems," *Appl. Energy*, vol. 230, no. February, pp. 62–77, 2018, doi: 10.1016/j.apenergy.2018.08.079.

[164] J. Hou, Z. Song, H. Hofmann, and J. Sun, "Adaptive model predictive control for hybrid energy storage energy management in all-electric ship microgrids," *Energy Convers. Manag.*, vol. 198, no. August, p. 111929, 2019, doi: 10.1016/j.enconman.2019.111929.

[165] F. Ni, Z. Zheng, Q. Xie, X. Xiao, Y. Zong, and C. Huang, "Enhancing resilience of DC microgrids with model predictive control based hybrid energy storage system," *Int. J. Electr. Power Energy Syst.*, vol. 128, no. November 2020, p. 106738, 2021, doi: 10.1016/j.ijepes.2020.106738.

[166] N. Chettibi, A. Mellit, G. Sulligoi, and A. M. Pavan, "Adaptive Neural Network-Based Control of a Hybrid AC/DC Microgrid," *IEEE Trans. Smart Grid*, vol. 9, no. 3, pp. 1667–1679, 2018, doi: 10.1109/TSG.2016.2597006.

[167] Y. Yuan, C. Sun, M. Li, S. S. Choi, and Q. Li, "Determination of optimal supercapacitor-lead-acid battery energy storage capacity for smoothing wind power using empirical mode decomposition and neural network," *Electr. Power Syst. Res.*, vol. 127, pp. 323–331, 2015, doi: 10.1016/j.epsr.2015.06.015.

[168] P. Singh and J. S. Lather, "Dynamic power management and control for low voltage DC microgrid with hybrid energy storage system using hybrid bat search algorithm and artificial neural network," *J. Energy Storage*, vol. 32, no. March, p. 101974, 2020, doi: 10.1016/j.est.2020.101974.

[169] P. García, C. A. García, L. M. Fernández, F. Llorens, and F. Jurado, "ANFIS-Based

control of a grid-connected hybrid system integrating renewable energies, hydrogen and batteries," *IEEE Trans. Ind. Informatics*, vol. 10, no. 2, pp. 1107–1117, 2014, doi: 10.1109/TII.2013.2290069.

[170] W. Jiang, L. Zhang, H. Zhao, H. Huang, and R. Hu, "Research on power sharing strategy of hybrid energy storage system in photovoltaic power station based on multi-objective optimisation," *IET Renew. Power Gener.*, vol. 10, no. 5, pp. 575–583, 2016, doi: 10.1049/iet-rpg.2015.0199.

[171] T. Mesbahi, N. Rizoug, P. Bartholomeüs, R. Sadoun, F. Khenfri, and P. Le Moigne, "Optimal energy management for a Li-ion battery/supercapacitor hybrid energy storage system based on a particle swarm optimization incorporating nelder-mead simplex approach," *IEEE Trans. Intell. Veh.*, vol. 2, no. 2, pp. 99–110, 2017, doi: 10.1109/TIV.2017.2720464.

[172] T. Zhou and W. Sun, "Optimization of battery-supercapacitor hybrid energy storage station in Wind/solar generation system," *IEEE Trans. Sustain. Energy*, vol. 5, no. 2, pp. 408–415, 2014, doi: 10.1109/TSTE.2013.2288804.

[173] U. Akram, M. Khalid, and S. Shafiq, "An innovative hybrid wind-solar and battery-supercapacitor microgrid system—development and optimization," *IEEE Access*, vol. 5, pp. 25897–25912, 2017, doi: 10.1109/ACCESS.2017.2767618.

[174] P. Lin, P. Wang, J. Xiao, J. Wang, C. Jin, and Y. Tang, "An Integral Droop for Transient Power Allocation and Output Impedance Shaping of Hybrid Energy Storage System in DC Microgrid," *IEEE Trans. Power Electron.*, vol. 33, no. 7, pp. 6262–6277, 2018, doi: 10.1109/TPEL.2017.2741262.

[175] Q. Xu *et al.*, "A Decentralized Dynamic Power Sharing Strategy for Hybrid Energy Storage System in Autonomous DC Microgrid," *IEEE Trans. Ind. Electron.*, vol. 64, no. 7, pp. 5930–5941, 2017, doi: 10.1109/TIE.2016.2608880.

[176] Q. Xu, J. Xiao, P. Wang, X. Pan, and C. Wen, "A Decentralized Control Strategy for Autonomous Transient Power Sharing and State-of-Charge Recovery in Hybrid Energy Storage Systems," *IEEE Trans. Sustain. Energy*, vol. 8, no. 4, pp. 1443–1452, 2017, doi: 10.1109/TSTE.2017.2688391.

[177] X. Chen, J. Zhou, M. Shi, L. Yan, W. Zuo, and J. Wen, "A Novel Virtual Resistor and Capacitor Droop Control for HESS in Medium-Voltage DC System," *IEEE Trans. Power Syst.*, vol. 34, no. 4, pp. 2518–2527, 2019, doi: 10.1109/TPWRS.2019.2894754.

[178] S. Faddel, A. A. Saad, T. Youssef, and O. Mohammed, "Decentralized Control Algorithm for the Hybrid Energy Storage of Shipboard Power System," *IEEE J. Emerg. Sel. Top. Power Electron.*, vol. 8, no. 1, pp. 720–731, 2020, doi: 10.1109/JESTPE.2019.2899287.

[179] X. Lin, R. Zamora, and C. A. Baguley, "A Coordinated Droop Controls and Power Management Scheme for Hybrid Energy Storage Systems in DC Microgrids," *2021 31st Australas. Univ. Power Eng. Conf.*, pp. 1–6, 2021, doi:

10.1109/aupec52110.2021.9597727.

[180] Y. Gu, W. Li, and X. He, “Frequency-coordinating virtual impedance for autonomous power management of DC microgrid,” *IEEE Trans. Power Electron.*, vol. 30, no. 4, pp. 2328–2337, 2015, doi: 10.1109/TPEL.2014.2325856.

[181] J. Duan, Z. Yi, D. Shi, C. Lin, X. Lu, and Z. Wang, “Reinforcement-Learning-Based Optimal Control of Hybrid Energy Storage Systems in Hybrid AC–DC Microgrids,” *IEEE Trans. Ind. Informatics*, vol. 15, no. 9, pp. 5355–5364, 2019, doi: 10.1109/tii.2019.2896618.

[182] Z. X. Xiao *et al.*, “Operation Control for Improving Energy Efficiency of Shipboard Microgrid including Bow Thrusters and Hybrid Energy Storages,” *IEEE Trans. Transp. Electrif.*, vol. 6, no. 2, pp. 856–868, 2020, doi: 10.1109/TTE.2020.2992735.

[183] M. Shi, X. Chen, J. Zhou, Y. Chen, J. Wen, and H. He, “Advanced Secondary Voltage Recovery Control for Multiple HESSs in a Droop-Controlled DC Microgrid,” *IEEE Trans. Smart Grid*, vol. 10, no. 4, pp. 3828–3839, 2019, doi: 10.1109/TSG.2018.2838108.

[184] R. Zhang, B. Hredzak, and T. Morstyn, “Distributed Control with Virtual Capacitance for the Voltage Restorations, State of Charge Balancing and Load Allocations of Heterogeneous Energy Storages in a DC Datacenter Microgrid,” *IEEE Trans. Energy Convers.*, vol. 34, no. 3, pp. 1296–1308, 2018, doi: 10.1109/TEC.2018.2889065.

[185] D. Gamage, X. Zhang, A. Ukil, and A. Swain, “Multi-Agent System Based Coordinated Consensus Control for Distributed Multi-Micro-grids,” *IECON Proc. (Industrial Electron. Conf.*, vol. 2020-Octob, pp. 1639–1644, 2020, doi: 10.1109/IECON43393.2020.9255328.

[186] P. Lin, T. Zhao, B. Wang, Y. Wang, and P. Wang, “A Semi-Consensus Strategy Toward Multi-Functional Hybrid Energy Storage System in DC Microgrids,” *IEEE Trans. Energy Convers.*, vol. 35, no. 1, pp. 336–346, 2020, doi: 10.1109/TEC.2019.2936120.

[187] B. Wang *et al.*, “Consensus-Based Control of Hybrid Energy Storage System with a Cascaded Multiport Converter in DC Microgrids,” *IEEE Trans. Sustain. Energy*, vol. 11, no. 4, pp. 2356–2366, 2020, doi: 10.1109/TSTE.2019.2956054.

[188] X. Chen *et al.*, “Distributed Cooperative Control of Multiple Hybrid Energy Storage Systems in a DC Microgrid Using Consensus Protocol,” *IEEE Trans. Ind. Electron.*, vol. 67, no. 3, pp. 1968–1979, 2020, doi: 10.1109/TIE.2019.2898606.

[189] C. Bordin, H. O. Anuta, A. Crossland, I. L. Gutierrez, C. J. Dent, and D. Vigo, “A linear programming approach for battery degradation analysis and optimization in offgrid power systems with solar energy integration,” *Renew. Energy*, vol. 101, pp. 417–430, 2017, doi: 10.1016/j.renene.2016.08.066.

[190] C. Zhou, K. Qian, M. Allan, and W. Zhou, “Modeling of the cost of EV battery wear due to V2G application in power systems,” *IEEE Trans. Energy Convers.*, vol. 26, no. 4, pp. 1041–1050, 2011, doi: 10.1109/TEC.2011.2159977.

[191] C. Ju, P. Wang, L. Goel, and Y. Xu, “A two-layer energy management system for

microgrids with hybrid energy storage considering degradation costs," *IEEE Trans. Smart Grid*, vol. 9, no. 6, pp. 6047–6057, 2018, doi: 10.1109/TSG.2017.2703126.

[192] Z. Tang *et al.*, "A Two-layer Receding-horizon Optimal Control Strategy for Battery Energy Storage System Participating in Peak Load Shifting Considering Degradation Cost," in *2021 IEEE Sustainable Power and Energy Conference (iSPEC)*, Dec. 2021, no. 521304200059, pp. 1189–1194. doi: 10.1109/iSPEC53008.2021.9735997.

[193] NREL, "End-Use Load Profiles for the U.S. Building Stock," 2021. doi: https://dx.doi.org/10.25984/1876417.

[194] EMC, "Energy Market Company (EMCSG)," *EMC Singapore*, 2022. https://www.emcsg.com/marketdata (accessed May 01, 2022).

[195] "Ergonomics ofthe Thermal Environment—Analytical Determination and Interpretation of Thermal Comfort Using Calculation of the PMV and PPD Indices and Local Thermal Comfort Criteria," *ISO 77302005*, 2005.

Local level energy management system

Chapter 3: A fully filter-based decentralized control with state of charge balancing strategy for battery energy storage systems in autonomous dc microgrid applications

Citation:

X. Lin, R. Zamora, and C. Baguley, "A fully filter-based decentralized control with state of charge balancing strategy for battery energy storage systems in autonomous dc microgrid applications," *IEEE Access*, vol. 9, pp. 15028–15040, Jan. 2021. **(Published)**

Preamble:

As discussed in Chapters 1 and 2, the intermittent nature of renewable energy sources causes significant challenges in providing stable electricity to households. In order to solve this problem, battery energy storage systems are adopted to improve the power quality and meet the power demand of users. Therefore, this chapter addresses the imbalance between the batteries and DC bus voltage deviations. This chapter proposes a fully decentralized control system for battery energy storage systems in DC microgrids. This approach enables state of charge (SoC) balancing among batteries regardless of whether the batteries have the same capacity. In addition, the proposed method can ensure that the bus voltage is within a safe range. Furthermore, the voltage restoration control in this chapter is equivalent to a high-pass filter (HPF) to remove the communication system between the primary and secondary controllers. Finally, the performance of the method is verified on a processor-in-the-loop (PIL) simulation platform.

Abstract:

State of charge (SoC) imbalance and dc bus voltage deviations are significant issues for distributed battery energy storage systems in autonomous dc microgrid applications. Accordingly, a high-pass filter (HPF) based SoC balancing method is proposed to achieve SoC balance by considering different SoCs and capacities, and a band-pass filter (BPF) based power droop control is used to accomplish power-sharing and voltage compensation. Through this approach battery storage units (BSUs) with higher SoC and capacity deliver more power during discharging mode than those with lower SoC and capacity. During charging mode, those BSUs with higher SoC and lower capacity are controlled to absorb less power than those with higher capacity and lower SoC. Therefore, SoC balance can be achieved between distributed BSUs. Besides, the dc bus voltage is maintained within the desired range by adopting the proposed method. In addition, the control method employed also considers the impact of line resistance. The proposed control strategy is implemented in a fully decentralized way which does not require any communication link, while maintaining system stability. MATLAB/Simulink and processor-in-the loop (PIL) simulation results verify that the proposed control strategy is effective and feasible.

Keywords: Decentralized control, state of charge (SoC) balance, high-pass-filter (HPF), band-pass-filter (BPF), battery storage system, dc microgrid.

1. Introduction

Globally, an increasing share of energy in an electrical form is being sourced from renewable energy resources (RERs). A microgrid is a small-scale power system that has a pivotal role in the integration of RERs into future societies, along with BSUs [1], [2]. Since the RERs, BSUs and many loads are dc in nature, these system components can be directly interconnected through a dc microgrid using dc-dc converters and without any dc-ac conversion stage [3]. This avoids incurring the problems related to frequency stability, reactive power compensation, and synchronization that are inherent to ac systems. Consequently, significant research effort has been expended on the dc microgrid concept, some examples of which include [4], [5].

The configuration of a dc microgrid is given in Fig. 1 [6]. Due to the stochastic nature of RERs, BSUs are employed to alleviate microgrid power fluctuations. This improves power quality and system stability [7], [8]. In the control system of BSUs, power converter systems (PCSs) are used to achieve power-sharing and SoC balancing among distributed BSUs [9]–[11].

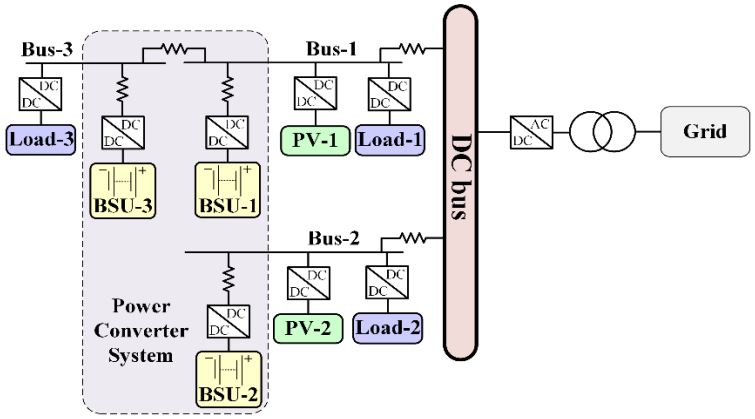

Fig. 1. DC microgrid structure.

Many studies have investigated PCSs [12]–[17]. In [12], a coordinated secondary control based on a current sharing method is proposed to achieve charge/discharge monitoring and SoC balance at the same time. In [14], an accurate power-sharing approach is presented to balance the SoC among BSUs in dc microgrid. In [16], a droop method is proposed based on voltage scheduling to guarantee the SoC balance of the BSUs. The mentioned distributed methods require a communication network to exchange system data. However, a single point of failure and communication delay can deteriorate the performance of the PCS controller [2], [18], [19]. To address these issues, a fully decentralized approach can be employed for dispersed BSUs [20]–[28], that does not require any communication link [20]. In [21], a multifunctional droop control method is proposed to achieve the SoC balancing by adopting the SoC-based frequency scheduling in ac microgrid. Nevertheless, this approach results in serious frequency error and

neglects the different capacities of BSUs. Due to the different capacities of each BSU, the SoC balancing process may fail to complete. By extending the approach in [21], a novel SoC balancing based droop control scheme in [22] is presented to balance the SoC with different capacities. However, these works are completed in the ac system. In [24], a droop approach based fuzzy logic control approach is proposed to balance the SoC among batteries by regulating virtual resistances in low voltage dc microgrids. In [9] and [11], the droop coefficient is set to be inversely proportional to the SoC^n in the discharging mode, but proportional to the SoC^n in charging mode, with *n* defined as the convergence factor. However, these control methods ignore the voltage deviation caused by droop control and SoC balancing scheme. In [25], an SoC-based virtual dc machine control strategy is proposed to achieve the SoC balance and to alleviate the dc bus voltage deviation. However, the methods do not consider the impact of BSU capacities on SoC balancing scheme. In [27], a SoC based droop control is presented to achieve the SoC balance. However, the proposed method is only suitable for SoC balance of batteries with the same capacities. Although the SoC balance with different capacities can be realized in [28], the method fails to consider the line resistance, and causes the voltage deviation. Hence, the SoC balancing strategy based on a fully decentralized manner needs to be further studied for dc microgrid applications.

In this paper, a novel filter-based droop control with SoC balancing scheme for dc microgrids is proposed, which does not require any local communication systems among BSUs. The major contributions of this paper are summarized as follows:

a) The proposed HPF-based SoC balancing approach can achieve SoC balance by considering different capacities and SoCs among BSUs.
b) Voltage recovery and power sharing are achieved by introducing BPF-based power droop control.
c) The proposed method eliminates the influence of different line impedances on output power-sharing and the SoC balancing scheme.
d) The design procedures on control parameters of the proposed method are elaborated in detail. Then, the system stability is analysed by using root locus method.

The rest of this paper is organized as follows. The SoC-based droop control is introduced in Section II. In Section III, the design procedures of system parameters and system stability are explained in detail. Section IV presents simulation results, which verifies the proposed approach. The conclusions are presented in Section V.

2. Proposed SoC-based droop control scheme

2.1. Basic operation of BSUs

In Fig. 1, BSUs can be used to compensate for the power shortage of the microgrid and to absorb the surplus power of RERs. During the operation of the BSUs, the SoC level among BSUs is required to be balanced. This avoids the overuse of any specific BSU, and thus improves BSU lifetimes.

2.2. SoC estimation method

Currently, the Coulomb counting method is widely used to estimate the SoC, using [11]:

$$\mathrm{SoC} = \mathrm{SoC}_{\mathrm{ini}} - \frac{1}{E_{b\_x}} \int I_{L\_x}\, dt \tag{1}$$

where, $\mathrm{SoC}_{\mathrm{ini}}$, E_{b_x}, and I_{L_x} are the initial value of SoC, battery capacity and output current for x^{th} BSU, (x=1, 2, …, n), respectively. Equation (1) can be further derived as:

$$\mathrm{SoC} = \mathrm{SoC}_{\mathrm{ini}} - \frac{1}{E_{b\_x} V_x} \int P_x\, dt \tag{2}$$

where, V_x and P_x are the output voltage and power of x^{th} BSU. From (2), the SoC of batteries is affected by the output power of BSUs. Therefore, SoC balancing can be achieved through regulating BSU output power levels.

2.3. Proposed filter-based droop control with SoC balancing strategy

Droop control in a dc microgrid setting can be implemented using:

$$V_{b\_x} = V_r - m_x P_{b\_x} \tag{3}$$

where, V_r and m_x are the reference voltage for dc bus and droop coefficient of x^{th} BSU, respectively, and V_{b_x} and P_{b_x} are the output voltage and power of BSUs converter, respectively. It should be noted that P_{b_x} is filtered by the low-pass filter (LPF), to attenuate high frequency components in the power waveform [11]. P_{b_x} is positive in discharging mode and negative in charging mode. The droop coefficient m_x is determined by the maximum allowable dc bus voltage deviation $V_{\max}$ and power rating P_{rating}.

$$m_x = \frac{\Delta V_{\max}}{P_{\mathrm{rating}}}. \tag{4}$$

In addition, if the line resistance is assumed to be omitted, and the output voltages of BSUs are considered to be equal, it yields

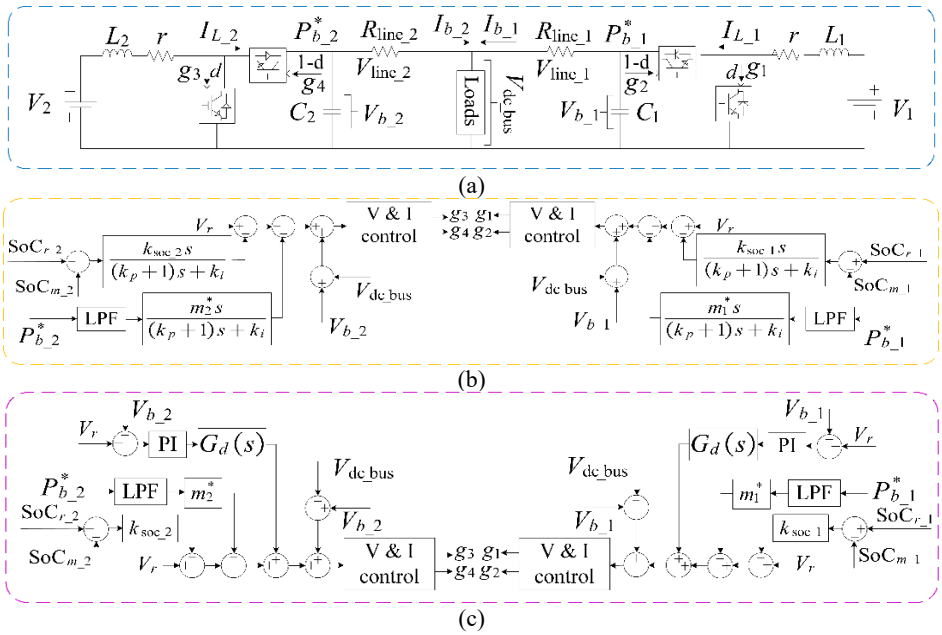

Fig. 2. Structure of the BSUs with the proposed control methods and a comparing control method, (a) dc-dc bidirectional converter, (b) proposed filtered-based SoC balancing scheme with the proposed voltage restoration for BSUs' converters, (c) proposed SoC balancing scheme with the voltage recovery from ref. [28] for BSUs' converters.

$$V_{b\_1} = V_{b\_2} = \ldots = V_{b\_x}. \tag{5}$$

From (3) and (5), if m_1=m_2=...=m_x, the output power of BSUs must be equivalently allocated at steady-state. This is a necessary condition for achieving the SoC balance. In order to balance the SoC among BSUs, an enhanced droop control is shown as follows:

$$V_{b\_x} = V_r - k_{soc\_x}(\mathrm{SoC}_{r\_x} - \mathrm{SoC}_{m\_x}) - \frac{m_x}{E_{b\_x}} P_{b\_x} \tag{6}$$

where k_{soc_x} , SoC_{r_x}, and SoC_{m_x} are the droop coefficient of SoC balancing scheme, reference SoC and measured SoC for x^{th} BSU.

In (6), the second and third terms are the SoC balancing and power droop control that cause the voltage variation. If the initially measured SoCs of two BSUs are described as SoC_{m_1} and SoC_{m_2}, SoC_{m_1} is assumed to be greater than SoC_{m_2}. Then, taking the same SoC droop coefficient and SoC reference, the second term of (6) satisfies $k_{soc\_1}(\mathrm{SoC}_{r\_1} - \mathrm{SoC}_{m\_1}) < k_{soc\_2}(\mathrm{SoC}_{r\_2} - \mathrm{SoC}_{m\_2})$. As a result, the voltage of the BSU with higher SoC descends less than the one of the BSU with lower SoC. Moreover, similar to the analysis of the second term, the power droop control shows that voltage drop caused by the low-capacity battery is larger than the ones with high-capacity. Finally, the BSU with higher voltage release more active power compared to the BSU with lower voltage.

As observed from (5) and (6), if two batteries with the same capacities are considered, it yields

$$\mathrm{SoC}_{m\_1} = \frac{k_{\mathrm{soc}\_1}\mathrm{SoC}_{r\_1} - k_{\mathrm{soc}\_2}(\mathrm{SoC}_{r\_2} - \mathrm{SoC}_{m\_2})}{k_{\mathrm{soc}\_1}}. \tag{7}$$

From (7), taking the same SoC droop coefficient and reference SoC, the SoCs of two BSUs reach a consistent value at steady-state. As analysis of equation (6), the BSU with higher capacity delivers more constant power compared to the ones with lower capacity at steady-state. Hence, the SoC disparity among the multiple BSUs is gradually reduced, and finally, the SoC balancing can be accomplished.

However, the SoC balancing scheme and droop control in (6) can result in serious bus voltage deviation in the steady-state. Therefore, the secondary control is widely adopted to compensate for the voltage loss by adjusting the set point for the primary control. Equation (6) can be modified as follows

$$V_{b\_x} = V_r - k_{\mathrm{soc}\_x}(\mathrm{SoC}_{r\_x} - \mathrm{SoC}_{m\_x}) - \frac{m_x}{E_{b\_x}} P_{b\_x} + \Delta V \tag{8}$$

$$\Delta V = [k_p(V_r - V_{b\_x}) + \frac{k_i}{s}(V_r - V_{b\_x})]G_d(s) \tag{9}$$

$$G_d(s) = \frac{\tau}{\tau s + 1} \tag{10}$$

where, ΔV, k_p, and k_i are the voltage compensating term and control parameters for the restoration control. The secondary control requires low-bandwidth-communication to achieve the data exchange with the primary control [29], [30]. $G_d(s)$ represents the delay in the communication system [31]. However, the communication delay and faults deteriorate the performance of the proposed method. In order to eliminate the communication issues, the secondary controller can be integrated with the primary control. A novel equation can be derived by combining (8) and (9):

$$V_{b\_x} = V_r - \frac{k_{\mathrm{soc}\_x} s}{(k_p+1)s + k_i}\Delta\mathrm{SoC} - \frac{m_x^* s}{(k_p+1)s + k_i} P_{b\_x} \tag{11}$$

where, $\Delta\mathrm{SoC} = (\mathrm{SoC}_{r\_x} - \mathrm{SoC}_{m\_x})$ and $m_x^* = m_x/E_{b\_x}$. From (11), the secondary control algorithm is equivalent to an HPF component that is added to the traditional power droop control and SoC balancing scheme. Therefore, the communication delay (10) is fully eliminated. By adding an HPF algorithm, the output voltage of BSUs can be restored to a pre-set value at steady-state. As a result, the voltage deviation caused by the power droop control and SoC balancing scheme is reduced by the proposed fully decentralized method.

Considering $P_{b\_x} = [\omega_L/(s+\omega_L)]P_{b\_x}^*$, (11) can be further modified as:

$$V_{b\_x} = V_r - G_{\mathrm{HPF}}(s)k_{\mathrm{soc}\_x}\Delta\mathrm{SoC} - G_{\mathrm{BPF}}(s)m_x^*P_{b\_x}^* \tag{12}$$

$$G_{\mathrm{BPF}}(s) = \frac{s}{(k_p{+}1)s{+}k_i} \cdot \frac{\omega_L}{s{+}\omega_L} \tag{13}$$

where, $G_{\mathrm{HPF}}(s) = s/[(k_p{+}1)s{+}k_i]$; ω_L and $P_{b\_x}^*$ are the cut-off frequency of the LPF and the output active power of the converter, respectively. The power-sharing and voltage restoration in the proposed controller are determined by the BPF, as shown by (12) and (13).

In practice, however, there is a line resistance between the terminal converter of BSUs and the dc voltage bus. The conventional droop control usually neglects the influence of line resistance on the system. In this case, the presence of line resistance deteriorates the performance of the proposed SoC balancing strategy. To overcome this issue, an extra control loop is added to the proposed scheme. In order to facilitate the observation, an equivalent circuit with the proposed control for BSUs is shown in Fig. 2(a). The SoC-based droop control with considering the line impedance can be derived as:

$$V_{b\_x} = V_r - G_{\mathrm{HPF}}(s)k_{\mathrm{soc}\_x}\Delta\mathrm{SoC} - G_{\mathrm{BPF}}(s)m_x^*P_{b\_x}^* + V_{\mathrm{line}\_x} \tag{14}$$

$$V_{\mathrm{line}\_x} = R_{\mathrm{line}\_x}\frac{P_{b\_x}^*}{V_{b\_x}} \tag{15}$$

$$P_{b\_x}^* = \frac{V_{b\_x} - V_{\mathrm{dc_{bus}}}}{R_{\mathrm{line}\_x}}V_{b\_x} \tag{16}$$

where, V_{line_x} and R_{line_x} are the line voltage and resistance for the x^{th} BSU. Subsequently, (14) can further be written as follows by considering (13), (15), and (16):

$$V_{b\_x} = V_r - \frac{k_{\mathrm{soc}\_x}s}{(k_p{+}1)s{+}k_i}\Delta SoC + (V_{b\_x} - V_{\mathrm{dc_{bus}}}) - \frac{m_x^*s}{(k_p{+}1)s{+}k_i} \cdot \frac{\omega_L}{s{+}\omega_L}P_{b\_x}^*. \tag{17}$$

It can be observed that the voltage drops produced by different line resistances are eliminated by introducing the third term of (17). Therefore, the SoC balancing and the improvement of power quality can be achieved regardless of the line resistance values, whether they are the same or different. The control structure is shown in Fig. 2(b).

3. Control parameters design and system stability analysis

For the proposed scheme, it is expected that BSUs with higher SoC supply more power compared with the ones with lower SoC. Generally, the BSUs are taken into account as the ideal voltage sources. Nevertheless, the converter systems with BSUs cannot be considered as the ideal voltage sources in practice. This is because the output voltage of the dc-dc bidirectional converter is

impacted by control system parameters. Therefore, the parameters are required to be designed better to guarantee the effectiveness of the proposed method. This section depicts the design process of the control parameters and the system stability analysis. From Fig. 2(a), the dynamic average model of the converter can be written as:

$$C_x \frac{dV_{b\_x}}{dt} = (1-d)I_{L\_x} - I_{b\_x} \tag{18}$$

$$rI_{L\_x} + L_x \frac{dI_{L\_x}}{dt} = V_x - (1-d)V_{b\_x} \tag{19}$$

where, r, C_x and L_x are the resistance of inductor, filter capacitor and inductor of the converters; I_{b_x} is the output current of BSUs converter; d denotes the duty cycle.

The dual-loop control is widely adopted for the dc-dc bidirectional converter. By considering (18) and (19), the control diagram for converter is shown in Figure 3. $G_v(s)$ and $G_c(s)$ are the regulator of the voltage and current, respectively; D is the steady-state value of the duty cycle. The equations are written as follows:

$$G_v(s) = k_{\mathrm{vp}} + \frac{k_{\mathrm{vi}}}{s} \tag{20}$$

$$G_c(s) = k_{\mathrm{cp}} + \frac{k_{\mathrm{ci}}}{s} \tag{21}$$

$$D = \frac{V_r - V_x}{V_r} \tag{22}$$

where, k_{vp}, k_{vi}, k_{cp} and k_{ci} are the control parameter for the voltage and current loops, respectively. As shown in Fig. 3, the open-loop transfer function of the current loop ($G_{\mathrm{co}}(s)$) can be written as:

$$G_{\mathrm{co}}(s) = \frac{k_{\mathrm{cp}}s + k_{\mathrm{ci}}}{s} \cdot \frac{V_r}{sL_x + r}. \tag{23}$$

According to (23), ω_c is assumed to be the control bandwidth of the current loop. In order to obtain enough phase margin, the corner frequency of the current regulator $k_{\mathrm{ci}}/k_{\mathrm{cp}}$ in (24) is required to be less than ω_c [32], [33]. Hence, the coefficient η must be less 1, which is set between 0.1 and 0.2 in this paper.

$$\frac{k_{\mathrm{ci}}}{k_{\mathrm{cp}}} = \eta\omega_c. \tag{24}$$

At a corner frequency of ω_c, the gain of the open-loop transfer function should equal to 0 dB. By considering (24), (23) can be modified as

$$G_{\mathrm{co}}(j\omega_c) = \left| \frac{j\omega_c k_{\mathrm{cp}} + \eta\omega_c k_{\mathrm{cp}}}{j\omega_c} \cdot \frac{V_r}{j\omega_c L_x + r} \right| = 1. \tag{25}$$

As observed in (25), η can be ignored since it is very small. Hence, the proportional and integral parameters for current loop can be obtained as follows:

$$k_{\mathrm{cp}} = \frac{\sqrt{\omega_c^2 L_x^2 + r^2}}{V_r} \tag{26}$$

$$k_{\mathrm{ci}} = \frac{\eta\omega_c\sqrt{\omega_c^2 L_x^2 + r^2}}{V_r}. \tag{27}$$

Since the response speed of the current regulator is much faster than the voltage regulator, the current loop can be considered as a gain of 1 when the voltage regulator is designed. Similar to the design procedure of the current regulator (23)-(27), the control parameters for the voltage loop can be derived as follows:

$$k_{\mathrm{vp}} = \frac{\omega_v C_x}{1 - D} \tag{28}$$

$$k_{\mathrm{vi}} = \frac{\eta\omega_v^2 C_x}{1 - D} \tag{29}$$

where, ω_v is the control bandwidth of the voltage control. Typically, ω_v is designed to be much less than ω_c, i.e. $\omega_c = 5\omega_v$, to guarantee the response of current control reaches steady state before any change is applied to reference current by the voltage control. Meanwhile, ω_c should also be selected to be much less than the switching frequency ω_s, i.e., $\omega_s = 10\omega_c$.

To compensate for the voltage drop due to deviation generated by the droop method and SoC balancing scheme, the voltage restoration is integrated with the power droop control. As it can be observed from (12) and (13), the performance of the proposed method is dominated by the cut-off frequency of BPF. Besides, the definition of cut-off frequency illustrates that the gain of BPF at the upper and lower cut-off frequency should be -3 dB [34]. Therefore, the effectiveness of the voltage compensation and SoC balancing can be guaranteed by this definition. Equation (13) can be further written as:

$$G_{\mathrm{BPF}}(s) = \frac{\omega_L s}{s^2 + (k_i + \omega_L)s + \omega_L k_i} \tag{30}$$

where, the cut-off frequency of HPF should be smaller compared with LPF ($k_i < \omega_L$). From second term of (12), $G_{\mathrm{HPF}}(s)$ can be further modified as (31).

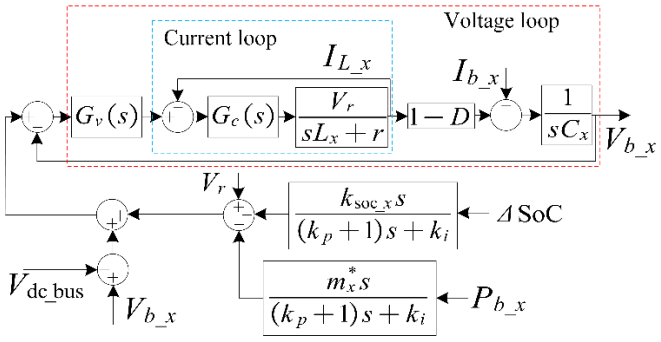

Fig. 3. Dual loop control architecture of the converter system.

$$G_{\mathrm{HPF}}(s) = \frac{s}{(k_p+1)s+k_i} = \frac{\frac{1}{k_p+1}s}{s+\frac{1}{k_p+1}k_i}. \tag{31}$$

From (31), the gain of $G_{\mathrm{HPF}}(s)$ is $1/(k_p+1)$, which affects the droop factor m_x and droop coefficient for SoC scheme k_{soc_x}. Therefore, the gain value must be as close to 1 as possible. Thus, k_p is chosen as 0 in this paper.

The system stability analysis can be achieved by using root-locus approach. By considering Figs. 2 and 3, the steady-state relationship between the output voltage of BSUs and reference voltage can be derived as follows:

$$V_{b\_x} = \frac{G_v(s)(1-D)[V_r - G_{\mathrm{HPF}}(s)(m^*P_{b\_x}+k_{\mathrm{soc}\_x}\Delta\mathrm{SoC})]}{C_x s+G_v(s)(1-D)} - \frac{1}{C_x s+G_v(s)(1-D)}I_{b\_x} \tag{32}$$

where, $G_v(s) = (\omega_v C_x s - \eta\omega_v^2 C_x)/[(1-D)s]$ and $G_{\mathrm{HPF}}(s) = s/(s+k_i)$.

If there is no voltage change, the current relationship in (18) can be expressed as $I_{L\_x} = I_{b\_x}/(1-D)$. Furthermore, substituting $I_{b\_x} = V_{b\_x}/R_L$ based on Figure 2, (1) can be written in s domain as (33).

$$\Delta\mathrm{SoC} = \frac{1}{(1-D)E_{b\_x}R_L s}V_{b\_x} \tag{33}$$

where, R_L is the load resistance. By combining (33) and small-signal disturbance, it produces

$$\Delta\widetilde{\mathrm{SoC}} = \frac{1}{(1-D)E_{b\_x}R_L s}\widetilde{V}_{b\_x}. \tag{34}$$

By considering the output power, it is obtained that

$$P_{b\_x} = \frac{\omega_L}{s+\omega_L} P^*_{b\_x} = \frac{\omega_L}{s+\omega_L} \cdot \frac{V^{*2}_{b\_x}}{R_L} \tag{35}$$

where, $V^*_{b\_x}$ is unfiltered output voltage the converters. If power loss caused by LPF is ignored, then $V^*_{b\_x} \approx V_{b\_x}$. After, the small-signal model can be written as

$$\widetilde{P}_{b\_x} = \frac{\omega_L}{s+\omega_L} \cdot \frac{2V_x}{R_L(1-D)} \widetilde{V}_{b\_x}. \tag{36}$$

By substituting (34) and (36) into (32), and performing small signal perturbation, it yields

$$\widetilde{V}_{b\_x} = \frac{G_v(s)(1-D)\widetilde{V}_r}{C_x s+G_v(s)(1-D)} - \frac{\widetilde{V}_{b\_x}}{[C_x s+G_v(s)(1-D)]R_L} - \frac{\widetilde{V}_{b\_x}}{[C_x s+G_v(s)(1-D)]R_L(1-D)}$$

$$- \frac{G_{\mathrm{HPF}}(s)k_{\mathrm{soc}\_x}\widetilde{V}_{b\_x}}{[C_x s+G_v(s)(1-D)]R_L E_{b\_x}}. \tag{37}$$

By considering two BSUs, the small-signal model of the relationship between the reference voltage and the output voltage of BSUs' converters are given by (38). Specifically, x=1 denotes the BSU_1, while x=2 denotes the BSU_2.

$$\widetilde{V}_{b\_x} = \frac{b_{x\_3}s^3+b_{x\_2}s^2+b_{x\_1}s+b_{x\_0}}{a_{x\_4}s^4+a_{x\_3}s^3+a_{x\_2}s^2+a_{x\_1}s+a_{x\_0}} \widetilde{V}_r \tag{38}$$

where, $a_{x\_4} = R_L E_{b\_x} C_x(1-D)$; $a_{x\_3} = R_L E_{b\_x} C_x(1-D)(k_i+\omega_L)+\omega_v R_L E_{b\_x} C_x(1-D) + E_{b\_x}(1-D)$; $a_{x\_2} = R_L E_{b\_x} C_x(1-D)k_i\omega_L+\omega_v R_L E_{b\_x} C_x(1-D)(k_i+\omega_L)+\eta\omega_v^2 R_L E_{b\_x} C_x(1-D)+\omega_v C_x(2m^*_x V_x E_{b\_x}\omega_L - k_{\mathrm{soc}\_x}) + E_{b\_x}(1-D)(k_i+\omega_L) + E_{b\_x}(1-D)(k_i+\omega_L)$; $a_{x\_1} = \omega_v R_L E_{b\_x} C_x(1-D)k_i\omega_L+R_L E_{b\_x}\eta\omega_v^2 C_x(1-D)\times(k_i+\omega_L)+\omega_v C_x k_{\mathrm{soc}\_x}\omega_L+E_{b\_x} C_x(1-D)k_i\omega_L +\eta\omega_v^2 C_x(2m^*_x V_x E_{b\_x}\omega_L - k_{\mathrm{soc}\_x})$; $a_{x\_0} = \eta\omega_v^2 C_x k_{\mathrm{soc}\_x}\omega_L+\eta\omega_v^2 C_x E_{b\_x} R_L(1-D)k_i\omega_L$; $b_{x\_3} = \omega_v C_x R_L(1-D)E_{b\_x}$; $b_{x\_2} = \omega_v C_x R_L(1-D)E_{b\_x}(k_i+\omega_L)+R_L E_{b\_x}\eta\omega_v^2 C_x(1-D)$; $b_{x\_1} = \omega_v C_x R_L(1-D)E_{b\_x}k_i\omega_L+\eta\omega_v^2 C_x R_L(1-D)E_{b\_x}\times(k_i+\omega_L)$; $b_{x\_0} = \eta\omega_v^2 C_x R_L(1-D)E_{b\_x}k_i\omega_L$.

Subsequently, considering the line resistances, the relationship between the dc bus voltage and output voltage of BSUs' converters is presented by (39).

$$\frac{\widetilde{V}_{\mathrm{dc\_bus}}}{R_L} = \frac{\widetilde{V}_{b\_1} - \widetilde{V}_{\mathrm{dc\_bus}}}{R_{\mathrm{line\_1}}} + \frac{\widetilde{V}_{b\_2} - \widetilde{V}_{\mathrm{dc\_bus}}}{R_{\mathrm{line\_2}}} \tag{39}$$

where, $R_{\mathrm{line\_1}}$ and $R_{\mathrm{line\_2}}$ are the line resistances between the dc bus and BSUs' converters 1 and 2, respectively.

Then, substituting (38) into (39), the characteristic function of the proposed control system is shown as (40).

$$a_8 s^8+a_7 s^7+a_6 s^6+a_5 s^5+a_4 s^4+a_3 s^3+a_2 s^2+a_1 s+a_0 = 0 \tag{40}$$

where $a_8 = a_{1\_4} a_{2\_4}$; $a_7 = a_{1\_4} a_{2\_3}+a_{1\_3} a_{2\_4}$; $a_6 = a_{1\_4} a_{2\_2}+a_{1\_3} a_{2\_3}+a_{1\_2} a_{2\_4}$; $a_5 = a_{2\_1}+a_{1\_3} a_{2\_2}+a_{1\_2} a_{2\_3}+a_{1\_1} a_{2\_4}$; $a_4 = a_{1\_4} a_{2\_0}+a_{1\_3} a_{2\_1}+a_{1\_2} a_{2\_2}+a_{1\_1} a_{2\_3}+a_{1\_0} a_{2\_4}$; $a_3 = a_{1\_3} a_{2\_0}+a_{1\_2} a_{2\_1}+a_{1\_1} a_{2\_2}+a_{1\_0} a_{2\_3}$; $a_2 = a_{1\_2} a_{2\_0}+a_{1\_1} a_{2\_1}+a_{1\_0} a_{2\_2}$; $a_1 = a_{1\_1} a_{2\_0}+a_{1\_0} a_{2\_1}$; $a_0 = a_{1\_0} a_{2\_0}$.

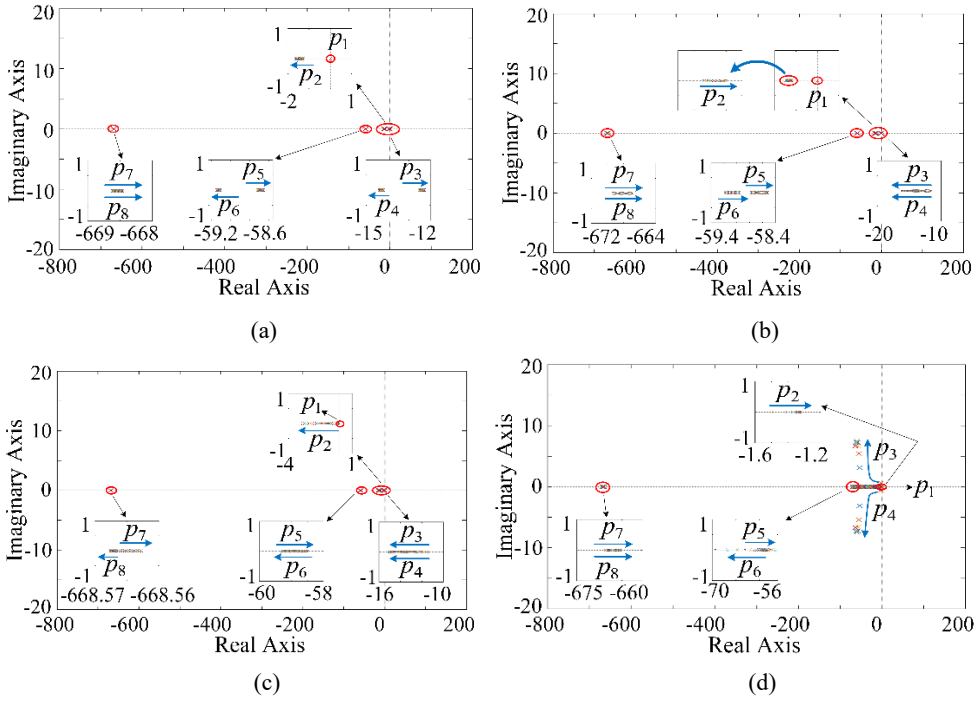

Fig. 4. Root locus diagram for droop parameters, (a) Root locus for different k_{soc}, (b) Root locus for different m, (c) Root locus for different k_i, (d) Root locus for different ω_L.

From (40), the system stability analysis can be accomplished by observing the placement of the dominant poles in the closed-loop characteristic equation. Therefore, the proper coefficients can be chosen to guarantee the effectiveness of the proposed method. Based on the specifications in Tables 1 and 2, the dominant poles with different droop coefficient for SoC balance are shown in Fig. 4(a), while the dominant poles with different droop coefficient for power droop is displayed in Fig. 4(b). It shows that the closed-loop dominant poles are sited in the left half of the s-plane with different droop parameters. Consequently, the system stability of the proposed control can be guaranteed. From Fig. 4(c), when k_i varies from 0 to 1×2π rad/s, the control system contains three negative real dominant poles (p_2, p_3 and p_4) that move to the left side. This means that the system has fast dynamic response capability and stability. From Fig. 4(d), when the cut-off frequency ω_L changes from 0 to 10×2π rad/s, the dominant pole p_2 is located on the left negative real axis. This illustrates that the stability and dynamic response of the control system can be guaranteed. At the beginning, the dominant poles p_3 and p_4 are on the left negative real axis, and

the moving span is relatively large. This means that the dynamic performance of the control system is accelerated. However, as ω_L increases, p_3 and p_4 change from negative real poles to complex conjugate poles. This indicates that the system may suffer oscillation. As a result, the HPF and LPF will not affect the dynamic performance and stability of the system by selecting appropriate parameters.

Table 1 Droop coefficient for system stability analysis

Items	Symbol	Value
Droop coefficient for power control	m_x	[0, 0.01] V/W
Droop coefficient for SoC balance	k_{soc_x}	[0, 5] V
Voltage compensating term	k_i	[0, 1×2π] rad/s
Cut-off frequency of LPF	ω_L	[0, 10×2π] rad/s

Table 2 System parameters

Items	Symbol	Value
Reference voltage	V_r	500 V
Battery voltage	V_x	300 V
Converter capacitor	C	200×10^{-6} F
Converter inductor	L	2×10^{-3} H
Resistance of inductor	r	0.01 Ω
Cut-off frequency of LPF	ω_L	2×2π rad/s
Voltage restoration gain	k_i	0.45×2π rad/s
Voltage control bandwidth	ω_v	100×2π rad/s
Current control bandwidth	ω_c	500×2π rad/s
Switch frequency	f_s	5000 Hz
Voltage control parameters	k_{vp}, k_{vi}	0.2094, 13.1595
Current control parameters	k_{cp}, k_{ci}	0.0126, 3.9483
Resistance load	R_L	28 Ω
Line resistance - 1	R_{line_1}	0.5 Ω
Line resistance - 2	R_{line_2}	1.2 Ω
Line resistance - 3	R_{line_3}	2.5 Ω
Reference SoC	SoC_{r_x}	100 %
Time constant	τ	0.5 s

Table 3 Droop coefficient for simulation verification

Items	Symbol	Value
Droop coefficient for power control	m_x	5.5×10^{-3} V/W
Droop coefficient for SoC balance	k_{soc_x}	2.25 V

4. Simulation verifications

To verify the effectiveness of the proposed filter-based droop scheme, an islanded microgrid including three BSUs is implemented in MATLAB/Simulink and processor-in-the loop (PIL). In cases 1 to 6, BSUs supply 9 kW power to the load at the beginning. The 3 kW load is added into the system at 20 s and removed from the system at 50 s. The scheduling equation is given as follows.

$$P_{load}(t)=\begin{cases} 9\ \text{kW},\ 0\ \text{s}\le t\le 20\ \text{s}, \\ 12\ \text{kW},\ 20\ \text{s}\le t\le 50\ \text{s}, \\ 9\ \text{kW},\ 50\ \text{s}\le t\le 140\ \text{s}. \end{cases} \quad \text{(Cases 1-6)}$$

Besides, the charging and discharging modes of BSUs are switched by regulating the dc bus voltage. From 0 s to 70 s, the dc bus voltage is less than the reference voltage, the BSUs run in discharging mode. After 70 s, the dc bus voltage is adjusted to be greater than the reference voltage, the BSUs will operate in charging mode. The system parameters are listed in Tables 2 and 3.

4.1. Case 1: Proposed method without voltage compensation and with LPF

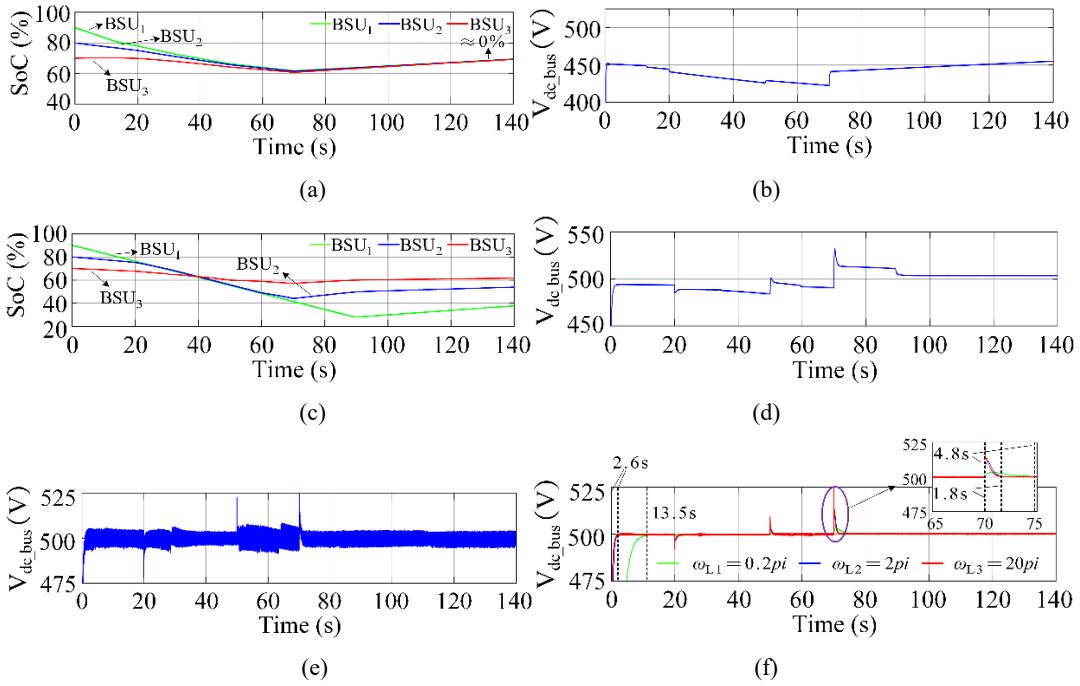

Fig. 5. Simulation results for case 1, (a) SoC of BSUs without voltage restoration, (b) DC bus voltage without voltage restoration, (c) SoC of BSUs without voltage compensation for line resistance, (d) DC bus voltage without voltage compensation for line resistance, (e) DC bus voltage without the LPF, (f) The influence of the different cut-off frequencies of the LPF on the output voltage.

Three sub-cases are studied: first case is the SoC-based droop control without the voltage recovery, where the simulation results are shown in Figs. 5(a) and 5(b). The second case is the voltage drop induced by different line resistance, where the simulation results are provided in Figs. 5(c) and 5(d). The third case is the time-delay caused by LPF, where the simulation results are shown in Figs. 5(e) and 5(f). Three BSUs consider the same capacities and different initial SoC condition (SoC_1=90%, SoC_2=80% and SoC_3=70%). Fig. 5(a) describes the SoC balance can gradually be reached by adopting the proposed method. However, the voltage deviation in Fig. 5(b) exceeds the acceptable range of ±5%. Meanwhile, the voltage drop caused by the load change cannot be restored to the pre-set value. Hence, the voltage error issue caused by the SoC-based droop control is not solved. From Fig. 5(c), the SoC balance cannot be accomplished by the proposed SoC balancing method since different voltage drop caused by the line resistance

deteriorates the equivalent power-sharing among BSUs. Moreover, the voltage deviation at steady state still exists in Fig. 5(d), and should further be minimized for better performance. From Fig. 5(e), without an LPF, the dc bus voltage is an instantaneous voltage with a high frequency band, which is not conducive to the stable operation of the system. Therefore, the LPF is required to be added to the system to remove unnecessary high-frequency parts. However, the LPF may cause time delay, hence, the relevant parameters should be selected appropriately. From Fig. 5(f), when the cut-off frequency of the LPF is selected as ω_{L1}, it takes 13.5s for the bus voltage to reach a steady state. However, when the cut-off frequency is ω_{L2} and ω_{L3}, the bus voltage only needs 2.6s to reach a steady state. Therefore, a lower cut-off frequency will cause more time delay, thereby reducing the dynamic response of the system. Finally, the cut-off frequency of this paper is 2×2π rad/s.

4.2. Case 2: SoC balancing scheme with the same capacities and different SoCs (SoC_1=90%, SoC_2=80%, SoC_3=70%)

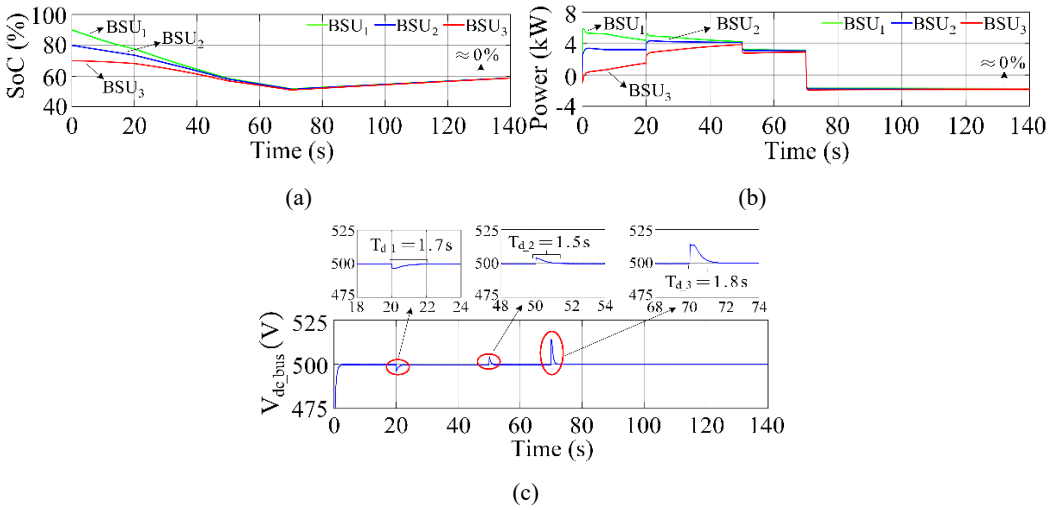

Fig. 6. Simulation results for case 2, (a) SoC of BSUs, (b) Output power of converters, (c) DC bus voltage.

In order to solve the issues in case 1, the voltage restoration loop for SoC-based droop scheme and different line resistance is considered in the proposed method. From Figs. 6(a) and 6(b), the BSUs are initially in discharging mode and then switched to charging mode. In discharging mode, BSU_1 and BSU_3, respectively, supply the highest and lowest power to the load due to their SoC level, so that the decrease rate in the SoC of BSU_1 is higher than that of BSU_3. Therefore, the SoC deviation among BSUs is gradually reduced. At 70 s, BSUs operate in charging mode. The SoC deviation progressively decreases to zero, and the power absorbed by each BSU is equivalent. Therefore, the SoC balance among BSUs can be achieved by adopting the proposed SoC balancing method. As observed in Fig. 6(c), the voltage deviation is maintained within the specified limit of ±5%.

To verify the superiority of the proposed method, the SoC balancing scheme that integrates the voltage recovery from ref. [28] is used to compare with the presented approach. The control

structure based on ref. [28] is shown in the purple dashed line in Fig. 2(c). From Figs. 7(a) and 7(b), the results of SoC balance scheme based on the voltage recovery from ref. [28] are the same as the presented method in Figs. 6(a) and 6(b). This shows that the proposed SoC balance method has good compatibility and can be combined with other control methods. However, when the load and dc bus voltage change suddenly, the voltage recovery in ref. [28] takes more time to restore the voltage to a stable state, as given in Fig. 7(c). The proposed method requires less time, as shown in Fig. 6(c). In addition, when a communication failure occurs between the primary and secondary controls at 100 s, this results in the inability to exchange data between the primary and secondary controls. Then the voltage recovery control cannot restore the voltage to the pre-set value. Therefore, the dc bus voltage has a serious voltage deviation, as given in Fig. 7(c).

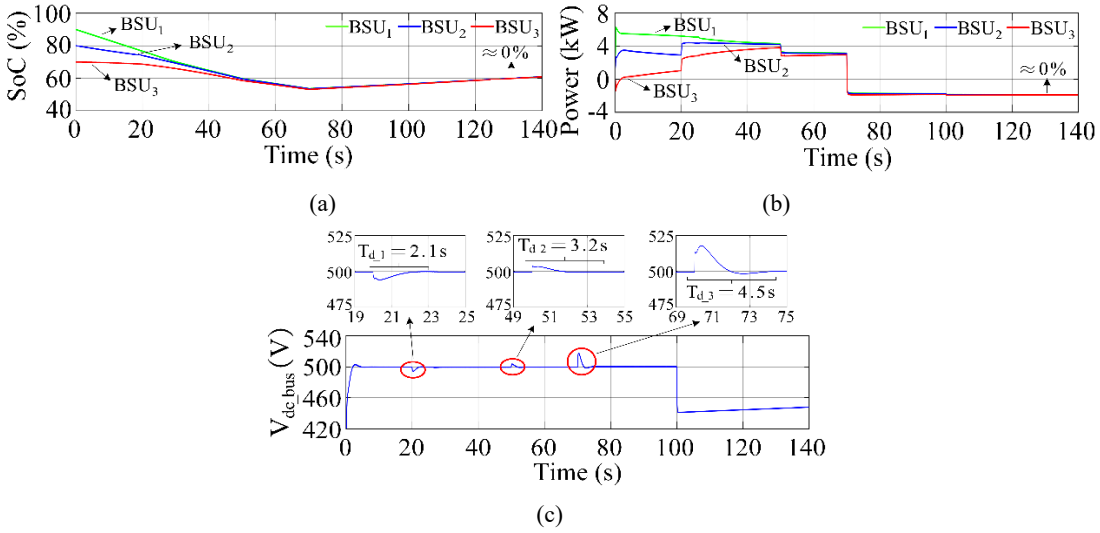

Fig. 7. Simulation results based on ref. [28] for case 2, (a) SoC of BSUs, (b) Output power of converters, (c) DC bus voltage.

4.3. Case 3: SoC balancing scheme with different capacities (BSU_1=1 Ah, BSU_2=2 Ah, AND BSU_3=3 Ah) and SoCs (SoC_1=90%, SoC_2=80%, SoC_3=70%)

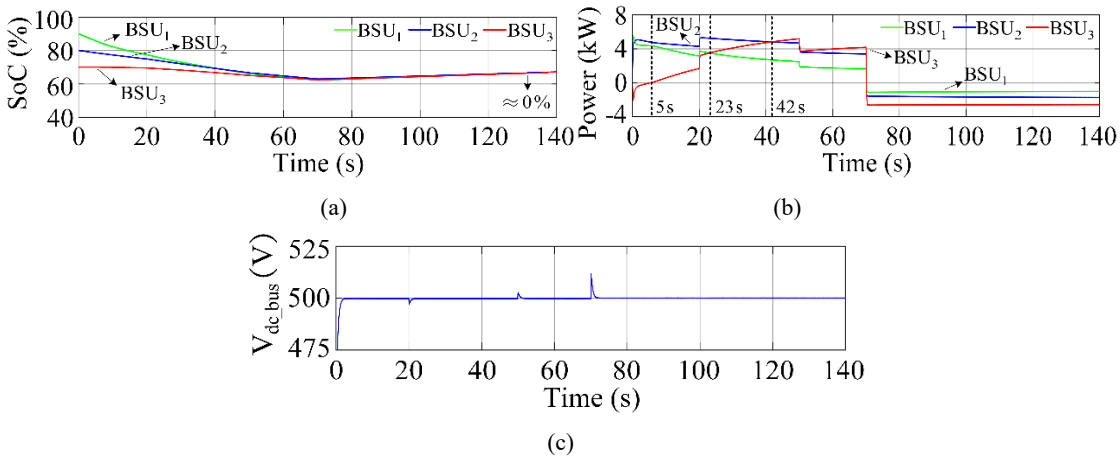

Fig. 8. Simulation results for case 3, (a) SoC of BSUs, (b) Output power of converters, (c) DC bus voltage.

In this case, the SoC balancing based droop control is tested by considering different battery capacities. From Figs. 8(a) and 8(b), although the initial SoC of BSU_1 is the highest, BSU_2

provides the maximum power from 0 to 42 s due to the capacity gap between BSUs. After 23 s, BSU_1 supplies the least amount of power due to the effect of capacity. BSU_3 absorbs a small amount of power at the beginning, and it supplies the lowest power from 5 s to 23 s. However, due to its maximum capacity, it provides the highest power after 42 s. In the following charging mode, the BSU_1 and BSU_3 absorb the lowest and highest power based on different capacities. The SoCs among BSUs gradually reaches an equilibrium value. Therefore, during the charging and discharging process, the low-capacity BSUs will not be overused, and the battery lifespan can be prolonged. Finally, Fig. 8(c) shows that the dc bus voltage is maintained within the defined range.

4.4. Case 4: SoC balancing scheme with different capacities (BSU_1=3 Ah, BSU_2=2 Ah, AND BSU_3=1 Ah) and SoCs (SoC_1=90%, SoC_2=80%, SoC_3=70%)

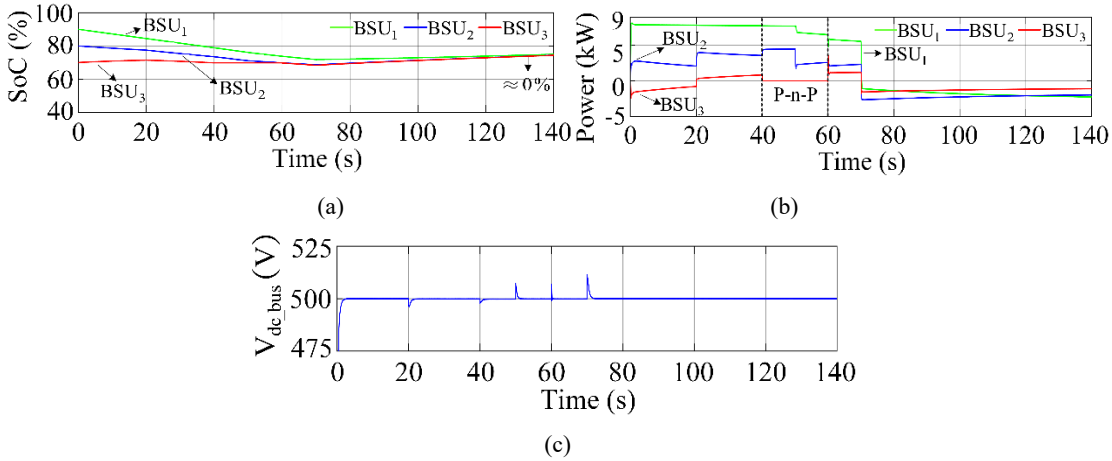

Fig. 9. Simulation results for case 4, (a) SoC of BSUs, (b) Output power of converters, (c) DC bus voltage.

BSU_1 and BSU_3 are defined to have the highest and lowest SoCs and capacities, respectively. As can be seen from Figs. 9(a) and 9(b), BSU_1 injects the highest power during discharging process. After 115 s, it absorbs the most power due to its highest capacity. At 0-20 s, BSU_3 is charged due to its minimum capacity and SoC level. In the following operation, the change in SoC of BSU_3 is the slightest. Therefore, the SoC of BSUs is balanced. Besides, plug-and-play (P-n-P) capability of the proposed method is verified. From Figs. 9(a) and 9(b), BSU_3 is disconnected from the system at 40 s. This means that BSU_3 stops supplying power to the system and the SoC of the BSU_3 stop changing. The proposed control method will automatically adjust the bus voltage and the power output of the installed BSUs, thereby ensuring the stable operation of the system. At 60 s, BSU_3 is reconnected. It can be seen from Fig. 9(b) that BSU_3 can supply power to the system normally as before disconnecting. Fig. 9(c) shows that bus voltage is restored to the acceptable range.

4.5. Case 5: compare with SoC balancing based on ref. [12]

In this case, the method in ref. [12] is used in comparison to show the advantages of the proposed approach. The simulation parameters in ref. [12] are consistent with cases 2 and 4. The results of

ref. [12] are shown in Figs. 10 and 11, which are compared with the results of case 2 and case 4, respectively. In the case of the same line resistance, SoC balance can be completed. However, when the load changes, the dc bus voltage cannot return to the initial value, as shown in Figs. 10(a) and 10(b). When the line resistance is different, the SoC balance fails to be achieved. At the same time, the deviation between the dc bus voltage and the reference value becomes larger, as given in Figs. 10(c) and 10(d). From Fig. 11(a), the SoC deviation between the BSUs cannot be narrowed when the different capacities are considered. This is because the method in ref. [12] does not consider the different capacities of the BSUs. Therefore, the SoC balance cannot be achieved. Besides, the voltage deviation still exists, as shown in Fig. 11(b).

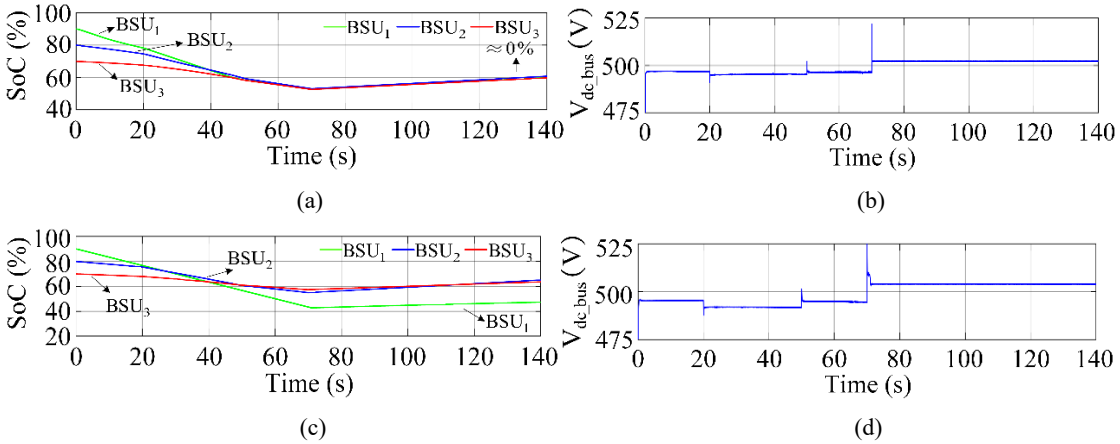

Fig. 10. Simulation results of ref. [12] for case 5, (a) SoC of BSUs with same line resistance, (b) DC bus voltage, (c) SoC of BSUs with different line resistance, (d) DC bus voltage.

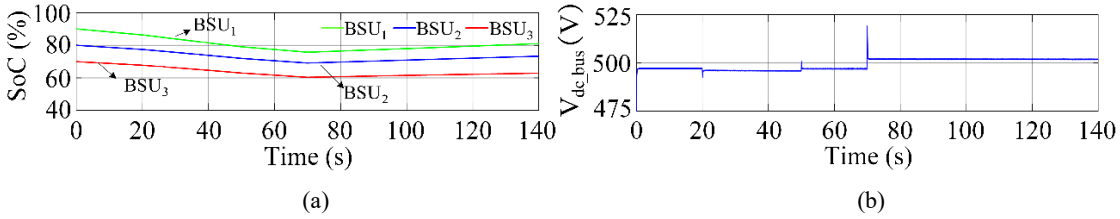

Fig. 11. Simulation results of ref. [12] for case 5, (a) SoC waveform with different BSUs' capacity, (b) DC bus voltage.

4.6. Case 6: Real controller based on PIL simulation

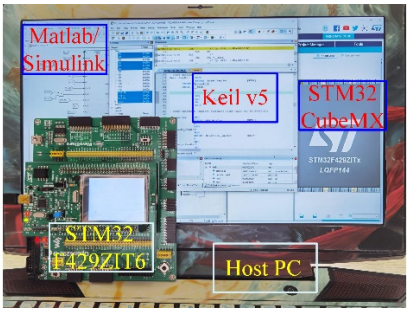

Fig. 12. Hardware and software setup.

In order to validate the feasibility of the proposed method in the real control system, a microcontroller based PIL is built. The microcontroller is implemented by using STM32F429-ZIT6, and a closed-loop simulation with the controlled object will be conducted. The hardware

and software interfaces are shown in Fig. 12. The parameters used in PIL are the same as in cases 2 and 3.

Fig. 13 shows the PIL simulation results for case 2. As can be observed, the SoC balance between BSUs can be achieved, and the bus voltage is restored to the initial value. Besides, as shown in Fig. 14, the PIL results are the same as the computer simulation results of case 3. Therefore, the proposed scheme when applied in a real control system can guarantee the expected performance.

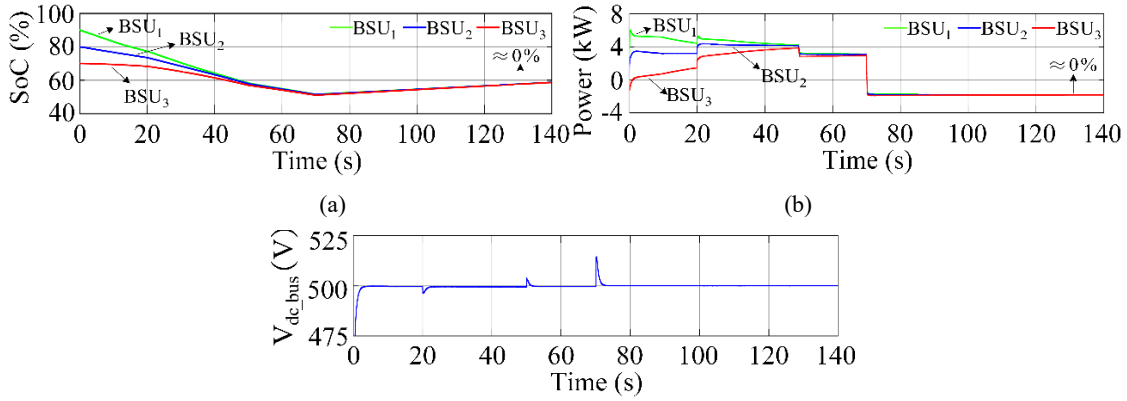

Fig. 13. PIL simulation results for case 2, (a) SoC of BSUs, (b) Output power of converters, (c) DC bus voltage.

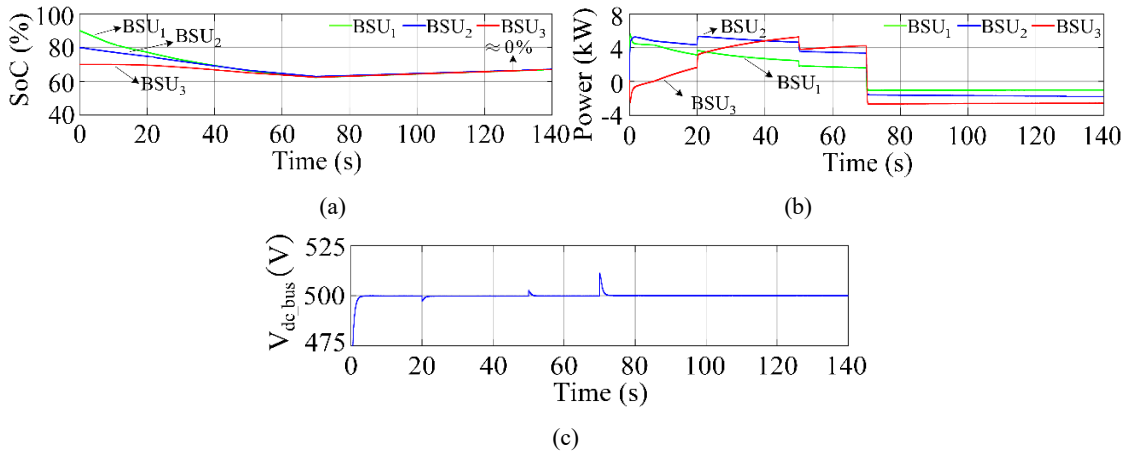

Fig. 14. PIL simulation results for case 3, (a) SoC of BSUs, (b) Output power of converters, (c) DC bus voltage.

4.7. Case 7: BSUs in DC Microgrid (BSU_1=3 Ah, BSU_2=2 Ah, AND BSU_3=1.5 Ah) AND SOCs (SOC_1=90%, SOC_2=80% AND SOC_3=70%)

The microgrid, integrated with a PV source, BSUs, pulse load and power converter load (PCL), is simulated in islanding mode, as shown in Fig. 1. The PCL consists of a buck converter and controller. The load scheduling equation is written as follows.

$$P_{Load}(t)=\begin{cases} 12\ \text{kW},\ 0\ \text{s}\le t\le 20\ \text{s}, \\ 16\ \text{kW},\ 20\ \text{s}\le t\le 30\ \text{s}, \\ 17\ \text{kW},\ 30\ \text{s}\le t\le 40\ \text{s} \\ 19\ \text{kW},\ 40\ \text{s}\le t\le 80\ \text{s}, \\ 15\ \text{kW},\ 80\ \text{s}\le t\le 100\ \text{s}, \\ 0\ \text{kW},\ 100\ \text{s}\le t\le 140\ \text{s}. \end{cases} \quad \text{(Case 7)}$$

In addition, the solar radiation and temperature data of PV source are obtained from the website of the Australian Government Bureau of Meteorology [35]. In Fig. 15(c), PV operates in maximum power point tracking (MPPT) mode. The output power of PV changes every 10 s. At the beginning, the PCL and resistive load with a total power of 12 kW are incorporated into the microgrid, as shown in Fig. 15(c). Then, 4 kW resistive load is added into the system at 20 s. During this period, BSU_1 with higher SoC and capacity provides maximum power, and BSU_3 is absorbing power to narrow the gap between SoCs due to its minimum capacity and SoC level, as shown in Fig. 15(b). From Fig. 15(c), 2 kW pulse load is connected to the system between 40-100 s. The frequency of the pulse load is set at 0.5 and 0.1 Hz during 40-60 s and 60-100 s, respectively. As observed in Fig. 15(b), the BSUs can respond to changes in pulse load at different frequencies. In addition, the proposed approach enables the BSUs to respond to changes in PV output power and load demand. From Fig. 15(c), when the output power of the PV source drops suddenly at 10 s, the BSU will quickly increase the output power to ensure the power balance of the system. At 20 s, The system load and the output power of the PV source increase simultaneously. At this time, the output power of the BSUs only slightly changes. It can be seen from Fig. 15(b) that the controller will automatically distribute power to each BSU. Besides, from Figs. 15(a) and 15(b), BSU_2 is disconnected from the system at 20 s. This means that BSU_2 no longer delivers power, hence, the SoC of BSU_2 will not change. Then, the controller will automatically regulate the output power of the other BSUs. At 30 s, 1 kW load is added to the system, the controller will distribute power to the installed BSUs. BSU_2 still does not release any power. At 40 s, BSU_2 is reconnected and able to work stably. The entire P-n-P process does not cause any negative impact on the system. After 100 s, all loads are disconnected, and the PV source charges the BSUs. From Fig. 15(a), the deviation between the SoCs of the BSUs gradually becomes smaller. Finally, the voltages of all buses between the branches of the BSUs are within the expected range, as shown in Fig. 5(d).

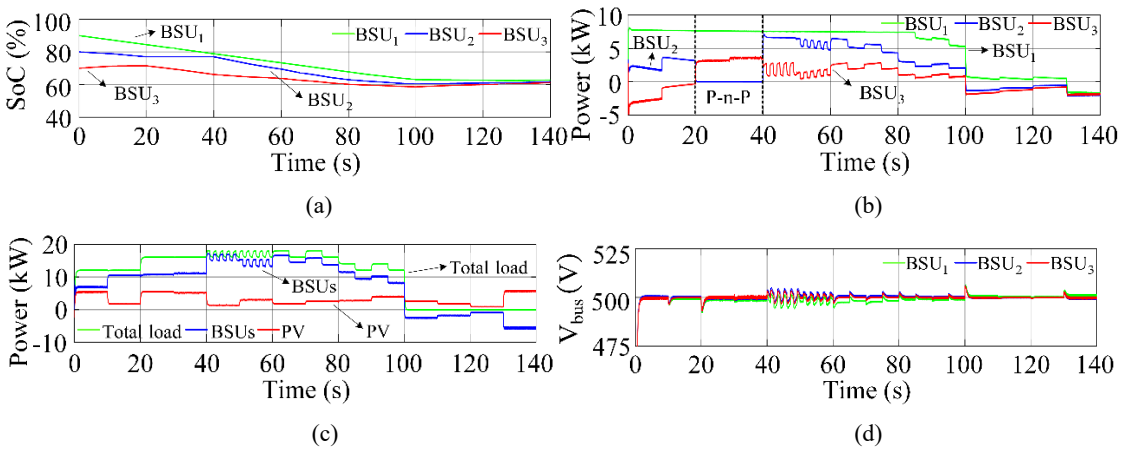

Fig. 15. Simulation results for case 7, (a) SoC of BSUs, (b) Output power of converters, (c) PV generation, total load demand and BSUs output, (d) Bus voltage for BSUs' branch.

4.8. Case 8: SoC limits for BSUs

In this paper, the safe limit of BSUs' SoC is set between 20% and 95%. In discharging mode, when the SoC of the BSUs drops to 20%, the BSUs will be forcibly charged, as shown in Figs. 16(a) and 16(b). If the system does not have additional power to charge the BSUs, the system will perform load shedding, as shown in Fig. 16(c). In charging mode, if the SoC of the BSUs reaches 95%, the BSUs are automatically discharged, as shown in Figs. 16(c) and 16(d). If the system does not have enough load demand to meet the battery discharge, the PV output power will be reduced and the system load will be increased, as shown in Fig. 16(f). Through the proposed control method, the SoC of the battery can be restricted to a safe range, thereby avoiding excessive use of the battery.

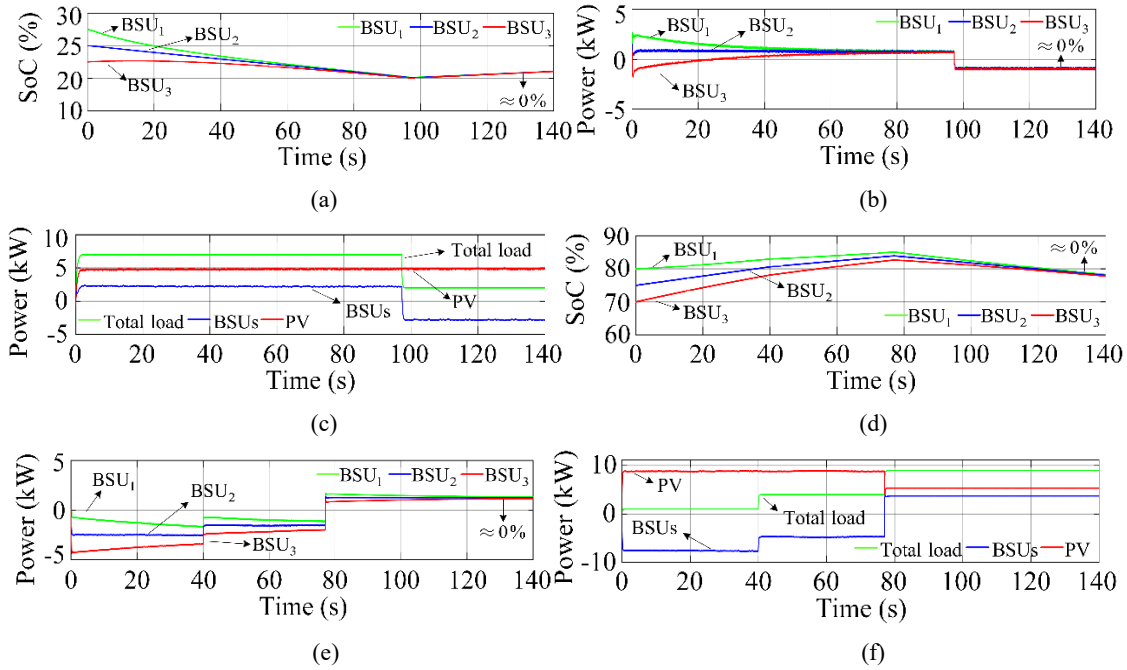

Fig. 16. Simulation results for case 8, (a) SoC of BSUs in discharging mode, (b) Output power of converters in discharging mode, (c) PV generation, total load demand and BSUs output power in discharging mode, (d) SoC of BSUs in charging mode, (e) Output power of converters in charging mode, (f) PV generation, total load demand and BSUs output power in charging mode.

5. Conclusion

The present research proposes a filter-based droop control to achieve SoC balancing by considering the different SoCs and capacities among BSUs in a dc microgrid. With the presented decentralized control algorithm, SoCs among BSUs can be balanced. Besides, the voltage deviation induced by the power droop and SoC balancing scheme can be eliminated. Moreover, the effectiveness of the proposed method is guaranteed regardless of the effect of different line resistances. Furthermore, the system stability analysis and the parameter design process are presented in detail. Finally, the performance and feasibility of the control algorithm is verified by MATLAB/Simulink and PIL simulation. The simulation results show that the proposed decentralized control scheme works satisfactorily for SoC balancing among BSUs in a dc microgrid.

Some works that have not been considered in this paper are left for future works. Therefore, future works will focus on applying this method to hybrid energy storage system (including battery and supercapacitor), while ensuring that the proposed method does not cause any adverse influences on the power-sharing between battery and supercapacitor. Besides, the state of health (SoH) of the storage device will also be taken into account in the hybrid energy storage system.

References

[1] R. Zamora and A. K. Srivastava, "Controls for microgrids with storage: Review, challenges, and research needs," *Renew. Sustain. Energy Rev.*, vol. 14, no. 7, pp. 2009–2018, 2010, doi: 10.1016/j.rser.2010.03.019.

[2] D. E. Olivares *et al.*, "Trends in microgrid control," *IEEE Trans. Smart Grid*, vol. 5, no. 4, pp. 1905–1919, 2014, doi: 10.1109/TSG.2013.2295514.

[3] X. Lu, J. M. Guerrero, K. Sun, and J. C. Vasquez, "An improved droop control method for dc microgrids based on low bandwidth communication with dc bus voltage restoration and enhanced current sharing accuracy," *IEEE Trans. Power Electron.*, vol. 29, no. 4, pp. 1800–1812, 2014, doi: 10.1109/TPEL.2013.2266419.

[4] T. Dragicevic, X. Lu, J. C. Vasquez, and J. M. Guerrero, "DC Microgrids - Part I: A Review of Control Strategies and Stabilization Techniques," *IEEE Trans. Power Electron.*, vol. 31, no. 7, pp. 4876–4891, 2016, doi: 10.1109/TPEL.2015.2478859.

[5] J. M. Guerrero, J. C. Vasquez, J. Matas, L. G. De Vicuña, and M. Castilla, "Hierarchical control of droop-controlled AC and DC microgrids - A general approach toward standardization," *IEEE Trans. Ind. Electron.*, vol. 58, no. 1, pp. 158–172, 2011, doi: 10.1109/TIE.2010.2066534.

[6] O. Cornea, G. D. Andreescu, N. Muntean, and D. Hulea, "Bidirectional Power Flow Control in a DC Microgrid Through a Switched-Capacitor Cell Hybrid DC-DC Converter," *IEEE Trans. Ind. Electron.*, vol. 64, no. 4, pp. 3012–3022, 2017, doi: 10.1109/TIE.2016.2631527.

[7] T. Morstyn, B. Hredzak, and V. G. Agelidis, "Control Strategies for Microgrids with Distributed Energy Storage Systems: An Overview," *IEEE Trans. Smart Grid*, vol. 9, no. 4, pp. 3652–3666, 2018, doi: 10.1109/TSG.2016.2637958.

[8] M. Faisal, M. A. Hannan, P. J. Ker, A. Hussain, M. Bin Mansor, and F. Blaabjerg, "Review of energy storage system technologies in microgrid applications: Issues and challenges," *IEEE Access*, vol. 6, pp. 35143–35164, 2018, doi: 10.1109/ACCESS.2018.2841407.

[9] X. Lu, K. Sun, J. M. Guerrero, J. C. Vasquez, and L. Huang, "State-of-charge balance using adaptive droop control for distributed energy storage systems in DC microgrid applications," *IEEE Trans. Ind. Electron.*, vol. 61, no. 6, pp. 2804–2815, 2014, doi: 10.1109/TIE.2013.2279374.

[10] S. Li, C. C. Mi, and M. Zhang, "A high-efficiency active battery-balancing circuit using

multiwinding transformer," *IEEE Trans. Ind. Appl.*, vol. 49, no. 1, pp. 198–207, 2013, doi: 10.1109/TIA.2012.2229455.

[11] X. Lu, K. Sun, J. M. Guerrero, J. C. Vasquez, and L. Huang, "Double-quadrant state-of-charge-based droop control method for distributed energy storage systems in autonomous DC Microgrids," *IEEE Trans. Smart Grid*, vol. 6, no. 1, pp. 147–157, 2015, doi: 10.1109/TSG.2014.2352342.

[12] T. R. Oliveira, W. W. A. Gonçalves Silva, and P. F. Donoso-Garcia, "Distributed secondary level control for energy storage management in DC microgrids," *IEEE Trans. Smart Grid*, vol. 8, no. 6, pp. 2597–2607, 2017, doi: 10.1109/TSG.2016.2531503.

[13] D. Xu, W. Zhang, B. Jiang, P. Shi, and S. Wang, "Directed-Graph-Observer-Based Model-Free Cooperative Sliding Mode Control for Distributed Energy Storage Systems in DC Microgrid," *IEEE Trans. Ind. Informatics*, vol. 16, no. 2, pp. 1224–1235, 2020, doi: 10.1109/TII.2019.2933227.

[14] K. D. Hoang and H. H. Lee, "Accurate power sharing with balanced battery state of charge in distributed DC microgrid," *IEEE Trans. Ind. Electron.*, vol. 66, no. 3, pp. 1883–1893, 2019, doi: 10.1109/TIE.2018.2838107.

[15] T. Morstyn, A. V. Savkin, B. Hredzak, and V. G. Agelidis, "Multi-agent sliding mode control for state of charge balancing between battery energy storage systems distributed in a DC Microgrid," *IEEE Trans. Smart Grid*, vol. 9, no. 5, pp. 4735–4743, 2018, doi: 10.1109/TSG.2017.2668767.

[16] C. Li, T. Dragicevic, M. G. Plaza, F. Andrade, J. C. Vasquez, and J. M. Guerrero, "Multiagent based distributed control for state-of-charge balance of distributed energy storage in DC microgrids," *IECON Proc. (Industrial Electron. Conf.*, pp. 2180–2184, 2014, doi: 10.1109/IECON.2014.7048804.

[17] Y. Guan, L. Meng, C. Li, J. C. Vasquez, and J. M. Guerrero, "A dynamic consensus algorithm to adjust virtual impedance loops for discharge rate balancing of AC microgrid energy storage units," *IEEE Trans. Smart Grid*, vol. 9, no. 5, pp. 4847–4860, 2018, doi: 10.1109/TSG.2017.2672882.

[18] Y. Han, K. Zhang, H. Li, and J. M. Guerrero, "MAS-Based Distributed Coordinated Control and Optimization in Microgrid and Microgrid Clusters: A Comprehensive Overview," *IEEE Trans. Power Electron.*, vol. 33, no. 8, pp. 6488–6508, 2018, doi: 10.1109/TPEL.2017.2761438.

[19] J. M. Guerrero, M. Chandorkar, T. L. Lee, and P. C. Loh, "Advanced control architectures for intelligent microgridspart i: Decentralized and hierarchical control," *IEEE Trans. Ind. Electron.*, vol. 60, no. 4, pp. 1254–1262, 2013, doi: 10.1109/TIE.2012.2194969.

[20] J. M. Rey, C. X. Rosero, M. Velasco, P. Martí, J. Miret, and M. Castilla, "Local Frequency Restoration for Droop-Controlled Parallel Inverters in Islanded Microgrids," *IEEE Trans. Energy Convers.*, vol. 34, no. 3, pp. 1232–1241, 2019, doi: 10.1109/TEC.2018.2886267.

[21] X. Sun, Y. Hao, Q. Wu, X. Guo, and B. Wang, “A Multifunctional and Wireless Droop Control for Distributed Energy Storage Units in Islanded AC Microgrid Applications,” *IEEE Trans. Power Electron.*, vol. 32, no. 1, pp. 736–751, 2017, doi: 10.1109/TPEL.2016.2531379.

[22] Q. Wu, R. Guan, X. Sun, Y. Wang, and X. Li, “SoC balancing strategy for multiple energy storage units with different capacities in islanded microgrids based on droop control,” *IEEE J. Emerg. Sel. Top. Power Electron.*, vol. 6, no. 4, pp. 1932–1941, 2018, doi: 10.1109/JESTPE.2018.2789481.

[23] D. Li, Z. Wu, B. Zhao, and L. Zhang, “An improved droop control for balancing state of charge of battery energy storage systems in AC microgrid,” *IEEE Access*, vol. 8, pp. 71917–71929, 2020, doi: 10.1109/ACCESS.2020.2987098.

[24] N. L. Diaz, T. Dragicevic, J. C. Vasquez, and J. M. Guerrero, “Intelligent distributed generation and storage units for DC microgrids - A new concept on cooperative control without communications beyond droop control,” *IEEE Trans. Smart Grid*, vol. 5, no. 5, pp. 2476–2485, 2014, doi: 10.1109/TSG.2014.2341740.

[25] N. Zhi, K. DIng, L. Du, and H. Zhang, “An SOC-Based Virtual DC Machine Control for Distributed Storage Systems in DC Microgrids,” *IEEE Trans. Energy Convers.*, vol. 35, no. 3, pp. 1411–1420, 2020, doi: 10.1109/TEC.2020.2975033.

[26] G. A. H. Pawitan and J. S. Kim, “MPC-Based Power Management of Renewable Generation Using Multi-ESS Guaranteeing SoC Constraints and Balancing,” *IEEE Access*, vol. 8, pp. 12897–12906, 2020, doi: 10.1109/ACCESS.2019.2962807.

[27] Y. Xia, M. Yu, P. Yang, Y. Peng, and W. Wei, “Generation-Storage Coordination for Islanded DC Microgrids Dominated by PV Generators,” *IEEE Trans. Energy Convers.*, vol. 34, no. 1, pp. 130–138, 2019, doi: 10.1109/TEC.2018.2860247.

[28] E. K. Belal, D. M. Yehia, and A. M. Azmy, “Adaptive droop control for balancing SOC of distributed batteries in DC microgrids,” *IET Gener. Transm. Distrib.*, vol. 13, no. 20, pp. 4667–4676, 2019, doi: 10.1049/iet-gtd.2018.6849.

[29] Q. Shafiee, J. M. Guerrero, and J. C. Vasquez, “Distributed secondary control for islanded microgrids-a novel approach,” *IEEE Trans. Power Electron.*, vol. 29, no. 2, pp. 1018–1031, 2014, doi: 10.1109/TPEL.2013.2259506.

[30] Y. Xia, W. Wei, Y. Peng, P. Yang, and M. Yu, “Decentralized coordination control for parallel bidirectional power converters in a grid-connected DC microgrid,” *IEEE Trans. Smart Grid*, vol. 9, no. 6, pp. 6850–6861, 2018, doi: 10.1109/TSG.2017.2725987.

[31] J. C. Vasquez, J. M. Guerrero, M. Savaghebi, J. Eloy-Garcia, and R. Teodorescu, “Modeling, analysis, and design of stationary-reference-frame droop-controlled parallel three-phase voltage source inverters,” *IEEE Trans. Ind. Electron.*, vol. 60, no. 4, pp. 1271–1280, 2013, doi: 10.1109/TIE.2012.2194951.

[32] S. Bacha, I. Munteanu, and A. I. Bratcu, *Power Electronic Converters Modelling and*

Control, no. 9781447154778. 2014. [Online]. Available: http://link.springer.com/10.1007/978-1-4471-5478-5_1

[33] Q. Xu *et al.*, "A Decentralized Dynamic Power Sharing Strategy for Hybrid Energy Storage System in Autonomous DC Microgrid," *IEEE Trans. Ind. Electron.*, vol. 64, no. 7, pp. 5930–5941, 2017, doi: 10.1109/TIE.2016.2608880.

[34] S. Liu *et al.*, "220GHz band-pass filter based on circular resonance cavities with low loss," *Eur. Microw. Week 2015 "Freedom Through Microwaves", EuMW 2015 - Conf. Proceedings; 2015 45th Eur. Microw. Conf. Proceedings, EuMC*, vol. 2, no. 1, pp. 1077–1079, 2015, doi: 10.1109/EuMC.2015.7345954.

[35] Australian Bureau of Meteorology, "Australian Government Bureau of Meteorology," *Australian Bureau of Meteorology*, 2020. http://www.bom.gov.au/index.php (accessed Oct. 05, 2020).

Chapter 4: A comprehensive multi-functional controller for hybrid energy storage systems in DC microgrids

Citation:

X. Lin, R. Zamora, and C. Baguley, "A comprehensive multi-functional controller for hybrid energy storage systems in DC microgrids," *IEEE Trans. Ind. Appl*. **(Under first review)**

Preamble:

Chapter 3 has presented a fully decentralized control system applied to battery energy storage systems in DC microgrids. However, as discussed in Chapter 4, the battery energy storage system is a kind of energy storage with high energy density, which cannot respond quickly to high-frequency changes in system load. Therefore, a hybrid energy storage system (HESS) adds supercapacitors (SCs) to solve this problem. In Chapter 4, a droop-based coordinated control is proposed to regulate the battery and SC. Among them, the v-dP droop control is proposed to regulate the battery converter to provide the average power, while the traditional v-P droop control is adopted to adjust the SC converter to provide the instantaneous power. This coordinated control also enables voltage regulation without any additional voltage control loops, aiming to simplify the overall controller. This chapter also proposes a consensus algorithm-based voltage compensator to achieve accurate power sharing and state of charge (SoC) balancing between batteries. Then, a SoC recovery of the SC is used to ensure that the SC has enough energy for future use. Finally, this chapter also proposes a power management system to keep the SoCs of the batteries within a safe range.

Abstract:

This article proposes a comprehensive multi-functional controller for a hybrid energy storage system (HESS), including a battery and supercapacitor (SC). In the presented method, a V-dP is proposed to control the output power of the battery converter with a slow dynamic response. The traditional V-P droop is employed to regulate the SC converter to give a fast response. The dc bus voltage can be maintained in a safe range by the SC converter control so that no voltage recovery loop is required. Hence, the order of the overall control system and the complexity of parameter design can be reduced. In addition, a novel consensus-based voltage compensator is proposed to achieve the state of charge (SoC) balance and accurate power sharing among batteries. Then, an SoC restoration of the SC is used to address the leakage current and ensure sufficient energy for future use. Next, a power management scheme (PMS) is proposed to protect the batteries from over-use under different operating modes. Finally, the output impedance characteristics, control system design, and stability analysis are elaborated. The processor in the loop (PIL) simulation results verified the effectiveness and feasibility of the proposed control method.

1. Introduction

Nowadays, dc microgrid is receiving more attention due to the increasing penetration of dc power sources, such as photovoltaic (PV) sources. Energy storage systems (ESSs) are an integral part of a dc microgrid that can suppress power fluctuations caused by the mismatch between power generation and demand [1], [2]. ESSs can be implemented using a variety of energy storage types, with each type having distinct characteristics that enable the realization of specific benefits [3]. For example, batteries with a slow dynamic response and a high energy density, may be employed to supply load power in steady state [4]. Conversely, supercapacitors (SCs), with a fast dynamic response but a low energy density, may be employed to serve loads with high power fluctuations [5]. No existing energy storage type has characteristics that suit all load and user demands. Therefore, hybrid energy storage systems (HESS), comprising multiple energy storage types have been proposed as an effective solution [6].

Many published works have presented various control methods for HESS research [7]–[11]. In [7], a frequency-coordinating virtual impedance control scheme is proposed to accomplish transient power allocations in HESS. However, the method fails to consider the bus voltage deviations. In [9], a novel energy management system is proposed for the grid-connected HESS under different operating modes. With the proposed method, the power sharing between battery and SC can be effectively achieved. Besides, the output power of the battery in HESS is based on the SoC level. Therefore, the over-use of the battery can be avoided. However, the methods mentioned above only use a single HESS to suppress the power fluctuations. As a result, the load pressure of the HESS will be increased, thereby reducing the service life of the ESS components.

To solve these shortcomings, control methods for multiple HESSs have also been studies in [12]–[17]. A novel droop control in [12] is proposed to achieve different dynamic power-sharing for multiple HESSs. By using this method, a conventional *V-P* droop control is used to regulate the battery converter to deliver the lower-frequency power, while an integral droop control is used to regulate the SC converter to supply the higher-frequency power. However, the proposed method does not consider the issue of the bus voltage deviation. In [13], a decentralized power management scheme (PMS) for HESSs is proposed to realize the power-split, voltage recovery and SoC of SC restoration. However, the order of overall control system is higher. In [15], an advanced secondary voltage recovery control is proposed for a battery and SC system in dc microgrid. In presented method, a voltage restoration based on consensus algorithm is used to maintain the dc bus voltage within the acceptable range. Another voltage recovery control is used to restore the SoC of the SC to pre-set value. In [16] and [17], a semi-consensus strategy is designed to implement the power sharing, SoC balance among batteries, and SoC restoration of SCs. Within the semi-consensus scheme, only the local controllers for batteries exchange data through a sparse communication link. However, the controllers for SCs do not need to carry out

the data exchange process, thus saving the system investment cost. In [18], a coordinated droop control is proposed to achieve power sharing and voltage recovery without the need for a voltage compensation loop. Besides, the proposed method can achieve SoC recovery of the SCs and SoC balance of batteries, as well as can ensure that SoCs of batteries are within a safe range. The aforementioned approaches do not take into account the inaccurate power distribution between energy stores caused by different line resistances, which degrades the performance of SoC balancing. Besides, the methods in [13]–[17] require a voltage compensation loop to eliminate voltage errors. However, the voltage compensation loop increases the complexity of the design of the system control parameters. Also, the methods in [13]–[17] ignore the protection of the battery, which may lead to excessive use of the battery. In addition, the method of [18] amplifies the noise of the system, thereby reducing the stability of the system.

To solve these drawbacks, a comprehensive multi-functional controller for HESSs in dc microgrid is proposed in this paper. The major contributions of this article can be summarized as follows:

a) A V-dP control is proposed to regulate the battery converter, while the traditional V-P droop method is employed to adjust the SC converter. By adopting the proposed method, the system power will be divided into low- and high-frequency parts, and distributed to the battery and SC, respectively. The bus voltage is regulated by the SC converter, hence, there is no need for any voltage recovery control. Therefore, the order of the control system and the complexity of parameter design are reduced.
b) A novel consensus-based voltage compensator including SoC balance and accurate power sharing schemes is proposed to eliminate the SoC imbalance among batteries and the adverse influence of the different line resistances. The voltage compensation control of the SC is employed to solve the leakage current and to guarantee sufficient energy for continuous operation.
c) The proposed PMS can protect batteries from over-use under different operating modes, including islanded, grid-connected, and plug-and-play (PnP) modes.
d) The impedance characteristics of the proposed strategy are analyzed in the frequency domain, and the root locus method is adopted to show system stability.

The rest of this paper is organized as follows. Section II presents the local control methods. Section III describes the consensus-based power compensator. In Section IV, the PMS is proposed for HESS. The parameter design and stability analysis of the proposed control methods are explained in detail in Section V. Section VI presents simulation results and discussions. The conclusions are presented in Section VII.

2. Proposed local control methods

2.1. System description

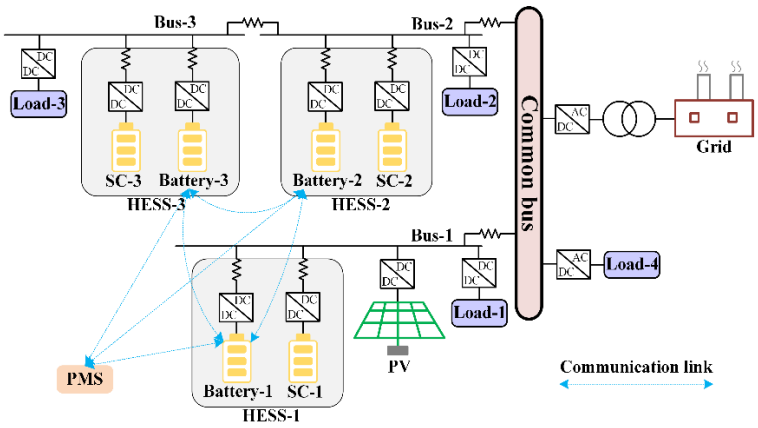

Fig. 1. The configuration of dc microgrid with the integration of HESSs.

Fig. 1. depicts a dc microgrid, which consists of renewable energy sources (RESs) such as PVs, multiple HESSs, and loads. PVs operate in maximum power point tracking (MPPT) and constant voltage control (CVC) modes. HESSs can suppress power fluctuations and maintain bus voltages. The PMS can ensure the SoC of the batteries within a safe horizon, thereby preventing batteries overuse.

2.2. *V*-dP and *V*-*P* droop controls

The *V*-d*P* control is discovered from the inductor characteristic, which appears as a short circuit at low-frequency and as an open-circuit at high frequency. Therefore, the battery converter can be controlled to provide low dynamic power instead of transient power at steady state. Based on the inductor characteristic, the relationship between inductor current and voltage can be written as (1).

$$i = i_o - \frac{1}{L}\int v_L dt \tag{1}$$

where L, i_o, i, and v_L are inductance, inductor initial current, the output current and voltage of the inductor, respectively. Then, (1) can be further modified as (2).

$$v_L = v_o - L\frac{di}{dt} \tag{2}$$

where $v_o = Ldi_o/dt$. The second term of (2) acts as an LPF that can filter out the high-frequency current. Similar to (2), the *V*-d*P* control shown in (3) is designed by replacing current with power and retaining the equivalent format as (2).

$$v_{b,j} = v_r - m\frac{dP_{b,j}}{dt} \tag{3}$$

where v_r, m, $v_{b,j}$, and $P_{b,j}$ are the reference voltage, droop coefficient, output voltage and power of the j^{th} battery converter, (j = 1, 2, …, N). The method in (3) contains a derivative term that amplifies system noise in the frequency domain. Therefore, (3) is further modified to (4).

$$P_{b,j} = \int \frac{v_r - v_{b,j}}{m} dt. \tag{4}$$

From (4), the derivative term has been eliminated. Besides, the ratio of output power to input voltage will be delivered to the current controller as the reference current. Therefore, the battery controller does not require a voltage controller, thereby simplifying the complexity of the control system.

The *V-P* droop control of the SC can be represented by (5) based on [19].

$$v_{\text{sc},j} = v_r - nP_{\text{sc},j} \tag{5}$$

where $v_{\text{sc},j}$ and $P_{\text{sc},j}$ are the output voltage and power of the j^{th} SC converter terminal, respectively. n is the droop coefficient that can be calculated by (6).

$$n = \frac{v_{\max} - v_{\min}}{P_{\text{sc},j}^{\max}} \tag{6}$$

where $v_{\min}$ and $v_{\max}$ are the minimum and maximum allowable dc bus voltage; $P_{\text{sc},j}^{\max}$ is the maximum transient power of the SC converter. Since the battery and SC can simultaneously meet the different dynamic power demands of the system, the total output power $P_{t,j}$ of HESS is the sum of the $P_{b,j}$ and $P_{\text{sc},j}$, as given in (7).

$$P_{t,j} = P_{b,j} + P_{\text{sc},j}. \tag{7}$$

By considering (4), (5), and (7), the power-split in the HESS can be written as (8).

$$\begin{cases} P_{b,j} = G_{\text{LPF}}(s) \cdot P_{t,j} = \dfrac{n}{ms+n} P_{t,j} \\ P_{\text{sc},j} = G_{\text{HPF}}(s) \cdot P_{t,j} = \dfrac{ms}{ms+n} P_{t,j}. \end{cases} \tag{8}$$

It can be seen from (8) that the essence of coordinated droop control is to form the low-pass filter (LPF) $G_{\text{LPF}}(s)$ and high-pass filter (HPF) $G_{\text{HPF}}(s)$ in HESS. Therefore, the output power of HESS can be automatically divided into low- and high-frequency parts, and then assigned each of them to the battery converter and SC converter, respectively. The desired power-sharing can be achieved by reasonably adjusting the corner frequency $\omega_c = n/m$ of both LPF and HPF.

2.3. Voltage recovery method

The characteristic of traditional *V-P* droop control is that power variations will cause bus voltage errors. In other words, if the power is constant, then the bus voltage will not change. Since SC converter only provides transient power instead of continuous power, the bus voltage can be restored to the set value at steady state, no extra control is required. In the case of a sudden power change, the SC converter will immediately respond to suppress the power fluctuation of the system. Based on (6), the maximum voltage deviation Δv is expressed as (9).

$$\Delta v = v_{\max} - v_{\min} \geq nP_{\mathrm{sc},j}^{\max} > 0. \tag{9}$$

From (9), the voltage change caused by the SC converter releasing/absorbing transient power will not be greater than the maximum voltage deviation.

After mitigating the power oscillation, the SC converter starts to slowly decrease its output power. When it reaches steady state, the SC converter no longer provides any output power to the system. Based on (5), the output voltage of the SC converter is equal to the reference bus voltage, as shown in (10).

$$v_{\mathrm{sc},j} = v_r. \tag{10}$$

Therefore, the bus voltage deviation is equal to zero, as given in (11).

$$\Delta v = v_{\max} - v_{\min} = nP_{\mathrm{sc},j}^{\max} = 0. \tag{11}$$

Finally, the bus voltage can be maintained within a safe range without the need for an additional voltage compensation loop.

2.4. Voltage recovery control for SCs

Due to the current leakage characteristics of the SC, the SoC of the SC will be reduced. To solve this problem, the *V-P* droop control with the SoC recovery is presented as (12).

$$v_{\mathrm{sc},j} = v_r - nP_{\mathrm{sc},j} - (k_{\mathrm{sc},j}^{p} + k_{\mathrm{sc},j}^{i}\frac{1}{s})(v_{\mathrm{sc},j}^{r} - v_{\mathrm{sc},j}^{\mathrm{in}}) \tag{12}$$

where $v_{\mathrm{sc},j}^{r}$ and $v_{\mathrm{sc},j}^{\mathrm{in}}$ are the reference and measured input voltage for the SC, respectively; $k_{\mathrm{sc},j}^{p}$ and $k_{\mathrm{sc},j}^{i}$ are the control parameters for the SC recovery method, respectively.

3. Consensus-based voltage compensator

In HESS, the batteries are employed to provide continuous power at steady state. For batteries, the SoC imbalance is a significant issue, which results in the over-charging and -discharging of a certain battery. In addition, different line resistances can lead to inaccurate power among

batteries, it may result in SoC balance not being successfully achieved. To address these issues, the consensus-based voltage compensator is proposed in this article.

3.1. Distributed consensus algorithm

A distributed consensus algorithm is an update rule that enables the status of distributed agents to be consistent by exchanging the information through sparse communication network [20]. In case of the HESSs, the distributed agents update their information status based on information gathered from neighbors. According to the information status of the distributed agents, the consensus algorithm generates a uniform value, which is sent as a control signal to the controllers of the distributed agents [21]. A distributed consensus algorithm is expressed as (13) – (14) based on [22].

$$h_j(k+1) = h_j(0) + \varepsilon \sum_{l \in N_j} \delta_{jl}(k+1) \tag{13}$$

$$\delta_{jl}(k+1) = \delta_{jl}(k) + a_{jl}\left[h_l(k) - h_j(k)\right] \tag{14}$$

where k is an iteration counter value. $h_j(k+1)$ is the information status of iteration at $k+1$ for j^{th} agent. N_j is the set of the agents that connect with j^{th} agent. $\delta_{jl}(k)$ is a variable, which can store cumulative difference between two agents j and l, and $\delta_{jl}(0) = 0$. a_{jl} is connection status between agents j and l. If agent j and agent l are not neighbors, then $a_{jl} = 0$, otherwise $a_{jl} = 1$. ε is used to regulate the convergence speed, which can be calculated by (15) based on [23].

$$\varepsilon = \frac{2}{\beta_1(L) + \beta_{n-1}(L)} \tag{15}$$

where $\beta_j(\cdot)$ is the j^{th} largest eigenvalue of the symmetric matrix. L is the Laplacian matrix; more detail can be found in [24].

3.2. Consensus-based voltage compensator for batteries

The consensus-based voltage compensator as defined by (16) – (17) is applied.

$$P_{b,j} = \int \frac{v_r - (v_{b,j} + \delta v_j)}{m} dt \tag{16}$$

$$\delta v_j = \delta v_{\text{SoC},j} - \delta v_{\text{acc.},j} \tag{17}$$

where δv_j is the voltage compensation term. $\delta v_{\text{SoC},j}$ and $\delta v_{\text{acc.},j}$ are used to adjust the setting voltage. $\delta v_{\text{SoC},j}$ is the consensus-based SoC balancing control, which is written as (18) – (20).

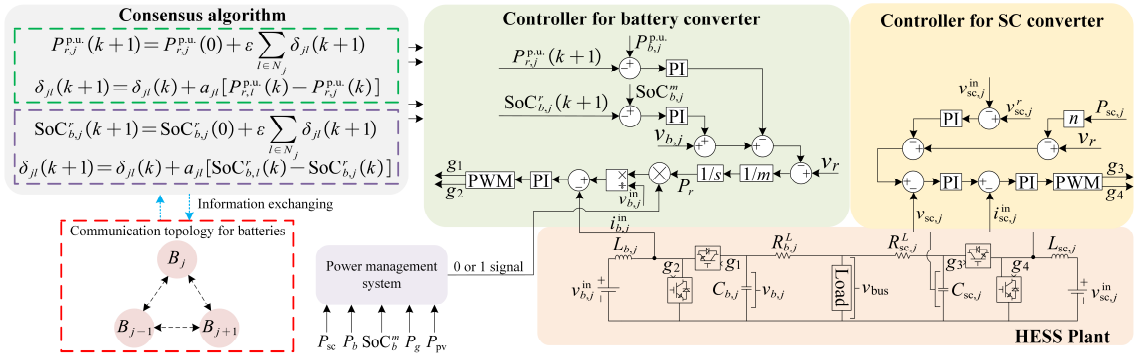

Fig. 2. The schematic diagram of the proposed control system for battery and SC converters.

$$\delta v_{\mathrm{SoC},j} = \left[\mathrm{SoC}^{r}_{b,j}(k{+}1) - \mathrm{SoC}^{m}_{b,j}\right]\left(k^{p}_{\mathrm{SoC},j} + k^{i}_{\mathrm{SoC},j}\frac{1}{s}\right) \tag{18}$$

$$\mathrm{SoC}^{r}_{b,j}(k{+}1) = \mathrm{SoC}^{r}_{b,j}(0) + \varepsilon \sum_{l\in N_j} \delta_{jl}(k{+}1) \tag{19}$$

$$\delta_{jl}(k{+}1) = \delta_{jl}(k) + a_{jl}\left[\mathrm{SoC}^{r}_{b,l}(k) - \mathrm{SoC}^{r}_{b,j}(k)\right] \tag{20}$$

where $\mathrm{SoC}^{r}_{b,j}(k{+}1)$ and $\mathrm{SoC}^{m}_{b,j}$ are the reference and measured SoC of the j^{th} battery. $\mathrm{SoC}^{r}_{b,j}(0)$ is the initial SoC level. $k^{p}_{\mathrm{SoC},j}$ and $k^{i}_{\mathrm{SoC},j}$ are the proportional and integral parameters for the SoC balancing scheme.

The consensus-based accurate power control $\delta v_{\mathrm{acc.},j}$ is presented as (21) – (23).

$$\delta v_{\mathrm{acc.},j} = \left[P^{\mathrm{p.u.}}_{r,j}(k{+}1) - P^{\mathrm{p.u.}}_{b,j}\right]\left(k^{p}_{\mathrm{acc.},j} + k^{i}_{\mathrm{acc.},j}\frac{1}{s}\right) \tag{21}$$

$$P^{\mathrm{p.u.}}_{r,j}(k{+}1) = P^{\mathrm{p.u.}}_{r,j}(0) + \varepsilon \sum_{l\in N_j} \delta_{jl}(k{+}1) \tag{22}$$

$$\delta_{jl}(k{+}1) = \delta_{jl}(k) + a_{jl}\left[P^{\mathrm{p.u.}}_{r,l}(k) - P^{\mathrm{p.u.}}_{r,j}(k)\right] \tag{23}$$

where $P^{\mathrm{p.u.}}_{r,j}(k{+}1)$ is the reference power in per unit. It should be noted that the per unit power is the ratio of the reference power to the maximum power ($P_{\max}$) of the battery converter. $P^{\mathrm{p.u.}}_{r,j}(0)$ is the initial output power of the battery converter. $k^{p}_{\mathrm{acc.},j}$ and $k^{i}_{\mathrm{acc.},j}$ are the proportional and integral parameters for the accurate power controller, respectively. The control equivalent diagram is shown in Fig. 2. Besides, the proposed method requires a sparse communication system. Therefore, the transfer function of the communication delay can be expressed as (24).

$$G_d = \frac{1}{\tau s + 1} \tag{24}$$

where τ is the communication delay.

4. Proposed PMS

The proposed PMS can ensure that the SoCs of the batteries are within a preset range. The equivalent circuit and flow chart of the proposed PMS is given in Figs. 2 and 3. It is worth noting that the SoC recovery loop of the SCs can ensure that the SoCs of the SCs are within a predetermined range. Therefore, PMS does not consider the SoC limitations of the SCs.

In the islanded mode, the dc bus voltage is regulated by the SC converters. The system power balance can be expressed as (25).

$$P_{\text{pv}} + P_b + P_{\text{sc}} = P_{\text{load}} + P_{\text{loss}} \tag{25}$$

where P_{load} is the load power; P_{loss} is the power loss caused by the line impedance and the converters. The upper limit (SoC_h) and lower limit (SoC_l) can ensure the safe operation of the batteries.

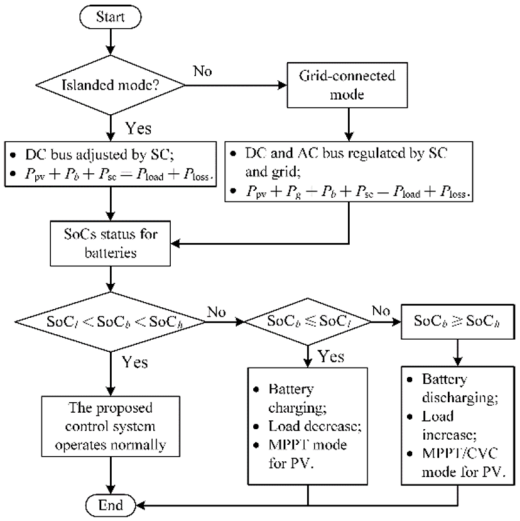

Fig. 3. The proposed PMS for HESSs.

Based on the SoC limits, the following three conditions are considered for the islanded mode:

1) $\text{SoC}_l < \text{SoC}_b < \text{SoC}_h$: the HESS operates normally. The SCs supply the transient power, while the batteries provide the average power. The SoC imbalance among batteries is eliminated by the proposed consensus-based voltage compensator.
2) $\text{SoC}_b \geq \text{SoC}_h$: the batteries operate in discharging mode. If the power supplied by the PV and batteries is greater than the power demand, then the system will decrease the generated power. Besides, the PV controller will be switched from MPPT to CVC to reduce output power. It should be noted that this article focuses on the HESS control system rather than the PV system. Therefore, the control structure diagram of the PV system will not be given. However, ref. [25] can be referred for more detail information.

3) $\mathrm{SoC}_b \leq \mathrm{SoC}_l$: PV works in MPPT mode to provide maximum power to charge the batteries. In addition, the system load will be appropriately reduced.

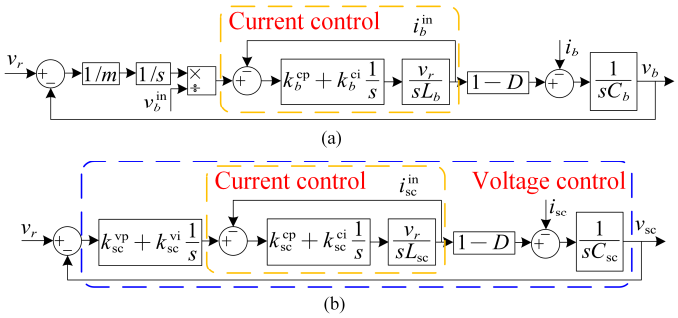

Fig. 4. The schematic diagram of the control circuit for dc-dc converter: (a) battery converter control, (b) SC converter control.

In the grid-connected mode, the grid, PV, and HESSs simultaneously deliver power to the load. The dc and ac bus voltages are controlled by the SC converters and grid. The total power balance can be written as (26).

$$P_{\mathrm{pv}} + P_g + P_b + P_{\mathrm{sc}} = P_{\mathrm{load}} + P_{\mathrm{loss}} \tag{26}$$

where P_g is the grid power. The grid-connected mode also contains three conditions similar to the islanded mode to ensure that the SoCs of the batteries are within a safe range.

5. Control system stability analysis

In HESS, the SC converter uses dual-loop control, while the battery converter employs inner loop current control. The parameters of the control need to be well designed to ensure that the slow and fast dynamic power sharing can be achieved. The schematic diagram of the control circuit for battery and SC is drawn in Fig. 4. The control parameters can be found by using (27) based on [13], [18].

$$\begin{aligned} k_x^{\mathrm{cp}} &= \frac{\omega_{x,c} L_x}{v_r} \qquad k_x^{\mathrm{vp}} = \frac{\omega_{x,v} C_x}{1 - D} \\ k_x^{\mathrm{ci}} &= \frac{\eta \omega_{x,c}^2 L_x}{v_r} \qquad k_x^{\mathrm{vi}} = \frac{\eta \omega_{x,v}^2 C_x}{1 - D} \end{aligned} \tag{27}$$

where k_x^{cp}, k_x^{vp}, k_x^{ci}, and k_x^{vi} are the proportional and integral parameters for the current and voltage control, respectively. $\omega_{x,c}$ is the control bandwidth of the current loop. $\omega_{x,v}$ is the control bandwidth of the voltage loop. D denotes the steady state value of the duty cycle. η is a coefficient. r, L_x, and C_x are the resistance of inductor, filter inductor and filter capacitor of the dc/dc converter, respectively. It should be noted that the response speed of the SC in HESS is faster than the response speed of the battery. Therefore, the current control bandwidth of the

battery is smaller than the bandwidths of the SC. Specifically, $x = b$ denotes the battery, while $x =$ sc denotes the SC component.

It is a common problem that the control system may suffer from potential degradation of stability caused by the coordination between interconnected converters [2]. Therefore, its stability analysis is an important step to ensure the safe operation of the system. According to Figs. 2 and 4, the small-signal model of the relationship between the bus voltage (v_{bus}) and the output voltage of the battery and SC converters is presented by (28).

$$\hat{v}_{\text{bus}} = \frac{R_{\text{sc}}^{L} R \hat{v}_b + R_b^{L} R \hat{v}_{\text{sc}}}{R_{\text{sc}}^{L} R + R_b^{L} R + R_b^{L} R_{\text{sc}}^{L}} \tag{28}$$

where R_b^L and R_{sc}^L are the line resistance of the battery or SC. R is the load impedance. The small signal of the output volage of the battery converter can be obtained from (29).

$$\hat{v}_b = \frac{b_{13}s^3 + b_{12}s^2 + b_{11}s + b_{10}}{a_{15}s^5 + a_{14}s^4 + a_{13}s^3 + a_{12}s^2 + a_{11}s + a_{10}} \tag{29}$$

where $a_{15} = E_b(1-D)RP_{\max}C_b m v_b^{\text{in}} L_b v_r$; $a_{14} = E_b RP_{\max}(1-D)C_b m v_b^{\text{in}} \omega_{b,c} L_b + E_b P_{\max}(1-D) m v_b^{\text{in}} L_b v_r$; $a_{13} = E_b(1-D)R\ P_{\max}C_b m v_b^{\text{in}} \eta \omega_{b,c} L_b + E_b P_{\max}(1-D)^2 R \omega_{b,c} L_b + E_b P_{\max} m v_b^{\text{in}} L_b (1-D)\omega_{b,c}$; $a_{12} = E_b P_{\max}(1-D)^2 R\eta\omega_{b,c}^2 L_b + P_{\max}(1-D)L_b\omega_{b,c}k_{\text{SoC},j}^{p} + 2v_b^{\text{in}}E_b k_{\text{acc.},j}^{p} + E_b(1-D)P_{\max} m v_b^{\text{in}} \eta L_b v_r$; $a_{11} = L_b\ P_{\max}(1-D)\omega_{b,c}k_{\text{SoC},j}^{i} + P_{\max}(1-D)\eta\omega_{b,c}^2 L_b k_{\text{SoC},j}^{p}$; $a_{10} = P_{\max}\ (1-D)\eta\omega_{b,c}^2 L_b k_{\text{SoC},j}^{i} + 2v_b^{\text{in}}E_b k_{\text{acc.},j}^{i}$; $b_{13} = E_b(1-D)^2 RP_{\max}L_b\omega_{b,c}v_r$; $b_{12} = E_b(1-D)^2 RP_{\max}\eta\omega_{b,c}^2 v_r L_b$; $b_{11} = b_{10} = 0$.

Similarly, the small-signal model of the output voltage of the SC converter is given by (30).

$$\hat{v}_{\text{sc}} = \frac{b_{23}s^3 + b_{22}s^2 + b_{21}s + b_{20}}{a_{24}s^4 + a_{23}s^3 + a_{22}s^2 + a_{21}s + a_{20}} \tag{30}$$

where $a_{24} = RE_{\text{sc}}(1-D)C_{\text{sc}}$; $a_{23} = RE_{\text{sc}}(1-D)\omega_{\text{sc},v}C_{\text{sc}} + 2n\omega_{\text{sc},v}C_{\text{sc}}E_{\text{sc}}v_{\text{sc}}^{\text{in}}$; $a_{22} = RE_{\text{sc}}(1-D)\eta\omega_{\text{sc},v}^2 C_{\text{sc}} + \omega_{\text{sc},v}C_{\text{sc}}k_{\text{sc},j}^{p} + 2n\eta\omega_{\text{sc},v}^2 C_{\text{sc}}E_{\text{sc}}v_{\text{sc}}^{\text{in}} + E_{\text{sc}}(1-D)$; $a_{21} = \omega_{\text{sc},v}C_{\text{sc}}k_{\text{sc},j}^{i} + \eta\omega_{\text{sc},v}^2\ C_{\text{sc}}$; $a_{20} = \eta\omega_{\text{sc},v}^2 C_{\text{sc}}k_{\text{sc},j}^{i}$; $b_{23} = \omega_{\text{sc},v}C_{\text{sc}}RE_{\text{sc}}(1-D)$; $b_{22} = \eta\omega_{\text{sc},v}^2 C_{\text{sc}} \times RE_{\text{sc}}(1-D)$; $b_{21} = b_{20} = 0$.

Then, substituting (28) and (29) into (27), the characteristics function of the relationship between the bus voltage and the reference voltage is given as (31).

$$0 = a_{39}s^9 + a_{38}s^8 + a_{37}s^7 + a_{36}s^6 + a_{35}s^5 + a_{34}s^4 + a_{33}s^3 + a_{32}s^2 + a_{31}s + a_{30} \tag{31}$$

where $a_{39} = a_{15}a_{24}$; $a_{38} = a_{15}a_{23} + a_{14}a_{24}$; $a_{37} = a_{15}a_{22} + a_{14}a_{23} + a_{13}a_{24}$; $a_{36} = a_{15}a_{21} + a_{14}a_{22} + a_{13}a_{23} + a_{12}a_{24}$; $a_{35} = a_{15}a_{20} + a_{14}a_{21} + a_{13}a_{22} + a_{12}a_{23} + a_{11}a_{24}$; $a_{34} = a_{14}\ a_{20} + a_{13}a_{21} + a_{12}a_{22} + a_{11}a_{23} + a_{10}a_{24}$; $a_{33} = a_{13}a_{20} + a_{12}a_{21}\ + a_{11}a_{22} + a_{10}a_{23}$; $a_{32} = a_{12}a_{20} + a_{11}a_{21} + a_{10}a_{22}$; $a_{31} = a_{11}\ a_{20} + a_{10}a_{21}$; $a_{30} = a_{10}a_{20}$.

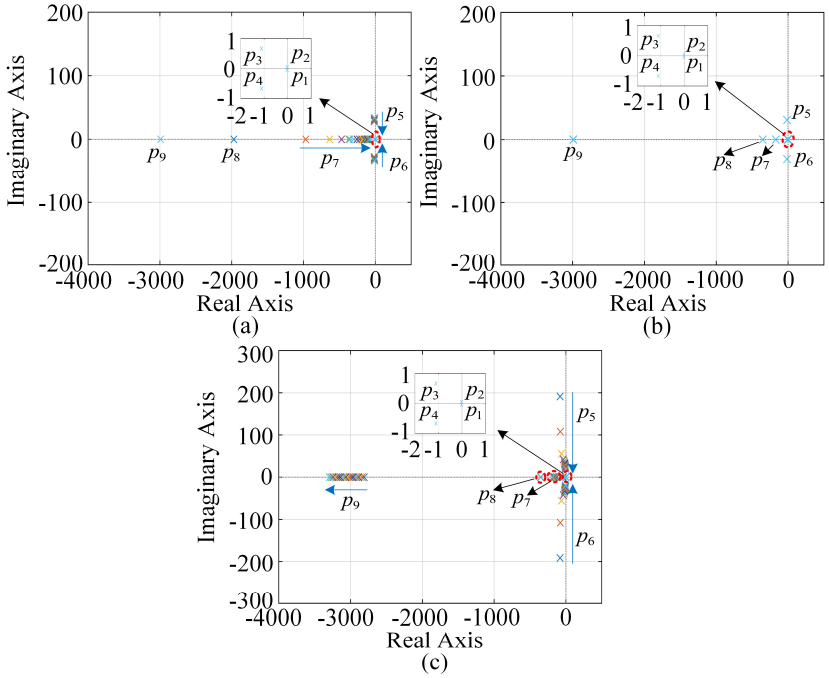

Fig. 5. Root locus diagrams: (a) C_b is between 10 μF and 200 μF, (b) C_{sc} is between 10 μF and 200 μF, and (c) n is between 0 and 0.01 V/W, while m is between 0 and 0.008 V/W.

According to equation (30), the system stability analysis can be achieved by observing the placement of the dominant pole in the root locus diagram. Then, selecting the appropriate parameters can ensure the performance of the controller and the safe operation of the system. From Fig. 5(a), there are nine negative eigenvalues, but only seven of them ($p_1, p_2, p_3, p_4, p_5, p_6$, and p_7) are dominant based on their position. With the variations of the filter capacitor C_b within the specified range, the dominant poles p_1, p_2, p_3, and p_4 are located in the left half of the s-plane. This indicates that the stability of the control system can be guaranteed. The poles p_5 and p_6 change from the complex conjugate poles to negative real poles. This indicates that the stability of the system is gradually improved. Meanwhile, although the dominant pole p_7 moves towards the right of the s-plane, it still sits on the left half of the s-plane. Therefore, the stability of the system can be guaranteed. Similarly, Figs. 5(b) and 5(c) show that the dominant eigenvalues of the system are located on the left half of the s-plane by changing the specified parameters. Thus, the instability of the proposed control system can be eliminated.

6. Simulation verifications

To verify the effectiveness of the proposed method in real control system, the PIL platform including a microcontroller (MC) and PC, is established. The MC is implemented by using STM32F429ZIT6, connected in a closed loop with the controlled object. The microgrid configuration is shown in Fig. 1. The key parameters are listed in Table I.

TABLE I
SYSTEM PARAMETERS

Items	Values	Items	Values	Items	Values
v_r	400 V	ω_c	0.2×2π rad/s	v_{sc}^r	180 V
v_b	180 V	m	0.0032 V/W	k_{SoC}^p	10
v_{sc}	200 V	n	0.004 V/W	k_{SoC}^i	1.1310
C_b	10 μF	k_b^{cp}	0.1257	$k_{acc.}^p$	10
C_{sc}	10 μF	k_b^{ci}	157.9137	$k_{acc.}^i$	0.6283
L_b	2 mH	k_{sc}^{cp}	0.0628	E_b	0.3 Ah
L_{sc}	5 mH	k_{sc}^{ci}	78.9568	$R_{b,1}^L$, $R_{sc,1}^L$	0.02 Ω
f_s	10 kHz	k_{sc}^{vp}	0.1257	$R_{b,2}^L$, $R_{sc,2}^L$	0.015 Ω
R	50 Ω	k_{sc}^{vi}	78.9568	$R_{b,3}^L$, $R_{sc,3}^L$	0.01 Ω
η	0.1	k_{sc}^p	2	P_{max}	10 kW
ε	1/3	k_{sc}^i	0.1257	τ	1 ms

6.1. Case 1: Different dynamic power-sharing

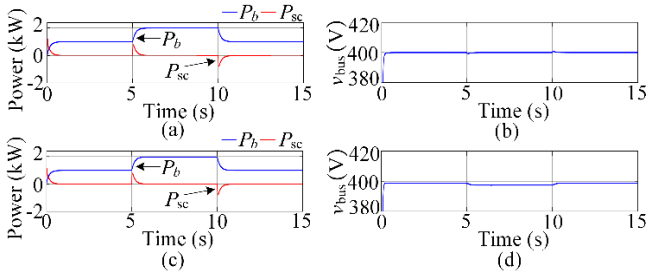

Fig. 6. Simulation results for case 1: (a) Dynamic power-sharing, (b) DC bus voltage, (c) Dynamic power-sharing from [12], and (d) DC bus voltage from [12].

In this case, the proposed method and the integral droop control from [12] are studied and compared. A single HESS including a battery and SC is used as the test object. From Fig. 6(a), HESS delivers 1 kW of power at the beginning. When the system load suddenly rises to 2 kW, the SC immediately responds to provide power and then gradually reduces to zero. The battery responds slowly to supply constant power at steady state. From Fig. 6(b), the dc bus voltage can be restored to the pre-set value through the SC control. According to the characteristics of *V-P* droop control, when SC provides the transient power, the dc bus voltage will have voltage deviations. After that, once the instantaneous power decreases to zero, the dc bus voltage will automatically return to the desired value. It can be seen from Fig. 6(c) that the simulation results produced by the control method from [12] are similar to the proposed method. However, when the system load changes, the dc bus voltage cannot be returned to the reference value, as shown in Fig. 6(d). This is because the dc bus voltage in [12] is regulated by the battery control (*V-P* droop control). This indicates that if the battery provides constant power, then the bus voltage error will always exist. Therefore, ref. [12] requires a voltage restoration loop to eliminate the

steady state error of the bus voltage. The results show that the proposed method can realize dynamic power distribution and maintain the voltage at the set value without an additional control. Hence, it confirms that the presented approach outperforms the comparing method.

6.2. Case 2: The performance of the consensus-based voltage compensator

From Fig. 7(a), the SoC balance among batteries is achieved at 20 s. After that, the SoC deviation among batteries gradually becomes larger due to the different line resistances in the microgrid system. From Fig. 7(b), the batteries cannot provide equivalent power to the load between 0-30 s. After 30 s, the consensus-based accurate power sharing control begins to operate, which can achieve a consistent output power from the batteries, thereby eliminating the negative effects of line resistance. It can be seen from Fig. 7(c) that the SoC of battery-1 (b_1) has the fastest drop rate, while the SoC of battery-3 (b_3) has the smallest drop rate. This means that the output power ($P_{b,1}$) of b_1 is the highest, while the output power ($P_{b,3}$) of b_3 is the least. Therefore, the SoC gap among batteries is gradually narrowing. In charging mode, the SoC of b_3 rises the fastest, and the SoC of b_1 rises the slowest. Therefore, SoC balance between batteries can be achieved, as shown in Fig. 7(d).

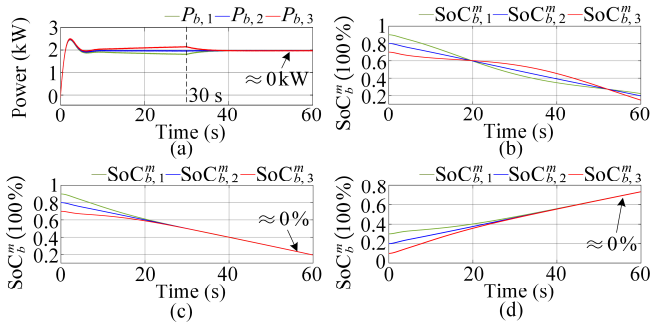

Fig. 7. Simulation results for case 2: (a) SoC balance without accurate power sharing control, (b) The performance of accurate power sharing control, (c) SoC balance in discharging mode, (d) SoC balance in charging mode.

6.3. HESS operation

In this scenario, the batteries are operating within a limited range ($10\% \leq \mathrm{SoC}_b^m \leq 90\%$). From Fig. 8(a), PV and HESSs initially supply 10.5 kW to the loads that include dc and ac loads. At 10 s, a 3 kW load is added to the system. At 20 s, the microgrid is connected to the main grid. The main grid shares the 3 kW load. Subsequently, a 1 kW pulse load is installed in the system from 30 to 50 s. The frequency of the pulse load is set at 0.4 and 0.2 Hz during 30-40 s and 40-50 s, respectively. After 60 s, the dc load is removed, and then the HESSs absorb the excess power of the system. At 80 s, the microgrid is disconnected from the main grid and returned to islanded mode. From Fig. 8(b), it can be seen that the bus voltages can be maintained within the set range even when the system power changes repeatedly. Besides, the difference among the three bus

voltages is small. As can be seen in Figs. 8(c) and 8(d), when the microgrid is connected to the main grid, the ac bus voltage does not exhibit any oscillations.

From Figs. 8(e) and 8(f), the output power $P_{b,1}$ of b_1 is the highest due to the existence of SoC balancing control, while the output power $P_{b,3}$ of b_3 is the least. Therefore, the SoC gap among batteries is gradually reducing. In addition, b_3 is disconnected from the system at 40 s. This means that b_3 stops supplying power. Other batteries will automatically deliver more power to ensure system stability. At 50 s, b_3 is reconnected to the system and supplies power normally. From Fig. 8(g), the SCs only release/absorb power when the system power changes suddenly. At 10 s, a 3 kW load is connected to the system and the SCs provide power rapidly. Then, SCs receive a brief charge from the batteries [n_1 from Fig. 8(e) and n_3 from Fig. 8(g)]. At 60 s, the load is removed and the SCs absorb instantaneous power. Subsequently, the SCs briefly release power that is absorbed by the batteries [n_2 from Fig. 8(e) and n_4 from Fig. 8(g)]. Therefore, the SoCs of the SCs can be maintained at the reference value, the continuous use of SCs can be guaranteed, as shown in Fig. 8(h).

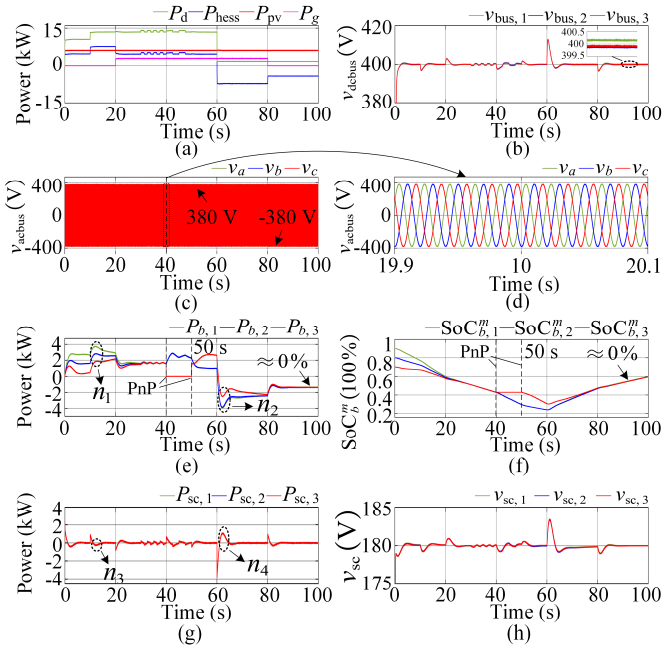

Fig. 8. Simulation results for case 3: (a) Power demand P_d, output power of the HESS, PV, and grid, (b) DC bus voltages, (c) AC bus voltage, (d) AC bus voltage between 19.9 s and 20.1 s, (e) Output power of batteries, (f) SoCs for batteries, (g) Output power of SCs, and (h) SoCs for SCs.

6.4. Case 4: SoC limitation for batteries

This case studies the batteries reaching the upper limit (90%) and lower limit (10%) of SoC. The initial states of the batteries' SoC are given in Table II.

From Figs. 9(a) and 9(c), the batteries are charged by the PV system. When the SoCs of the batteries reaches 90%, the proposed controller will automatically disconnect the battery to prevent

overcharging. The power generated by PV will be greater than the load demand. Therefore, PV control will switch from MTTP mode to CVC mode to reduce output power at 32 s. At 34 s, all the batteries stop working. Then, an 11 kW load is installed in the system at 40 s. At this time, the total load of the system is greater than the power generated by the PV, hence the batteries will participate in providing power to the load. The SoC among the batteries is able to maintain balance throughout the operation. It should be noted that SCs are connected to the system during the entire operation to maintain the stability of the dc bus voltages, as shown in Figs. 9(b) and 9(d).

TABLE II
SOC LIMITATIONS FOR BATTERIES

Upper limits of SoC		Lower limits of SoC	
$SoC^m_{b,1}$	70 %	$SoC^m_{b,1}$	50 %
$SoC^m_{b,2}$	60 %	$SoC^m_{b,2}$	40 %
$SoC^m_{b,3}$	50 %	$SoC^m_{b,3}$	30 %

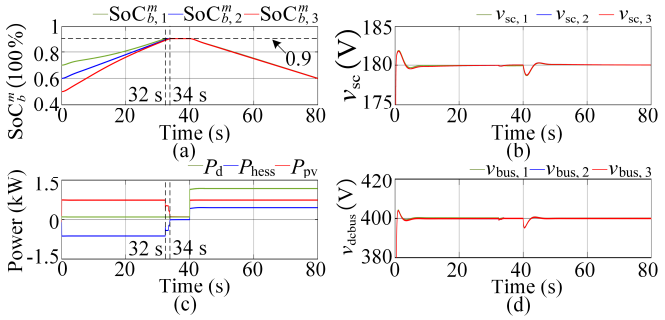

Fig. 9. Simulation results for case 4 ($SoC_b \geq 90\%$): (a) SoCs for batteries, (b) SoCs for SCs, (c) Power demand P_d, output power of the HESS and PV, and (d) DC bus voltages.

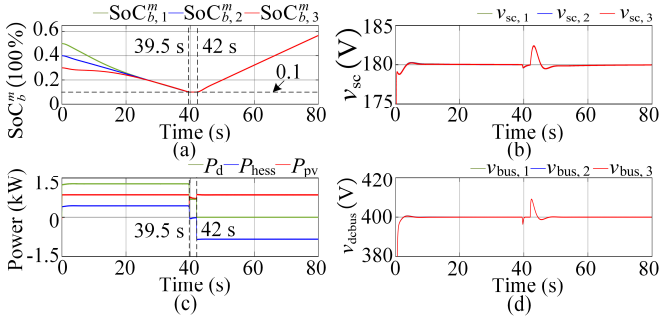

Fig. 10. Simulation results for case 4 ($SoC_b \leq 10\%$): (a) SoCs for batteries, (b) SoCs for SCs, (c) Power demand P_d, output power of the HESS and PV, and (d) DC bus voltages.

From Figs. 10(a) and 10(c), the batteries run in discharge mode. When the SoC of the batteries drops to 10% at 39.5 s, the batteries stop supplying power to the load. In addition, PV will switch to CVC mode, and the system load will be reduced appropriately. In addition, PV will switch to CVC mode, and the system load will be reduced appropriately. At 42 s, the system load was completely removed. The PV switches to MPPT mode to charge the batteries. During the entire operation process, SCs play a role in suppressing power fluctuations in the microgrid and ensuring that the bus voltages are within the safe range, as shown in Figs. 10(b) and Fig. 10(d).

7. Conclusion

The novel coordinated droop controls are proposed in this paper. The *V*-d*P* control is proposed to adjust the battery converter to deliver the low-frequency power, while the *V-P* droop control is employed to regulate the SC converter to supply the high-frequency power. In addition, the bus voltage can be restored to the desired range through the SC control without an extra voltage recovery loop. The consensus-based voltage compensator is proposed to achieve the SoC balance among batteries and accurate power sharing. The proposed PMS can ensure that batteries operate within a safe range to prevent overuse. Then, the SoC of the SC can be automatically restored to the set value. In addition, the root locus method is employed to verify the stability of the proposed control system. Finally, the performance and feasibility of the proposed control method are verified by PIL simulation. The results of the simulation show that the proposed control works as expected.

References:

[1] R. Zamora and A. K. Srivastava, "Multi-Layer Architecture for Voltage and Frequency Control in Networked Microgrids," *IEEE Trans. Smart Grid*, vol. 9, no. 3, pp. 2076–2085, 2018, doi: 10.1109/TSG.2016.2606460.

[2] T. Dragicevic, X. Lu, J. C. Vasquez, and J. M. Guerrero, "DC Microgrids - Part I: A Review of Control Strategies and Stabilization Techniques," *IEEE Trans. Power Electron.*, vol. 31, no. 7, pp. 4876–4891, 2016, doi: 10.1109/TPEL.2015.2478859.

[3] T. Morstyn, B. Hredzak, and V. G. Agelidis, "Control Strategies for Microgrids with Distributed Energy Storage Systems: An Overview," *IEEE Trans. Smart Grid*, vol. 9, no. 4, pp. 3652–3666, 2018, doi: 10.1109/TSG.2016.2637958.

[4] X. Qiu, T. A. Nguyen, and M. L. Crow, "Heterogeneous Energy Storage Optimization for Microgrids," *IEEE Trans. Smart Grid*, vol. 7, no. 3, pp. 1453–1461, 2016, doi: 10.1109/TSG.2015.2461134.

[5] D. B. W. Abeywardana, B. Hredzak, V. G. Agelidis, and G. D. Demetriades, "Supercapacitor sizing method for energy-controlled filter-based hybrid energy storage systems," *IEEE Trans. Power Electron.*, vol. 32, no. 2, pp. 1626–1637, 2017, doi: 10.1109/TPEL.2016.2552198.

[6] J. Shen and A. Khaligh, "A Supervisory Energy Management Control Strategy in a Battery/Ultracapacitor Hybrid Energy Storage System," *Ieee Trans. Transp. Electrif.*, vol. 1, no. 3, pp. 223–231, 2015.

[7] Y. Gu, W. Li, and X. He, "Frequency-coordinating virtual impedance for autonomous power management of DC microgrid," *IEEE Trans. Power Electron.*, vol. 30, no. 4, pp. 2328–2337, 2015, doi: 10.1109/TPEL.2014.2325856.

[8] S. K. Kollimalla, M. K. Mishra, A. Ukil, and H. B. Gooi, "DC Grid Voltage Regulation

Using New HESS Control Strategy," *IEEE Trans. Sustain. Energy*, vol. 8, no. 2, pp. 772–781, Apr. 2017, doi: 10.1109/TSTE.2016.2619759.

[9] U. Manandhar *et al.*, "Energy management and control for grid connected hybrid energy storage system under different operating modes," *IEEE Trans. Smart Grid*, vol. 10, no. 2, pp. 1626–1636, 2019, doi: 10.1109/TSG.2017.2773643.

[10] X. Gao and L. Fu, "SOC Optimization Based Energy Management Strategy for Hybrid Energy Storage System in Vessel Integrated Power System," *IEEE Access*, vol. 8, pp. 54611–54619, 2020, doi: 10.1109/ACCESS.2020.2981545.

[11] Q. Zhang and G. Li, "Experimental study on a semi-active battery-supercapacitor hybrid energy storage system for electric vehicle application," *IEEE Trans. Power Electron.*, vol. 35, no. 1, pp. 1014–1021, 2020, doi: 10.1109/TPEL.2019.2912425.

[12] P. Lin, P. Wang, J. Xiao, J. Wang, C. Jin, and Y. Tang, "An Integral Droop for Transient Power Allocation and Output Impedance Shaping of Hybrid Energy Storage System in DC Microgrid," *IEEE Trans. Power Electron.*, vol. 33, no. 7, pp. 6262–6277, 2018, doi: 10.1109/TPEL.2017.2741262.

[13] Q. Xu, J. Xiao, X. Hu, P. Wang, and M. Y. Lee, "A Decentralized Power Management Strategy for Hybrid Energy Storage System with Autonomous Bus Voltage Restoration and State-of-Charge Recovery," *IEEE Trans. Ind. Electron.*, vol. 64, no. 9, pp. 7098–7108, 2017, doi: 10.1109/TIE.2017.2686303.

[14] T. Morstyn, B. Hredzak, and V. G. Agelidis, "Cooperative Multi-Agent Control of Heterogeneous Storage Devices Distributed in a DC Microgrid," *IEEE Trans. Power Syst.*, vol. 31, no. 4, pp. 2974–2986, 2016, doi: 10.1109/TPWRS.2015.2469725.

[15] M. Shi, X. Chen, J. Zhou, Y. Chen, J. Wen, and H. He, "Advanced Secondary Voltage Recovery Control for Multiple HESSs in a Droop-Controlled DC Microgrid," *IEEE Trans. Smart Grid*, vol. 10, no. 4, pp. 3828–3839, 2019, doi: 10.1109/TSG.2018.2838108.

[16] P. Lin, T. Zhao, B. Wang, Y. Wang, and P. Wang, "A Semi-Consensus Strategy Toward Multi-Functional Hybrid Energy Storage System in DC Microgrids," *IEEE Trans. Energy Convers.*, vol. 35, no. 1, pp. 336–346, 2020, doi: 10.1109/TEC.2019.2936120.

[17] R. Zhang, B. Hredzak, and T. Morstyn, "Distributed Control with Virtual Capacitance for the Voltage Restorations, State of Charge Balancing and Load Allocations of Heterogeneous Energy Storages in a DC Datacenter Microgrid," *IEEE Trans. Energy Convers.*, vol. 34, no. 3, pp. 1296–1308, 2018, doi: 10.1109/TEC.2018.2889065.

[18] X. Lin, R. Zamora, and C. A. Baguley, "A Coordinated Droop Controls and Power Management Scheme for Hybrid Energy Storage Systems in DC Microgrids," *2021 31st Australas. Univ. Power Eng. Conf.*, pp. 1–6, 2021, doi: 10.1109/aupec52110.2021.9597727.

[19] X. Lu, K. Sun, J. M. Guerrero, J. C. Vasquez, and L. Huang, "State-of-charge balance using adaptive droop control for distributed energy storage systems in DC microgrid

applications," *IEEE Trans. Ind. Electron.*, vol. 61, no. 6, pp. 2804–2815, 2014, doi: 10.1109/TIE.2013.2279374.

[20] C. Li, E. A. A. Coelho, T. Dragicevic, J. M. Guerrero, and J. C. Vasquez, "Multiagent-Based Distributed State of Charge Balancing Control for Distributed Energy Storage Units in AC Microgrids," *IEEE Trans. Ind. Appl.*, vol. 53, no. 3, pp. 2369–2381, 2017, doi: 10.1109/TIA.2016.2645888.

[21] H. J. Yoo, T. T. Nguyen, and H. M. Kim, "Consensus-based distributed coordination control of hybrid AC/DC microgrids," *IEEE Trans. Sustain. Energy*, vol. 11, no. 2, pp. 629–639, 2020, doi: 10.1109/TSTE.2019.2899119.

[22] M. Kriegleder, "A correction to algorithm A2 in 'asynchronous distributed averaging on communication networks,'" *IEEE/ACM Trans. Netw.*, vol. 22, no. 6, pp. 2026–2027, 2014, doi: 10.1109/TNET.2013.2292800.

[23] L. Meng, T. Dragicevic, J. Roldan-Perez, J. C. Vasquez, and J. M. Guerrero, "Modeling and Sensitivity Study of Consensus Algorithm-Based Distributed Hierarchical Control for DC Microgrids," *IEEE Trans. Smart Grid*, vol. 7, no. 3, pp. 1504–1515, May 2016, doi: 10.1109/TSG.2015.2422714.

[24] R. Olfati-Saber, J. A. Fax, and R. M. Murray, "Consensus and cooperation in networked multi-agent systems," *Proc. IEEE*, vol. 95, no. 1, pp. 215–233, 2007, doi: 10.1109/JPROC.2006.887293.

[25] F. Zhang, K. Thanapalan, A. Procter, S. Carr, and J. Maddy, "Adaptive Hybrid Maximum Power Point Tracking Method for a Photovoltaic System," *IEEE Trans. Energy Convers.*, vol. 28, no. 2, pp. 353–360, Jun. 2013, doi: 10.1109/TEC.2013.2255292.

System level energy management system

Chapter 5: A hybrid short-term load forecasting approach for individual residential customer

Citation:

X. Lin, R. Zamora, C. Baguley, and Anurag K. Srivastava, "A hybrid short-term load forecasting approach for individual residential customer," *IEEE Trans. Power Del.* 2022. **(Published)**

Preamble:

The randomness of end-user behavior and real-time changes in electricity prices lead to irregularities in the consumption of household loads. For this reason, forecasting household loads in the home energy management system (HEMS) is highly challenging. Chapter 5 proposes a hybrid forecasting model for single household load consumption forecasting. This hybrid forecasting model consists of two parts. The first part is an ensemble model consisting of support vector machine (SVM), back propagation neural network (BPNN), and generalized regression neural network (GRNN). Among them, SVM and BPNN are optimized by genetic algorithm. Then, the chapter also proposes a thermal dynamic model to track the variation of indoor temperature, which is used as input to the ensemble model to predict the use of air conditioners and heaters. The other part is a deep ensemble model that is used to predict lighting and other loads. The model consists of three bidirectional long short-term memory (Bi-LSTM) networks, which uses a Bayesian algorithm to optimize their hyperparameters. Next, an illuminance algorithm is used to calculate outdoor illuminance, which is used as input to the deep ensemble model to track lighting load usage. Finally, the results of both ensemble and deep ensemble models are merged by the trimmed algorithm.

Abstract:

This article proposes a hybrid method (HM) to improve the accuracy of short-term individual residential load forecasting. The HM includes an ensemble model (EM), deep ensemble model (DEM), and thermal dynamic model expressed by resistance-capacitance (RC). The EM consists of three predictors of support vector machine (SVM), back propagation neural network (BPNN), and generalized regression neural network (GRNN). The genetic algorithm (GA) is used to optimize SVM and BPNN to enhance their performance. The DEM includes multiple bi-directional long-short term memory (Bi-LSTM) networks. The Bayesian algorithm (BA) is used to optimize the hyperparameters of the Bi-LSTM. The outputs of individual predictors are aggregated using an optimal trimmed algorithm. At first, the total load is separated into the heater and air conditioning (HAC), and non-HAC loads. Then, the RC model is presented to predict the indoor temperature, which integrates outdoor weather and less HAC historical data as the input of the EM to forecast the HAC load. After that, non-HAC loads are further divided into electric

lighting and other loads. A daylight equation is used to calculate the illuminance, which is combined with less lighting historical data as the input of DEM to predict electric lights usage. Then, other loads are captured by DEM through less historical data. Finally, the total load is obtained by combining the predicted HAC and non-HAC loads. The datasets from the UMass Smart Microgrid and Flexhouse projects are used to test the proposed method. The comparison with existing models proves that the presented model can provide accurate short-term individual load forecasting.

1. Introduction

Accurate short-term load forecasting (STLF) plays a vital role in modern power systems [1]. Through STLF, power companies can formulate strategies to adjust power dispatch in real-time, thereby improving their energy efficiency and economic benefits. Residential customers can evaluate power consumption and control the usage of electrical equipment to reduce electricity tariffs [2].

Although many articles have studied the STLF in the residential sector, most of them track the load usage trajectory of a group of households rather than a single household [3]-[6]. A small number of articles discusses the electricity usage forecast of a single user [7]-[11]. However, they all directly predict the total load demand without taking into account key influencing factors, including temperature and illuminance

To address these issues, a hybrid method (HM) for the STLF of the individual residential user is proposed in this paper. The major contributions of this article are summarized as follows:

a) The thermal dynamic model represented by resistance-capacitance (RC) is proposed to estimate indoor mean temperature, which combines output weather conditions and less historical data for the heater and air conditioning (HAC) as the input of the ensemble model (EM).
b) The HAC load is forecasted by adopting the EM integrating back propagation neural network (BPNN), support vector machine (SVM), and generalized regression neural network (GRNN). The genetic algorithm (GA) is employed to search the optimal hyperparameters of BPNN and SVM to enhance the forecasting accuracy. Therefore, the HAC physical model does not need to be built.
c) The non-HAC loads are further divided into electric lighting and other loads. A daylight equation is used to calculate the solar illuminance, which is combined with the historical data of the electric light power as input of a deep ensemble model (DEM) to track the power consumption of the electric light. Other loads are forecasted by DEM based on historical data. The DEM integrating multiple bi-directional long short-term memory (Bi-

LSTM) networks is developed to track the non-HAC load usage. Besides, the Bayesian algorithm (BA) is adopted to search the optimal hyperparameters of the Bi-LSTM.

The rest of this paper is organized as follows. The literature review is described in Section II. Section III presents the indoor temperature prediction and illuminance calculation. Section IV describes the proposed HM. Section V presents the case studies and discussions. The conclusion is shown in Section VI.

2. Literature review

Time series models are the typical method applied to STLF, including autoregressive integrated moving average models [12], grey model [13], and regression analysis model [14]. However, these models are insufficient to deal with nonlinear problems and will lead to lower prediction accuracy. Therefore, nonlinear forecasting models, including support vector regression [15], and artificial neural networks [16], such as Elman neural network (ELM), BPNN, and radial basis functions (RBF), have been employed to solve nonlinear problems in load forecasting.

ELM is one of the recurrent neural networks (RNN), which has a good ability to solve discrete-time series problems. In [17], an improved ELM is proposed to predict the short load usage for residential buildings. The method considers the consumers' comfort index to improve the prediction accuracy. In [18], a hybrid quantization ELM with inputs, historical load, and temperature is proposed to realize STLF. A GA is used to optimize the hyperparameters in ELM. BPNN is a kind of feed-forward neural network, which has strong nonlinear mapping ability and generalization. In [19], a short-term prediction model based on the decomposition of load components is proposed to track changes in the cooling load of residential buildings. The prediction model includes a BPNN and auto-regressive integrated moving average algorithm. RBF neural network is a type of feed-forward neural network, which is developed to solve the slow training process caused by the size of the large network. In [9], a prediction framework based on RBF is proposed to track short-term load changes. The methods consider weather and load historical data as input. In [10], a prediction model based on LSTM and convolutional neural network (CNN) is proposed to solve the STLF issue for a single customer. In the proposed method, CNN is used to extract features of the data, and LSTM uses these features for time series prediction. In [11], a predictive model based on RNN is developed to implement STLF for residential and commercial buildings. In addition, some missing energy data can be repaired by the proposed model. However, all the above methods use a single predictive model. Due to the performance limitations of a single predictor, different data quality and evaluation metrics may reduce the generalization capability of the model, so that the predicted output may have outliers, and hence, the deviation will increase [20], [21].

TABLE I
A COMPARATIVE SUMMARY OF STLF

References	Load characteristics		Ensemble model	Individual residential user
	HAC	Lights		
[7], [10], [11], [19]	×	×	×	✓
[17], [18]	×	×	×	×
[28]	×	×	✓	✓
[4]-[6], [8], [23]	×	×	✓	×
[30]-[32]	✓	×	×	✓
This research	✓	✓	✓	✓

The aforementioned issues can be addressed by an EM that includes multiple predictors [22]. Ref. [23] proposes an ensemble model including multiple RBF to achieve short-term and mid-term load forecasting. The LSTM network will extract features from the load sequence to train multiple RBFs in the ensemble model. Ref. [4] proposes an online second learning method that combines the original feature, forecasting output of the multiple models, and actual data to produce a new training dataset. The multiple models consist of a least-square support vector machine (LSSVM), BPNN, and gradient boosting regression trees. In [5], an evolutionary neural machine inference model combining least-square support vector regression and RBF is used to forecast residential energy usage. Then, a symbiotic organism search is employed to find the optimal tuning parameters of forecasting models. Ref. [6] proposes an ensemble method to forecast energy consumption in residential buildings. Three generative adversarial networks integrated memristor array are used as predictors. However, these methods mainly focus on the study of load forecasting for large-scale systems (e.g., more than thousands of residential users) rather than an individual residential customer. Since the individual load has the characteristics of fast change and randomness, its prediction is still a challenge [3], [7]. Besides, the above methods mainly focus on the user's total power prediction and do not include the power consumption prediction of high-power equipment, such as HAC. Since HAC occupies a large proportion of electricity, it is the potential for energy-saving [24]. Furthermore, the power consumption forecast for HAC can enable users to understand the specific situation of the power usage, so as to make necessary adjustments to achieve the goal of power-saving [25]. There are three prediction methods for HAC systems: physics-based, data-driven, and hybrid models [26]. The physics-based model predicts the load by establishing a complex physical model. However, the parameters of the physical model are often difficult to measure [27]. Data-driven uses machine learning and time-series statistical analysis methods to predict load, but it requires a lot of historical data [28]. In order to solve these issues, a hybrid model including physical-based and data-driven models is presented because it only requires a simple physical model and less historical data [29]. In [30], a thermodynamic model based on RC was built as the physical part of the building. Then, a Gaussian process based on explicit basis functions was proposed to estimate building temperature and predict overall energy consumption. The results show the higher forecasting accuracy. Ref.

[31] proposes a hybrid model for building energy consumption forecasting. The air conditioning power usage is forecasted by using the building thermal dynamic model and air conditioning model. The non-air-conditioning power usage is forecasted by using LSSVM. The real dataset is collected to validate the effectiveness of the proposed method. In [32], a hybrid model including building thermal dynamic model and empirical model of heating, ventilation, and air conditioning system is proposed to forecast building load demand in the campus. Table I provides a comparative summary of the current articles investigating STLF.

According to the literature review, the motivations of this article can be summarized as follows:

a) The HAC accounts for a significant proportion of typical household energy in the USA, which can reach 51% of the total loads [33]. Therefore, the household load will be split into HAC and non-HAC loads in this article. The consumption of the HAC load is affected by indoor and outdoor temperatures. The current hybrid models require the construction of a thermal dynamic model and a complex HAC model, which leads to an increase in the unknown parameters of the model. In addition, data-driven methods require the collection of large amounts of data for training and prediction.
b) The non-HAC loads have fast time-varying and random characteristics. For example, electric lights are determined by the unpredictable behavior of users and environmental conditions. Although traditional predictors can extract the non-linear characteristics of the data, they cannot remember the important state of the past and the future. As a result, the prediction accuracy is reduced.
c) In the case of single residential forecasting, only one predictor is used to implement load prediction. However, a single predictor may produce undesirable outliers, thereby increasing the prediction error.

3. Indoor temperature prediction & illuminance calculation

3.1. Proposed thermal dynamic model

A thermodynamic mathematical model is proposed to predict the indoor temperature of a house. It should be noted that the indoor temperature refers to the average temperature. The schematic diagram of the RC thermal model for k^{th} house (k=1, 2, …, n) is given in Fig. 1.

The heat transfer of the house exterior wall is expressed by a differential equation, as shown in (1).

$$C_k^w \frac{dT_k^w}{dt} = \frac{T_k^i - T_k^w}{R_k^{\text{iw}}} + \frac{T_k^a - T_k^w}{R_k^{\text{aw}}} \tag{1}$$

where T_k^w and C_k^w are the temperature and capacity of exterior wall; T_k^I and T_k^a are the temperature of indoor and ambient; R_k^{iw} is the resistance between indoor air and exterior wall; R_k^{aw} is the resistance between ambient and exterior wall.

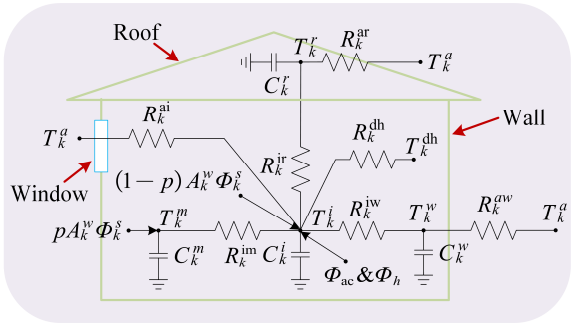

Fig. 1. The schematic diagram of house thermal dynamic model.

The heat balance model for the medium in the inner wall can be written as (2).

$$C_k^m \frac{dT_k^m}{dt} = \frac{T_k^i - T_k^m}{R_k^{\mathrm{im}}} + p\mathrm{A}_k^w \Phi_k^s \tag{2}$$

where T_k^m, C_k^m, and R_k^{im} are the temperature, capacity, and resistance of the medium in the inner wall; A_k^w and Φ_k^s are the window area and solar radiation; p is the proportion of the solar radiation acting on the inner wall medium.

The thermal transfer of the house roof is given in (3).

$$C_k^r \frac{dT_k^r}{dt} = \frac{T_k^i - T_k^r}{R_k^{\mathrm{ir}}} + \frac{T_k^a - T_k^r}{R_k^{\mathrm{ar}}} \tag{3}$$

where T_k^r and C_k^r are the temperature and capacity of the house roof; R_k^{ir} is the resistance between roof and indoor air; R_k^{ar} is the resistance between roof and ambient.

The heat balance of the indoor air will be affected by many factors, such as the external temperature and the HAC. The equivalent mathematical model of the heat balance of the indoor air is formulated as (4).

$$C_k^i \frac{dT_k^i}{dt} = \frac{T_k^r - T_k^i}{R_k^{\mathrm{ir}}} + \frac{T_k^a - T_k^i}{R_k^{\mathrm{ai}}} + \frac{T_k^w - T_k^i}{R_k^{\mathrm{iw}}} + \frac{T_k^m - T_k^i}{R_k^{\mathrm{im}}} + \frac{T_k^{\mathrm{dh}} - T_k^i}{R_k^{\mathrm{dh}}} + (1-p)\mathrm{A}_k^w \Phi_k^s + \Phi_k^{\mathrm{ac}} + \Phi_k^h \tag{4}$$

where C_k^I is the capacity of the indoor air; T_k^{dh} and R_k^{dh} are the temperature and resistance caused by humidity; R_k^{ai} is resistance between indoor air and ambient; Φ_k^h and Φ_k^{ac} is the power input from the heater and air conditioning.

Based on (1)-(4), the thermal dynamic model can be further modified as deterministic linear state space model in continuous time, as shown in (5).

$$\begin{aligned} \frac{dT_k}{dt} &= \mathrm{A}T_k + \mathrm{B}U_k \\ T_k^o &= \mathrm{C}T_k \end{aligned} \tag{5}$$

where $T_k = \left[T_k^w, T_k^m, T_k^r, T_k^i\right]^{'}$ is the state vector; $U_k = \left[T_k^a, T_k^{\mathrm{dh}}, \Phi_k^s, \Phi_k^{\mathrm{ac}}, \Phi_k^h\right]^{'}$ is the input vector of the thermal dynamic model; T_k^o denotes the measured parameters; A, B, and C are the system behavior, input behavior, and constant matrices. The matrices in (5) are shown in (6)-(8).

$$A = \begin{bmatrix} a_{11} & 0 & 0 & a_{14} \\ 0 & a_{22} & 0 & a_{24} \\ 0 & 0 & a_{33} & a_{34} \\ a_{41} & a_{42} & a_{43} & a_{44} \end{bmatrix} \tag{6}$$

where each element is shown as follows:

$a_{11} = \frac{1}{C_k^w R_k^{\mathrm{iw}}}$; $a_{14} = -\frac{1}{C_k^w}\left(\frac{1}{R_k^{\mathrm{iw}}} + \frac{1}{R_k^{\mathrm{aw}}}\right)$; $a_{22} = -\frac{1}{C_k^m R_k^{\mathrm{im}}}$; $a_{24} = \frac{1}{C_k^m R_k^{\mathrm{im}}}$; $a_{33} = -\frac{1}{C_k^r}\left(\frac{1}{R_k^{\mathrm{ir}}} + \frac{1}{R_k^{\mathrm{ar}}}\right)$; $a_{34} = \frac{1}{C_k^r R_k^{\mathrm{ir}}}$; $a_{41} = \frac{1}{C_k^i R_k^{\mathrm{iw}}}$; $a_{42} = \frac{1}{C_k^i R_k^{\mathrm{im}}}$; $a_{43} = \frac{1}{C_k^i R_k^{\mathrm{ir}}}$; $a_{44} = -\frac{1}{C_k^i}\left(\frac{1}{R_k^{\mathrm{ai}}} + \frac{1}{R_k^{\mathrm{iw}}} + \frac{1}{R_k^{\mathrm{im}}} + \frac{1}{R_k^{\mathrm{dh}}} + \frac{1}{R_k^{\mathrm{ir}}}\right)$.

$$B = \begin{bmatrix} \frac{1}{C_k^w R_k^{\mathrm{aw}}} & 0 & 0 & 0 & 0 \\ 0 & 0 & \frac{p\mathrm{A}_k^w}{C_k^m} & 0 & 0 \\ \frac{1}{C_k^r R_k^{\mathrm{ar}}} & 0 & 0 & 0 & 0 \\ \frac{1}{C_k^i R_k^{\mathrm{ai}}} & \frac{1}{C_k^i R_k^{\mathrm{dh}}} & \frac{(1-p)\mathrm{A}_k^w}{C_k^i} & \frac{1}{C_k^i} & \frac{1}{C_k^i} \end{bmatrix} \tag{7}$$

$$C = [0 \quad 0 \quad 0 \quad 1] \tag{8}$$

Since real data is collected in discrete time, the differential equation (5) in continuous time can be further written in discrete time based on Euler discretization method with sample time τ.

$$\begin{aligned} T_k(t{+}1) &= \mathrm{A}_{\mathrm{dis}}\mathrm{T}_k(t) + \mathrm{B}_{\mathrm{dis}}\mathrm{U}_k(t) \\ T_k^o(t) &= \mathrm{C}_{\mathrm{dis}}\mathrm{T}_k(t) \end{aligned} \tag{9}$$

where

$$A_{\mathrm{dis}} = \exp(\mathrm{A}\tau);\ B_{\mathrm{dis}} = \int_0^{\tau} \exp(\mathrm{A}\sigma)\mathrm{B}d\sigma;\ C_{\mathrm{dis}} = C.$$

The discrete thermal dynamic model in (9) is used to predict the indoor temperature at the next time. However, there are physical parameters that cannot be measured in the thermal dynamic model, such as heat capacity and resistance. Therefore, the maximum likelihood method can be used to evaluate these unknown parameters. After that, a Kalman filter is employed to perform a one-step prediction of equation (9) to obtain the indoor temperature [34].

3.2. Illuminance calculation

The strength of indoor daylight will affect residents' use of electric light [35]. In addition, the intensity of indoor daylight is mainly determined by the strength and length of outdoor sunlight [36]. Hence, the article integrates the daylight illuminance equation to evaluate the outdoor illuminance to improve the accuracy of the power usage of the electric light. The equation of the solar illuminance is given in (10) [37].

$$L_o = K_m \int_{0.38}^{0.78} v_\lambda E_\lambda \mathrm{d}\lambda \tag{10}$$

where L_o is the outdoor illuminance; K_m is the maximum luminous efficacy, which is 683 lm/W; v_λ is the luminous efficiency functions, which can be found from Commission Internationale de l'Éclairage (CIE) 1988 data [38]; E_λ is global irradiance; λ indicates the wavelength.

4. The proposed hybrid method

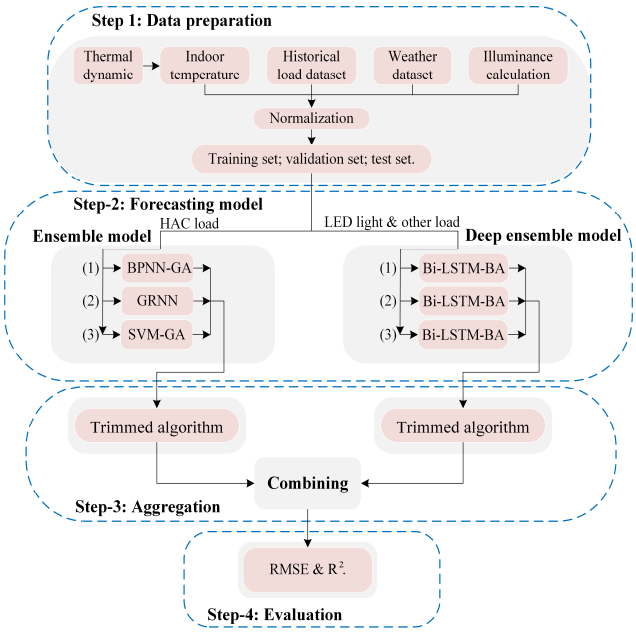

Fig. 2. The schematic diagram of the HM.

The HM divides the total data into HAC and non-HAC parts. The indoor temperature obtained by the thermal dynamic model integrates weather and a small amount of HAC historical data,

which will be used as the input of the EM to forecast HAC consumption. Non-HAC loads are further divided into electric lighting and other loads. A daylight equation is used to calculate the solar illuminance, which is combined with the historical data of the electric light power as input of the DEM to track the power consumption of the electric light. Other loads are directly predicted by DEM using its historical data. Finally, the HAC, lightings and other loads will be merged. The schematic diagram of the HM is displayed in Fig. 2.

4.1. Data preparation

During operation, the raw dataset will be divided into training (Y_{train}), verification (Y_{vald}), and test (Y_{test}) datasets. Y_{train} and Y_{vald} are used to train and select the optimal model and parameters. Y_{test} is used to test the performance of the HM. In addition, reasonable preprocessing of the mentioned datasets can effectively improve the performance of the predictor in the HM. Therefore, the min-max normalization method is employed to deal with these mentioned datasets. The normalization method can convert raw data to a scalar value between 0 and 1. The related equation can be expressed as (11).

$$\tilde{y}_k = \frac{y_k - y_{\min}}{y_{\max} - y_{\min}} \tag{11}$$

where y_k is the actual raw data; $y_{\max}$ and $y_{\min}$ are the maximum and minimum values in y_k; $\tilde{y}_k$ is the converted value.

4.2. The proposed EM method

The preprocessed data will be fed into the EM as input. It can be observed from Fig. 2 that the EM contains three predictors of SVM-GA, BPNN-GA, and GRNN. These three predictors operate independently of each other. This means that there is no mathematical mechanism between SVM-GA, BPNN-GA, and GRNN. The output of these three predictors will be sent to the trimmed algorithm to be combined and then remove undesirable outliers to improve the prediction accuracy. The detail of the individual predictor is shown below.

4.2.1. SVM-GA

The SVM is realized by the principle of structural risk minimization, the goal of which is to try to minimize the upper limit of generalization errors [39]. The forecasting performance of SVM is mainly determined by kernel functions and setting parameters, hence, they need to be selected reasonably. This article chooses the RBF kernel function because its performance is better than other kernel functions. GA is used to optimize the kernel parameters, insensitive loss parameters

and penalty parameters in SVM. The fitness function is represented by the mean square error (MSE) between actual and validation values.

4.2.2. BPNN-GA

The BPNN is a multi-layer mapping neural network algorithm, which can reverse the error of each node to adjust the relevant layer weights. However, the main disadvantage of BPNN is that it sometimes fails to find the global optimal value during the iterative calculation process [40]. Therefore, GA is used to address the problem of not being able to find the global optimum. In BPNN-GA, the initial weights, and thresholds of BPNN will be optimized by GA. The MSE is used as fitness function.

4.2.3. GRNN

The GRNN is a form of RBFNN deformation. Based on non-parametric regression, the GRNN calculates the expected output of the network with the maximum probability. In addition, the GRNN has better nonlinear approximation capabilities [41]. Therefore, the GRNN is suitable for solving nonlinear problems, such as STLF.

4.3. The proposed DEM method

LSTM network is a time series prediction model, which is proposed to address the problem of information loss and gradient disappearance caused by RNN [1], [3]. The schematic diagram of the LSTM network is given in Fig. 3. The computation formula can be written as (12)-(14).

$$\begin{bmatrix} f_t \\ i_t \\ o_t \\ \tilde{c}_t \end{bmatrix} = \begin{bmatrix} \sigma \\ \sigma \\ \sigma \\ \tanh \end{bmatrix} (\boldsymbol{w} \begin{bmatrix} x_t \\ h_{t-1} \end{bmatrix} + \boldsymbol{b}) \tag{12}$$

$$c_t = \tilde{c}_t * i_t + c_{t-1} * f_t \tag{13}$$

$$h_t = o_t * \tanh(c_t) \tag{14}$$

where f_t, i_t, o_t and $\tilde{c}_t$ are forget gate, input gate, output gate, and candidate value, respectively; x_t, h_t and c_t are the input, output, and cell state of the LSTM at the time t; h_{t-1} and c_{t-1} are the output and cell state at the previous time $t-1$; σ and tanh are the sigmoid and tanh functions; $\boldsymbol{w}$ and $\boldsymbol{b}$ indicate the weight matrices and bias vectors of the network activation function; * is an element-wise product.

In the LSTM network, input x_t is combined with previous output h_{t-1} to generate the value of f_t (0,1) to determine whether to let previous cell state c_{t-1} pass. In addition, the input x_t and output

h_{t-1} are sent to the sigmoid and tanh functions to update the cell state c_t. After, c_t passes through the tanh function and multiplies the signal from the output gate o_t to obtain the target output h_t.

The LSTM is a one-direction time series prediction method, which suffers from insufficient usage of temporal features [42]. Therefore, the Bi-LSTM as the latest derivative structure of the RNN is presented to address this problem [43]. The schematic structure of the Bi-LSTM is drawn in Fig. 4. In each layer, the Bi-LSTM consists of the backward layer and forward layer. The backward layer can obtain the future information from the data, while the forward layer can process the past feature of the data. Therefore, Bi-LSTM can realize two-way information transmission. The hidden layer state ($\boldsymbol{H}_t$) including forward state ($\overrightarrow{h}_t$) and backward state ($\overleftarrow{h}_t$) can be written as (15).

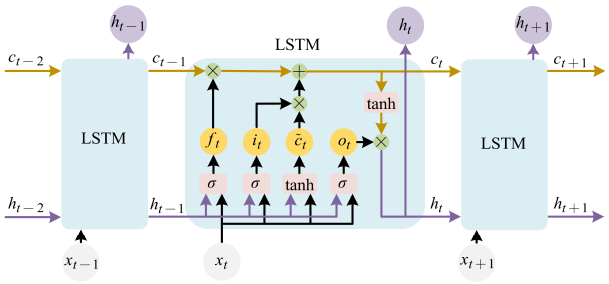

Fig. 3. The schematic diagram of the LSTM network.

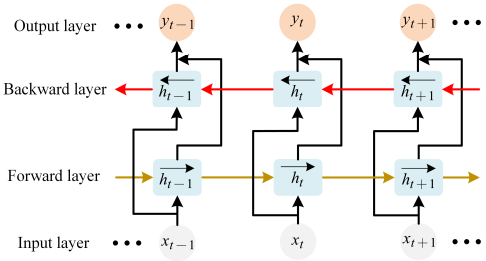

Fig. 4. The schematic diagram of the Bi-LSTM network.

$$\begin{cases} \overrightarrow{h}_t = \overrightarrow{\mathrm{LSTM}}(h_{t-1}, x_t, c_{t-1}) \\ \overleftarrow{h}_t = \overleftarrow{\mathrm{LSTM}}(h_{t+1}, x_t, c_{t+1}) \\ \boldsymbol{H}_t = [\overrightarrow{h}_t, \overleftarrow{h}_t] \end{cases} \tag{15}$$

The hyperparameters of Bi-LSTM is required to be carefully adjusted to get the best prediction results. The BA is selected as the optimization tool to search the optimal hyperparameters for Bi-LSTM. In a network model $\mathcal{M}_i(\cdot)$, θ_i is marked as a vector including the configured hyperparameters. The purpose of the BA is to search for the optimal hyperparameters (θ_i^{opt}) in a way that minimizes the performance errors of the network $\mathcal{M}_i(\cdot)$.

$$\theta_i^{\mathrm{opt}} = \underset{\theta}{\operatorname{argmin}}\, \mathcal{L}(\theta) \tag{16}$$

where $\mathcal{L}(\cdot)$ is expressed as the real dataset and the errors evaluated by the model $\mathcal{M}_i(\cdot)$. The steps of the BA are summarized as follows:

1. The BA will consider the error function $\mathcal{L}(\cdot)$ as a Gaussian process (GP) model. Subsequently, the input information (θ) is used to adjust and optimize the model.
2. θ_i is selected from the GP model. The selection standard is that θ_i can maximize the acquisition function.
3. The value of $\mathcal{L}(\theta)$ is calculated. If the maximum iteration is reached, the output result is displayed. Otherwise, BA will go back to step 2. More detail regarding BA can be found in [44].

The optimized hyperparameters of Bi-LSTM are given below:

1. Initial learning rate: refers to the value used for the initial training of the network.
2. L2 regularization coefficient: indicates regularization term which can attenuate the weights, thereby preventing the phenomenon of model overfitting.
3. Hidden size: represents the number of neurons in each hidden layer.

4.4. Trimmed algorithm

Each predictor in the EM and DEM will produce a related expected result. This means that the results from individual predictors need to be appropriately combined. In this article, multiple results are aggregated by adopting a trimmed algorithm, which can effectively remove the extreme values in the results to improve the prediction accuracy [45]. In order to calculate the optimal trimming mean, the predicted value of each row in Y_{vald} should be arranged in ascending order. Then, the forecast trimming number (n_{trim}) is defined as (17).

$$n_{\text{trim}} = \frac{\alpha}{100} n_{\text{total}} \tag{17}$$

where n_{total} is the total number of the predictors; $\alpha \in [1,100]$ is the amount of the trimming. Then, the number of elements contained in each row of Y_{vald} can be expressed as (18).

$$I_\alpha = \{\frac{n_{\text{trim}}}{2} + 1, \frac{n_{\text{trim}}}{2} + 2, \ldots, n_{\text{total}} - \frac{n_{\text{trim}}}{2}\}. \tag{18}$$

Finally, the optimal trimming mean in the l^{th} row of Y_{vald} can be calculated by using (19).

$$\hat{y}_l^\alpha = \frac{1}{n_{\text{total}} - n_{\text{trim}}} \sum_{j \in I_\alpha} \hat{y}_{l,j} \tag{19}$$

where $l = 1, 2, \ldots, n_{\text{vald}}$. It should be noted that n_{vald} refers to the number of rows in Y_{vald}. After the optimal trimming mean is obtained, the root mean squared error (RMSE) is used to test its performance, as shown in (20).

$$\text{RMSE}^{\alpha} = \left[\frac{1}{n_{\text{vald}}}\sum_{l=1}^{n_{\text{vald}}}(\hat{y}_l^{\alpha} - y_l)^2\right]^{1/2} \tag{20}$$

where y_l is the actual value. The above steps will be repeated within the scope of α. Once the smallest RMSE^{α} is reached, then the optimal α can be determined. After that, the predicted samples in Y_{test} will be trimmed appropriately based on the optimal α.

4.5. Evaluation metrics

In order to evaluate the prediction performance, RMSE, and coefficient of determination (R^2) are chosen as evaluation metrics. RMSE are used to measure the difference between the forecasting and actual values, as shown in (20). R^2 is employed to measure the fit of the prediction model. If R^2 is closer to 1, then this means better predictive ability and data fit. R^2 can be written as (21).

$$R^2 = 1 - \frac{\sum_{l=1}^{N}(y_l - \hat{y}_l)^2}{\sum_{l=1}^{N}(y_l - \bar{y}_l)^2} \tag{21}$$

where $\hat{y}_l$ is the predicted value; $\bar{y}_l$ is the average actual value; N is the number of the data.

5. Case studies and discussions

In this section, the public datasets from the UMass Smart Microgrid Project [46] and Flexhouse project [47] are used to verify the performance and feasibility of the proposed method. The purpose of the UMass project is to optimize user power usage by analyzing collected household load data. Therefore, the UMass project deploys intelligent real-time systems in three real homes located in Western Massachusetts to continuously collect environmental and power consumption data. The UMass project focuses on collecting indoor environment, outdoor weather and power usage of household appliances. This article selects the data of houses A and B as the test objects. Houses A and B use a gas-powered heating system to increase the indoor temperature in winter. In summer, house A uses natural ventilation, while house B uses central air-conditioning to cool down. Therefore, the load data of house A mainly includes lighting usage and other loads (e.g., refrigerator and dishwash). The load data for house B consists of air conditioning, lighting, and other loads. The Flexhouse project is an experimental building located at the Technical University of Denmark, it collects the power usage of heater to study the energy performance of buildings. The experiment time range is from February 2009 to April 2009. The data of the Flexhouse project is composed of indoor environment, weather, and heater. The data sampling interval of Flexhouse

and UMass is 5 minutes. Finally, BPNN-PSO, ELM-GA, RBF, and the method from Ref. [31] will be used to compare the proposed models.

5.1. Case 1: indoor temperature prediction

Unknown parameters that cannot be measured from (5) are estimated in Table II. Due to the different structure, material, and environment of house B and Flexhouse, the unknown parameters of their thermal dynamic models are different. For both houses, the heat capacity C_k^r of the roof is larger than other heat capacity parameters. Therefore, the roofing material has better heat storage capability and slower temperature changes. The estimated heat capacity C_k^i of indoor air is the smallest. This indicates that the indoor air has a low heat-gathering capacity, hence, its temperature will change faster. The resistance against thermal convection from the outdoor ambient to the house roof R_k^{ar} and wall R_k^{aw} is almost the same. This shows that the external environment of the roof and the wall is the same. In house B, the resistance against thermal convection from the indoor air to the roof R_k^{ir}, external wall R_k^{iw}, and inner medium R_k^{im} is the lowest. In Flexhouse, the thermal resistance R_k^{im} is the smallest. Also, the p of both houses is 0.869 and 0.915, which means that most of the solar radiation passing through the window is absorbed by the indoor medium.

TABLE II
CASE 1: ESTIMATED PARAMETERS

Buildings	C_k^i	C_k^m	C_k^r	C_k^w	R_k^{ar}	R_k^{aw}	R_k^{dh}	R_k^{ai}	R_k^{im}	R_k^{ir}	R_k^{iw}	p
House B	0.109	19.288	65.798	21.51	15.994	15.616	13.758	14.218	0.686	0.658	0.73	0.869
Flexhouse	0.1073	1.9707	31.188	21.835	81.723	86.403	2.544	89.754	0.988	76.591	77.677	0.915

Note: the units of C_k^x and R_k^x are kWh/℃ and ℃/kW; x represents the unified symbol of upper labels.

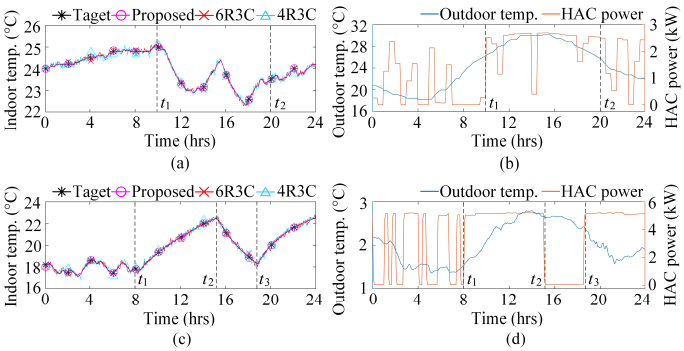

Fig. 5. Simulation results for case 1: (a) Indoor temperature for house B, (b) Outdoor temperature and HAC power for house B, (c) Indoor temperature for Flexhouse, (d) Outdoor temperature and HAC power for Flexhouse.

TABLE III
CASE 1: EVALUATION METRICS FOR INDOOR TEMPERATURE

	House B			Flexhouse		
	Proposed	6R3C	4R3C	Proposed	6R3C	4R3C
RMSE (℃)	0.0245	0.078	0.0974	0.0751	0.1778	0.1676
R^2	0.9987	0.9872	0.9801	0.998	0.9899	0.9886

After the unknown parameters in the thermal dynamic model are calculated, the indoor temperature can be predicted by using Kalman filter. In addition, the thermal dynamic model 6R3C (including six thermal resistances and three thermal capacities) and 4R3C from [31] and [48] are used for comparison. It can be seen from Fig. 5(a) that the predicted indoor temperature can accurately track the changes in the actual measured temperature. Besides, the indoor temperature is the lowest between t_1 and t_2, but the outdoor temperature rises to about 30 ℃. This indicates that the central air conditioning delivers power to adjust the indoor temperature, as shown in Fig. 5(b). From Table III, the proposed method has the lowest RMSE (0.0245). The R^2 value is 0.9987, which is very close to 1. Besides, 4R3C method produces the highest error and the smallest R^2. From Fig. 5(c) and 5(d), The predicted temperature experiences three points: t_1, t_2 and t_3. Between t_1 and t_2, the indoor temperature rises to about 22.5°C, while the outdoor temperature is only about 2°C. This means that the heater is working to improve the indoor temperature. Since the heater stops transferring heat between t_2 and t_3, the indoor temperature starts to drop. From Table III, the proposed method performance RMSE (0.0751) are the lowest, and R^2 (0.998) is the highest. The prediction results of 6R3C are slightly higher than 4R3C method. From the above results, the indoor temperature can reflect the usage of the heater and AC system. In addition, the proposed thermal dynamic model outperforms the comparing methods.

5.2. Case 2: illumination and light study

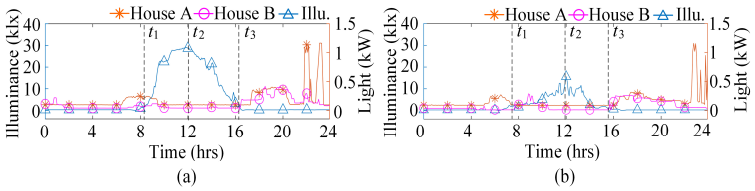

Fig. 6. Simulation results for case 2: (a) Illumination and light on January 25, 2016, (b) Illumination and light on September 30, 2016.

The relationship between illuminance and power usage of the electric light will be analyzed in Case 2. The data collected from January 25, 2016 and September 30, 2016 are used as test targets. From Fig. 6(a), the daylight illuminance is an upward trend between t_1 and t_2, this means that the visibility inside and outside has improved. The lighting energy in house A begins to decrease, and the energy usage of the lights in house B does not change significantly. Since the illuminance will be the lowest at t_3, the indoor and outdoor visibility will decrease. Therefore, the energy consumption of lights in houses A and B have been significantly increased. From Fig. 6(b), the illuminance starts to increase at t_1. The energy consumption of lights in houses A and B has slightly changed. The illuminance reaches the highest at t_2, and the lighting power in houses A and B are both low. Since the illuminance reaches its lowest at t_3, the energy usage of the lights

in houses A and B is significantly increased. From the above results, it can be seen that the intensity of illuminance can also reflect the use of lighting energy.

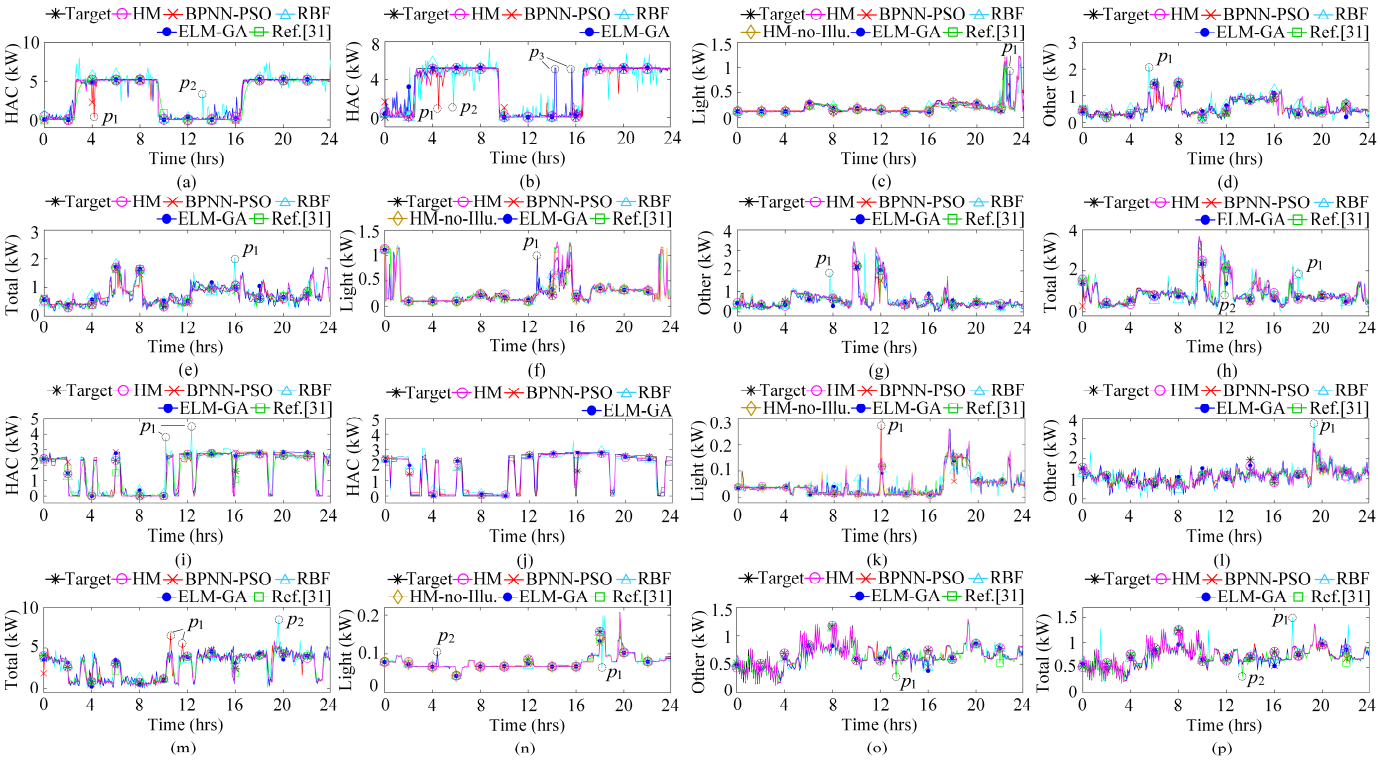

Fig. 7. Simulation results for case 3: (a) HAC usage for Flexhouse in winter, (b) HAC usage for Flexhouse without indoor temperature in winter, (c) Lighting usage for house A in summer, (d) Other load usage for house A in summer, (e) Total load usage for house A in summer, (f) Lighting usage for house A in winter, (g) Other load usage for house A in winter, (h) Total load usage for house A in winter, (i) HAC usage for house B in summer, (j) HAC usage for house B without indoor temperature in summer, (k) Lighting usage for house B in summer, (l) Other load usage for house B in summer, (m) Total load usage for house B in summer, (n) Lighting usage for house B in winter, (o) Other load usage for house B in winter, (p) Total load usage for house B in winter.

TABLE IV
CASE 3: EVALUATION METRICS FOR 1 DAY LOAD FORECASTING

	Flexhouse				House A									
	HAC in winter		HAC in winter (no indoor temp.)		Light usage in summer		Other load usage in summer		Total load usage in summer		Light usage in winter		Other load usage in winter		Total load in winter	
Methods	RMSE (kW)	R^2	RMSE (kW)	R^2	RMSE (kW)	R^2	RMSE (kW)	R^2	RMSE (kW)	R^2	RMSE (kW)	R^2	RMSE (kW)	R^2	RMSE (kW)	R^2
HM	0.2521	0.9898	0.3533	0.98	0.026	0.9785	0.0363	0.9853	0.0441	0.9832	0.0532	0.9602	0.0725	0.9835	0.0892	0.9763
BPNN-PSO	0.4801	0.9631	0.2534	0.9467	0.0731	0.83	0.1227	0.8317	0.1473	0.8126	0.1134	0.8192	0.234	0.8279	0.225	0.8495
ELM-GA	0.4652	0.9654	0.7408	0.9122	0.0866	0.7618	0.1141	0.8545	0.1327	0.8479	0.1116	0.8251	0.2208	0.8467	0.223	0.8522
RBF	0.6501	0.9324	0.7647	0.9064	0.0826	0.7832	0.1331	0.8019	0.1565	0.7884	0.1171	0.8074	0.2479	0.8068	0.2478	0.8175
Ref. [31]	0.5475	0.952	-	-	0.0528	0.9113	0.0655	0.9521	0.0834	0.9398	0.078	0.9146	0.1425	0.9362	0.1559	0.9278
HM (no-Illu.)	-	-	-	-	0.0337	0.9639	-	-	-	-	0.0683	0.9344	-	-	-	-
	House B															
	HAC in summer		HAC in summer (no indoor temp.)		Light usage in summer		Other load usage in summer		Total load usage in summer		Light usage in winter		Other load usage in winter		Total load in winter	
Methods	RMSE (kW)	R^2	RMSE (kW)	R^2	RMSE (kW)	R^2	RMSE (kW)	R^2	RMSE (kW)	R^2	RMSE (kW)	R^2	RMSE (kW)	R^2	RMSE (kW)	R^2
HM	0.2031	0.9732	0.2451	0.9610	0.0059	0.9835	0.0363	0.9853	0.2162	0.9806	0.0025	0.9828	0.0396	0.9613	0.0396	0.9624
BPNN-PSO	0.2908	0.945	0.3189	0.9339	0.0172	0.8579	0.2012	0.7474	0.4737	0.9069	0.0066	0.879	0.1026	0.7405	0.1014	0.7529
ELM-GA	0.24	0.9626	0.3163	0.9350	0.0186	0.8331	0.2121	0.7194	0.4779	0.9052	0.0068	0.8705	0.1016	0.7458	0.0966	0.7755
RBF	0.3608	0.9154	0.3914	0.9004	0.0232	0.7417	0.2268	0.679	0.5436	0.8773	0.008	0.8231	0.1067	0.7197	0.1082	0.7187
Ref. [31]	0.2989	0.9419	-	-	0.0138	0.9082	0.1342	0.8877	0.3387	0.9524	0.0053	0.9216	0.0811	0.8379	0.0813	0.8412
HM (no-Illu.)	-	-	-	-	0.0101	0.9514	-	-	-	-	0.0045	0.9431	-	-	-	-

5.3. Case 3: house daily load forecast

The Flexhouse data collected on February 10, 2009, and houses A and B measured on February 27, 2016 and July 28, 2016 were used as test targets (Note: February is winter, and July is summer). In the collected dataset, HAC power is predicted using forecasted indoor temperature, meteorological and less historical data as the input of the EM. The DEM combining the calculated illuminance data is used to track the trajectory of lighting energy and other loads. Tables IV lists the comparison of RMSE and R^2 for the load prediction between the HM and other methods. Fig. 7 shows the forecasting results and the corresponding targets.

It can be seen from the results of Flexhouse in Table IV that the RMSE of HM (0.2521) are smaller than other single predictors. In addition, the HM has the highest coefficient of determination (0.9898), which indicates that the HM model has a strong fitting ability. The RBF model shows the largest RMSE (0.6501), and the smallest R^2 (0.9324). The prediction performance of ELM-GA and BPNN-PSO are relatively close. The method from Ref. [31] produces a prediction error between BPNN-PSO and RBF. Fig. 7(a) shows that the proposed HM can accurately predict the change of HAC load. However, a single model such as BPNN-PSO and RBF will have larger extreme values (p_1 and p_2), thereby increasing the forecasting error. In addition, Fig. 7(b) presents the result of removing the indoor temperature from the input in the predictor. Although the HM, ELM-GA, BPNN-PSO, and RBF can predict changes in HAC load, their prediction accuracy and fitting capability are reduced, as shown in Table IV. It should be noted that the method from Ref. [31] is to evaluate the energy consumption of HAC by indoor temperature. Therefore, the method cannot be operated under the condition of removing the indoor temperature.

From the results of house A in Table IV, the proposed method can accurately predict the lighting in summer and winter. The proposed method provides the lowest RMSE (0.026 and 0.0532) and the highest R^2 (0.9785and 0.9835). After removing the daylight illuminance, the prediction accuracy and fit of the proposed method are reduced. The results (0.0337 and 0.0683 for RMSE; 0.9639 and 0.9344 for R^2) are still better than the other single predictors. The power consumption trajectories of other loads (such as refrigerator and dishwasher) can also be accurately captured by the proposed method. The total load forecast is achieved by combining the predicted lighting energy and other loads. This means that the total load forecast can provide lower RMSE (0.0441 and 0.0892) and the highest R^2 (0.9832 and 0.9763). However, due to the poor generalization and training network capabilities of a single predictor, ELM-GA, BPNN-PSO, RBF, and the method from Ref. [31] give lower R^2 and RMSE. The forecasting results of the house A are shown in Fig. 7(c) - 7(h).

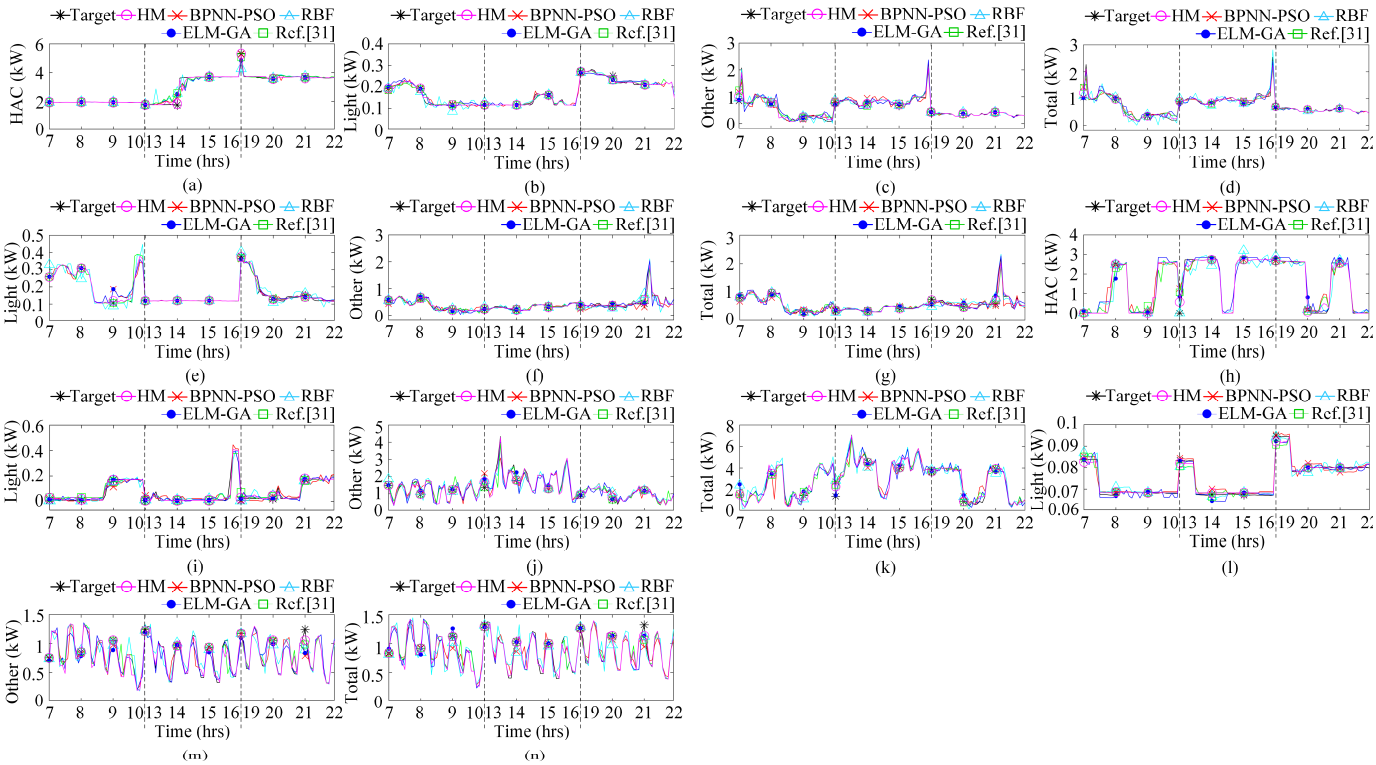

Fig. 8. Simulation results for case 4: (a) HAC usage for Flexhouse in winter, (b) Lighting usage for house A in summer, (c) Other load usage for house A in summer, (d) Total load usage for house A in summer, (e) Lighting usage for house A in winter, (f) Other load usage for house A in winter, (g) Total load usage for house A in winter, (h) HAC usage for house B in summer, (i) Lighting usage for house B in summer, (j) Other load usage for house B in summer, (k) Total load usage for house B in summer, (l) Lighting usage for house B in winter, (m) Other load usage for house B in winter, (n) Total load usage for house B in winter.

TABLE V
CASE 4: EVALUATION METRICS FOR 3 HOURS LOAD FORECASTING

	Flexhouse			House A											
	HAC in winter (R^2)			Light usage in summer (R^2)			Other load in summer (R^2)			Total load in summer (R^2)			Light usage in winter (R^2)		
Methods	M	A	E	M	A	E	M	A	E	M	A	E	M	A	E
HM	0.9835	0.9661	0.9839	0.9795	0.9833	0.9788	0.9706	0.9469	0.9507	0.9765	0.9492	0.9593	0.9815	0.9393	0.9832
BPNN-PSO	0.9213	0.9026	0.9064	0.9259	0.9144	0.8999	0.8889	0.8814	0.8608	0.8998	0.8727	0.8638	0.8916	0.8978	0.9186
ELM-GA	0.9439	0.9081	0.9327	0.9311	0.9177	0.9012	0.9058	0.9019	0.8999	0.9003	0.8773	0.8749	0.9067	0.8958	0.9114
RBF	0.9187	0.8781	0.9088	0.9095	0.8701	0.8891	0.9341	0.8836	0.858	0.8953	0.8079	0.8184	0.919	0.872	0.9298
Ref. [31]	0.9677	0.9108	0.9028	0.9332	0.9462	0.9464	0.9104	0.9013	0.9062	0.924	0.9051	0.9025	0.9458	0.9241	0.9416
	House A						House B								
	Other load in winter (R^2)			Total load in winter (R^2)			HAC in summer (R^2)			Light usage in summer (R^2)			Other load in summer (R^2)		
Methods	M	A	E	M	A	E	M	A	E	M	A	E	M	A	E
HM	0.9802	0.9691	0.9366	0.9864	0.9687	0.9307	0.9869	0.9819	0.9876	0.9656	0.9558	0.979	0.9399	0.9376	0.9255
BPNN-PSO	0.8679	0.8579	0.8697	0.922	0.8234	0.8636	0.9357	0.9255	0.9505	0.9266	0.9144	0.9232	0.8611	0.8443	0.8387
ELM-GA	0.8839	0.8669	0.8852	0.9411	0.8541	0.8722	0.9414	0.944	0.9794	0.9482	0.9249	0.9399	0.8883	0.8675	0.8563
RBF	0.8462	0.8107	0.8349	0.9122	0.8046	0.8315	0.9101	0.9163	0.9454	0.9335	0.9122	0.92	0.8526	0.8413	0.8251
Ref. [31]	0.9119	0.8757	0.8899	0.9443	0.8744	0.8812	0.9492	0.9445	0.9651	0.9188	0.919	0.9377	0.8927	0.8715	0.8809
	House B												-		
	Total load in summer (R^2)			Light usage in winter (R^2)			Other load in winter (R^2)			Total load in winter (R^2)			-		
Methods	M	A	E	M	A	E	M	A	E	M	A	E	-	-	-
HM	0.9768	0.9633	0.9873	0.9882	0.9716	0.9542	0.9546	0.9392	0.9439	0.955	0.9404	0.9443	-	-	-
BPNN-PSO	0.9141	0.906	0.9385	0.9193	0.9372	0.9038	0.8917	0.8405	0.8596	0.8815	0.8316	0.8786	-	-	-
ELM-GA	0.9315	0.9172	0.9408	0.936	0.9454	0.9444	0.9007	0.8817	0.8618	0.8953	0.848	0.8821	-	-	-
RBF	0.9073	0.8915	0.924	0.9356	0.9449	0.9103	0.8851	0.8494	0.8437	0.8903	0.8123	0.8745	-	-	-
Ref. [31]	0.9478	0.9233	0.9707	0.9553	0.9289	0.9207	0.9096	0.8675	0.9002	0.9102	0.8697	0.9011	-	-	-

Note: M – morning, A – afternoon, E – evening.

The summer power data of the house B includes HAC, lightings and other loads. From Fig. 7(i) and 7(j), the HM can accurately track the HAC power trajectory such that its prediction has a

better fit with the target value. Although other single predictors can also predict HAC load consumption, they may have undesirable extreme values, thereby reducing the accuracy of prediction. From Fig. 7(k) and 7(l), HM can effectively predict lighting and other loads that have high frequency change characteristics. The HM gives the highest R^2 (0.9835 and 0.9853) and lowest RMSE (0.0059 and 0.0363). However, the prediction errors of other methods are significantly larger, as shown in Table IV. Since the prediction error of HM for each load is low, the prediction accuracy of the total load is high, as shown in Fig. 7(m). In addition, the HM can also accurately predict the daily load usage of house B in winter, and its results are also significantly better than a single prediction method. The results are shown in Table IV and Fig. 7(n) - 7(p). From the above results, the proposed HM can accurately and stably predict the daily load in various houses and seasons. The result is obviously better than BPNN-PSO, ELM-GA, RBF, and the method from Ref. [31].

5.4. Case 4: house load forecast for 3 hours

The performance of the HM in 3 hours load forecasting will be studied. The Flexhouse data collected on March 4, 2009, and houses A and B measured on February 29, 2016 and July 26, 2016 were used as test data. In order to show the change characteristics of the load in different time periods, Case 4 will select the load data from 7:00 to 10:00, 13:00 to 16:00, and 19:00 to 22:00 as the test targets. The prediction results are presented in Fig. 8 and Table V.

From Fig. 8(a), the HAC load in Flexhouse does not change in the morning and evening. Therefore, the R^2 values of all predictors are above 0.9, and R^2 values of the proposed HM are the highest at 0.9835 and 0.9839. In the afternoon, the HAC load had a sudden change. Hence, the accuracy of all predictors decreases. However, the prediction fit of the HM is still the highest, it is 0.9661. It can be seen from Fig. 8(b) - 8(g) that the HM's prediction accuracy of the load energy consumption for house A is significantly better than other single predictors. The maximum and minimum of R^2 for the proposed HM are 0.9876 and 0.9307. In addition, the load change frequency of house B is relatively fast, and the HM can still achieve accurate prediction, as shown in Fig. 8(h) - 8(n). From the above results, it can be concluded that the prediction ability of the proposed HM is obviously better than the compared methods.

5.5. Case 5: long-term house load forecast

The HM is used to realize the long-term load forecast of the houses for 3 months. Houses A and B data collected from July 2016 to September 2016 are used as the test targets. It should be noted that the data from February to April 2009 provided by the Flexhouse project is intermittent. Therefore, Flexhouse is not studied in Case 5. The prediction results are presented in Fig. 9 and Table VI.

From Fig. 9(a) - 9(g), it can be observed that the three-month load change frequency of houses A and B is relatively fast. Due to the poor generalization and training network capabilities of a single predictor, ELM-GA, BPNN-PSO, RBF and the method from Ref. [31] give lower R^2 and higher RMSE. However, the HM can still guarantee high prediction accuracy and determination coefficient. For example, in the total load prediction result of house B, the HM provides the highest R^2 (0.9677) and the lowest RMSE (0.2064). Meanwhile, RBF shows the highest RMSE (0.5461) and the lowest R^2 (0.7738). Although the prediction performance of ELM-GA, BPNN-PSO, and the method from Ref. [31] is better than RBF, they are still lower than the HM. Therefore, the proposed HM is better than a single predictor in long-term house load prediction.

From the above results, it can be seen that the HM has the best generalization ability, and it can maintain good prediction accuracy in different buildings (Flexhouse, houses A and B), season (summer and winter) and time horizons (3 hours, 1 day and 3 months). Meanwhile, ELM-GA, BPNN-PSO, RBF and the method from Ref. [31] have different prediction accuracy under different conditions. This means that the prediction stability of a single predictor is poor. Therefore, the proposed HM prediction has better stability and can be used for various household load predictions.

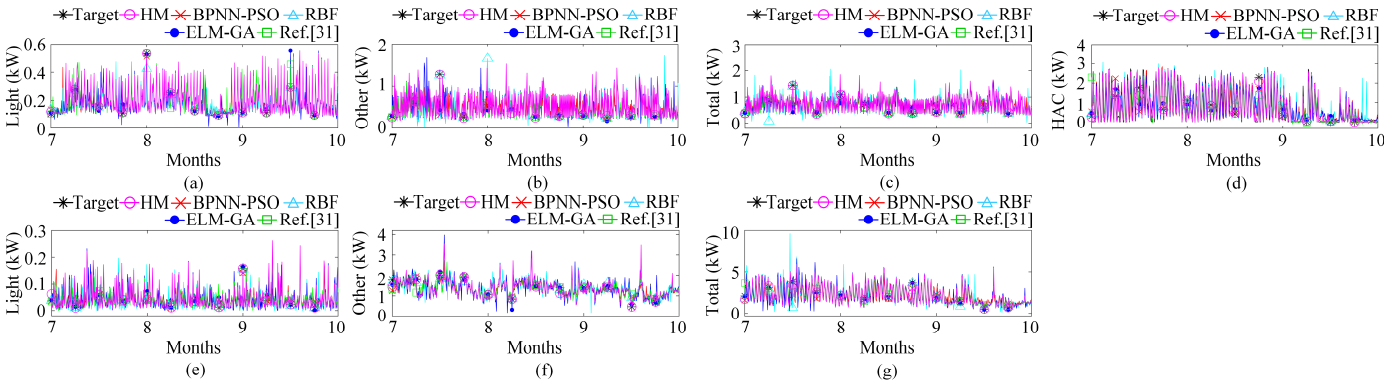

Fig. 9. Simulation results for case 5: (a) Lighting usage for house A, (b) Other load usage for house A, (c) Total load usage for house A, (d) HAC usage for house B, (e) Lighting usage for house B, (f) Other load usage for house B, (g) Total load usage for house B.

TABLE VI
CASE 5: EVALUATION METRICS FOR 3 MONTHS LOAD FORECASTING

	House A						House B							
	Light usage		Other load usage		Total load usage		HAC in summer		Light usage in		Other load usage		Total load usage	
Methods	RMSE (kW)	R^2	RMSE (kW)	R^2	RMSE (kW)	R^2	RMSE (kW)	R^2	RMSE (kW)	R^2	RMSE (kW)	R^2	RMSE (kW)	R^2
HM	0.0229	0.9536	0.0579	0.9572	0.0688	0.9524	0.1731	0.959	0.0127	0.9003	0.0895	0.9575	0.2064	0.9677
BPNN-PSO	0.0483	0.7946	0.1482	0.7195	0.1618	0.737	0.4391	0.736	0.022	0.6996	0.2171	0.7503	0.5327	0.7847
ELM-GA	0.0465	0.8096	0.1475	0.7221	0.1503	0.773	0.4055	0.7749	0.0213	0.7178	0.2019	0.784	0.4828	0.8231
RBF	0.0494	0.7851	0.1582	0.6802	0.1656	0.7244	0.4562	0.715	0.0223	0.6926	0.2193	0.7453	0.5461	0.7738
Ref. [31]	0.0359	0.8866	0.0879	0.9012	0.0941	0.911	0.3664	0.8161	0.0199	0.7537	0.1893	0.8101	0.4261	0.8622

6. Conclusion

In this paper, a HM method is proposed for the STLF of the individual residential user. The HM includes a thermal dynamic model, DEM, and EM. The thermal dynamic model is used to predict

the indoor temperature, which integrates meteorological and a small amount of HAC historical data as the input of the EM to forecast the HAC load usage. In addition, non-HAC loads are divided into lightings and other loads. An illuminance calculation method is used to generate daylight illuminance, which will be combined with lighting historical data as input of the DEM to predict light usage. Other loads are directly predicted by DEM. The EM includes SVM, BPNN, and GRNN. GA is used to optimize the hyperparameters of SVM and BPNN. The DEM consists of the multiple Bi-LSTM networks. The BA is used to search the optimal hyperparameters of the Bi-LSTM. The outputs of the individual predictors are aggregated by a trimmed algorithm. The total load forecast is obtained by combining HAC, lighting and other loads. The data of the UMass microgrid and Flexhouse projects is used as the test target. The results show that the predictive performance of the proposed HM works as expected.

References:

[1] J. Li, D. Deng, J. Zhao, D. Cai, W. Hu, M. Zhang, *et al*., "A novel hybrid short-term load forecasting method of smart grid using MLR and LSTM neural network," *IEEE Trans. Ind. Informat*., vol. 17, no. 4, April 2021.

[2] K. Aurangzeb, M. Alhussein, K. Javaid, and S.I. Haider "A pyramid-CNN based deep learning model for power load forecasting of similar-profile energy customers based on clustering," *IEEE Access,* vol.9, pp. 14992-15003, Jan. 2021.

[3] W. Kong, Z. Y. Dong, Y. Jia, D. J. Hill, Y. Xu, and Y. Zhang, "Short-term residential load forecasting based on LSTM recurrent neural network," *IEEE Trans. Smart Grid*, vol. 10, no. 1, pp. 841–851, Jan. 2019.

[4] M. Zhou, and M. Jin, "Holographic ensemble forecasting method for short-term power load," *IEEE Trans. Smart Grid*, vol. 10, no. 1, pp. 425-434, Jan. 2019.

[5] D. Tran, D. Luong, and J. Chou, "Nature-inspired metaheuristic ensemble model for forecasting energy consumption in residential buildings," *Energy*, vol. 191, pp. 116552, Jan. 2020.

[6] G. Zhang, and J. Guo "A novel ensemble method for residential electricity demand forecasting based on a novel sample simulation strategy," *Energy*, vol. 207, no. 118265, Sep. 2020.

[7] H. Shi, M. Xu, and R. Li, "Deep learning for household load forecasting— A novel pooling deep RNN," *IEEE Trans. Smart Grid*, vol. 9, no. 5, pp. 5271–5280, Sep. 2018.

[8] M. Q. Raza, M. Nadarajah, and C. Ekanayake, "An improved WT and NN ensemble demand forecast model for PV integrated smart buildings," *IEEE PES Innov. Smart Grid Technol. Conf. Eur*., pp. 781–786, 2016.

[9] W. Mai, C. Y. Chung, T. Wu, and H. Huang, "Electric load forecasting for large office building based on radial basis function neural network," *IEEE Power Energy Soc. Gen. Meet*., pp. 1–5, Oct. 2014.

[10] A. Musaed, A. Khursheed, and I. Syed, “Hybrid CNN-LSTM Model for Short-Term Individual Household Load Forecasting,” *IEEE Access*, vol. 8, pp. 180544-180557, Oct. 2020.

[11] R. Aowabin, M. Gilanifar, S. Vivek, and S. Amanda, “Predicting electricity consumption for commercial and residential buildings using deep recurrent neural networks,” *Appl. Energy*, vol. 212, pp. 372–385, Feb. 2018.

[12] J. C. López, M. J. Rider and Q. Wu, “Parsimonious short-term load forecasting for optimal operation planning of electrical distribution systems,” *IEEE Trans. Power Syst.*, vol. 34, no. 2, pp. 1212-1219, Mar. 2019.

[13] A. Dejamkhooy, A. Dastfan and A. Ahmadyfard, “Modeling and forecasting nonstationary voltage fluctuation based on grey system theory,” *IEEE Trans. Power Del.*, vol. 32, no. 3, pp. 1212-1219, Jun. 2017

[14] J. Zhao and X. Liu, “A hybrid method of dynamic cooling and heating load forecasting for office buildings based on artificial intelligence and regression analysis,” *Energy Build*., vol. 174, pp. 293-308, 2018.

[15] Y. Wang, Q. Chen, T. Hong, and C. Kang, “Review of smart meter data analytics: Applications, methodologies, and challenges,” *IEEE Trans. Smart Grid*, vol. 10, no. 3, pp. 3125–3148, May 2019.

[16] C. Cecati, J. Kolbusz, P. Ró˙zycki, P. Siano, and B. M. Wilamowski, “A novel RBF training algorithm for short-term electric load forecasting and comparative studies,” *IEEE Trans. Ind. Electron*., vol. 62, no. 10, pp. 6519–6529, Oct. 2015.

[17] Y. Yu, X. Wang, and R. Bründlinger, “Improved Elman Neural Network Short-Term Residents Load Forecasting Considering Human Comfort Index,” *J. Electr. Eng. Technol*., vol. 14, no. 6, pp. 2315–2322, 2019.

[18] P. Li, Y. Li, Q. Xiong, Y. Chai, and Y. Zhang, “Application of a hybrid quantized Elman neural network in short-term load forecasting,” *Int. J. Electr. Power Energy Syst*., vol. 55, pp. 749–759, 2014.

[19] X. Lin, Z. Tian, Y. Lu, H. Zhang, and J. Niu, “Short-term forecast model of cooling load using load component disaggregation,” *Appl. Therm. Eng*., vol. 157, pp. 113630, Feb. 2019.

[20] A. O. Hoori, A. Al Kazzaz, R. Khimani, Y. Motai, and A. J. Aved, “Electric Load Forecasting Model Using a Multicolumn Deep Neural Networks,” *IEEE Trans. Ind. Electron*., vol. 67, no. 8, pp. 6473–6482, Aug. 2020.

[21] H. Su, T. Liu, and H. Hong, “Adaptive residual compensation ensemble models for improving solar energy generation forecasting,” *IEEE Trans. Sustain. Energy*, vol. 11, no. 2, pp. 1103-1105, April 2020.

[22] M. Q. Raza, M. Nadarajah, J. Li, and K. Y. Lee, "Multivariate Ensemble Forecast Framework for Demand Prediction of Anomalous Days," *IEEE Trans. on Sustain. Energy*, vol. 11, no. 1, pp. 27-36, Nov. 2020.

[23] C. Lai *et al*, "Multi-view neural network ensemble for short and mid-term load forecasting," *IEEE Trans. Power Syst*., to be published. DOI: 10.1109/TPWRS.2020.3042389.

[24] Y. Yu, S. You, H. Zhang, T. Ye, Y. Wang, and S. Wei, "A review on available energy saving strategies for heating, ventilation and air conditioning in underground metro stations," *Renew. Sustain. Energy Rev*., vol. 141, no. 110788, May 2021.

[25] Y. Chen, G. Fu, and X. Liu, "Air-conditioning load forecasting for prosumer based on meta ensemble learning," *IEEE Access*, vol. 8, pp. 123673-123682, 2020.

[26] Y. Ding, H. Su, X. Kong, and Z. Zhang, "Ultra-short-term building cooling load prediction model based on feature set construction and ensemble machine learning," *IEEE Access*, vol. 8, pp. 178733-178745, Sep. 2020.

[27] A. Foucquier, S. Robert, F. Suard, L. Stéphan and A. Jay, "State of the art in building modelling and energy performances prediction: A review," *Renew. Sustain. Energy Rev.*, vol. 23, pp. 272-288, Jul. 2013.

[28] J.-S. Chou, S.-C. Hsu, N.-T. Ngo, C.-W. Lin and C.-C. Tsui, "Hybrid machine learning system to forecast electricity consumption of smart grid-based air conditioners," *IEEE Syst. J.*, vol. 13, no. 3, pp. 3120-3128, Sep. 2019.

[29] M. Bourdeau, X. Q. Zhai, E. Nefzaoui, X. Guo and P. Chatellier, "Modeling and forecasting building energy consumption: A review of data-driven techniques," *Sustain. Cities Soc.*, vol. 48, 2019.

[30] F. M. Gray, and M. Schmidt, "A hybrid approach to thermal building modelling using a combination of Gaussian processes and grey-box models," *Energy Build*., vol. 165, pp. 56-63, Jan. 2018.

[31] D. Dong, Z. Li, S. M. Rahman, and R. Vega, "A hybrid model approach for forecasting future residential electricity consumption," *Energy Build*., vol. 117, pp. 341-351, April 2016.

[32] W. Collinge, J. Deblois, A. Landis, and L. Schaefer, "Hybrid dynamic-empirical building energy modeling approach for an existing campus building," *J. Architect. Eng*., vol. 22, no. 1, Mar. 2016.

[33] "Energy use in homes". [Online]. Available at: https://www.eia.gov/ energyexplained/use-of-energy/homes.php, Accessed on: Feb. 2022.

[34] A. Thavlov, "Dynamic optimization of power consumption," M.S. thesis, Tech. Univ. Denmark, Kongens Lyngby, Denmark, 2008.

[35] Y. Yoon, J. W. Moon, and S. Kim, “Development of annual daylight simulation algorithms for prediction of indoor daylight illuminance,” *Energy Build*., vol. 118, pp. 1–17, 2016.

[36] M. Ayoub, “A review on machine learning algorithms to predict daylighting inside buildings,” *Sol. Energy*, vol. 202, no., pp. 249–275, Jan. 2020.

[37] C. A. Gueymard, “REST2: High-performance solar radiation model for cloudless-sky irradiance, illuminance, and photosynthetically active radiation - Validation with a benchmark dataset,” *Sol. Energy*, vol. 82, no. 3, pp. 272–285, 2008.

[38] “Appendix 7 Spectral Luminous Efficiency Functions”. [Online]. Available at https://onlinelibrary.wiley.com/doi/pdf/10.1002/047002427 5.app7, Accessed on: Nov, 2021.

[39] B. Ji, F. Xie, X. Wang, S. He and D. Song, “Investigate contribution of multi-microseismic data to rockburst risk prediction using support vector machine with genetic algorithm,” *IEEE Access*, vol. 8, pp. 58817-58828, 2020.

[40] Y. Wang, Y. Shen, S. Mao, G. Cao and R. M. Nelms, “Adaptive learning hybrid model for solar intensity forecasting,” *IEEE Trans. Ind. Informat.*, vol. 14, no. 4, pp. 1635-1645, Apr. 2018.

[41] L. Ge, Y. Xian, J. Yan, B. Wang, and Z. Wang, “A hybrid model for short-term PV output forecasting based on PCA-GWO-GRNN,” *J. Mod. Power Syst. Clean Energy*, vol. 8, no. 6, pp. 1268-1275, Sep. 2020.

[42] X. Ma, J. Zhang, B. Du, C. Ding, and L. Sun, “Parallel architecture of convolutional bi-directional lstm neural networks for network-wide metro ridership prediction,” *IEEE Trans. Intell. Transp. Syst.*, vol. 20, no. 6, pp. 2278–2288, 2018.

[43] H. Jahangir, H. Tayarani, S. S. Gougheri, M. A. Golkar, A. Ahmadian and A. Elkamel, “Deep learning-based forecasting approach in smart grids with micro-clustering and bi-directional LSTM network,” *IEEE Trans. Ind. Electron*., to be published. DOI: 10.1109/TIE.2020.3009604.

[44] E. Brochu, V. M. Cora, and N. de Freitas, “A tutorial on Bayesian optimization of expensive cost functions, with application to active user modeling and hierarchical reinforcement learning,” Dec. 2010. [Online]. Available: arXiv:1012.2599.

[45] S. Hassan, A. Khosravi, and J. Jaafar, “Examining performance of aggregation algorithms for neural network–based electricity demand forecasting,” *Int. J. Elect. Power Energy Syst*., vol. 64, pp. 1098–1105, Jan. 2015.

[46] “Umass smart dataset”. [Online]. Available at: http://traces.cs.umass.edu/ index.php/Smart/ Smart, Accessed on: May 2021.

[47] “Data and experiments for building energy performance”. [Online]. Available at: http://www2.compute.dtu.dk/~pbac/buildingdata09/, Accessed on: Nov. 2021.

[48] F. Luo, G. Ranzi, C. Wan, Z. Xu, and Z. Y. Dong, “A multistage home energy management system with residential photovoltaic penetration,” *IEEE Trans. Ind. Informat*., vol. 15, no. 1, pp. 116–126, Jan. 2019.

Chapter 6: A multi-level home energy management system (HEMS) suited to DC-based home microgrid

Citation:

X. Lin, R. Zamora, C. Baguley, Yazhou Jiang and Anurag K. Srivastava, "A multi-level home energy management system (HEMS) suited to DC-based home microgrid," *IEEE Trans. Sustain. Energy*, 2022 (**To be submitted**).

Preamble:

The home energy management system (HEMS) will formulate an optimal power dispatch plan through the collected data and user needs, which will determine the charging and discharging operation of the hybrid energy storage system, and purchase/sell electric energy from/to the utility. Therefore, Chapter 6 proposes a multi-level HEMS for home microgrids, which consists of two parts. The first part is the system level HEMS, which is proposed to reduce operating costs and improve user comforts. This system level HEMS is the long- and short-time scales optimization method based on model predictive control (MPC). The long-time scale optimization is proposed to minimize the operating cost of the system and maximize user comforts. The total operating cost consists of electricity cost, PV power generation cost, battery and SC wear costs. Then, a predicted mean vote - percentage people dissatisfied (PMV-PPD) model is adopted to evaluate thermal environment comfort. An illuminance model is employed to assess the indoor visual comfort. The objective of the short-time scale optimization is to alleviate the power fluctuations caused by the randomness of end-user behaviors and PV generation, as well as to ensure the capacity of the SC within a safe range. The second part of this chapter is the local level energy management system, which is further improved based on the method in Chapter 4. Furthermore, the control method is more simplified and has better performance.

Abstract:

A multi-level home energy management system (HEMS) in this article is proposed to minimize operating cost and to maximize user comfort in the DC-based home microgrid. The presented HEMS includes the system- and local-level HEMS. The system-level HEMS consists of long- and short-time optimization based on model predictive control (MPC). The long-time optimization (LTO) optimizes load usage by using data collected with the goal of minimizing house operating costs and maximizing user comfort. The purpose of the short-time optimization (STO) is to alleviate the power oscillations caused by the randomness of user behavior and PV generation, and to ensure that the voltage level of the supercapacitor (SC) is within a safe range. Besides, a predicted mean vote - percentage people dissatisfied (PMV-PPD) model is used to estimate comfort level in thermal environment. An illuminance model is employed to assess the

intensity of indoor light. Battery and SC degradation cost models are proposed to evaluate the wear cost during operation. The local-level HEMS is used to achieve DC voltage restoration, power sharing between batteries and SCs, as well as voltage recovery of SC. Besides, a consensus-based voltage regulator is proposed to achieve state of charge (SoC) balance and accurate power sharing between batteries. The dataset from National Renewable Energy Lab (NREL) and energy market company of Singapore are used to validate the proposed method.

1. Introduction

Recently, approximately one third of energy usage is contributed to residential sector. Integration of small-scale power systems including renewable energy resource (RES) and energy storage system (ESS) into residential buildings has become an emerging technology to reduce energy consumption and alleviate environmental concerns. These power systems are also defined as home microgrid [1]. Besides, the energy generated by photovoltaic (PV) systems is DC power, and a large number of DC electrical loads are applied in houses, such as LED lights and air conditioners. DC-based microgrids can be better used in housing scenarios, which can improve energy efficiency and simplify power conversion [2]. In DC home microgrid, the home energy management system (HEMS) plays a significant role in optimizing energy usage. HEMS can effectively coordinate the power supply of various energy resources and provide decision support for the customers' demand [3].

Many existing works have presented the HEMS with different purposes [4]–[7]. In [8], a two level HEMS is proposed for residential energy optimization. The first level of the HEMS is to minimize the electricity tariff by regulating the time usage of the appliances. The second level of the HEMS is to optimize the operation cost of the microgrid. In [9], a model predictive control (MPC) based HEMS is designed to optimize energy usage based on the information of the electricity tariff, load demand and power generation. In [5], a multi-objective mixed integer nonlinear programming model is proposed for energy cost saving and comfortable lifestyle in residential building. In the method, energy saving, indoor thermal comfort and user satisfaction rate are used as optimization objectives. In [10], a stochastic HEMS model is proposed to minimize the energy cost in the long-term period. A response fatigue index is designed to maintain the users' satisfaction. Ref. [11] proposes a novel differential dynamic programing based HEMS to minimize the electricity expense in the house integrating PV system, ESS, and controllable load. This HEMS takes into account the uncertainty caused by PV generation, and battery degradation cost. Ref. [12] develops an energy management system based on Lyapunov optimization technique for grid-connected PV integrated buildings. The objective of this method is to minimize the energy usage by considering real-time price, energy storage degradation cost and user comfort level. In [13], a multi-stage HEMS is proposed to maintain indoor thermal

comfort and minimize home operation cost. This work also intends to reduce the energy deviation between day-ahead scheduling and actual operation.

Although the above-mentioned articles have studied HEMS in depth, their shortcomings can be summarized as follows:

a. The methods in the above articles only consider the battery as an energy buffer, thereby increasing the power supply burden on the battery and shortening the cycle life of battery. This is because the intermittent power generation of RES and the randomness of household load usage can lead to high frequency power fluctuations and power mismatch between hourly power scheduling and intra-hourly power usage. This means that HEMS requires the ESS to respond quickly to power changes. Hence, a high-power density ESS such as supercapacitor (SC) should also be integrated into HEMS to compensate for the fluctuations.
b. The thermal comfort in Refs. [5], [7], and [9]–[11] is evaluated only by the indoor temperature, which cannot fully reflect the indoor comfort conditions. According to the ISO 7730:2005 standard, thermal comfort includes indoor temperature, humidity and user clothing conditions. Therefore, the method in [13] integrates a predicted mean vote (PMV) model to evaluate indoor comfort. However, ref. [13] regards PMV as a constraint condition rather than an objective function, hence, indoor comfort is not the optimal value. Besides, very few articles such as [12] consider indoor visual comfort. However, the method in this article does not consider the users' work and rest time.
c. The mentioned articles focus on designing system-level HEMS and ignore the interaction between local and system level HEMS.

Recently, battery-SC hybrid energy storage system (HESS) has been widely applied in different scenarios such as shipboard microgrid and electric vehicle [14], [15]. Many works have investigated the HESS [16]–[19]. For example, ref. [16] proposes an advanced droop-controlled secondary control to achieve voltage recovery. Ref. [18] develops a coordinating control method for power sharing, voltage restoration, state of charge (SoC) balance of batteries and SoC recovery of SCs in DC microgrid. However, the method in [16] and [18] contains many control loops, which makes the system complicated. Therefore, the method in [19] simplifies the controller and ensures versatility of the controller. However, this method may amplify the system noise in frequency domain, thereby deteriorating the system stability. Besides, refs. [16]–[19] does not consider inaccurate power sharing caused by line resistance.

To address the issues mentioned above, a multi-level HEMS is proposed for DC home microgrid in this article. The main contributions are summarized as follows:

a. The system-level HEMS is composed of multi-time scale optimization based on MPC. The goal of long-time optimization (LTO) is to minimize the operating costs of the house microgrid and to maximize user comfort. The goal of short-time optimization (STO) is to suppress the power oscillations caused by the randomness of user behavior and PV generation, and to ensure that the SoC level of the SC is within a safe range.
b. To design a more practical HEMS, a modified battery degradation model based on lifetime throughput and a SC degradation model are presented to be integrated into the HEMS in order to reduce the operating cost and to prolong the energy storage lifespan.
c. A PMV - percentage people dissatisfied (PPD) model is employed to be an optimization objective for improving indoor thermal comfort. Indoor illuminance model is used to maintain visual comfort within an acceptable range.
d. The purpose of the local level HEMS is to achieve power sharing between batteries and SCs, as well as voltage compensation for SCs. The DC bus volage can be maintained within a desired range. Besides, a consensus-based voltage regulator is proposed to achieve accurate power sharing and SoC balancing between batteries.

The rest of this article is organized as follows. Section II presents system configuration and model. Section III describes system-level HEMS. Section IV presents local-level HEMS. Simulation results are discussed in Section V. Finally, the conclusion of this article is given in Section VI.

2. System configuration and model

2.1. System configuration

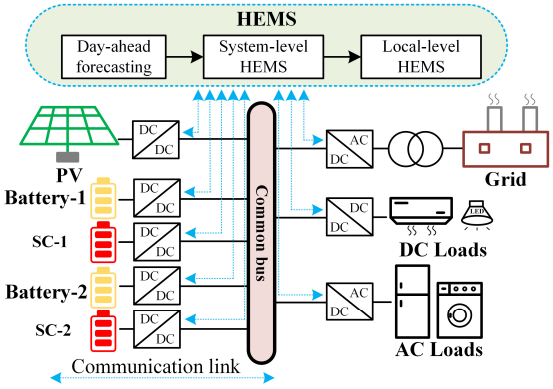

Fig. 1. The schematic diagram of the HEMS in DC house microgrid.

The equivalent structure diagram of the proposed HEMS is shown in Fig. 1. The system consists of a PV generation, two HESSs and household appliances. In the day-ahead forecasting step, the house load consumption is forecasted by the authors' previous research [20]. The PV generation and real time price are predicted by using artificial neural network. It should be noted that this article mainly focuses on the studies of multi-level HEMS. Hence, the day-ahead forecasting will not be discussed. Then, the system-level HEMS provides decision-making for house energy usage

and generates power references based on forecasted data. Finally, the local-level HEMS determine the charging and discharging of the HESS, and the purchase/sell the electricity from/to main grid according to the power reference.

2.2. Battery degradation model

Battery degradation models can be divided into physical models and semi-empirical models. The physical model is built based on the chemical structure and material parameters of the battery, while the semi-empirical model is established based on battery operating parameters such as SoC, voltage, depth of discharge (DOD), etc. [21]. In this article, the semi-empirical model is employed since the establishment of the physical model requires experimental parameters. A linear degradation model is a kind of semi-empirical model, which has been widely used in several works [22]–[24]. For example, the linear degradation models in [22] and [23] are developed based on the lifetime throughput. However, the estimation of battery degradation costs in this model is achieved under fixed DOD conditions. In practice, DOD varies during battery operation. Therefore, degradation costs estimated by above method may be inaccurate. In [24], the battery degradation model is represented by a constant, which cannot accurately represent the process of battery degradation. Hence, this article presents a modified degradation model. The lifetime throughput is written as (1) [22].

$$\mathrm{LTT}_B^* = Q_B \times \mathrm{DoD}_B \times L_B \tag{1}$$

where LTT_B^* is the lifetime throughput of battery (kWh). Q_B, DoD_B, L_B are the battery capacity (kWh), battery DoD, and lifetime. The battery degradation cost per kWh can be written as (2) [22].

$$C_{B,\mathrm{per}}^* = \frac{B_{\mathrm{price}}}{\mathrm{LTT}_B \times \sqrt{\mu}} \tag{2}$$

where B_{price} and μ are the replacement cost ($) and charging and discharging efficiency.

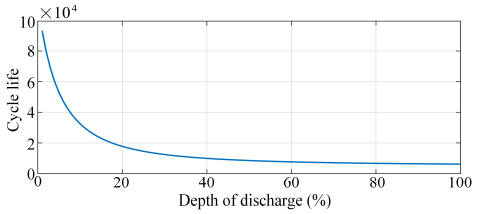

Fig. 2. Relationship between cycle life and DoD.

The characteristic relationship between life cycle and DOD is displayed in Fig. 2 [25]. When DOD increases during battery operation, the life cycle decreases and vice versa. The fitting function of the curve in Fig. 2 can be described as (3) [26], [27].

$$L_B(\mathrm{DoD}_B(\Delta t)) = a_B \times \mathrm{DoD}_B(\Delta t)^{-b_B} \times e^{c_B \times \mathrm{DoD}_B(\Delta t)} \tag{3}$$

$$\mathrm{DoD}_B(\Delta t) = \frac{P_B(t) \times \Delta t}{Q_B} \tag{4}$$

where a_B, b_B, c_B are the curve-fitting coefficients for equation (2). Δt is the time interval. $P_B(t)$ is the battery power at time t (kW). By combining (1) - (4), the total battery degradation cost model with time variable can be expressed as (5).

$$C_B(t) = \frac{B_{\text{price}} \times P_B(t) \times \Delta t}{Q_B \times \mathrm{DoD}_B(\Delta t) \times L_B(\mathrm{DoD}_B(\Delta t)) \times \sqrt{\mu}} \tag{5}$$

where C_B is the total battery degradation cost.

2.3. SC degradation cost model

SC is a power density energy storage with high lifetime and fast response characteristics. Therefore, SC is usually used to provide transient power, thereby reducing the power supply burden of the battery [28]. Since SC is also degraded during operation, HEMS needs to consider the degradation cost of SC to maximize the economic benefits of the operating cost in the house microgrid. The SC degradation model has been studied in several works [29]–[31]. However, these models are more complex. Since the lifetime parameters of SC under normal working conditions are available from the manufacturer, a linear model based on the lifetime can be developed to estimate the degradation cost of SC, as shown in (6).

$$C_{\text{sc}}(t) = \frac{\mathrm{SC}_{\text{price}}}{L_{\text{sc}} \times 2 \times Q_{\text{sc}}} \times P_{\text{sc}}(t) \times \Delta t \tag{6}$$

where $\mathrm{SC}_{\text{price}}$, Q_{sc} and L_{sc} are the SC price, SC capacity and total lifetime. $P_{\text{sc}}(t)$ is SC power (kW). $\mathrm{SC}_{\text{price}}/(L_{\text{sc}} \times 2 \times Q_{\text{sc}})$ refers to the degradation cost in per kWh. $P_{\text{sc}}(t) \times \Delta t$ indicates the energy variation of SC during time interval Δt.

2.4. PV generation and grid power cost model

The daily cost of PV power generation can be expressed as (7).

$$C_{\text{pv}} = \frac{\mathrm{PV}_{\text{price}}}{N_{\text{year}} \times 365 \times 24} \tag{7}$$

where $\mathrm{PV}_{\text{price}}$ and N_{year} are the PV price and number of guaranteed years of the photovoltaic. Equation (7) refers to the fixed wear cost per hour of PV. The main grid electricity cost is written as (8).

$$C_g(t) = P_g(t) \times \eta_{\text{pr}}(t) \times \Delta t \tag{8}$$

where $\eta_{\text{pr}}(t)$ is the hourly electricity price at time t (\$), and $P_g(t)$ is the grid power at time t (kW).

2.5. Thermal comfort model

Thermal comfort refers to the users' satisfaction with the current thermal environment, and it has a significant impact on the user's health [32]. Low thermal comfort causes overcooling and overheating of the environment, which can lead to discomfort to the environment for customers. According to ISO 7730:2005 standard, the thermal comfort model considers indoor temperature and humidity [33]. In this article, the indoor temperature is estimated by the thermal dynamic model in [20], which is written as (9).

$$\begin{aligned} T(t+1) &= A \times T(t) + B \times U(t) \\ T_{\text{in}}(t) &= C \times T(t) \end{aligned} \tag{9}$$

where $T(t) = [T_w(t), T_m(t), T_r(t), T_{\text{in}}(t)]^{'}$ is the state vector. $T_w(t)$ is the temperature of exterior wall at time t (℃). $T_m(t)$ is the temperature of the medium in the inner wall at time t (℃). $T_r(t)$ is the temperature of the house roof at time t (℃). $T_{\text{in}}(t)$ is the indoor temperature at time t (℃). $U(t) = [T_a(t), T_{\text{dh}}(t), \Phi_s(t), P_{\text{ac}}(t), P_h(t)]^{'}$ is the input vector of the thermal dynamic model. $T_a(t)$ is the ambient temperature at time t (℃). $T_{\text{dh}}(t)$ is the temperature caused by humidity at time t (℃). $\Phi_s(t)$ is the solar irradiation at time t (kW/m^2). $P_{\text{ac}}(t)$ and $P_h(t)$ the power input from the heater and air conditioning (AC) at time t (kW). A, B, and C are the system behavior, input behavior, and constant matrices, which can be found in [20].

The indoor temperature obtained from (9) cannot accurately reflect the user's thermal comfort satisfaction. Therefore, the PMV model is incorporated into the HEMS to evaluate thermal comfort. PMV is expressed as the users' perception of thermal comfort in the environment. Based on Table I [33], when the PMV is between -0.2 and +0.2, the higher comfort is reached. The users feel comfortable when PMV is between -0.5 and +0.5. The PMV model is given in (10) and (11).

TABLE I
PMV-PPD Standard

Category	PMV	PPD (%)
A	-0.2 < PMV < +0.2	< 6
B	-0.5 < PMV < +0.5	< 10
C	-0.7 < PMV < +0.7	< 17

$$P_v(t) = \text{rh}(t) \times 10 \times e^{(16.6536 - 4030.183)/(T_{\text{in}}(t) + 273)} \tag{10}$$

$$\text{PMV}(t) = a_{\text{PMV}} \times T_{\text{in}}(t) + b_{\text{PMV}} \times P_v(t) + c_{\text{PMV}} \tag{11}$$

where $P_v(t)$ and rh(t) are the vapor pressure and relative humidity at time t. a_{PMV}, b_{PMV} and c_{PMV} are the clothing thermal insulation factors, which can be found from [34]. However, PMV refers to the average thermal comfort of the house members, thus ignoring individual differences in the house. A PPD model is used to assess the dissatisfaction of users in the house with the thermal environment. A lower PPD value means that fewer users in the house are dissatisfied with the thermal environment. The PPD model can be written as (12), while the PPD(t) cost function can be present as (13) [35].

$$\mathrm{PPD}(t) = 100 - 95 \times e^{-\left(0.03353 \times \mathrm{PMV}(t)^4 + 0.2179 \times \mathrm{PMV}(t)^2\right)}. \tag{12}$$

$$C_{\mathrm{PPD}}(t) = w_{\mathrm{PPD}} \times \mathrm{PPD}(t) \tag{13}$$

where w_{PPD} is the weight factor ($).

2.6. Visual comfort model

Visual comfort refers to the intensity of indoor light, which is usually expressed in illuminance. The indoor illuminance is produced by the electric lights and the outdoor sunlight. The illuminance generated by electric lights can be formulated as (14).

$$L_{\mathrm{light}}(t) = \frac{P_{\mathrm{light}}(t) \times \mathrm{MF} \times \mathrm{UF}}{A} \tag{14}$$

where $L_{\mathrm{light}}(t)$ and $P_{\mathrm{light}}(t)$ are the lighting illuminance and lighting power at time t. A, MF and UF are the illuminated area, maintenance factor and utilization factor.

The intensity of outdoor brightness can be represented by outdoor illuminance, which is determined by solar irradiance. Ref. [36] establishes a linear relationship between outdoor illuminance and solar irradiance through experimental measurement, which can be expressed as (15).

$$L_o^*(t) = a_o \times (\Phi_{\mathrm{dni}}(t) + \Phi_{\mathrm{dhi}}(t)) + b_o \tag{15}$$

where $L_o^*(t)$ is outdoor illuminance (lx). $\Phi_{\mathrm{dni}}(t)$ and $\Phi_{\mathrm{dhi}}(t)$ are the direct normal irradiance and diffuse horizontal irradiance at time t (W/m^2). a_o and b_o are the measured parameters that can be obtained from [36]. Since most of the surface area of the house is impermeable to light, only a small part of the outdoor illuminance is converted into indoor illuminance. The daylight factor is introduced to represent the conversion rate between outdoor and indoor illuminance, which can be expressed as (16) [37].

$$L_o(t) = L_o^*(t) \times \mathrm{DF} \tag{16}$$

where DF is daylight fact. $L_o(t)$ is the component of indoor illuminance at time t (lx). The indoor illuminance ($L_{\text{in}}(t)$) is written as (17).

$$L_{\text{in}}(t) = L_{\text{light}}(t) + L_o(t). \tag{17}$$

The visual comfort requires the reasonable setups and assumptions, which can be summarized as follows:

a. In the daytime, the indoor illuminance is mainly provided by the outdoor illuminance. If the indoor illuminance is lower than 320 lx, the electric lamp will provide lighting to make the indoor illuminance meet the requirement [38]. If the room illuminance exceeds 1800 lx, it is assumed that the users will take actions to reduce the indoor illuminance such as closing the window [39].
b. At night, the indoor illuminance is only provided by electric lights, and the poor illuminance generated by moonlight is assumed to be ignored. During sleeping time (22:00 – 6:00), the indoor illumination is recommended to be set between 0 and 5 lx, which is helpful for users to sleep [40].

3. Proposed system-level HEMS

The system-level HEMS consists of LTO and STO based on MPC. It should be noted that the long- and short-time scales in this article are 1 hour and 5 minutes. LTO is to minimize the operating cost, maintain user comfort and schedule power dispatch based on hourly forecasted data. However, PV generation and household loads may vary within an hour depending on meteorological factors and user behavior, thus reducing the accuracy of LTO. STO is developed to reduce the deviation between the power optimized by LTO and the intra-hourly power usage. The equivalent structure diagram of system-level HEMS is shown in Fig. 3. The stages can be summarized as follows:

a. Forecasted dataset is imported to system-level HEMS.
b. LTO-MPC steps:
    1. At time $t_{\text{LT,1}}$, LTO collects the state information of the system components containing the PV power, load demand, electricity price, as well as the SoC and output power of battery and SC.
    2. The predictive sequence is obtained by solving finite horizon optimization problem.
    3. The first element in the predictive sequence is sent to STO-MPC step. At $t_{\text{LT,1}} + \Delta t_{\text{LT}}$, the predictive window moves by one time interval. The process starts from step b-1.
c. STO-MPC steps:
    1. At time $t_{\text{ST,1}}$, STO collects data information from LTO-MPC step.

2. The predictive sequence is obtained by solving finite horizon optimization problem.
3. The first element in the predictive sequence is sent to b-1 and local-level HEMS. At time $t_{ST,1} + \Delta t_{ST}$, the predictive window moves by one time interval. Then, optimization process starts from step c-1.

3.1. System operation constraints

The power balance constraint for LTO and STO can be written as (18).

$$P_L(t) + P_{\text{light}}(t) + P_{\text{ac}}(t) + P_h(t) = P_g(t) + P_{\text{pv}}(t) + P_{\text{HESS}}(t) \tag{18}$$

where $P_L(t)$ is the house load that does not include lights, air conditioner and heater at time t (kW). $P_{\text{pv}}(t)$ is the PV power at time t (kW). $P_{\text{HESS}}(t) = P_B(t) + P_{\text{sc}}(t)$, which is output power of the HESS.

The SoC variation models of the battery and SC can be expressed as (19) and (22).

$$\text{SoC}_B(t+1) = \text{SoC}_B(t) - \frac{\eta_B^c \times P_B(t) \times \Delta t}{Q_B}, P_B(t) \le 0 \tag{19}$$

$$\text{SoC}_B(t+1) = \text{SoC}_B(t) - \frac{P_B(t) \times \Delta t}{Q_B \times \eta_B^d}, P_B(t) > 0 \tag{20}$$

$$\text{SoC}_{\text{sc}}(t+1) = \text{SoC}_{\text{sc}}(t) - \frac{\eta_{\text{sc}}^c \times P_{\text{sc}}(t) \times \Delta t}{Q_{\text{sc}}}, P_{\text{sc}}(t) \le 0 \tag{21}$$

$$\text{SoC}_{\text{sc}}(t+1) = \text{SoC}_{\text{sc}}(t) - \frac{P_{\text{sc}}(t) \times \Delta t}{Q_{\text{sc}} \times \eta_{\text{sc}}^d}, P_{\text{sc}}(t) > 0 \tag{22}$$

where $\text{SoC}_B(t)$ and $\text{SoC}_{\text{sc}}(t)$ are the SoC of battery and SC. η_B^c, η_{sc}^c, η_B^d and η_{sc}^d are the charging and discharging coefficients for battery and SC. The SoC and power constraints of the battery and SC can be written as (23) - (26).

$$\text{SoC}_B^{\min} \le \text{SoC}_B(t) \le \text{SoC}_B^{\max} \tag{23}$$

$$\text{SoC}_{\text{sc}}^{\min} \le \text{SoC}_{\text{sc}}(t) \le \text{SoC}_{\text{sc}}^{\max} \tag{24}$$

$$P_B^{\min} \le P_B(t) \le P_B^{\max} \tag{25}$$

$$P_{\text{sc}}^{\min} \le P_{\text{sc}}(t) \le P_{\text{sc}}^{\max} \tag{26}$$

where $\text{SoC}_B^{\min}$, $\text{SoC}_{\text{sc}}^{\min}$, $\text{SoC}_B^{\max}$ and $\text{SoC}_{\text{sc}}^{\max}$ are the minimum and maximum SoC of the battery

and SC. $P_B^{\min}$, $P_{\text{sc}}^{\min}$, $P_B^{\max}$ and $P_{\text{sc}}^{\max}$ are the minimum and maximum power of the battery and SC. The power constraints of the grid, lighting, AC and heater are given in (27) – (29).

$$P_g^{\min} \le P_g(t) \le P_g^{\max} \tag{27}$$

$$P_{\text{light}}^{\min} \le P_{\text{light}}(t) \le P_{\text{light}}^{\max} \tag{28}$$

$$P_{\text{hac}}^{\min} \le P_{\text{hac}}(t) \le P_{\text{hac}}^{\max} \tag{29}$$

where $P_{\text{hac}}(t)$ is the power of heater or AC (HAC). $P_g^{\min}$, $P_{\text{light}}^{\min}$, $P_{\text{hac}}^{\min}$, $P_g^{\max}$, $P_{\text{light}}^{\max}$, and $P_{\text{hac}}^{\max}$ are the minimum and maximum power of the grid, lighting and HAC.

The thermal and illuminance constraints are present as (30) and (31).

$$|\text{PMV}_{\text{in}}(t) - \text{PMV}_d(t)| \le \varepsilon_{\text{PMV}} \tag{30}$$

$$L_{\text{in}}^{\min} \le L_{\text{in}}(t) \le L_{\text{in}}^{\max} \tag{31}$$

where $L_{\text{in}}^{\min}$and $L_{\text{in}}^{\max}$ are the minimum and maximum illuminance. $\text{PMV}_d(t)$ is the desired PMV value. ε_{PMV} is the deviation between desired and actual PMV.

3.2. The objective function of LTO and STO

The objective function of LTO considering indoor comfort and the degradation cost model of HESS is proposed to reduce the operating cost of the house microgrid, it can be expressed as (32).

$$\min F_{\text{LTO}} = \sum_{t_{\text{LT}} \in \{1,\ldots,T_{\text{LT}}\}} (C_g(t_{\text{LT}}) + C_B(t_{\text{LT}}) + C_{\text{sc}}(t_{\text{LT}}) + C_{\text{PPD}}(t_{\text{LT}})) + C_{\text{pv}} \tag{32}$$

s.t. (5) – (8), (10) – (31)

variables: $\{P_g(t_{\text{LT}}), P_B(t_{\text{LT}}), P_{\text{sc}}(t_{\text{LT}}), P_{\text{hac}}(t_{\text{LT}}), P_{\text{light}}(t_{\text{LT}})\}_{t_{\text{LT}}=1}^{T_{\text{LT}}}$

where T_{LT} is the time horizon for LTO. t_{LT} is time in LTO. Then, the objective function of STO can be written as (33).

$$\min F_{\text{STO}} = \sum_{t_{\text{ST}} \in \{1,\ldots,T_{\text{ST}}\}} C_{\text{sc}}(t_{\text{ST}}) + \sum_{t_{\text{ST}} \in \{1,\ldots,T_{\text{ST}}\}} \left| P_B^{\text{LT}}(t_{\text{LT}}) - P_B^{\text{ST}}(t_{\text{ST}}) \right|$$

$$+ \sum_{t_{ST} \in \{1,\ldots,T_{ST}\}} \left| P_g^{LT}(t_{LT}) - P_g^{ST}(t_{ST}) \right|$$

$$+ \sum_{t_{ST} \in \{1,\ldots,T_{ST}\}} \left| P_{light}^{LT}(t_{LT}) - P_{light}^{ST}(t_{ST}) \right|$$

$$+ \sum_{t_{ST} \in \{1,\ldots,T_{ST}\}} \left| P_{hac}^{LT}(t_{LT}) - P_{hac}^{ST}(t_{ST}) \right|$$

$$+ \sum_{t_{ST} \in \{1,\ldots,T_{ST}\}} \left| SoC_{sc}^{ref} - SoC_{sc}^{ter}(t_{ST,\,end}) \right| \qquad (33)$$

s.t. (6), (18) – (31)

variables:

$$\{P_g(t_{ST}), P_{sc}(t_{ST}),\ P_B(t_{ST}), P_{hac}(t_{ST}), P_{light}(t_{ST})\}_{t_{ST}=1}^{T_{ST}}$$

where SoC_{sc}^{ref} is the reference SoC. $SoC_{sc}^{end}(t_{ST,\,end})$ is the SoC of the end time in the predictive horizon.

4. Proposed local-level HEMS

The local-level HEMS regulates the power supply of the main grid and the HESSs by receiving the power reference signal from the system-level HEMS. If the communication link between the system-level and local-level HEMS suddenly fails, the local HEMS is able to operate independently to ensure the stability of the house microgrid. In the local-level HEMS, a *v-dP* droop control and *v-P* droop control with voltage recovery loop are employed to regulate the battery and SC converters to achieve power distribution, DC bus voltage restoration and voltage recovery of the SC.

4.1. v-dP droop control and v-P droop control with voltage recovery

A *v-dP* droop control is employed to regulate the battery converter, it is given in (34) [19].

$$v_{b,\,n} = v_r - k_b \times \frac{d(P_{b,\,n} - P_{b,\,n}^{ref})}{dt} \qquad (34)$$

where k_b, v_r and $v_{b,\,n}$ are the droop coefficient, reference and output voltage of the n^{th} battery converter, (n = 1, 2, …, N). $P_{b,\,n}$ is the output power of the battery converter. $P_{b,\,n}^{ref}$ is the reference power from system-level HEMS. Equation (34) contains a derivative term that amplifies the noise in the control system, thereby reducing the stability of the system. Thus, equation (34) can be further modified as (35).

$$P_{b,n} = P_{b,n}^{\text{ref}} + \int \frac{v_r - v_{b,n}}{k_b} dt. \tag{35}$$

The traditional *v*-*P* control with voltage recovery can be written as (36) and (37).

$$v_{\text{sc},n} = v_r - k_{\text{sc}} \times (P_{\text{sc},n} - P_{\text{sc},n}^{\text{ref}}) - \delta v_{\text{sc},n} \tag{36}$$

$$\delta v_{\text{sc},n} = (k_{\text{sc},n}^{p} + k_{\text{sc},n}^{i} \frac{1}{s}) \times (v_{\text{sc},n}^{r} - v_{\text{sc},n}^{\text{in}}) \tag{37}$$

where k_{sc}, $v_{\text{sc},n}$ and $P_{\text{sc},n}$ are droop coefficient, the output voltage and power of the n^{th} SC converter. $P_{\text{sc},n}^{\text{ref}}$ is the reference power from system-level HEMS. $\delta v_{\text{sc},n}$ is the voltage recovery method. $v_{\text{sc},n}^{r}$ and $v_{\text{sc},n}^{\text{in}}$ are the reference and measured voltage for the SC. $k_{\text{sc},n}^{p}$ and $k_{\text{sc},n}^{i}$ are the control parameters. When the system- and local-level HEMS are operating normally, the voltage recovery control of SC stops working to avoid conflict with the SoC recovery in the system level HEMS.

4.2. Consensus-based voltage regulator

The purpose of the consensus algorithm is to exchange information through a sparse communication network to ensure that the stored information state of distributed agents remains consistent [41]. A consensus algorithm can be written as (38) – (39) based on [42].

$$h_n(k+1) = h_n(0) + \varepsilon \sum_{j \in N_n} \delta_{nj}(k+1) \tag{38}$$

$$\delta_{nj}(k+1) = \delta_{nj}(k) + a_{nj} \left[h_j(k) - h_n(k) \right] \tag{39}$$

where $h_n(k)$ is the information state at iteration k for n^{th} agent. N_n is the set of the agents. $\delta_{nj}(k)$ is a variable that stores cumulative difference between agents n and j, and $\delta_{nj}(0) = 0$. a_{nj} is the connection state between agents n and j. ε can adjust the convergence speed, which can be calculated by (40) based on [43].

$$\varepsilon = \frac{2}{\beta_1(L) + \beta_{N-1}(L)} \tag{40}$$

where $\beta_n(\cdot)$ is the n^{th} largest eigenvalue of the symmetric matrix. L is the Laplacian matrix.

The consensus-based voltage regulator is defined by (41) – (43).

$$P_{b,n} = P_{b,n}^{\text{ref}} + \int \frac{v_r - v_{b,n} + \delta v_n}{k_b} dt \tag{41}$$

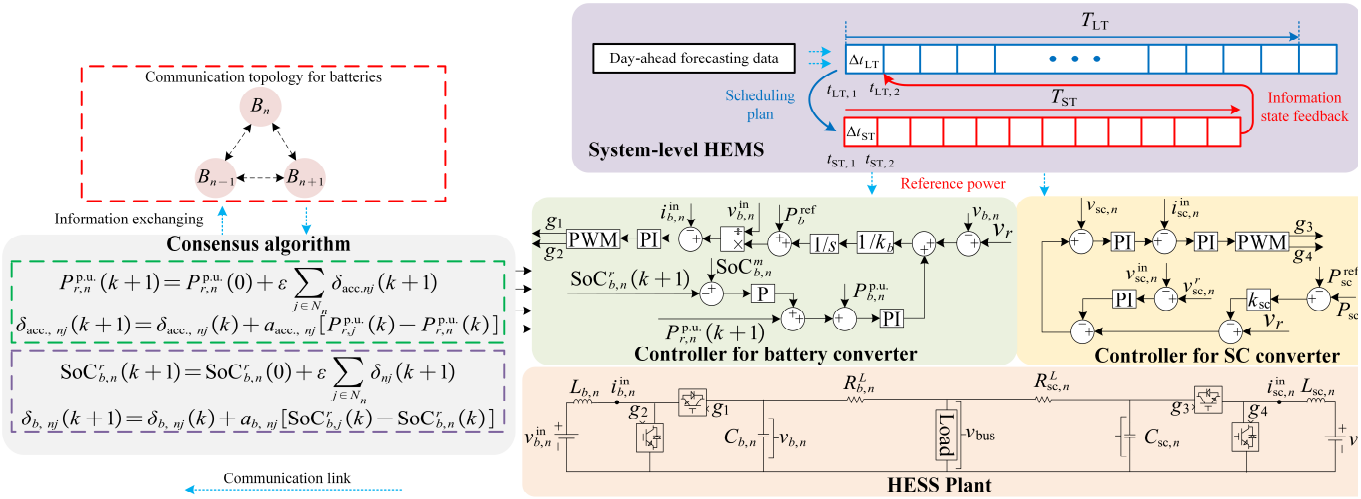

Fig. 3 The schematic diagram of the multi-level HEMS.

$$\delta v_n = \left[P_{r,n}^{\text{p.u.}}(k+1) + \delta v_{\text{SoC},n} - P_{b,n}^{\text{p.u.}}\right] \times \left(k_{\text{acc.},n}^{p} + k_{\text{acc.},n}^{i}\frac{1}{s}\right) \tag{42}$$

$$\delta v_{\text{SoC},n} = \left[\text{SoC}_{b,n}^{m} - \text{SoC}_{b,n}^{r}(k+1)\right] \times k_{\text{SoC},n} \tag{43}$$

where δv_n is the voltage compensation term. $\delta v_{\text{SoC},n}$ is the SoC balance term. $P_{r,n}^{\text{p.u.}}(k+1)$ and $P_{b,n}^{\text{p.u.}}$ are the reference and output power in per unit for battery. $k_{\text{acc.},n}^{p}$ and $k_{\text{acc.},n}^{i}$ are the accurate power control parameters. $\text{SoC}_{b,n}^{r}(k+1)$ and $\text{SoC}_{b,n}^{m}$ are the average and measured SoC of the n^{th} battery. $k_{\text{SoC},n}$ is the SoC balance control parameter. Then, $P_{r,n}^{\text{p.u.}}(k+1)$ and $\text{SoC}_{b,n}^{r}(k+1)$ can be obtained by (44) – (47).

$$P_{r,n}^{\text{p.u.}}(k+1) = P_{r,n}^{\text{p.u.}}(0) + \varepsilon \sum_{j \in N_n} \delta_{\text{acc.},nj}(k+1) \tag{44}$$

$$\delta_{\text{acc.},nj}(k+1) = \delta_{\text{acc.},nj}(k) + a_{\text{acc.},nj}\left[P_{r,j}^{\text{p.u.}}(k) - P_{r,n}^{\text{p.u.}}(k)\right] \tag{45}$$

$$\text{SoC}_{b,n}^{r}(k+1) = \text{SoC}_{b,n}^{r}(0) + \varepsilon \sum_{j \in N_n} \delta_{\text{SoC},nj}(k+1) \tag{46}$$

$$\delta_{\text{SoC},nj}(k+1) = \delta_{\text{SoC},nj}(k) + a_{\text{SoC},nj}\left[\text{SoC}_{b,j}^{r}(k) - \text{SoC}_{b,n}^{r}(k)\right] \tag{47}$$

where $\text{SoC}_{b,j}^{r}(0)$ is the initial SoC level. $P_{r,j}^{\text{p.u.}}(0)$ is the initial output power of the battery converter. The control equivalent diagram is shown in Fig. 3. Besides, the presented approach needs a sparse communication network. The communication delay can be represented as a transfer function that is given in (48).

$$G_d = \frac{1}{\tau s + 1} \tag{48}$$

where τ is the communication delay.

5. Simulation results

In this section, the public datasets consisting of load and meteorological data for individual house are obtained from NREL database [44] to verify the performance of the proposed multi-level HEMS. Then, the hourly electricity price data is collected from energy market company of Singapore [45]. The long- and short-time intervals are 1 h and 5 min, respectively. The equivalent structure of the house DC microgrid is shown in Fig. 1, which contains a PV generation, two batteries and SCs, as well as house loads. The total optimization period is 24 h. The total system parameters are given in Table II. Three case studies focus on discussing and analyzing the user comfort, uncertainties of house load and PV generation and interaction between local- and system-level HEMS. The designed model is executed in Matlab/Simulink.

TABLE II
PARAMETERS FOR MULTI-LEVEL HEMS

System-level HEMS					
B_{price}	600 \$/kWh	$\text{SoC}_{\text{sc}}^{\min}$	10 %	$P_g^{\min}$	-10 kWh
Q_B	12 kWh	$\text{SoC}_{\text{sc}}^{\max}$	90 %	$P_g^{\max}$	10 kWh
$\text{SoC}_B^{\min}$	10 %	$P_{\text{sc}}^{\min}$	-5 kW	$P_{\text{light}}^{\min}$	0 kWh
$\text{SoC}_B^{\max}$	90 %	$P_{\text{sc}}^{\max}$	5 kW	$P_{\text{light}}^{\max}$	1 kWh
$P_B^{\min}$	-5 kW	L_{sc}	50000	$P_{\text{hac}}^{\min}$	0 kWh
$P_B^{\max}$	5 kW	PV_{price}	\$ 6220	$P_{\text{hac}}^{\max}$	6 kWh
μ	0.98	N_{year}	25	$\text{PMV}_d(t)$	0
ε_{PMV}	0.2	η_B^c, η_B^d	0.98	ε_{PMV}	0.2
a_B	4980	η_{sc}^c, η_{sc}^d	0.98	DF	0.1
b_B	1.98	Illuminance comfort			
c_B	0.016	22:00 – 6:00		6:00 – 22:00	
SC_{price}	2400 \$/kWh	$L_{\text{in}}^{\min}$	0 lx	$L_{\text{in}}^{\min}$	320 lx
Q_{sc}	2 kWh	$L_{\text{in}}^{\max}$	5 lx	$L_{\text{in}}^{\max}$	1800 lx
Local-level HEMS					
v_b, v_{sc}	150 V	k_{sc}^p	0.25	k_{SoC}	150
C_b, C_{sc}	10 μF	k_{sc}^i	0.157	$R_{b,1}^L$, $R_{\text{sc},1}^L$	0.02 Ω
L_b, L_{sc}	2 mH	v_{sc}^r	75 V	$R_{b,2}^L$, $R_{\text{sc},2}^L$	0.01 Ω
k_b	0.016 V/W	$k_{\text{acc.}}^p$	100	τ	1 ms
k_{sc}	0.02 V/W	$k_{\text{acc.}}^i$	62.83	v_r	220 V

TABLE III
HAC ENERGY FOR DIFFERENT WEIGHTS

w_{PPD}	0.1	0.2	0.3
HAC energy	76.5159 kWh	79.4329 kWh	80.3446 kWh

5.1. Case 1: User comfort

This case study discusses the user comfort in the residential environment. The change in thermal comfort level is observed by adjusting the PPD weights w_{PPD} (0.1-0.3) in the thermal comfort scenario. From Fig. 4(a), it can be seen that the PMV waveform gets closer to the neutral line as the w_{PPD} becomes larger. This means that the average users' thermal satisfaction is higher. In addition, the difference between PMV at w_{PPD} = 0.1 and 0.2 is larger than the difference between PMV at w_{PPD} = 0.2 and 0.3. This implies that the PMV variation decreases gradually when the w_{PPD} becomes larger. From Fig. 4(b), a higher w_{PPD} causes the PPD waveform to approach a straight line of 5%. This indicates that the percentage of users dissatisfied with the current housing thermal environment is at the lower level. From Fig. 4(c) and 4(d), outdoor temperatures begin to warm up after 6:00 and can reach 40 ℃. Then, the indoor temperature can be fluctuated around 22 ℃. This means that HAC is working to reduce the indoor temperature. In addition, the indoor temperature is fluctuated around 22 ℃ as the weight w_{PPD} changes. The energy usages of HAC in 24 h are shown in Table III under different weighting conditions. It can be observed that the PPD weights can control the energy consumption of HAC. At weights 0.1 and 0.2, the energy consumption of the HAC increases significantly, while the energy of HAC varies less between weights 0.2 and 0.3. From the above results, it can be seen that the designed w_{PPD} can effectively regulate the indoor thermal comfort and HAC energy consumption. In this article, the w_{PPD} is set to 0.2.

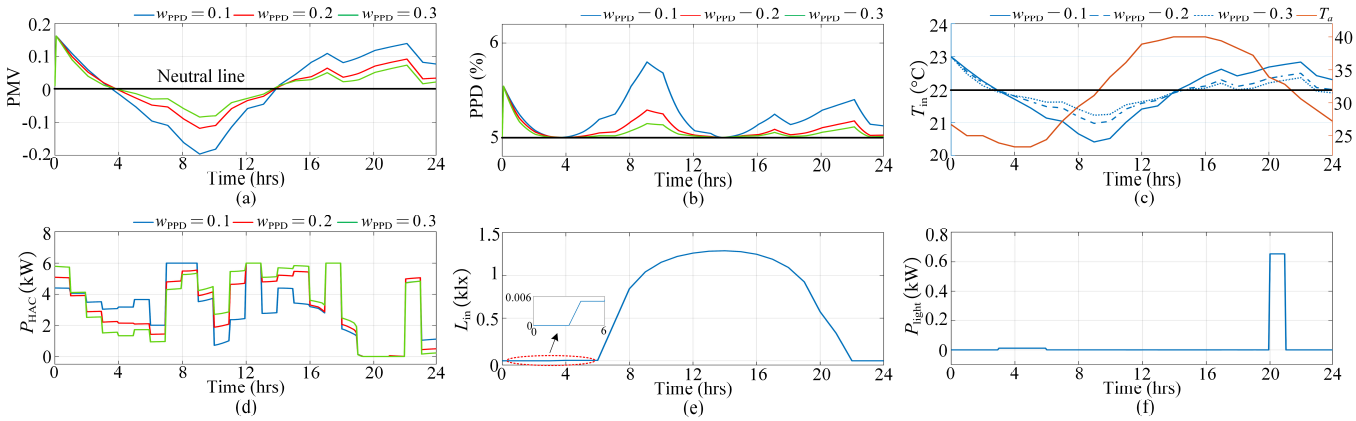

Fig. 4 Simulation results for case 1: (a) PMV with different w_{PPD}, (b) PPD with different w_{PPD}, (c) HAC power with different w_{PPD}, (d) Outdoor temperature and indoor temperature with different w_{PPD}, (e) Indoor illuminance, (f) Lighting power.

In this article, indoor illuminance is used to estimate visual comfort. From Fig. 4(e) and 4(f), the indoor illuminance is mainly provided by the outdoor illuminance between 6:00 and 20:00. After 22:00, the indoor illuminance converted from the outdoor illuminance does not satisfy the visual comfort of the users. Therefore, the electric lights start working to increase the intensity of the indoor light. During sleep time, the electric light provides only a small amount of illuminance (0 - 5 lx) to ensure the users' sleep quality.

5.2. Case 2: The uncertainties of house load and PV power

LTO provides power scheduling decisions based on day-ahead forecast data. However, the uncertainties generated by the random behavior of users and the intermittent nature of PV system can cause the power mismatch between hourly power scheduling and intra-hourly power usage. Therefore, an SC is employed to eliminate the power mismatch. In this case, power stochastic errors are generated in the house load and PV power data to indicate the power mismatch. The error rates are 5 %, 10 % and 20 %. The case consists of three scenarios: PV power data with errors, household load data with errors, and both with errors. In addition, cost efficiency (CE) is introduced to assess the percentage of savings in operating costs, it can be written as (47).

$$\mathrm{CE} = \frac{\mathrm{C_{no}} - \mathrm{C}_w}{\mathrm{C_{no}}} \times 100\ \% \tag{47}$$

where $\mathrm{C_{no}}$ and C_w are the operating cost with and without HEMS ($).

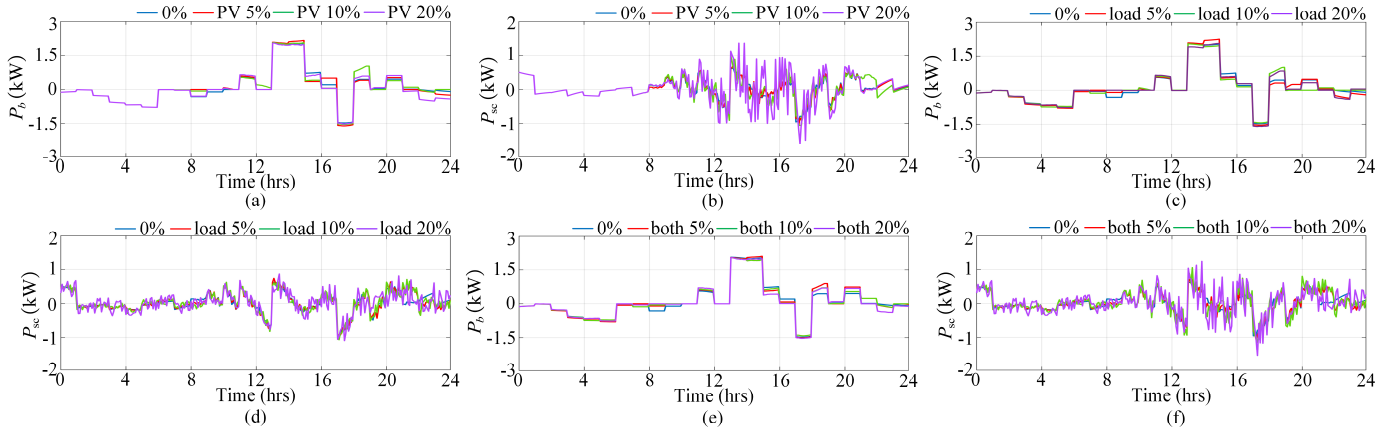

Fig. 5 Simulation results for case 2: (a) The output power of battery under PV error, (b) The output power of SC under PV error, (c) The output power of battery under house load error, (d) The output power of SC under house load error, (e) The output power of battery under both PV and house load errors, (f) The output power of SC under both PV and house load errors.

TABLE IV
CASE II: ESTIMATED PARAMETERS

PV errors	5 %	10 %	20 %	Load errors	5 %	10 %	20 %	Both errors	5 %	10 %	20 %
Total cost ($)	11.8088	11.7153	11.9210	Total cost ($)	11.7741	11.7221	11.7386	Total cost ($)	11.7562	11.6550	11.8583
CE (%)	19.1107	19.7512	19.1358	CE (%)	19.3481	19.7043	19.5918	CE (%)	20.0299	20.5237	19.6918
PMV	0.0527	0.0526	0.0528	PMV	0.0512	0.0513	0.0514	PMV	0.0513	0.0518	0.0522
PPD (%)	5.0575	5.0573	5.0577	PPD (%)	5.0543	5.0545	5.0547	PPD (%)	5.0545	5.0556	5.0564

As can be seen from Fig. 5(a), 5(c) and 5(e), the change in error does not result in a large variation in the output power of the battery since the output power of the battery tracks the power scheduling decision provided by the LTO. From Fig. 5(b), 5(d) and 5(f), the SC is able to respond quickly to oscillation in system load. In addition, the output power fluctuation of SC becomes larger with the increase of power error. This is because the SC is regulated by the STO that is used to suppress the power mismatch caused by stochastic errors. As can be observed from Table IV, the total cost, cost efficiency, average PMV and PPD do not display significant changes with power errors variations. As a comparison, the total cost, CE, PMV and PPD of the optimization

without errors are 11.9067 $, 19.3383 %, 0.0521 and 5.0562 %, respectively. Therefore, the proposed method can effectively suppress the power mismatch without increasing the operating cost and ensuring the user comfort.

5.3. Case 3: Interaction between system- and local-level HMES

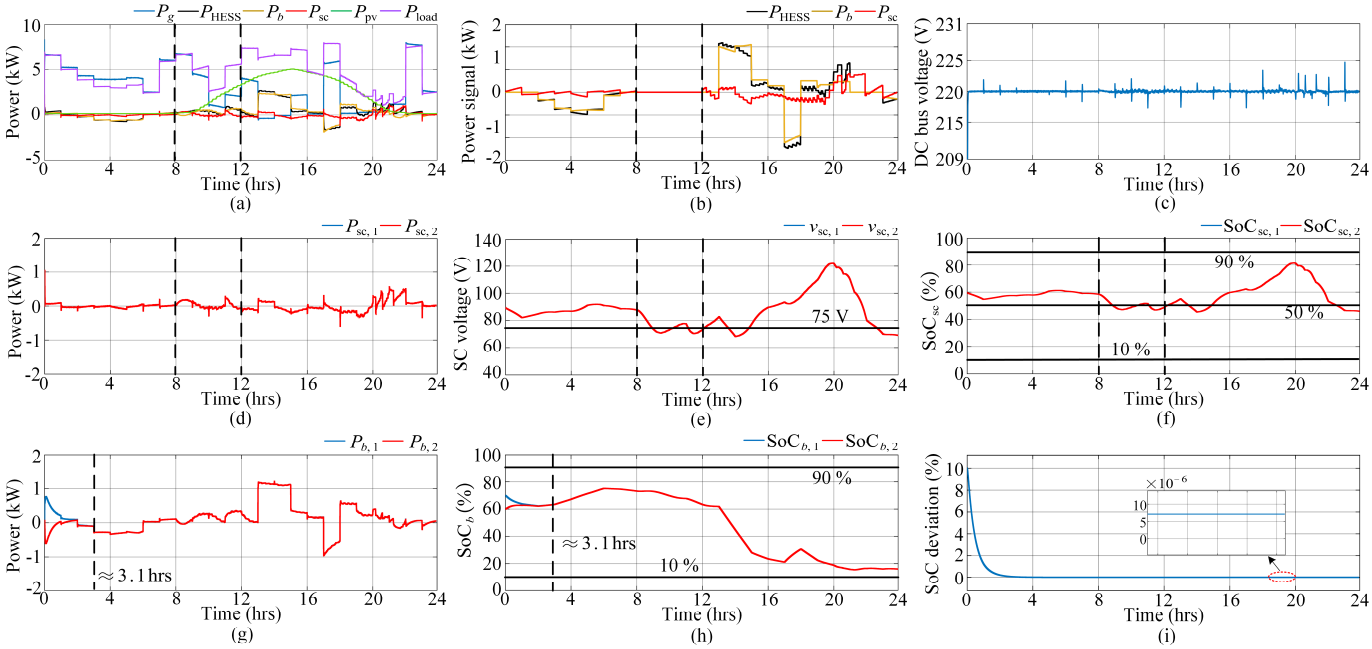

Fig. 6 Simulation results for case 3: (a) Power profile in home microgrid, (b) Power signal from system-level HEMS, (c) DC bus voltage, (d) Output power of SCs, (e) SC voltages, (f) SC SoCs, (g) Output power of batteries, (h) battery SoCs, (i) SoC deviation.

This case study will analyze and discuss the interaction between system level and local level HEMS. From Fig. 6(a) and 6(b), the local-level HEMS will provide power demands for the house based on the power scheduling decisions provided by the system-level HEMS. A communication failure between the system and the local-level HEMS suddenly occurs between 8 and 12 hours. The local-level HEMS is unable to receive the information command from system-level HEMS, and thus it will achieve battery and SC power sharing through *v-dP* and *v-P* droop controls. After 12 hours, system- and local-level HEMS regained communication connectivity. The system-level HEMS re-updates the power scheduling decision based on the current system data. The local level HEMS will supply power to the house based on the updated reference power. During this period, the DC bus voltage can be maintained within the desired range (220 × (1 ± 5%) V), as shown in Fig. 6(c). In addition, the SC voltage recovery control in the local-level HEMS will ensure that the voltage and SoC of SCs fluctuate around the preset value for future use, as shown in Fig. 6(d) - 6(f). As can be observed from Fig. 6(g) – 6(h), the initial values of the SoC for both batteries are set to 70% and 60%, respectively. The proposed consensus-based voltage regulator will force the battery with higher SoC to provide more power to the system than the ones with lower SoC, thus avoiding the overcharging and discharging of the smaller SoC battery. Then, the SoC balance between batteries is implemented regardless of the system line resistance consistency. Besides, it

can be observed from Fig. 6(i) that the SoC deviation between the batteries is very small. Therefore, the performance of the proposed consensus-based voltage regulator meets the expected requirements.

6. Conclusion

In this article, multi-level HEMS is proposed for minimizing operating cost and maximizing user comfort in a DC home microgrid. The multi-level HEMS consists of a system-level and local-level HEMS. In the system-level HEMS, the LTO-MPC is proposed to minimize the operating cost and to maximize the user comfort. The STO-MPC is presented to eliminate the power mismatch caused by randomness of user behavior and intermittent PV generation. The PMV-PPD model is employed to estimate the thermal comfort. The visual comfort is represented by the illuminance model. Besides, the battery and SC degradation model is integrated into the HEMS to assess the wear cost. In the local-level HEMS, a consensus-based voltage regulator is proposed to achieve the accurate power sharing and SoC balance between batteries. The power sharing between battery and SC is achieved by using *v-dP* and *v-P* droop controls. The DC bus voltage and SC voltage can be restored within a safe range.

References

[1] K. Vatanparvar and M. A. Al Faruque, "Design Space Exploration for the Profitability of a Rule-Based Aggregator Business Model Within a Residential Microgrid," *IEEE Trans. Smart Grid*, vol. 6, no. 3, pp. 1167–1175, 2015, doi: 10.1109/TSG.2014.2380318.

[2] A. Chub, D. Vinnikov, E. Liivik, and T. Jalakas, "Multiphase Quasi-Z-Source DC-DC Converters for Residential Distributed Generation Systems," *IEEE Trans. Ind. Electron.*, vol. 65, no. 10, pp. 8361–8371, 2018, doi: 10.1109/TIE.2018.2801860.

[3] Y. Deng, Y. Zhang, F. Luo, and G. Ranzi, "Many-Objective HEMS Based on Multi-Scale Occupant Satisfaction Modelling and Second-Life BESS Utilization," *IEEE Trans. Sustain. Energy*, vol. 13, no. 2, pp. 934–947, 2022, doi: 10.1109/TSTE.2022.3140765.

[4] S. L. Arun and M. P. Selvan, "Intelligent Residential Energy Management System for Dynamic Demand Response in Smart Buildings," *IEEE Syst. J.*, vol. 12, no. 2, pp. 1329–1340, Jun. 2018, doi: 10.1109/JSYST.2017.2647759.

[5] A. Anvari-Moghaddam, H. Monsef, and A. Rahimi-Kian, "Optimal smart home energy management considering energy saving and a comfortable lifestyle," *IEEE Trans. Smart Grid*, vol. 6, no. 1, pp. 324–332, 2015, doi: 10.1109/TSG.2014.2349352.

[6] M. Gholami and M. J. Sanjari, "Multiobjective energy management in battery-integrated home energy systems," *Renew. Energy*, vol. 177, pp. 967–975, 2021, doi: 10.1016/j.renene.2021.05.162.

[7] J. Engel, T. Schmitt, T. Rodemann, and J. Adamy, "Hierarchical Economic Model

Predictive Control Approach for a Building Energy Management System With Scenario-Driven EV Charging," *IEEE Trans. Smart Grid*, vol. 3053, no. c, pp. 1–12, 2022, doi: 10.1109/TSG.2022.3160390.

[8] H. Çimen, N. Bazmohammadi, A. Lashab, Y. Terriche, J. C. Vasquez, and J. M. Guerrero, "An online energy management system for AC/DC residential microgrids supported by non-intrusive load monitoring," *Appl. Energy*, vol. 307, no. October 2021, p. 118136, 2022, doi: 10.1016/j.apenergy.2021.118136.

[9] Y. Zhang, R. Wang, T. Zhang, Y. Liu, and B. Guo, "Model predictive control-based operation management for a residential microgrid with considering forecast uncertainties and demand response strategies," *IET Gener. Transm. Distrib.*, vol. 10, no. 10, pp. 2367–2378, 2016, doi: 10.1049/iet-gtd.2015.1127.

[10] M. Shafie-Khah and P. Siano, "A stochastic home energy management system considering satisfaction cost and response fatigue," *IEEE Trans. Ind. Informatics*, vol. 14, no. 2, pp. 629–638, 2018, doi: 10.1109/TII.2017.2728803.

[11] B. Jeddi, Y. Mishra, and G. Ledwich, "Differential Dynamic Programming Based Home Energy Management Scheduler," *IEEE Trans. Sustain. Energy*, vol. 11, no. 3, pp. 1427–1437, 2020, doi: 10.1109/TSTE.2019.2927237.

[12] A. Ahmad and J. Y. Khan, "Real-Time Load Scheduling, Energy Storage Control and Comfort Management for Grid-Connected Solar Integrated Smart Buildings," *Appl. Energy*, vol. 259, no. August 2019, p. 114208, 2020, doi: 10.1016/j.apenergy.2019.114208.

[13] F. Luo, G. Ranzi, C. Wan, Z. Xu, and Z. Y. Dong, "A Multistage Home Energy Management System with Residential Photovoltaic Penetration," *IEEE Trans. Ind. Informatics*, vol. 15, no. 1, pp. 116–126, 2019, doi: 10.1109/TII.2018.2871159.

[14] S. Faddel, A. A. Saad, T. Youssef, and O. Mohammed, "Decentralized Control Algorithm for the Hybrid Energy Storage of Shipboard Power System," *IEEE J. Emerg. Sel. Top. Power Electron.*, vol. 8, no. 1, pp. 720–731, 2020, doi: 10.1109/JESTPE.2019.2899287.

[15] Q. Zhang and G. Li, "Experimental study on a semi-active battery-supercapacitor hybrid energy storage system for electric vehicle application," *IEEE Trans. Power Electron.*, vol. 35, no. 1, pp. 1014–1021, 2020, doi: 10.1109/TPEL.2019.2912425.

[16] M. Shi, X. Chen, J. Zhou, Y. Chen, J. Wen, and H. He, "Advanced Secondary Voltage Recovery Control for Multiple HESSs in a Droop-Controlled DC Microgrid," *IEEE Trans. Smart Grid*, vol. 10, no. 4, pp. 3828–3839, 2019, doi: 10.1109/TSG.2018.2838108.

[17] M. M. S. Khan, O. Faruque, and A. Newaz, "Fuzzy Logic Based Energy Storage Management System for MVDC Power System of All Electric Ship," *IEEE Trans. Energy Convers.*, vol. 32, no. 2, pp. 798–809, 2017.

[18] R. Zhang, B. Hredzak, and T. Morstyn, "Distributed Control with Virtual Capacitance for the Voltage Restorations, State of Charge Balancing and Load Allocations of

Heterogeneous Energy Storages in a DC Datacenter Microgrid," *IEEE Trans. Energy Convers.*, vol. 34, no. 3, pp. 1296–1308, 2018, doi: 10.1109/TEC.2018.2889065.

[19] X. Lin, R. Zamora, and C. A. Baguley, "A Coordinated Droop Controls and Power Management Scheme for Hybrid Energy Storage Systems in DC Microgrids," *2021 31st Australas. Univ. Power Eng. Conf.*, pp. 1–6, 2021, doi: 10.1109/aupec52110.2021.9597727.

[20] X. Lin, R. Zamora, C. Baguley, and A. Srivastava, "A Hybrid Short-Term Load Forecasting Approach for Individual Residential Customer," *IEEE Trans. Power Deliv.*, vol. 8977, no. c, pp. 1–1, 2022, doi: 10.1109/tpwrd.2022.3178822.

[21] H. Ekhteraei Toosi, A. Merabet, and A. Swingler, "Impact of battery degradation on energy cost and carbon footprint of smart homes," *Electr. Power Syst. Res.*, vol. 209, no. December 2021, p. 107955, 2022, doi: 10.1016/j.epsr.2022.107955.

[22] C. Bordin, H. O. Anuta, A. Crossland, I. L. Gutierrez, C. J. Dent, and D. Vigo, "A linear programming approach for battery degradation analysis and optimization in offgrid power systems with solar energy integration," *Renew. Energy*, vol. 101, pp. 417–430, 2017, doi: 10.1016/j.renene.2016.08.066.

[23] Y. Guo, S. Sheng, N. Anglani, and B. Lehman, "Optimal Power Management for Grid-Connected Microgrid Considering Modelling of Different Electricity Cost and Battery Degradation Cost," *2019 IEEE 20th Work. Control Model. Power Electron. COMPEL 2019*, 2019, doi: 10.1109/COMPEL.2019.8769640.

[24] M. Gitizadeh and H. Fakharzadegan, "Battery capacity determination with respect to optimized energy dispatch schedule in grid-connected photovoltaic (PV) systems," *Energy*, vol. 65, pp. 665–674, 2014, doi: 10.1016/j.energy.2013.12.018.

[25] S. Drouilhet and B. L. Johnson, "A battery life prediction method for hybrid power applications," *35th Aerosp. Sci. Meet. Exhib.*, no. January 1997, 1997, doi: 10.2514/6.1997-948.

[26] C. Zhou, K. Qian, M. Allan, and W. Zhou, "Modeling of the cost of EV battery wear due to V2G application in power systems," *IEEE Trans. Energy Convers.*, vol. 26, no. 4, pp. 1041–1050, 2011, doi: 10.1109/TEC.2011.2159977.

[27] C. Ju, P. Wang, L. Goel, and Y. Xu, "A two-layer energy management system for microgrids with hybrid energy storage considering degradation costs," *IEEE Trans. Smart Grid*, vol. 9, no. 6, pp. 6047–6057, 2018, doi: 10.1109/TSG.2017.2703126.

[28] U. Manandhar *et al.*, "Energy management and control for grid connected hybrid energy storage system under different operating modes," *IEEE Trans. Smart Grid*, vol. 10, no. 2, pp. 1626–1636, 2019, doi: 10.1109/TSG.2017.2773643.

[29] P. Kreczanik, P. Venet, A. Hijazi, and G. Clerc, "Study of supercapacitor aging and lifetime estimation according to voltage, temperature, and RMS current," *IEEE Trans. Ind. Electron.*, vol. 61, no. 9, pp. 4895–4902, 2014, doi: 10.1109/TIE.2013.2293695.

[30] P. Roy, J. He, and Y. Liao, “Cost Minimization of Battery-Supercapacitor Hybrid Energy Storage for Hourly Dispatching Wind-Solar Hybrid Power System,” *IEEE Access*, vol. 8, pp. 210099–210115, 2020, doi: 10.1109/ACCESS.2020.3037149.

[31] A. Prasanthi, H. Shareef, M. Asna, A. Asrul Ibrahim, and R. Errouissi, “Optimization of hybrid energy systems and adaptive energy management for hybrid electric vehicles,” *Energy Convers. Manag.*, vol. 243, no. May, p. 114357, 2021, doi: 10.1016/j.enconman.2021.114357.

[32] S. Zhang, Y. Cheng, Z. Fang, and Z. Lin, “Improved algorithm for adaptive coefficient of adaptive Predicted Mean Vote (aPMV),” *Build. Environ.*, vol. 163, no. May, p. 106318, 2019, doi: 10.1016/j.buildenv.2019.106318.

[33] “Ergonomics ofthe Thermal Environment—Analytical Determination and Interpretation of Thermal Comfort Using Calculation of the PMV and PPD Indices and Local Thermal Comfort Criteria,” *ISO 77302005*, 2005.

[34] C. Buratti, P. Ricciardi, and M. Vergoni, “HVAC systems testing and check: A simplified model to predict thermal comfort conditions in moderate environments,” *Appl. Energy*, vol. 104, pp. 117–127, 2013, doi: 10.1016/j.apenergy.2012.11.015.

[35] L. Xiao, L.-L. Qin, and S.-Y. Wu, “Proposal and application of comprehensive thermal comfort evaluation model in heating seasons for buildings with solar Trombe wall,” *Appl. Therm. Eng.*, vol. 213, no. May, p. 118774, 2022, doi: 10.1016/j.applthermaleng.2022.118774.

[36] P. R. Michael, D. E. Johnston, and W. Moreno, “A conversion guide: Solar irradiance and lux illuminance,” *J. Meas. Eng.*, vol. 8, no. 4, pp. 153–166, 2020, doi: 10.21595/jme.2020.21667.

[37] S. Vaisi and F. Kharvari, “Evaluation of Daylight regulations in buildings using daylight factor analysis method by radiance,” *Energy Sustain. Dev.*, vol. 49, pp. 100–108, 2019, doi: 10.1016/j.esd.2019.02.002.

[38] J. Seo, A. Choi, and M. Sung, “Recommendation of indoor luminous environment for occupants using big data analysis based on machine learning,” *Build. Environ.*, vol. 198, no. March, p. 107835, 2021, doi: 10.1016/j.buildenv.2021.107835.

[39] G. Hoffmann *et al.*, “Effects of variable lighting intensities and colour temperatures on sulphatoxymelatonin and subjective mood in an experimental office workplace,” *Appl. Ergon.*, vol. 39, no. 6, pp. 719–728, 2008, doi: 10.1016/j.apergo.2007.11.005.

[40] T. Cao, Z. Lian, S. Ma, and J. Bao, “Thermal comfort and sleep quality under temperature, relative humidity and illuminance in sleep environment,” *J. Build. Eng.*, vol. 43, no. March, p. 102575, 2021, doi: 10.1016/j.jobe.2021.102575.

[41] C. Li, E. A. A. Coelho, T. Dragicevic, J. M. Guerrero, and J. C. Vasquez, “Multiagent-Based Distributed State of Charge Balancing Control for Distributed Energy Storage Units in AC Microgrids,” *IEEE Trans. Ind. Appl.*, vol. 53, no. 3, pp. 2369–2381, 2017, doi:

10.1109/TIA.2016.2645888.

[42] M. Kriegleder, “A correction to algorithm A2 in ‘asynchronous distributed averaging on communication networks,’” *IEEE/ACM Trans. Netw.*, vol. 22, no. 6, pp. 2026–2027, 2014, doi: 10.1109/TNET.2013.2292800.

[43] L. Meng, T. Dragicevic, J. Roldan-Perez, J. C. Vasquez, and J. M. Guerrero, “Modeling and Sensitivity Study of Consensus Algorithm-Based Distributed Hierarchical Control for DC Microgrids,” *IEEE Trans. Smart Grid*, vol. 7, no. 3, pp. 1504–1515, May 2016, doi: 10.1109/TSG.2015.2422714.

[44] NREL, “End-Use Load Profiles for the U.S. Building Stock,” 2021. doi: https://dx.doi.org/10.25984/1876417.

[45] EMC, “Energy Market Company (EMCSG),” *EMC Singapore*, 2022. https://www.emcsg.com/marketdata (accessed May 01, 2022).

Conclusion and future work

Chapter 7: Conclusion and future work

7.1. Conclusion

This chapter summarizes the findings and results of this PhD thesis. It draws conclusions based on the methodology and results mentioned in the previous chapters. Finally, it provides recommendations for future research.

This thesis investigates the modeling of home energy management systems (HEMS) with solar PV and hybrid energy storage systems (HESS). It provides accurate forecasting and optimal power scheduling for household electricity usage. The thesis also studies the control technology of the HESS to ensure the stable operation of household microgrid. The results and verification under different conditions presents that the proposed method can help reduce the cost of home microgrid operation and improve user comfort.

Chapter 2 provides a comprehensive literature review on the application technologies and related challenges of HEMS in home microgrids. It discusses and studies various proposed solutions for addressing the associated challenges. It also exposes the shortcomings of the current HEMS research field and points out possible future challenges. Research areas with challenges suggested in future trends of this chapter need to be researched more to get valuable solutions for implementation. The discussion in this chapter shows that HEMS can enable end customers to understand the structure of household energy use and change customers' consumption behavior to reduce electricity costs. It can further transform end users from traditional consumer roles to prosumers, who can actively participate in energy market transactions. Therefore, the development of this HEMS needs to consider load forecasting, optimization and control to ensure the normal operation of the home microgrid. Furthermore, this complete system can increase the penetration rate of renewable energy sources in houses.

Chapter 3 designs a control method for battery energy storage systems in DC microgrids. The proposed method is able to achieve state of charge (SoC) balancing among batteries regardless of whether the batteries have the same capacity or not. In this method, the voltage recovery control is equivalent to a high-pass filter (HPF) to realize DC bus voltage regulation. That is to say, the method removes the communication connection between the primary and secondary controllers and simplifies the controller structure. Therefore, the control method proposed in this chapter is a fully decentralized type to regulate the battery operation in the DC microgrid.

Chapter 4 proposes an integrated multifunctional controller for multiple HESSs consisting of batteries and supercapacitors (SCs) in a DC microgrid. In the proposed method, the v-dP droop control method is developed to regulate the battery converter, while the traditional v-P droop control method is adopted to regulate the SC converter. This combination of two droop control

methods can realize power sharing between battery and SC as well as voltage regulation without additional voltage restoration controller, thus simplifying the complexity of the controller. This method also designs a voltage compensator based on a consensus algorithm to achieve SoC balancing and accurate power sharing among batteries. Finally, a power management system is proposed to prevent battery overuse.

Chapter 5 proposes a hybrid model for short-term household load forecasting, which consists of two parts. The first part is an ensemble model consisting of support vector machine (SVM), back propagation neural network (BPNN), and generalized regression neural network (GRNN). Then, a genetic algorithm is used to optimize BPNN and SVM to improve their forecasting performance. Also, a thermal dynamic model is proposed to predict the indoor temperature, which is used as input of the ensemble model to estimate the power consumption of air conditioning and heater. The other part is a deep ensemble model that is used to predict lighting and other loads. The model consists of three bidirectional long short-term memory (Bi-LSTM) networks. A Bayesian algorithm is adopted to search the optimal hyperparameters of the BI-LSTM. After, an illuminance algorithm is used to calculate outdoor illuminance, which is used as input of the deep ensemble model to track lighting load usage. Finally, a trimmed algorithm is used to integrate the results of ensemble and deep ensemble models. The datasets from the UMass Smart Microgrid and Flexhouse projects are used to verify the performance of the proposed method. The results show that the proposed method has better prediction accuracy.

Finally, Chapter 6 presented a multi-level HEMS for home microgrids. In HEMS at the system level, long-time scale optimizations are proposed to minimize the overall system operating cost and user comfort requirements. The operating cost covers electricity cost, PV power generation cost, battery and SC wear costs. Then, the method also employs a predicted mean vote - percentage people dissatisfied (PMV-PPD) model to evaluate the thermal comfort of users. Besides, an illuminance model is adopted to evaluate the user's visual comfort. The objective of the short-time scale optimization is to alleviate the power fluctuations caused by the randomness of end-user behaviors and PV generation, as well as to ensure the SoC of the SC within a safe range. Then the local level HEMS is proposed to receive the power reference from the system level HEMS to adjust the charging and discharging operation of the HESS, and purchase/sell the electricity from/to utility.

The main concluding results and remarks of this thesis are summarized as follows:

- As an emerging power system, a home microgrid needs a smart HEMS integrating multiple functions to ensure its stable operation and meet the needs of users and utility.

- Compared with traditional energy storage systems, HESS can effectively suppress high-frequency power fluctuations caused by the randomness of user behavior and the uncertainty of renewable energy resources.
- The fully decentralized approach can achieve SoC balancing among batteries and DC bus voltage regulation
- The versatility and simplicity of the HESS control system can be achieved at the same time.
- Household load forecasting is very significant to assist users understand household load usage and planning.
- Considering different optimization objectives and system constraints can minimize the operating cost of the system and maximize user comfort.

7.2. Future work

Despite the valuable contributions and findings of this study, there are still opportunities for future research and prospects to expand the topics covered in this study. Some of research areas that require further investigation are as follows:

- Most of the HESSs mentioned in the literature are a combination of batteries and SCs. There are few introductions for other types of energy storage combinations. Therefore, scholars can consider further research on the low-cost combination and high economic benefits of multiple type energy storage systems.
- HEMS needs to receive and send data through a communication network. This means that communication delays are unavoidable. Therefore, it is necessary to develop a delay compensation algorithm in HEMS to reduce the negative impact of communication delay.
- Coordination algorithms need to be developed in HEMS for both home-to-home and home-to-grid. This is very important for the energy trading mechanism.